Cranial and Postcranial Morphology of the Insectivoran-grade Mammals *Hsiangolestes* and *Naranius* (Mammalia, *Eutheria*) with Analyses of Their Phylogenetic Relationships

Suyin Ting, Xiaoming Wang, and Jin Meng

Bulletin of the American Museum of Natural History

CRANIAL AND POSTCRANIAL MORPHOLOGY OF THE INSECTIVORAN-GRADE MAMMALS *HSIANGOLESTES* AND *NARANIUS* (MAMMALIA, EUTHERIA) WITH ANALYSES OF THEIR PHYLOGENETIC RELATIONSHIPS

SUYIN TING
LSU Museum of Natural Science
Louisiana State University, Baton Rouge

XIAOMING WANG
Department of Vertebrate Paleontology
Natural History Museum of Los Angeles County, Los Angeles;
Division of Paleontology
American Museum of Natural History

JIN MENG
Division of Paleontology
American Museum of Natural History

BULLETIN OF THE AMERICAN MUSEUM OF NATURAL HISTORY
Number 463, 127 pp., 56 figures, 3 tables
Issued June 26, 2023

 ISSN 0003-0090

CONTENTS

ABSTRACT

Early Cenozoic "insectivorans" possess some of the most primitive morphologies among eutherian mammals. Studies of these archaic mammals offer insights into the early diversifications of basal eutherians. Despite such importance, early fossil "insectivorans" from Asia are poorly known due to a scarcity of fossil remains, which often consist only of fragmentary jaws and teeth. Discoveries of remarkably well-preserved fossil "insectivorans", including complete skulls and articulated postcranial skeletons, from the early Eocene Hengyang Basin in south-central Hunan Province, China, offer a rare opportunity to thoroughly study two taxa belonging to different families.

Fine-grained red beds from Hengyang Basin preserve extraordinary fossils with morphological structures rarely seen elsewhere. Thin sections of a skull of *Hsiangolestes youngi* Zheng and Huang, 1984, for example, reveal the extremely delicate nasal and maxillary turbinates, which, as far as we are aware, are the first known from fossils of this age. We thus take this opportunity to document in detail the cranial and dental morphology, as well as postcranial skeletons, of the Hengyang "insectivorans.".

In this monograph, we describe several complete skulls and serial sections of a skull, as well as many partial skulls, mandibles, and postcranial skeletons of *Hsiangolestes youngi*, an Asian early Eocene insectivoran-grade mammal. We also report a new species of *Naranius* Russell and Dashzeveg, 1986—*N. hengdongensis*—an Asian early Eocene cimolestid and describe its well-preserved skulls and mandibles.

Hsiangolestes is endemic to Asia. It is currently known only from the earliest Eocene Lingcha Formation, Hengyang Basin, Hunan Province, China. *Naranius* closely resembles *Cimolestes* Marsh, 1889, the type genus of the family Cimolestidae. It is mainly distributed in Asia and known from the earliest Eocene deposits in the Bumban Member of the Naran Bulak Formation, Nemegt Basin, of Mongolia, and the Lingcha Formation, Hengyang Basin, Hunan Province, China. The only record of *Naranius* reported outside of Asia is *N. americanus* from the early Wasatchian Red Hot Local Fauna, Mississippi, United States.

Using PAUP and TNT search algorithms, we place these Hengyang taxa within phylogenetic context of other fossil "insectivorans" from the Mesozoic and early Cenozoic of Asia together with some well-known Holarctic taxa. A phylogenetic analysis of 290 cranial and dental characters from 36 fossil and modern insectivoran-grade taxa is presented, focusing on new materials of *Hsiangolestes youngi* and *Naranius hengdongensis*. Based on the results of our phylogenetic analyses, we propose that (1) *Hsiangolestes*, *Prosarcodon*, *Sarcodon*, and *Sinosinopa*, form a monophyletic group, for which we propose the family name Sarcodontidae; (2) the family Cimolestidae should be restricted to *Naranius* and *Cimolestes*, which are sister taxa; (3) the systematic position of *Naranius americanus* is uncertain; and (4) the family Micropternodontidae should be restricted to *Micropternodus* and its allies in North America.

INTRODUCTION

Early Cenozoic "insectivorans" (we use this term as a grade descriptor) comprise a controversial and ill-defined group long been associated with the basal radiation of placental mammals (eutherians) that trace their origins to the Mesozoic (Huxley, 1880; Matthew, 1909; Butler, 1972; Wyss, 1987; Douady and Douzery, 2003; Meredith et al., 2011; Asher, 2018a; and citations within). With their small size and primitive tribosphenic dental morphology, some early fossil "insectivorans" were suspected to be basal or distantly related to living eutherians (e.g., McKenna, 1963, 1968; Novacek, 1986). As such, records of early Cenozoic "insectivoran" diversifications were often viewed as crucial in our understanding of how several eutherian mammal clades evolved from a primitive "insectivoran" stock (e.g., Butler, 1948, 1956, 1972; Novacek, 1986; Asher et al., 2002). As a result, much attention has been devoted to fossil "insec-

tivorans" with an eye for resolving eutherian relationships, although in recent years, the explosive growth of DNA sequence data has played an increasingly important role in formulating higher-level relationships and teasing out discrete clades that were previously difficult to resolve based on morphology alone (e.g., Douady et al., 2004; Springer et al., 2004; O'Leary et al., 2013; Tarver et al., 2016; Álvarez-Carretero et al., 2022; Foley et al., 2023).

Despite these attentions, fossil records of Asian early Paleogene "insectivores" are generally poor as compared to those from Europe and North America, and as a result, Asian taxa did not figure importantly in the discussion of insectivoran-grade phylogeny (e.g., Butler, 1948; Novacek, 1986; Asher et al., 2002; Wible et al., 2004). Much of this poor state of knowledge can be attributed to rare and poorly preserved fossil records as their small, fragile skeletal remains are prone to destruction in the sediments. The long history of the early fossil "insectivores," often going back to the late Mesozoic and early Cenozoic, is also unfavorable for their preservations because of the drastically reduced exposures suitable for explorations. It is thus particularly rare that complete skulls and postcranial skeletons of early "insectivorans" are preserved. Discovery of exquisite fossils from the Hengyang Basin in the south-central part of Hunan Province, China, is such an occasion.

Fossils from fine-grained red beds in Hengyang Basin are so well preserved that extremely delicate nasal and maxillary turbinates are beautifully preserved, as revealed by thin sectioning, which, as far as we are aware, are unprecedented in fossils of this age. In addition, delicate bones in the ear regions are also preserved, as well as articulated partial vertebrae and limb bones. The Hengyang materials thus preserve such a wealth of information that monographic treatment is warranted.

In addition to the remarkable preservation of fossils, the Hengyang Basin is one of four currently known sites in Asia where continental deposits spanning the Paleocene-Eocene boundary are preserved (the others being the Erlian Basin, Inner Mongolia; the Nanyang Basin, Henan Province of China; and the Nemegt Basin, Mongolia) (Dashzeveg, 1988; Bowen et al., 2005; Zhu et al., 2010). It is also one of two currently known sites in Asia (the other being the Nanyang Basin), where the remarkable negative shift in δ^{13} C values of carbonates (carbon isotope excursion, CIE) that marks the Paleocene-Eocene boundary has been found (Bowen et al., 2002; Ting et al., 2003, 2011; Zhu et al., 2010).

This negative shift of carbonate isotopes in both marine (Kennett and Scott, 1991; Thomas and Shackleton, 1996) and continental deposits (Koch et al., 1992, 1995) suggests a significant global climatic warming during the Paleocene-Eocene transition (Paleocene-Eocene Thermal Maximum, PETM, Zachos et al, 2003). The materials of *Hsiangolestes youngi* and *Naranius hengdongensis* were collected from deposits about 15 m above the local Paleocene-Eocene boundary, which also yielded the euprimate, *Teilhardina asiatica* (Ni et al., 2004), and other mammalian and reptilian fossils. Such a globally well-dated carbon isotope excursion not only helps to constrain the age of Hengyang "insectivoran" fossils but also places them within the context of global climatic changes.

The purpose of this study is to describe new materials of skulls and partial postcranial skeleton of an Asian early Eocene insectivoran-grade mammal, *Hsiangolestes youngi* (Zheng and Huang, 1984), and to report a new species of *Naranius*, *Naranius hengdongensis* (*N.* cf. *infrequens* of Ting, 1995, 1998), an Asian early Eocene cimolestid (where Cimolestidae is herein restricted to *Cimolestes* + *Naranius*; see Phylogenetic Analysis below). We also use their cranial and dental information for phylogenetic analysis and discuss their phylogenetic positions.

Both *Hsiangolestes* and *Naranius* are mainly distributed in Asia. *Hsiangolestes*, represented by the only known species, *H. youngi*, is from the earliest Eocene Lingcha Formation, Hengyang Basin, Hunan Province, China (Bowen et al., 2002; Ting et al., 2003, 2011). The type species of

Naranius, *N. infrequens*, occurs in the earliest Eocene deposits in the Bumban Member of the Naran Bulak Formation, Nemegt Basin, of Mongolia (Russell and Dashzeveg, 1986), and the new species, *H. hengdongensis*, is from the Lingcha Formation in Hengyang Basin. *Naranius americanus,* the only record of *Naranius* reported outside of Asia, is from the early Wasatchian Red Hot Local Fauna, Mississippi in the United States (Beard and Dawson, 2009); however, its phylogenetic position is uncertain.

The phylogenetic positions of *Hsiangolestes* and *Naranius* and their relationships with other early "insectivoran" eutherians are poorly understood due to the lack of complete specimens. In this study, *Hsiangolestes* and *Naranius* are represented by well-preserved complete skulls, lower jaws, and partial postcranial skeletons, which, for the first time, provide a unique opportunity to understand their cranial anatomy and to analyze their phylogenetic relationships. In order to understand the internal cranial structures of *Hsiangolestes*, we ground down a complete skull into 377 serial sections, which exposed the internal structures of the ear region and nasal cavity, including nasal and maxillary turbinates (this work was undertaken in 1990 when noninvasive computed tomography was not available). To reconstruct the phylogenetic relationships of *Hsiangolestes* and *Naranius*, we used cladistic methods, involving 36 fossil and modern insectivoran-grade taxa and 290 cranial and dental characters for comparison. Our study focuses on the phylogenetic position of these two taxa at the family level. A phylogenetic analysis of all eutherian insectivoran-grade mammals is beyond our scope; however, the detailed cranial and dental anatomy of these two taxa and the phylogenetic analysis presented herein should encourage future research on Asian stem eutherian insectivoran-grade mammals.

Institutional Abbreviations

AMNH Division of Paleontology, American Museum of Natural History, New York

CM Carnegie Museum of Natural History, Pittsburgh, Pennsylvania

IVPP Institute of Vertebrate Paleontology and Paleoanthropology, Chinese Academy of Sciences, Beijing, China

PSS Mongolian Academy of Sciences, Institute of Geology, Palaeontology and Stratigraphy Section, Ulan Bator, Mongolia

HISTORY OF RESEARCH

Hsiangolestes and *Naranius* are important components in the Hengyang Fauna. The discovery of the Hengyang fossils began early last century when the Hengyang "Red Beds" were investigated (Tien et al., 1933; Young et al., 1938). Tien et al. (1933) distinguished two sets of red beds: the older named the "Hengyang Red Beds" or "Hengyang Sandstone" with a suggested Eocene age, the younger the "Tanshih Red Beds" with a suggested Miocene age. Based on the discovery of plants and fishes, Tien (1936) then proposed that "Tanshih Red Beds" probably were Eocene in age and "Hengyang Red Beds" were Cretaceous. Young (1944) reported the first mammalian fossil, *Propalaeotherium hengyangensis* (*Propachynolophus hengyangensis* of Li et al., 1979), found at Changpiliang (now Lingcha village of Hengdong County, Li et al., 1979) about 15 km northeast of Hengyang city in the Hengyang Basin. He suggested that the "Hengyang Red Beds" (or "Hengyang Sandstone") containing this fossil were middle Eocene in age; however, he also pointed out that "*P. hengyangensis* is derived from a lower level of the Red Beds," so it "does not necessarily mean that the whole formation is middle Eocene in age" (Young, 1944: 3).

Research on the Hengyang red beds has continued since the 1960s and some invertebrate and palynologic fossils were found (Li, 1965; Zhang, 1979; Guan, 1979, 1989; Hu and Zheng, 1980; Zhang, 1982; Liang and Zhang, 1984; Chu, 1986; Hsu et al., 1990). The Hunan Petroleum Team subdivided the "Hengyang Red Beds" into the Paleocene-Eocene "Xialiushi Formation" and

the Eocene-Oligocene "Limuping Formation" in 1976 (Zheng and Huang, 1984).

Major progress in defining the early Tertiary strata came from the study of fossil vertebrates, when Li et al. (1979) discovered a small mammal fauna about 15 km southwest of Hengdong, a small town in the Hengdong County, in the northeast part of the Hengyang Basin. They named the fossil-bearing layer the Lingcha Formation and subdivided it into the "Upper Fossil Layer" and the "Lower Fossil Layer." In the "Upper Fossil Layer," they found at least five mammalian species, *Propachynolophus hengyangensis*, *Cocomys lingchaensis*, *Matutinia nitidulus*, ?*Asiocoryphodon* sp., *Hunanictis inexpectatus*, plus additional unidentified insectivoran-grade mammals. The insectivoran-grade mammals in the upper fossil layer are represented by two small skulls (IVPP V5352, 5353), now identified as *Naranius hengdongensis*. In the "Lower Fossil Layer," they found one species, *Archaeolambda* sp., and suggested that the "Upper Fossil Layer" represented the early Eocene (no later than the Cuisian European Land Mammal Age, ELMA) and was probably equivalent to the Sparnacian ELMA, and the "Lower Fossil Layer" represented the earliest Eocene (perhaps correlative with the fauna from the Naran Bulak Formation of Mongolia) (Li et al., 1979).

A few years later, Zheng and Huang (1984) found an anterior part of a skull from the same area and named it *Hsiangolestes youngi*. Based on this discovery, Zheng and Huang (1984) suggested that both upper and lower fossil layers of the Lingcha Formation may be early Eocene in age and may be comparable to the Graybullian of the Wasatchian North American Land Mammal Age (NALMA). They also resumed the name "Limuping Formation," replacing the "Lingcha Formation" proposed by Li et al. (1979), because they think both names represent the same formation and the name "Limuping Formation" was used first. Li and Ting (1983) reused the name "Lingcha Formation" to represent early Eocene in the Hengyang Basin and created the name "Lingchan" to tentatively represent the early Eocene Chinese Provincial Age.

The intensive study and fossil collecting in the Hengyang Basin by C.K. Li, S. Ting, and S.H. Xie during the 1982–1986 field season greatly improved both the quality and quantity of collections (Li and Ting, 1983, 1985; Ting and Li, 1984, 1987; Ting, 1993, 1995; Ting et al., 2002, 2004). Many specimens of *Hsiangolestes* and *Naranius* collected during the 1987 field season by S. Ting, J.L. Li, and S.H. Xie made this study possible. In the early 21th century, a multidisciplinary project, including biostratigraphic, chemostratigraphic, and magnetostratigraphic studies, on the early Paleogene strata in the Hengyang Basin by S. Ting, P.L. Koch, W.C. Clyde, Y.Q. Wang, M.C. McKenna, Y. Wang, and S.H. Xie has led to a breakthrough in defining the age of the Hengyang Fauna and correlating the geochronologically constrained Paleocene-Eocene boundary record in the Hengyang Basin to the geological time scale (Bowen et al., 2002; Ting et al., 2003).

The type species of *Hsiangolestes*, *H. youngi*, was first described by Zheng and Huang (1984) based on the anterior part of a skull with right and left C-M3 (IVPP V7353) collected from the Lingcha Formation (Early Eocene Limuping Formation of Zheng and Huang, 1984) about 150 m south of Lingcha village (field number: 78006), Hengyang Basin, Hunan, China. This specimen has been the only reported material of the genus *Hsiangolestes* since then. Based on the dental formula and morphology (P3-4 slightly molarized, molars transversely elongated with very well-developed conules and styles), *H. youngi* was assigned to subfamily Wyolestinae under family Didymoconidae (Zheng and Huang, 1984). Ting and Li (1987) suggested that *Hsiangolestes youngi* differs from didymoconids in both dental and cranial morphology, but noticed that it is slightly similar to *Bogdia orientalis*, a pantolestid, from the middle Eocene Tsagan-Khutel, Mongolia (Dashzeveg and Russell, 1985).

In her dissertation, Ting (1995) described the cranial morphology of *Hsiangolestes youngi* and assigned it to the family Micropternodontidae, under suborder Soricomorpha, order Insectivora, based on its dental similarities to palaeoryc-

toids. McKenna and Bell (1997) grouped *Hsiangolestes* with *Wyolestes* and *Mongoloryctes* into Wyolestinae under order Cimolesta (see our redefined Cimolestidae within our own phylogenetic framework). In his overall review of Asian Paleogene insectivoran-grade mammals, Lopatin (2006) suggested that the Asian early Paleogene "insectivoran" mammals can be divided into two groups: true insectivorans, including orders Lipotyphla (Erinaceoumorpha and Soricomorpha), Didymoconida, and Leptictida, and insectivoran-like placental, including Cimolesta (Didelphodonta, Palaeoryctida, and Pantolesta). He assigned *Hsiangolestes*, with *Sinosinopa* and *Bogdia,* to subfamily Micropternodontinae under family Micropternodontidae, suborder Soricomorpha of order Lipotyphla, and grouped *Carnilestes*, *Prosarcodon*, *Sarcodon*, *Hyracolestes*, and *Metasarcodon* into subfamily Sarcodontinae (Lopatin and Kondrashov, 2004; Lopatin, 2006) under the same family Micropternodontidae.

The type species of *Naranius*, *N. infrequens*, was first described by Russell and Dashzeveg (1986). The holotype of *N. infrequens* is a fragmentary left mandible with p3–m1 and alveoli of p1-2 (PSS 20-73), collected from the Bumban Member of the Naran-Bulak Formation, Tsagan-Khushu, Nemegt Basin, Mongolia, where many isolated or fragmentary teeth were referred. Russell and Dashzeveg (1986) considered that the lower molars of *N. infrequens* are quite similar to those of the late Cretaceous *Procerberus formicarum*, except that *N. infrequens* is less than half the size of *P. formicarum*, and is also similar to *Batodon tenuis*, but less similar to Cretaceous species of *Cimolestes* and the Eocene *Bessoecetor diluculi*. They pointed out that *N. infrequens* lower molars are very similar to those of various species of Eocene *Centetodon*. They assigned *Naranius* to subfamily Didelphodontinae, family Palaeoryctidae, order Proteutheria. In her dissertation, Ting (1995) described a skull of *Naranius* cf. *infrequens* (now *Naranius hengdongensis*), and assigned it to the family ?Palaeoryctidae, under superfamily Palaeoryctoidea, Soricomorpha, Insectivora. McKenna and Bell (1997) reassigned *N. infrequens* to family Cimolestidae under Didelphodonta of the order Cimolesta. Lopatin (2005) reported some new materials of *Naranius infrequens* collected from the same locality in Mongolia, including a left maxilla with P4–M2, a right lower jaw with p4–m3, and many isolated teeth. He emphasized that the "most prominent characters distinguishing *Naranius* from the majority of genera of Cimolestidae are well-developed lingual cingula of M1-3 and the considerably reduced p2-3" (Lopatin, 2005: 322), and also pointed out the dental differences of *Naranius* from *Didelphodus*, *Procerberus*, *Alveugena*, *Gelastops*, etc., and assigned *Naranius* to family Cimolestidae within the order Cimolesta. Subsequently, Lopatin (2006) reconfirmed the family Cimolestidae classification under suborder Didelphodonta of order Cimolesta.

GEOLOGICAL SETTING

The Hengyang Basin is located in the south-central part of Hunan Province, China (27°05′ N, 112°57′ E) (fig. 1). It is roughly square, with an area of ~5200 km^2 (Liu and Fu, 1986), and bounded by the Heng Shan mountains to the north and by hills of late Paleozoic rocks to the south near Laiyang city (Young et al., 1938). The basement of the Hengyang basin is composed of Protozoic and early Paleozoic low-grade metamorphic rocks and late Paleozoic limestone (417 Geological Team, 1979). It is one of the rift basins of south China that formed from extension in the back arc of the Kula-Pacific subduction complex during the late Cretaceous and early Tertiary (Ren et al., 2002). Active subsidence associated with these extensional structures created considerable space for the clastic detritus that accumulated from the erotion of nearby uplands, which formed the widely distributed fossiliferous syntectonic late Cretaceous and early Paleogene deposits, "Red Beds," in the basin.

The early Paleogene red beds in the Hengyang Basin are mainly distributed in the eastern part of the basin, and have been subdivided into two for-

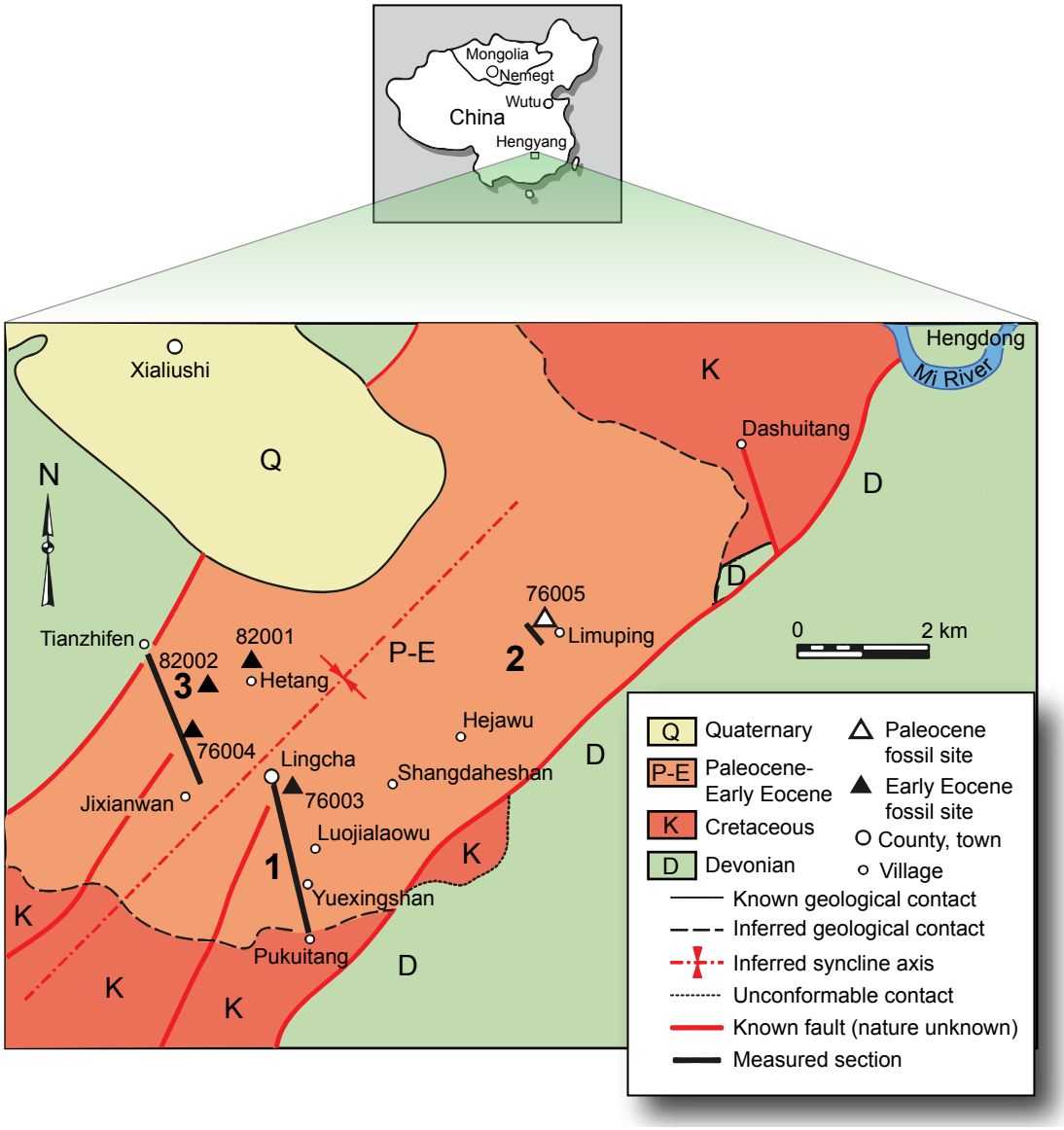

FIG. 1. Geological sketch map of fossil sites near Hengdong County, Hengyang Basin, Hunan Province, China. At top is a map of central Asia, showing the location of Hengyang Basin (modified from Ting et al., 2003).

mations from the oldest to the youngest: the Limuping Formation (Lower Lingcha Formation of Bowen et al., 2002, and Ting et al., 2003; Tong et al., 2006) and the Lingcha Formation (Upper Lingcha Formation of Bowen et al., 2002, and Ting et al., 2003; Tong et al., 2006). Both the Limuping and Lingcha formations are distributed in the north and south limbs of a NE-SW extended syncline that defines the Hengyang Basin. The Limuping Formation is ~530 m thick (Ting et al., 2011), brick red in color, and composed of mudstone intercalated with channel sandstone and laminated siltstone (fig. 2). The only known mammalian fossil, *Archaeolambda* sp., occurs near the

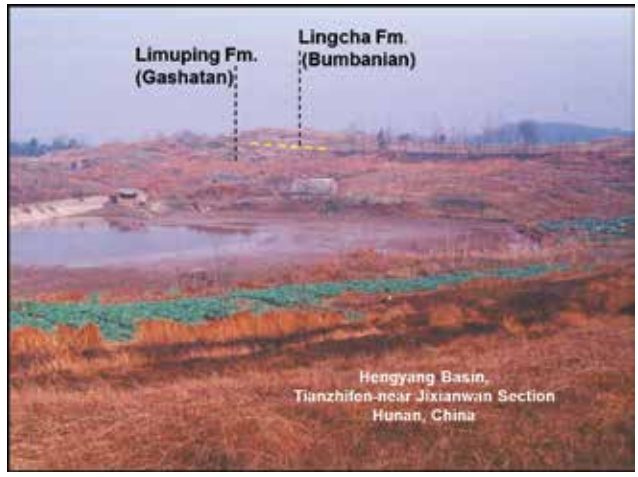

FIG. 2. Photo of the Tianzhifen-near Jixianwan Section, showing the strata of Limuping Formation (Late Paleocene, Gashatan ALMA) and Lingcha Formation (Early Eocene, Bumbanian ALMA).

middle part of section 2, and is Gashatan (Asian Land Mammal Age, ALMA) in age (fig 3). The overlying Lingcha Formation is very thin, only ~20 m thick, exposed at the top of the section (fig. 2). It is lithologically more heterogeneous, and composed of brick-red and gray mudstone intercalated with thin layers of sandstone or siltstone, and includes many discrete horizons with pedogenic carbonate nodules. The abundant calcareous nodules contain many early Eocene (Bumbanian ALMA) mammalian fossils, especially skulls. A multidisciplinary project studying the Hengyang early Tertiary strata has measured three sections (fig. 3) (Bowen et al., 2002; Ting et al., 2003). Section 1, from Pukuitang to Lingcha villages, is in the south limb of the syncline and about 550 m thick. Section 2, near Limuping village, is also in the south limb of the syncline and about 16 m thick. A simple trigonometric projection was used to make an approximate correlation between sections 1 and 2, because bedding orientations along the south limb of the fold are broadly consistent and local topography is precisely known. Section 3, from Tianzhifen village to near Jixianwan village, is on the north limb of the syncline and about 280 m thick. A combination of field observations and isotopic and paleomagnetic data was used to correlate the three sections into a single composite section (fig. 3A). The similar composition and lithostratigraphic associations of the Lingcha fauna from section 1 and 3 suggests that these horizons may be correlative (fig. 3B). The early Eocene fossils, including *Hsiangolestes youngi* and *Naranius hengdongensis,* were found on the top of Section 1 and 3.

AGE OF FAUNAS FROM HENGYANG BASIN

Paleomagnetic and isotopic results in the Hengyang Basin show two well-delineated magnetic polarity zones and a dramatic negative shift in paleosol carbonate δ^{13} C values (CIE) within the upper reversed-polarity zone. The Paleocene-Eocene boundary is placed at 516 m in the composite section, the first level producing unusually low δ^{13} C values (fig. 3). The uppermost reversed-polarity interval within the Hengyang composite section is correlated to Chron C24r, and the underlying normal polarity interval to Chron C25n (Cande and Kent, 1995; Bowen et al., 2002; Ting et al., 2003). The Lingcha fauna, where *Hsiangolestes* and *Naranius* were produced, occurs between ~15 m above the Paleocene-Eocene boundary and the carbon isotope minimum at 548 m. Therefore, Lingcha fauna correlates to the earliest

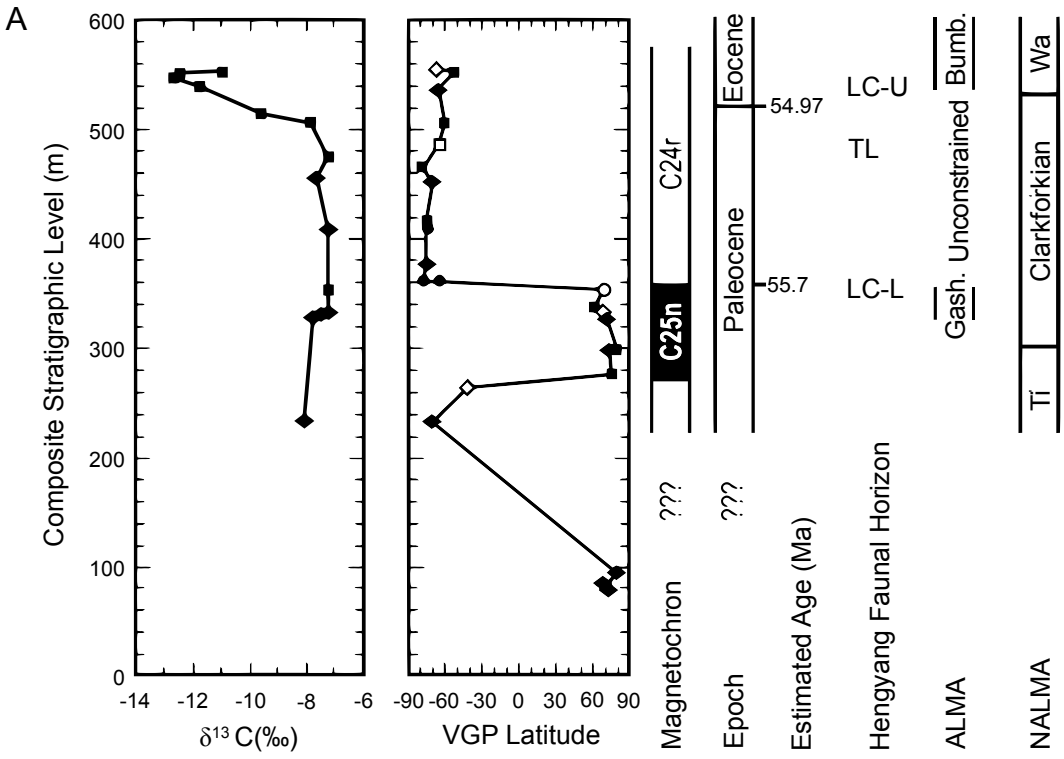

FIG. 3. Composite carbon isotope and magnetic stratigraphy of the Hengyang Basin Paleocene/Eocene boundary interval. **A.** (*above*) Composite stratigraphic data from local sections 1 (diamonds), 2 (circles) and 3 (squares) projected on the section 1 stratigraphic scale. The positions of Hengyang Basin (HB) faunal horizons are indicated by LC-L: lower Lingcha fauna from Limuping Formation, LC-U: upper Lingcha fauna from Lingcha Formation. Paleomagnetic data, presented as the latitude of the Virtual Geomagnetic Pole (VGP) corresponding to the average site direction for each sampling locality. Solid symbols represent data from alpha sites, and open circles represent beta sites. Magnetochron assignments are made with reference to marine Paleocene/Eocene boundary section (Kennett and Stott, 1991). **B. (***opposite page***)** The Paleocene/Eocene boundary is placed at the base of the carbon isotope excursion, and assigned an age of 54.97 Ma after Wing et al. (1999). Modified from Ting et al. (2003).

Wasatchian (North American Land Mammal Age, NALMA, Wa0 zone) on a scale of ~10^4 yr, and the Limuping fossils, found within meters of the Chron C25n/C24r reversal, can be correlated with the earliest subzone of the Clarkforkian NALMA (Bowen et al., 2002; Ting et al., 2003). The Lingcha fauna shares the occurrence of *Orientolophus*, *Homogalax*, and *Hapalodectes* with the Wutu fauna from the Wutu Formation, Wutu Basin, Shandong Province, China, and the fauna from the Bumban Member of the Naran Bulak Formation, Nemegt Basin, Mongolia, and represents the basal Bumbanian Asian Land Mammal Age. The Bumbanian Asian Land Mammal Age is marked by abrupt synchronous first appearances of several modern mammalian orders, represented by *Orientolophus* and *Homogalax* (Perissodactyla), *Teilhardina* and *Altanius* (Primates), *Wutuhyus* (Artiodactyla), and by the last occurrences of the extinct mammalian order, Acreodi, represented by *Dissacus zengi* and *D. bohaiensis*, a mammalian taxon commonly distributed in Paleocene deposits. The Bumbanian ALMA is also characterized by sharing several taxa with those of the early Wasatchian NALMA, includ-

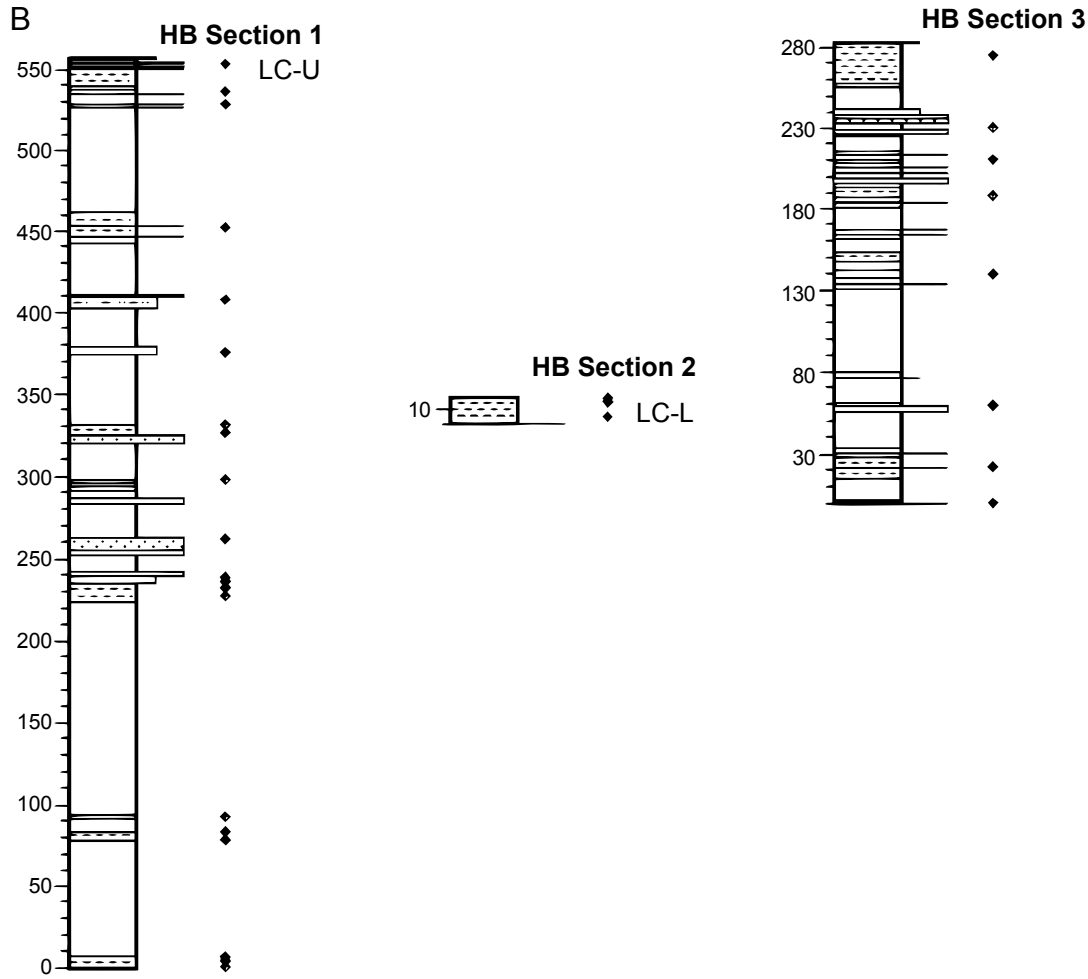

ing (at the family level) Omomyidae, Coryphodontidae, Hyaenodontidae, Viverravidae, Miacidae, Mesonychidae, and Hyopsodontidae, and (at the generic level) *Teilhardina*, *Coryphodon*, *Hyopsodus*, *Homogalax*, and *Heptodon*. It indicates that Bumbanian faunas are cosmopolitan. The transient carbon isotope excursion found in the Hengyang Basin precisely correlates the Asian Paleocene-Eocene boundary to the geological time scale, indicating that the Gashatan-Bumbanian faunal turnover is closely related to the PETM global climate change, and records a major wave of migration between Asia and other continents (Ting et al., 2003).

The following faunas are an updated lists of taxa from Hengyang Basin (classification based on McKenna and Bell, 1997).

Fauna from Lingcha Formation

Class Mammalia Linnaeus, 1758
Order Incertae sedis
Family Sarcodontidae (Sarcodontinae, Lopatin and Kondrashov, 2004), new family
Hsiangolestes Zheng and Huang, 1984
Hsiangolestes youngi Zheng and Huang, 1984

? Insectivoran-grade mammal, uncertain
Family Cimolestidae Marsh, 1889
Naranius Russell and Dashzeveg, 1986
Naranius hengdongensis, new species
Order Simplicidentata Weber, 1904
Family Eurymylidae Matthew, Granger, and Simpson, 1929
Matutinia Li, Chiu, Yan, and Hsieh, 1979
Matutinia nitidulus Li, Chiu, Yan, and Hsieh, 1979
Order Acreodi Matthew, 1909
Family Hapalodectidae (Szalay and Gould, 1966) Ting and Li, 1987
Hapalodectes Matthew, 1909
Hapalodectes hetangensis Ting and Li, 1987
Family Mesonychidae Cope, 1875
Dissacus Cope, 1881
Dissacus zengi Ting et al., 2004
Order Pantodonta Cope, 1873
Family Coryphodontidae Marsh, 1876
?*Asiocoryphodon* Xu, 1976
?*Asiocoryphodon* sp. Li et al., 1979
Order Primates Linnaeus, 1758
Family Omomyidae Trouessart, 1879
Teilhardina Simpson, 1940
Teilhardina asiatica Ni et al., 2004
Order Rodentia Bowdich, 1821
Family Chapattimyidae Hussain, de Bruijn, and Leinders, 1978
Cocomys (Li et al., 1979) Dawson et al., 1984
Cocomys lingchaensis (Li et al., 1979) Dawson et al., 1984
Tsagamys Russell and Dashzeveg, 1986
? cf. *Tsagamys subitus* Russell and Dashzeveg, 1986 (Ting, 1995)
Order Perissodactyla Owen, 1848
Family ?Isectolophidae Paterson, 1919
Orientolophus Ting, 1993
Orientolophus hengdongensis Ting, 1993 (*Erihippus tingae* Bai et al., 2018, Equidae Gray, 1821, suborder Hippomorpha Wood, 1937, for IVPP V5789.1 and V5790)
Family incertae sedis
Propachynolophus Li et al., 1979
Propachynolophus hengyangensis (*Propalaeotherium* of Young, 1944) Li et al., 1979 (*Protomoropus*? *hengyangensis* Bai et al., 2018, *Protomoropus* Hooker and Dashzeveg, 2004, Family incertae sedis, Infraorder Ancylopoda Cope, 1889, Suborder Tapiromorpha Haeckel, 1866, for IVPP V214 and V7453; *Danjiangia lambdodon* Bai et al., 2018, *Danjiangia* Wang, 1995, Brontotheriidae Marsh, 1873, Suborder Titanotheriomorpha Hooker, 1989, for IVPP V5349)
Superorder Leptictida McKenna, 1975
Family Didymoconidae Kretzoi, 1943
Hunanictis Li, Chiu, Yan, and Hsieh, 1979
Hunanictis inexpectatus Li et al., 1979
?Didymoconidae, uncertain

Fauna from Limuping Formation

Class Reptilia Laurenti, 1768
Order Crocodilia, Gmelin, 1788
Family Crocodylidae Gmelin, 1788
Planocrania Li, 1976
Planocrania hengdongensis, Li, 1976
Class Mammalia Linnaeus, 1758
Order Pantodonta Cope, 1873
Family Archaeolambdidae Flerov, 1952
Archaeolambda Flerov, 1952
Archaeolambda sp. Li et al., 1979

MATERIALS AND METHODS

Materials

The specimens described in this monograph were collected in the Hengyang Basin by teams from the Institute of Vertebrate Paleontology and Paleoanthropology, Chinese Academy of Sciences, in field seasons of 1976 (C.K. Li, Z.X. Qiu, D.F. Yan, and S.H. Xie), 1982–1986 (C.K. Li, S. Ting, and S.H. Xie), 1987 (S. Ting, J.L. Li,

and S.H. Xie), and in 2000 (an international collaborative team: S. Ting, P.L. Koch, W.C. Clyde, Y.Q, Wang, M.C. McKenna, Y. Wang, and S.H. Xie). The specimens were prepared by hand, using sewing needles: Hongyepai #10, produced by the Qingdao Needle Factory, and Dongfengpai #12, produced by the Dongfeng Needle Factory, China.

A few of *Hsiangolestes* specimen numbers in this paper may differ from the ones in Ting's (1995) dissertation, because some numbers in the dissertation overlapped with preoccupied IVPP catalog numbers; for example, V5791 in the dissertation has been changed to V5346. The dissertation included initial identifications on some of specimens that were not completely prepared. We marked the numbers found in the dissertation in parentheses when they differ those in this paper and we have deleted V7437, which was wrongly identified as *Hsiangolestes* in the dissertation. Bai et al. (2018) recently revised the perissodactyl material from the Hengyang fauna. It is beyond the scope of our research to study the classification of the perissodactyls. We list *Orientolophus hengdongensis* and *Propachynolophus hengyangensis* Bai et al. (2018) systematic position and provide revised information for each taxon.

We made measurements of the specimens using an iGaging OriginCal digital caliper and measurements of the teeth using a Wild Heerbrugg M7 Microscope (figs. 4, 5). The dental terminology basically follows Lopatin (2006) and is illustrated in figure 6.

Serial Sections

The serial section of specimen IVPP V7438 was made in the laboratory at the Museum of Comparative Zoology, Harvard University, in 1990, by the first author with the help of Zhexi Luo, using a Croft parallel grinder apparatus (Croft, 1950; Luo and Eastman, 1995). The specimen was first embedded in plaster and subjected to serial grinding to obtain a series of exposures. The structures exposed by serial grinding were first drawn with the aid of a microscope's camera lucida and then photographed. The internal structures of the skull were documented by a series of drawings and photographic slides of each serial section. We obtained 377 serial sections from IVPP V7438 at 100 μ intervals at the basicranial and ear regions and 200 μ intervals at the rest of the cranial region. Digital scans of the serial sections are available at MorphoSource.org (see Online Data Archives below).

Fossil Localities

The following fossil sites produced all of the specimens described herein:

IVPP V76003, 200 m south of Lingcha village, where *Propachynolophus hengyangensis* (*Propalaeotherium* of Young, 1944) was found
IVPP V76004, 1.5 km northwest of Lingcha village
IVPP V82001, north of Hetang village
IVPP V82002, 1 km southwest of Hetang village

Anatomical Abbreviations

ac	anterior crura of tympanic ring
alic	alisphenoid canal
as	alisphenoid
bn	body of navicular
bocc	basioccipital
bs	basisphenoid
C	upper canine
c	lower canine
cha	choenae
coc	cochlea
cond	condylar process
dl	dorsal lamina
dnm	dorsal nasal meatus
ec-1, 2, 3	ectoturbinal 1, 2, 3
en-I, II, III, IV	entoturbinal I, II, III, IV
er	epitympnic recess

etf ethmoid foramen
exocc exoccipital
ff foramen for facial nerve
fo fenestra ovalis (fenestra vestibuli)
for fenestra rodunda (fenestra cochleae)
fov foramen ovale
fr frontal
fs frontal sinus
ftt fossa for tensor tympani
glf glenoid fossa
hf hypoglossal foramen
hpm (ma) horizontal process of maxilla
hpp (pal) horizontal process of palatine
I1–3 upper incisors 1 through 3
i1–3 lower incisors 1 through 3
iam internal acoustic meatus
ica groove for internal carotid artery
itf inner table of frontal
iof infraorbital foramen
jaf jacobson's fossa
jf jugular foramen
jp jugular process of condyle
ju jugal
la lacrimal
laf lacrimal foramen
lfs lateral part of frontal sinus
ll lateral lamina
llen-II, III, IV lateral lamina of en-II, III, IV
M1–3 upper molars 1 through 3
m1–3 lower molars 1 through 3
ma maxilla
mc maxilloturbinate crest
mfs medial part of frontal sinus
mg magnum
mm medial malleolus of tibia
mnm middle nasal meatus
mp mastoid process
mph II–V middle phalange of digits II through V
ms maxillary sinus
mt mastoid tubercle
mt I–V metatarsals I through V
na nasal
na/fr nasal-frontal articulation
np nasal pharynx
occ occipital
opf optic foramen
os orbitosphenoid
P1–4 upper premolars 1 through 4
p1–4 lower premolars 1 through 4
pa parietal
pal palatine
pa/sq parietal-squamosal articulation
pal/ma palatine-maxilla articulation
pc posterior crura of tympanic ring
pcr palatine crest
pgf postglenoid foramen
pgp postglenoid process
pif piriform fenestra
plf posterior lacerate foramen
pm premaxilla
pma groove for promontory artery
pocp posterior opening of cribriform plate
poi posterior opening of infraorbital canal
ppe perpendicular process of ethmoid
pph I proximal phalange of hallux
pph II–IV proximal phalange of digits II through IV
ppn plantar process of navicular
ppp (pal) perpendicular process of palatine
pr promontorium
ps presphenoid
pt posttympanic process of squamosal
sa groove for stapedial artery
saf subarcurate fossa
sesa sesamoid bone
sf stapedius fossa
sfs septum of frontal sinus
slp sphenoethmoid lamina of palatine
soc supraoccipital
spf septal plate of frontal
sphorb sphenorbital fissure
sq squamosal
tlv transverse (ventral) lamina (transverse, dorsal convex arch)
tr tympanic ring
tph II–V terminal phalange of digits II through V
tt tentorium
vo vomer
zgp zygomatic process of maxilla

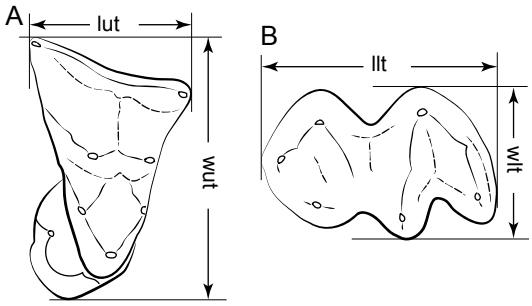

FIG. 4. Dental measurements: **A.** upper molar; **B.** lower molar. Abbreviations: **llt,** length of lower teeth; **lut,** length of upper teeth; **wlt,** width of lower teeth; **wut,** width of upper teeth.

Online Data Archivies

Digital data and image files related to this paper are all uploaded to online repositories. A nexus file containing character matrix is available at Dryad (https://doi.org/10.5061/dryad.69p8cz94s) as well as an online supplementary document (https://doi.org/10.5531/sd.sp.59).

Digitized thin section slides of a complete skull are available at MorphoSource.org (https://www.morphosource.org/dashboard/collections/000457564/edit?locale=en&).

SYSTEMATIC PALEONTOLOGY

Class Mammalia Linnaeus, 1758

Order Incertae sedis

Family Sarcodontidae Lopatin and Kondrashov, 2004, new family

Included Genera: *Hsiangolestes* Zheng and Huang, 1984; *Sinosinopa* Qi, 1987; *Sarcodon* Matthew and Granger, 1925; *Prosarcodon* McKenna et al., 1984; *Metasarcodon* Lopatin and Kondrashov, 2004.

Geographic Distribution and Ages: *Hsiangolestes* (Early Eocene Lingcha Formation, Hengyang Basin, Hunan Province, China); *Sinosinopa* (Middle Eocene Arshanto Formation, Erlian, Inner Mongolia, China); *Sarcodon* (Late Paleocene Gashato Formation, Nemegt Basin, Mongolia, and Early Eocene Bayan Ulan Formation, Erlian, Inner Mongolia, China); *Prosarcodon* (Late Paleocene Fangou Formation, Shimen, Lonan County, Shaanxi Province, China); *Metasarcodon* (Middle Eocene Khaychin Formation, southwestern Mongolia).

Diagnosis: Dental formula 3.1.4.3(2)/3.1.4.3(2), presence of two molars in *Prosarcodon* (char. 70), presence of diastema posterior to p2 (char. 56), M1 narrower than M2 in width (char. 73), metastylar lobe more labially situated (char. 74), paraconid crestiform (char. 112), trigonid wide open (but narrow in *Hsiangolestes*) (char. 114), coronoid process broad, roughly two molar lengths (char. 134), foramen ovale situated in alisphenoid (char. 224), and absence of basisphenoid tympanic process (char. 242).

Hsiangolestes Zheng and Huang, 1984

Type Species: *Hsiangolestes youngi*, Zheng and Huang, 1984.

Included Species: Type species only.

Distribution and Age: Early Eocene (Bumbanian Asian Land Mammal Age), Lingcha Formation, Hengyang Basin, Hunan Province, China.

Revised Diagnosis: The size of this "insectivoran" is similar to that of the Asian house shrew (*Suncus murinus*) (see figs. 7, 8 for size variation and tables 1, 2, 3 for measurements), dental formula being 3.1.4.3/3.1.4.3, I1 subequal to I2 in size (char. 6), presence of diastema posterior to P2 (char. 30), P3 paracone greatly enlarged (char. 32), anterior edge of P4 slightly shorter than the posterior (P4 less asymmetrical) (char. 48), p3 subequal to p2 in size (char. 57), p3 protoconid subequal to p4 in size (char. 58), paracrista weak (char. 85), protocristid transversely situated (char. 116), talonid basin shaped with multicusps (char. 118), internal carotid artery transpromontorial (char. 245), fenestra cochlear posteromedially situated to fenestra vestibuli (char. 264).

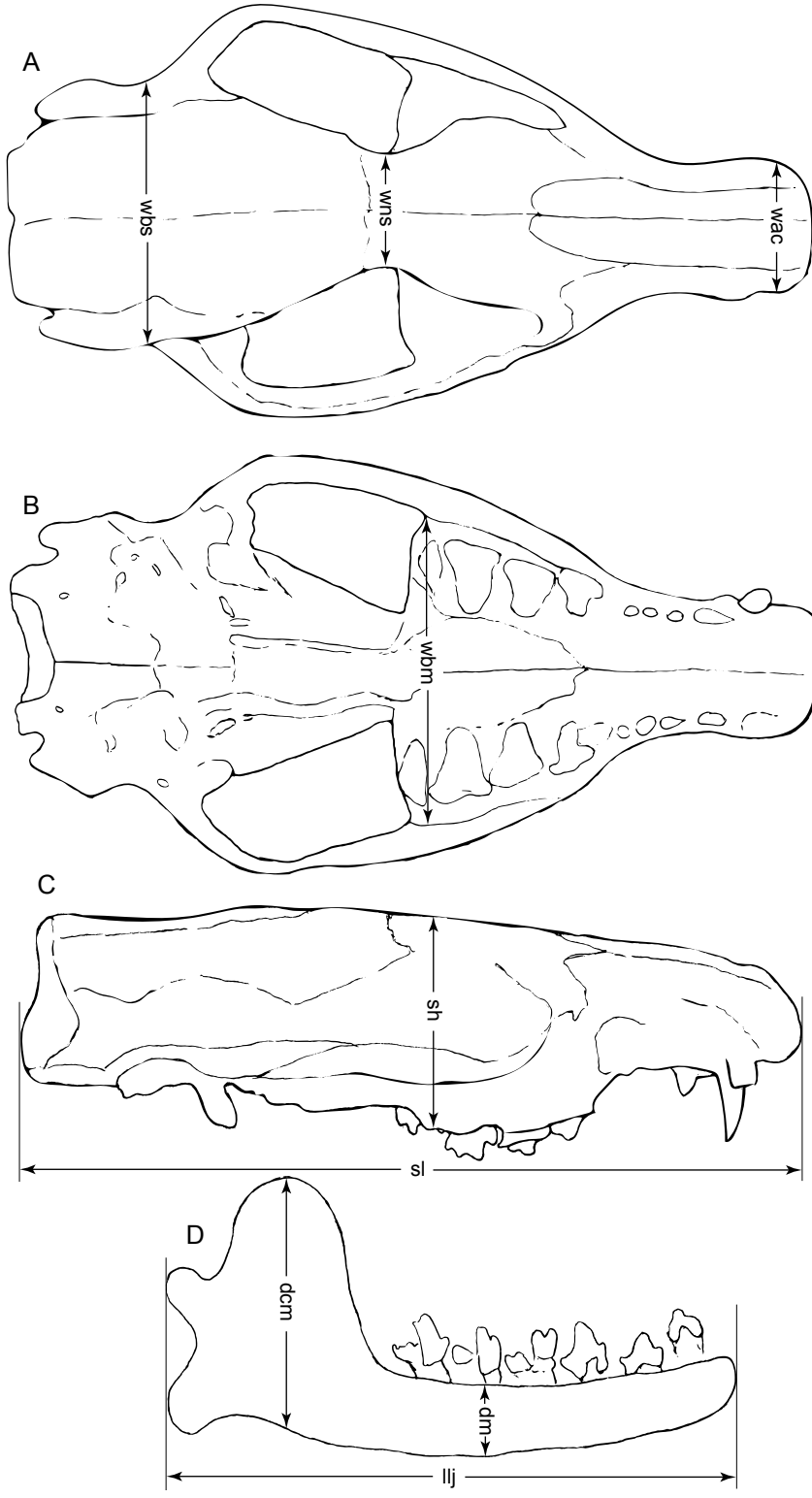
A
wbs
wns
wac
B
wbm
C
sh
sl
D
dcm
dm
llj

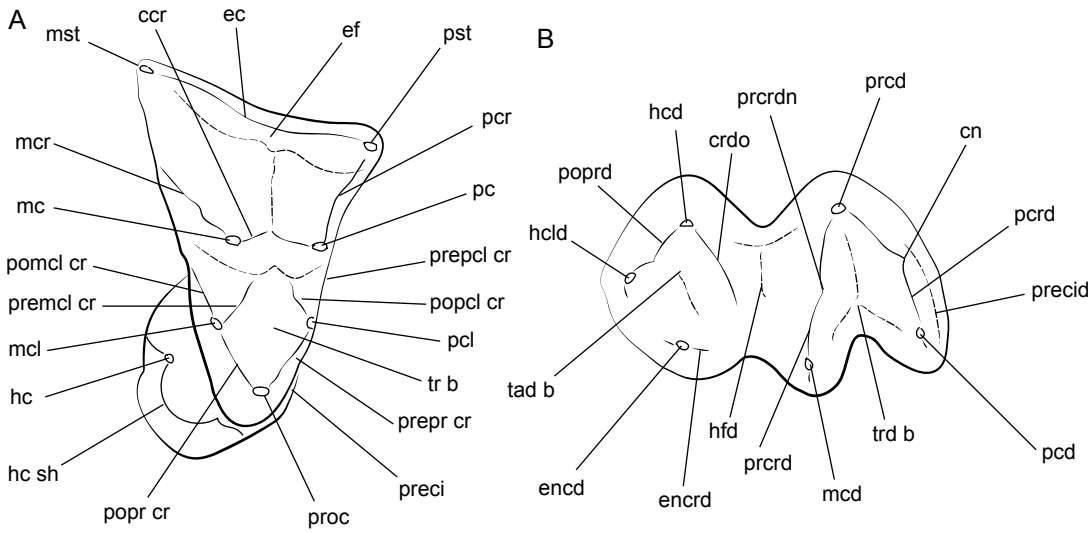

FIG. 6. Dental nomenclature: **A.** upper molar; **B.** lower molar. Abbreviations: **ccr,** centrocrista; **cn,** carnassial notch; **crdo,** cristid obliqua; **ec,** ectocingulum; **ef,** ectoflexus; **encd,** entoconid; **encrd,** entocristid; **hc,** hypocone; **hcd,** hypoconid; **hcld,** hypoconulid; **hfd,** hypoflexid; **hc sh,** hypoconal shelf; **mc,** metacone; **mcd,** metaconid; **mcl,** metaconule; **mcr,** metacrista; **mst,** metastyle; **pc,** paracone; **pcd,** paraconid; **pcl,** paraconule; **pcr,** paracrista; **pcrd,** paracristid; **pomcl cr,** postmetaconule crest; **popcl cr,** postparaconule crest; **popr cr,** postprotocrista; **poprd,** postcristid; **prcd,** protoconid; **preci,** precingulum; **precid,** precingulid; **prcrd,** protocristid; **premcl cr,** premetaconule crest; **prepcl cr,** preparaconule crest; **prepr cr,** preprotocrista; **prcrdn,** protocristid notch; **proc,** protocone; **pst,** parastyle; **tad b,** talonid basin; **trd b,** trigonid basin; **tr b,** trigon basin.

Similar to *Sinosinopa* in having seven postcanine teeth (char. 1), absence of P1 procumbent (char. 23), presence of diastema posterior to P2 (char. 30), P3 paracone greatly enlarged (char. 32), P4 smaller than M1 in size (char. 47), p4 talonid narrower than trigonid (char. 66), centrocrista V-shaped (char. 86), small hypocone on postcingulum (char. 101), moderate hypoconal shelf (char. 102), paracristid carnassial shaped (char. 113), protocristid transversely situated (char. 116), and talonid basin shaped with multicusps (char. 118). Differing from *Sinosinopa* in having P1 with two roots (char. 24), anterior edge of P4 slightly shorter than the posterior (P4 less asymmetrical) (char. 48), p4 talonid ridge shaped instead of heel (char. 67), trigonid anteroposteriorly compressed (char. 114), and presence of entocristid (char. 126).

Similar to *Sarcodon* in having M1–2 parastylar lobe anterolabial to paracone (char. 76), metacone and paracone base adjoined (char. 84), paraconid situated in lingual margin (char. 111), and talonid basin shaped and multicuspid (char. 118), and anteriormost mental foramen below p1 (char 132). Differing from *Sarcodon* in having p4 talonid with median longitudinal ridge instead of heel (char. 67), presence of a weak paracrista (char. 85), centrocrista V-shaped (char. 86), better developed hypocone on postcingulum (char. 101), hypocone shelf moderate instead of broad

FIG. 5. Measurements of skull and lower jaw: **A.** dorsal view; **B.** ventral view; **C.** lateral view; **D.** lower jaw, lateral view. Abbreviations: **dcm,** depth of ascending ramus of mandible (from coronoid process to lower edge of mandible); **dm,** depth of mandible (under m2); **llj,** length of lower jaw (posterior edge of angular process to anterior end of lower jaw); **sh,** skull height (between skull roof and M2); **sl,** skull length (between anterior edge of nasal and condyle); **wac,** width of skull anterior to canine; **wbm,** width of skull between maxilla ventral edge lateral to M3; **wbs,** width of skull between squamosal; **wns,** width of the narrowest part of skull.

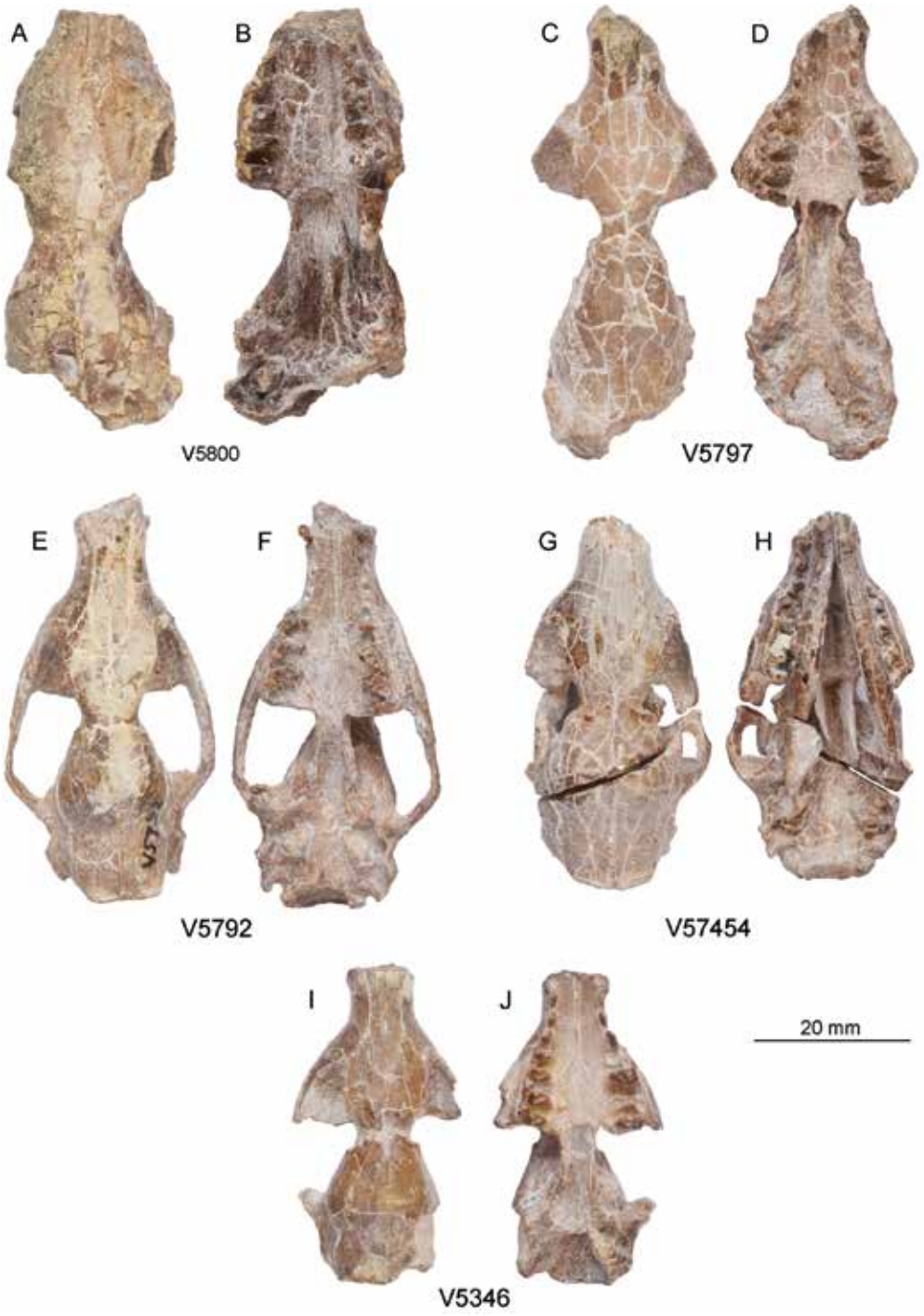

FIG. 7. *Hsiangolestes youngi* skulls in dorsal (A, C, E, G, I) and ventral views (B, D, F, H, J), showing size variation. IVPP V5800 (A, B), V5797 (C, D), V5792 (E, F), V7454 (G, H), V5346 (I, J).

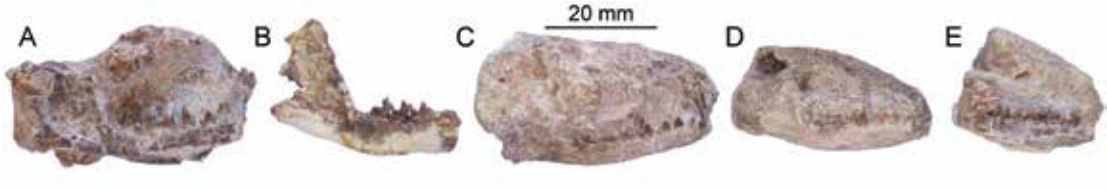

FIG. 8. *Hsiangolestes youngi* lower jaws in lateral view, showing size variation. **A.** IVPP V7435, **B.** V5793, **C.** V5794, **D.** V5795, **E.** V5801.

(char. 102), trigonid much narrower (char. 114), protocristid transversely situated instead of obliquely (char. 116), and cristid oblique attaching base of metaconid instead of to notch in protocristid (char. 119).

Similar to *Prosarcodon* in having I1 subequal to I2 in size (char. 6), presence of diastema posterior to P2 (char. 30), P3 paracone greatly enlarged (char. 32), p1 unicuspid (char. 51), p3 subequal to p2 in size (char. 57), presence of ectocingulum (char. 80), centrocrista V-shaped (char. 86), and talonid basin-shaped with multicusps (char. 118). Differing from *Prosarcodon* in having P1 with two roots instead of one (char. 24), P4 less asymmetrical (char. 48), p3 protoconid subequal to p4 instead of shorter (char. 58), absence of p4 metaconid (char. 65), p4 talonid narrower than trigonid instead of same width (char. 66), three molars instead of two (char. 70), hypocone on postcingulum distinct (char. 101), hypocone shelf wider (char. 102), and protocristid transversely situated instead of obliquely (char. 116).

Hsiangolestes youngi Zheng and Huang, 1984

Figures 7–43; tables 1–3

Type Specimen: IVPP V7353, anterior part of skull, with left and right upper canine roots and left and right P1-M3, collected by J.J. Zheng and X.S. Huang in 1978.

Referred Specimens: IVPP V5346 (V5791 of Ting, 1995), complete skull, with partial left P1, left P2–3, left M1 and M3, and right P1–M3; IVPP V5792, complete skull, with left and right canines, left P1, left P4–M3, and right P4–M2; IVPP V5793, anterior half of skull and partial right lower jaw, with fragmentary left and right C–M3 and right m1–3; IVPP V5794, anterior half of skull with associated mandibles, with left and right I1–3, left and right C, left P1–M3, right P1, right P4–M3, left i2–3, left c and incomplete right c, and left and right p1–m3; IVPP V5795, anterior half of skull with associated mandibles, with fragmentary left C, left P1, left P3–M1, left M3, right P1–M3, fragmentary right c, left p2–m3, and right p1–m3; IVPP V5796, a fragmentary anterior half of skull without well preserved teeth; IVPP V5797, nearly complete skull, with fragmentary left and right P1–M3, also with a rib, partial right pelvic girdle, partial left femur, partial right tibia, and nearly complete left and right pedes; IVPP V5798, anterior half of skull and associated partial left lower jaw, with fragmentary left and right M2, and vary fragmentary left m2–3; IVPP V5799 (V5800 of Ting, 1995), crushed anterior part of skull with associated mandibles, with fragmentary left I2–3, left C, left P3–M3, fragmentary right C, right P4–M3, left and right c, and right p2–3; IVPP V5800 (V5799 of Ting, 1995), nearly complete skull, with very fragmentary left P3–M3 and fragmentary right P3–M3; IVPP V5801, anterior half of skull with associated mandibles, with left P1–2, left P4–M3, right P1–M3, and left and right p1–m3; IVPP V5802, anterior half of skull with associated mandibles, with left P1–M3, right P2–M1, left p1–4, and right p3–m3; IVPP V7431, fragmentary partial skull with associated fragmentary mandibles, with right P1–4 and right p2–4; IVPP V7432, fragmentary partial skull with associated fragmentary mandible, with very fragmentary left

TABLE 1

Measurements (mm) of Skull and Dentary

	Skull						Dentary		
IVPP no.	sl	sh	wac	wbm	wbs	wns	dcm	dm	llj
Hsiangolestes youngi									
5346	38.5	13.0	8.0	17.0	17.0	7.0			
5792	50.3	15.2	8.3	19.1	16.3	6.8			
5793	32.2*	11.5	8.4	19.4			19.0	6.8	32.5*
5794	42.4*	10.9	6.9				13.7*	4.0	35.7
5795	34.4*	11.1	8.4	18.0			9.9*	4.2	32.7*
5796	31.9*		8.9						
5797	57.4	13.8	8.4	19.6	16.1	6.2			
5798	33.0*	16.8	8.5	16.6		8.1		7.2	21.4*
5800	51.5	17.8		18.7	19.1*	9.7			
5801	20.2*	13.7	7.8	18.7					
5802	32.6*	13.1	7.9*	15.5*					
7431	45.5*	13.9							
7432	39.4*								
7433	23.5*	5.4*	6.8						
7434	25.0*	10.6*							
7435	37.1*	12.2					18.1	5.5	35.6*
7436	27.2*	11.6*						8.0	29.8*
7454	43.0	14.0	8.3	15.5	18.0*	7.5	15.5	4.5	35.8
Naranius hengdongensis									
5352	18.8	5.9	3.3		7.2	3.6	5.9	2.3	11.2*
5353	16.9*	4.4			6.2	3.6	4.6*	2.2	12.0*
7439	21.5	4.7	3.6	6.7	8.3	3.2	6.3	2.2	15.4
7440	12.7*	4.7	3.0					1.5	9.3*
?Didymoconid									
7441	25.0*		8.1	10.3		7.3			
?Insectivora									
7442	22.2*			7.7		7.5			

*Measurement estimated or preserved.

TABLE 2

Measurements (mm) of Upper Dentition

	P1		P2		P3		P4		M1		M2		M3	
IVPP no.	lut	wut	lut	wut	lut	wut	lut	wut	lut	wut	lut	wut	lut	wut
Hsiangolestes youngi														
5346	1.8	0.7	2.0	0.8	1.5	1.0	2.5	2.5	2.7	3.7	3.0	4.5	1.9	3.5
5792	1.8	0.9					2.9	3.5	3.5	4.0	3.5	4.5	2.0	4.2
5793	1.5*	0.6*	2.0*	0.9*	2.5*	1.0*	3.4*	2.8*	3.0*	4.5*	3.7*	4.5*		
5794	1.5*	0.7*	2.0	0.8*	2.5*		3.0	3.5	3.5		3.4	4.5	1.9	3.9
5795	1.2		2.0		2.5		3.0	3.0	3.0	4.0	3.0		2.0	4.0
5797	1.9		2.3		2.5		3.1		3.0		3.2		2.5	
5799							2.5*		3.3*		3.4		2.5	
5800					3.1	1.5	3.0*	3.0*	3.5*	4.5*	3.3	5.0*	2.5*	4.4*
5801	1.3		2.0		2.2*		3.0		3.1		3.4		1.9*	
5802	1.2		2.0		2.3		3.3		3.4		3.3*		2.3*	
7431	1.3		2.0		2.1		3.0							
7434							3.0		3.1		3.2		2.5	
7435									3.0*	3.3*	3.0*	4.7*	2.0*	3.8*
7436							4.4		5.0		5.1		5.0	
7454	1.5		2.1		2.5		3.0		3.1		3.3		2.3	
Naranius hengdongensis														
5352			0.4		0.3		1.5		1.2		1.0		0.8	
5353							0.7*	0.4*	1.2*	1.5*	1.0	1.8	0.9	1.9
7439	0.6	0.3	0.5	0.2	0.3	0.2	1.0	1.2	1.1	1.7	1.0	1.9	0.8	1.9
7440			0.5		0.5		1.0	0.4*	1.2	0.9*	1.1	1.0*	0.8	0.9*
?Didymoconid														
7441			1.8*	1.0*	2.0*	1.2*	2.0*	1.6*	2.2*	3.0*				
?Insectivoran														
7442	0.7*	0.3*	1.1*	0.5*	1.1*	0.7*	1.4*	1.2*						

*Measurement estimated or preserved.

TABLE 3

Measurements (mm) of Lower Dentition

	p1		p2		p3		p4		m1		m2		m3	
IVPP no.	lut	wut	lut	wut	lut	wut	lut	wut	lut	wut	lut	wut	lut	wut
Hsiangolestes youngi														
5793									3.5	1.8	3.5	2.2	4.0	2.0
5794	1.0		2.0	1.2	2.5	1.3	2.7	1.3	3.5		3.4		3.5	
5795	1.0		2.3		2.5		2.7		3.5		3.4			
5798							3.0*	1.5*	3.0*	2.0*	2.8*	2.0*	3.5*	1.8*
5801	1.1		2.0		2.2		2.4		2.6		3.0			
5802	1.1		2.0		2.5		2.7		3.0		3.0		3.0	
7431			2.0		2.5		2.6							
7433	1.2		2.0		2.7		2.7		3.1		3.5			
7434	1.0		2.0		2.3		2.6		2.8		3.0		3.2	
7435			2.2	1.0	2.8	1.0	3.1	1.2	3.3	2.0	3.4	2.3	4.0	2.8
7436							4.2		5.0		4.9		6.4	
7454	1.4		2.2		2.5				2.9		2.9			
Naranius hengdongensis														
5352							1.0	0.4	1.1	0.7	1.2	0.8*	1.4	0.7
5353							1.0		1.1		1.1		1.4	
7439	0.5	0.2	0.4	0.1	0.3	0.1	0.9	0.4	1.2	0.6	1.3	1.0	1.5	1.0
7440			0.4		0.3		0.8		1.2		1.0*		1.7	

*Measurements estimated or preserved.

P4; IVPP V7433, fragmentary anterior part of skull with associated mandibles, with left p4–m2, right i2, and right p1–4; IVPP V7434, fragmentary anterior part of skull with associated mandibles, with left P4–M3, right P1–4, left p3–m3, and right p1–m3; IVPP V7435, crushed anterior part of skull with associated mandibles, with fragmentary right M1–3, a loose crown of lower canine, left p3–m3, and right p2–m3; IVPP V7436, left maxillary fragment with associated dentary, with left P4–M3 and p4–m3; IVPP V7454, complete skull with associated mandibles, with partial left C, left and right P1–M3, left and right p1–m3, atlas, axis, third and fourth cervical vertebrae; IVPP V7438, a skull that has been processed into serial sections (field numbers: 76004, 82001, 82002).

Distribution and Age: Same as for the genus.

Revised Diagnosis: Same as for the genus.

Dentition

Dental Formula: 3.1.4.3/3.1.4.3. There are no specimens with deciduous teeth in this study.

Incisors: There are three upper and lower incisors well preserved in IVPP V5794. They are about the same size and shape, and are crowded at the tip of the upper and lower jaws (fig. 9). An isolated, complete, unworn tooth stuck in the matrix above the right M1 in IVPP V5802 is most likely a loose incisor from this specimen. The incisors are leaflike, anteroposteriorly compressed, with three cusps at the tip of the cutting

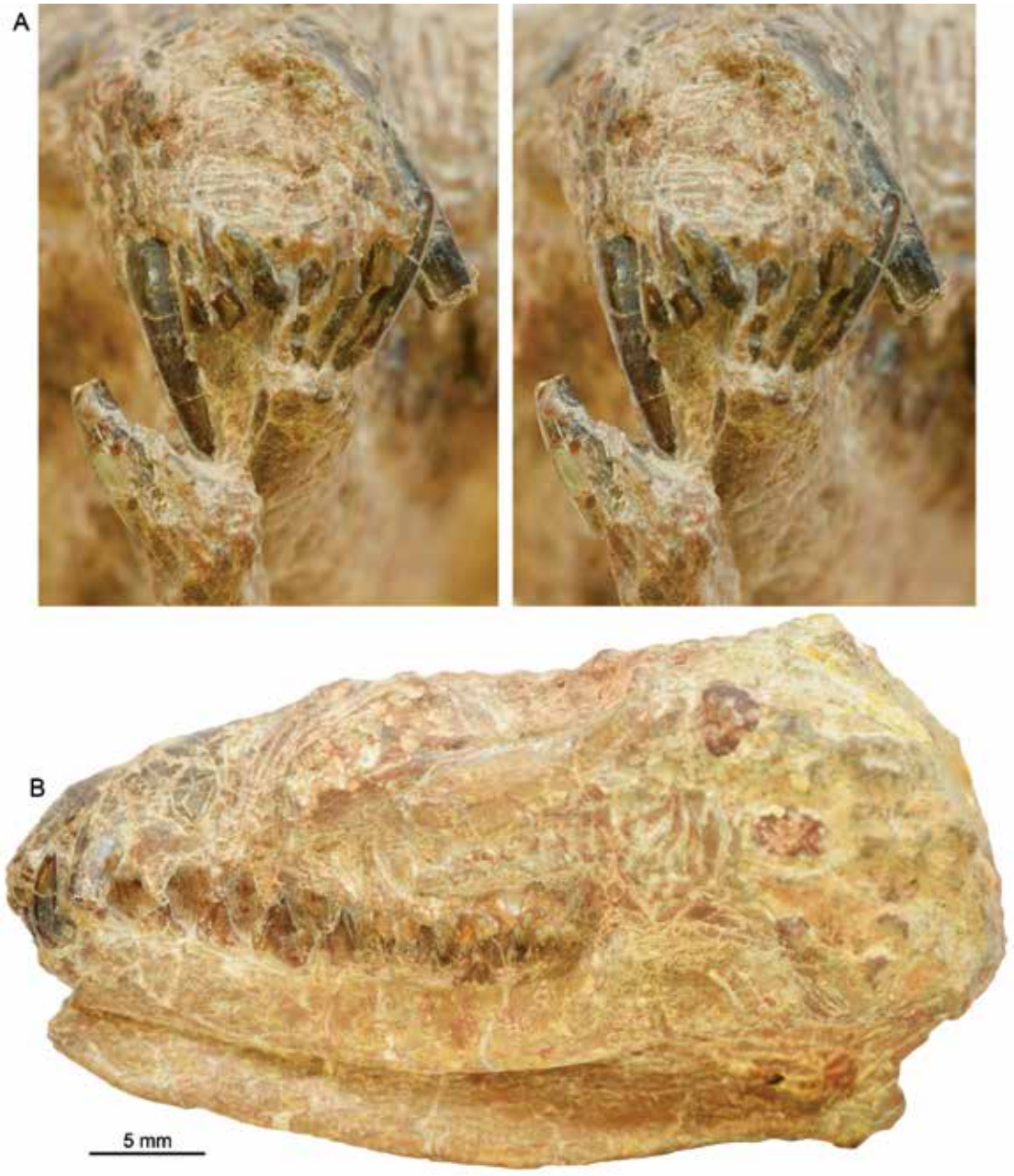

FIG. 9. Anterior part of skull of *Hsiangolestes youngi*, IVPP V5794: **A.** stereophotographs in front view; and **B.** photo in lateral view.


A
B
5 mm

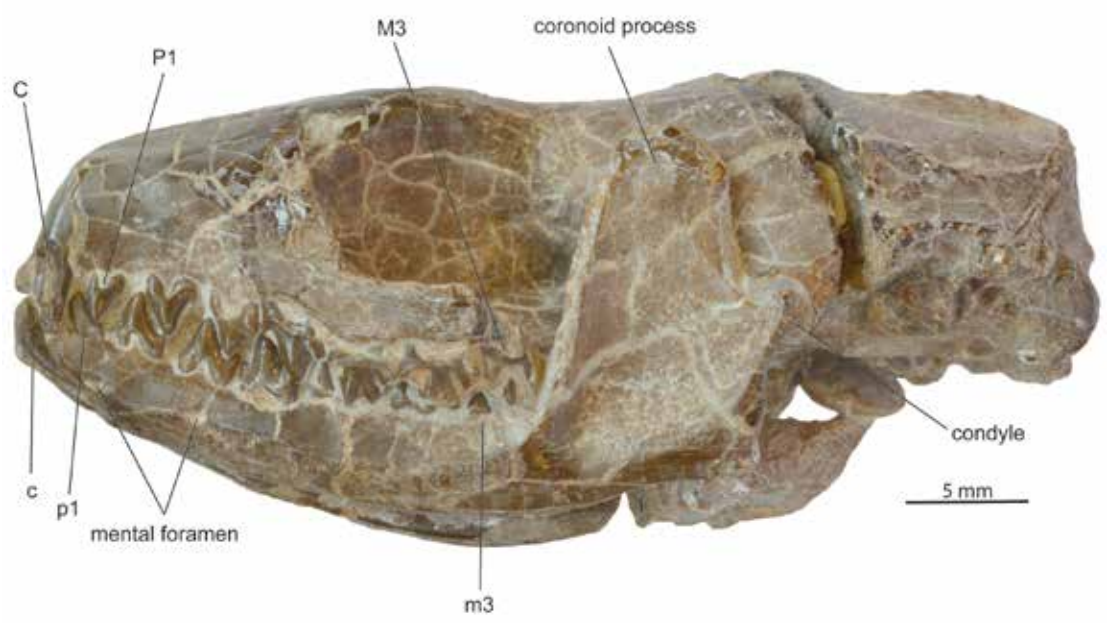

FIG. 11. Skull and lower jaw of *Hsiangolestes youngi*, IVPP V7454.

edge, and single rooted. The middle part of the tooth is convex on both labial and lingual sides, making the tooth in this part thicker than the rest of the tooth. The roots of both upper and lower incisors are large, long, strong, and compressed transversely.

Canines: The upper canines are well preserved in IVPP V5792, 5794, and partially preserved in IVPP V7454. The upper canine is situated just posterior to the premaxillary-maxillary suture (figs. 9, 10, 11). It is much larger and longer than both upper incisors and P1, projecting vertically with a sharp, piercing tip slightly pointing posteriorly. The upper canine has a large, single, transversely compressed root and is oval in cross section. The anterior surface of the upper canine is smooth; however, there are two gentle ridges on the medial and lateral surface respectively, and a sharp, thin ridge in the middle of the posterior surface extending from the tip to the base of the crown. A nearly complete lower canine is well preserved in IVPP V7435, but it is loose and out of original position due to the lateral compression of the mandible (fig. 8A). The lower canines are also partially preserved in IVPP V7434 and 7454. The lower canine is situated at the anterior tip of the mandible, close to the incisor (fig. 11). The morphology of the lower canine is almost identical to that of the upper, but slightly smaller and slenderer. It is much larger and longer than both lower incisors and the first lower premolar, and situated medial and anterior to the upper canine in occlusion.

Premolars: The P1 is a small, simple tooth (figs. 12, 13). It is unicuspid and double rooted. The posterior root is slightly greater in diameter than the anterior. The P1 is mediolaterally compressed and triangular in lateral view, with a single cusp. The main cusp is conical and piercing. The anterior surface of the tooth is broad with a ridge medially and tilts slightly anteriorly; the posterior surface is sharp edged with a keel. The labial surface of the main cusp is slightly convex, and the lingual surface is flat. There are no anterior and posterior accessory cusps.

FIG. 10. *Hsiangolestes youngi* skull, IVPP V5792: **A.** right lateral and **B.** left lateral views.

FIG. 12. *Hsiangolestes youngi* skull, IVPP V5792, ventral view.

FIG. 13. *Hsiangolestes youngi* skull, IVPP V5346, ventral view.

FIG. 14. Right maxilla of *Hsiangolestes youngi*, IVPP V5346, stereophotograph in occlusal view.

The P2 is slightly larger than P1, and is a double-rooted tooth (fig. 13). P2 has a main cusp and a small but distinct posterior accessory cusp, but has no an anterior accessory cusp. The posterior accessory cusp is well separated from the main cusp and located at the extremity of the posterior edge of the tooth. The development of the posterior accessory cusp varied among specimens. This cusp in IVPP V7454 is larger and stronger than that of IVPP V5346. The main cusp is larger and taller than that of P1. A crest at the anterior surface of the main cusp extends lingually from the tip of the tooth to about two-thirds of the tooth height. The posterior edge of the tooth is sharp and extends from the tip of the main cusp to the base of tooth. There are no clear cingula on the tooth.

The P3 is larger than the latter (figs. 13, 14). It is a double-rooted tooth and the posterior root is slightly larger than the anterior. The P3 is laterally compressed and triangular in lateral view with a large main cusp and a small posterior accessory cusp (figs. 13, 14). The main cusp is tall, conical, and has its apex above the midpoint of the anteroposterior axis of the tooth. A sharp ridge at the anterior surface of the main cusp extends from the tip of the cusp, turning lingually to terminate at the base of the crown. There is no indication of an anterior accessory cusp; however, the anterior edge of the tooth is projecting. The posterior edge of the main cusp is keellike and extends from its apex to end at the base of the tooth. In IVPP V5346, this edge turns slightly lingually to meet the cingulum at the base of tooth, but in IVPP V7454, the edge turns posteriorly toward the midpoint of the tooth row to form a deep notch between the main cusp and the posterior accessory cusp. The posterior acces-

FIG. 15. Anterior part of skull and lower jaw of *Hsiangolestes youngi*, IVPP V7433, in **A.** occlusal, **B.** left lateral, and **C.** right lateral views.

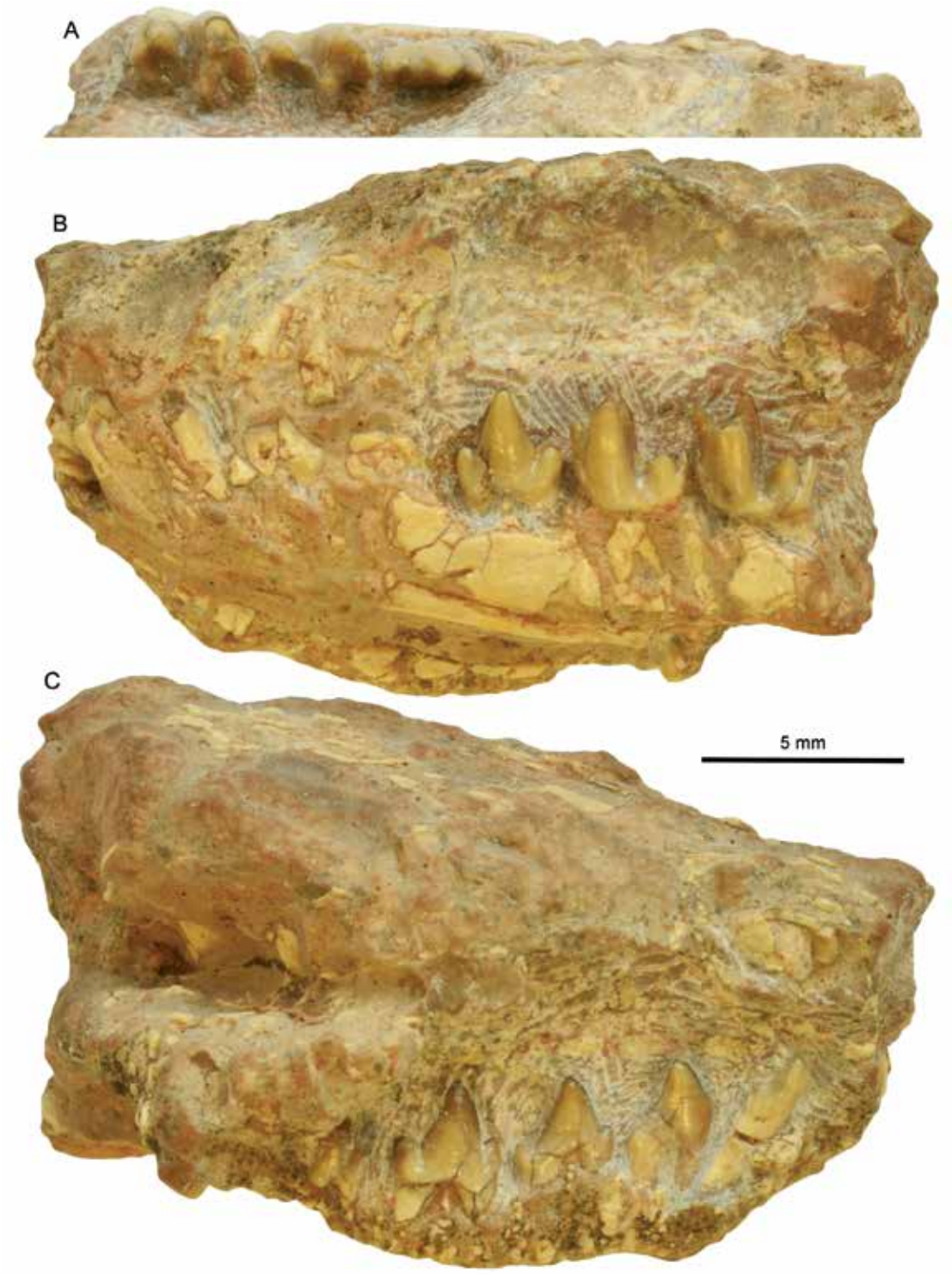
A
B
C
5 mm

sory cusp is well separated from the main cusp by a deep notch. A distinct lingual cingulum begins at the midpoint of the anteroposterior axis of the tooth and ends at the base of the posterior accessory cusp. The labial cingulum begins posterior to the midpoint of the anteroposterior axis of the tooth and meets the lingual cingulum at the posterior accessory cusp. In IVPP V5346, anterior to the posterior accessory cusp is a slightly concave surface closed by the labial cingulum, but in IVPP V7454, anterior to the posterior accessory cusp are two surfaces, one closed by the lingual cingulum and the other closed by the labial cingulum.

The P4 is closely posterior to P3, and is the largest and the only upper premolar with three roots (figs. 12–14). The lingual root is the largest, and two labial ones are smaller and about equal in size. The P4 is triangular in occlusal view, and has a distinctive protocone, paracone, and hypocone, but no metacone. The paracone is the most prominent and the tallest cusp. It is large and conical. The apex of the paracone is at the midpoint of the labial edge of the tooth. The paracrista is a sharp ridge and extends from a little above the apex of the paracone anteriorly to the anterior base of the crown. It is well separated from the parastyle cusp by a broad low-lying area. The parastyle is distinct, conical, and connected with the preparaconule crest lingually. There is no sign of a precingulum, but a weak ectocingulum runs from the parastyle to the metastyle. A sharp ridge at the posterior surface of the paracone extends steeply from a little above the apex of the paracone posteriorly to end at the base of the tooth. It is separated from the metastyle cusp by a narrow notch. The metastyle is strong, ridgelike, and labial-lingually compressed. The protocone is smaller and shorter than the paracone, but it is robust and conical. The preprotocrista is very weak, which shows better in IVPP V5792, but not in IVPP V5346. The paraconule is located at about the midpoint of the anterior transverse surface of the tooth. It is a strong and very distinctive cusp, and is slightly anteroposteriorly compressed in IVPP V5346, but weak in IVPP V5792. A well-developed preparaconule crest runs between the paraconule and parastyle. A short, distinct crest, the postprotocrista, is situated labially to the protocone, and separated from a tiny cusp by a narrow notch. This cusp is located on the lingual side at the base of the paracone. It may be considered the metaconule. It is small and anteroposteriorly compressed. The postprotocrista and the metaconule can be seen clearly in IVPP V5436; however, in IVPP V5792, the surface between the paracone and protocone is heavily worn and only a vestigial postprotocrista can be seen. There is no indication of an entocingulum; however, the postcingulum is well developed and runs from the posterior surface at a little above the apex of the protocone, to end at almost two-thirds of the way to the posterior edge of the tooth. A distinct, but small, hypocone is located at the lingual part of the posterior cingulum. The hypocone is slightly anteroposteriorly compressed.

The p1 is a small, simple, unicuspid, and double-rooted tooth (fig. 11). The posterior root is larger than the anterior one. The p1 is labiolingually compressed and its labial side is convex, and the lingual side is relatively flat (figs. 15C, 16A). Both crown and root are inclined anteriorly. The main cusp is conical with a sharp anterior ridge extending from the tip of the main cusp running anteroventrally and then turning posteriorly, so that the anterior surface of the tooth curves anteriorly. The posterior ridge is sharp, curves at the middle, and is projected posteriorly near the base of the crown. The posterior projection is large, not separated from the ridge, and heellike.

The p2 is larger than p1 (fig. 11). It is a double-rooted tooth and the anterior and posterior roots are narrowly, but well separated. The posterior root is slightly larger than the anterior. The crown is labiolingually compressed with the labial surface convex (figs. 15C, 16, 17B). The main cusp is tall, conical, and its apex lies over the posterior edge of the anterior root. The anterior surface has a sharp ridge extending from the tip of the main cusp to meet the anterior acces-

sory cusp at about two-thirds the depth of the crown. The anterior accessory cusp is distinct and well separated from the main cusp by a notch. The size of this cusp varies in different individuals. The posterior surface is sharply ridged. The ridge extends from the tip of the main cusp to meet the posterior accessory cusp near the base of the crown. The posterior accessory cusp is distinct, large, and conical, and its size varies in different individuals. The posterior accessory cusp is separated from the ridge by a wide notch.

The p3 is slightly larger than p2 (figs. 11, 15C, 16, 17B). It is double rooted, labiolingually compressed, and has three well-developed cusps. The main cusp is conical, and considerably taller than the others. It is labiolingually compressed with both labial and lingual side slightly convex. The anterior surface of the crown is ridged. A sharp ridge extends anteriorly from the tip of the main cusp to near the base of the crown. The appearance of the anterior accessory cusp varies in different individuals. In IVPP V7435, there is a large and distinctive cusp, the anterior accessory cusp, well separated from the anterior edge and located at the anterolingual corner of the tooth near the base of the crown; however, in V7454, there is no indication of an anterior accessory cusp, instead, there is a projection in the area. The posterior edge is sharp and extends from the tip of the main cusp to near the base of the crown. The posterior accessory cusp is enlarged as an unbasined talonid with a low central ridge, well separated from the posterior ridge by a wide gentle groove. Both the labial and lingual side of the posterior accessory cusp is slightly convex. The size of the posterior accessory cusp varies in different individuals. This cusp in IVPP V7454 is larger, higher, and stronger than that in IVPP V7435, and like an unbasined talonid.

The p4 is slightly larger than the p3 (figs. 11, 15C, 16, 17B, 18B). It is a double-rooted tooth. The two roots are basically equal in size. The main cusp is tall, conical, and labiolingually compressed with both the labial and lingual surfaces convex. Its anterior surface is sharply ridged with a ridge extending from the tip of the main cusp to terminate near the base of the crown, where it meets the anterior accessory cusp. The anterior accessory cusp is large, distinct, and separated from the anterior ridge by a deep notch. Both the labial and lingual surfaces of the anterior accessory cusp are convex. The posterior edge of the main cusp is sharp and extends steeply to terminate near the base of the crown to meet the talonid. The talonid has a ridge at the middle and it is separated from the posterior ridge by a deep notch, so the talonid is not really basined; however, there is a flat surface extending obliquely from the middle ridge to form a wide area at the base of the talonid. The area where these two surfaces meet forms a cingulumlike projective edge; however, there is no real cingulum.

Molars: All three upper molars are transverse and three rooted, the lingual root the largest and most robust (figs. 12, 13, 14, 19A). The labial roots are parallel to one another and about equal in size. The M2 is the largest among the upper molars, and the M3 is reduced in size. All upper molars have high piercing cusps. The protocone is much shorter than the paracone, but slightly shorter than the metacone. Both the anterior and posterior faces of the protocone are steep. The preprotocrista and postprotocrista are well developed, but the former is shorter than the latter. The paracone and metacone are well separated and approximately parallel to the labial edge of the crown. The paracone is the tallest among the three cusps in all upper molars. The metacone is slightly reduced in size in M3. The lingual surface of the paracone and metacone are convex and project lingually, and the labial surface of the paracone and metacone are flat. The paracrista is moderately developed as a thin ridge with a steep anterior face. The ridge terminates anterolabially near the base of the paracone, and is separated from the parastyle by a shallow groove. The parastylar shelf is small in M1, but increasingly developed from M1 to M3, and becomes a very prominent stylar shelf lobe in M3. The parastyle cusp is vestigial or absent.

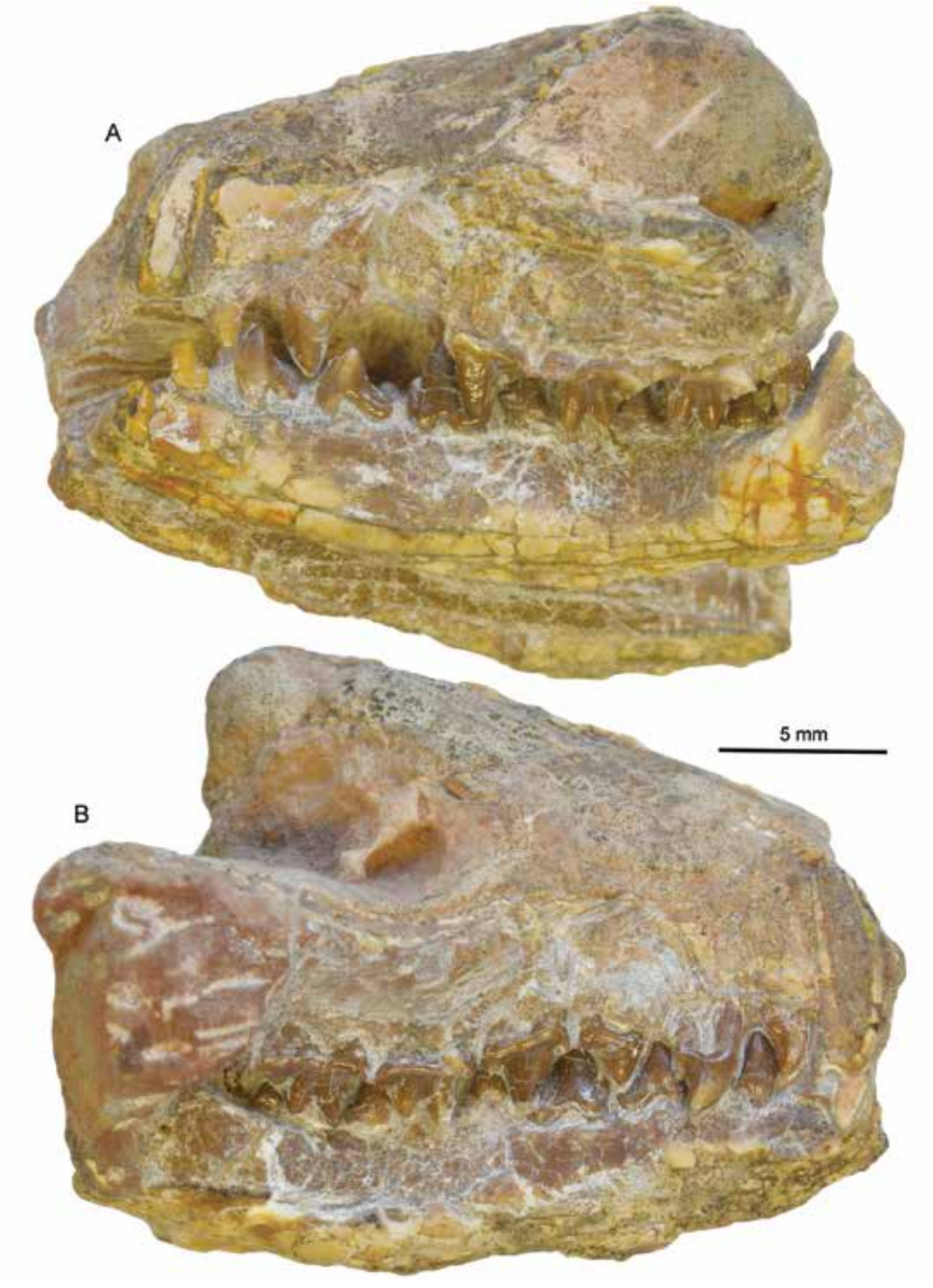

FIG. 16. Anterior part of skull of *Hsiangolestes youngi*, IVPP V5081: **A.** right lateral and **B.** left lateral views.

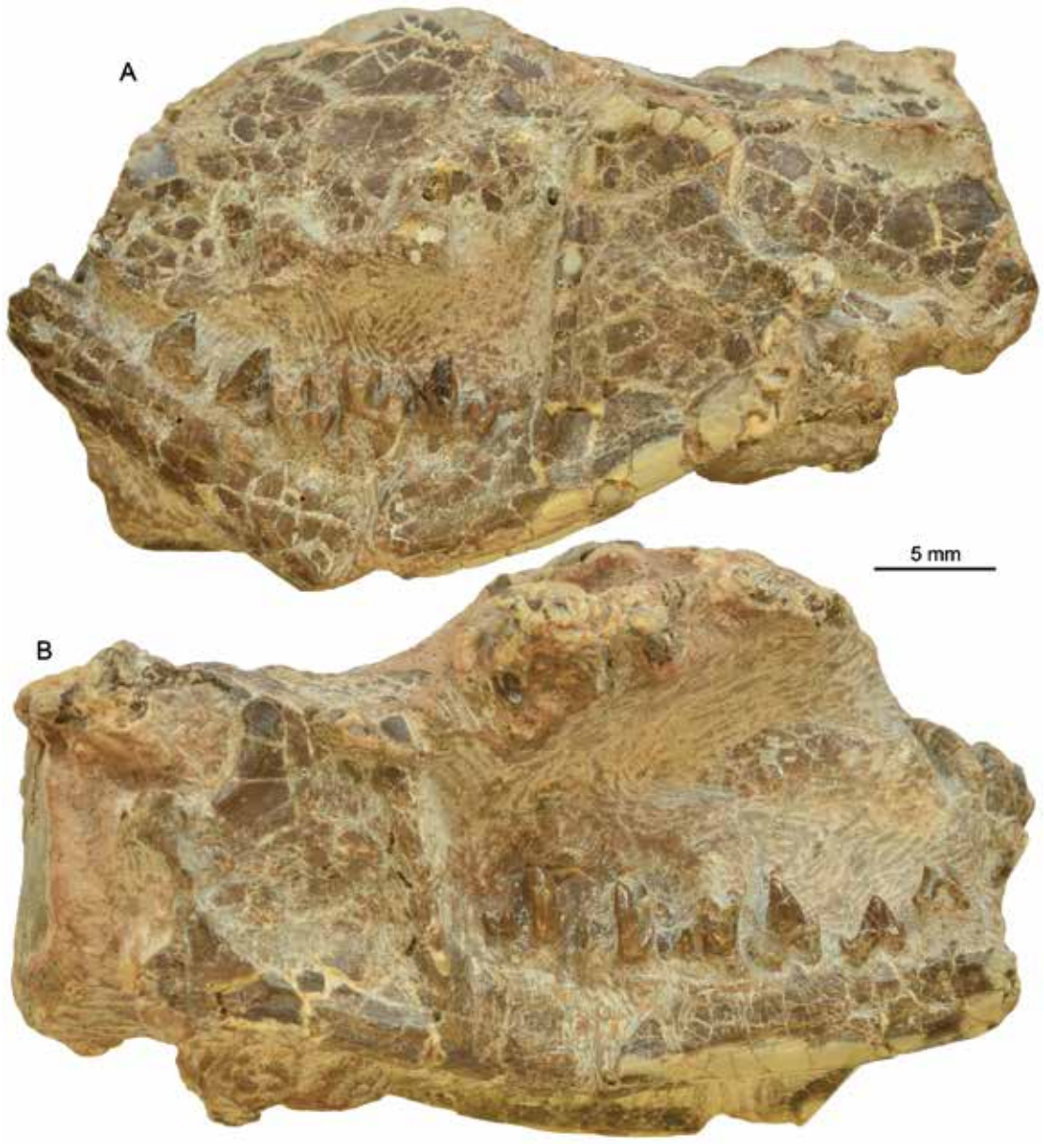

FIG. 17. *Hsiangolestes youngi* lower jaw, IVPP V7435: **A.** left lateral and **B.** right lateral views.

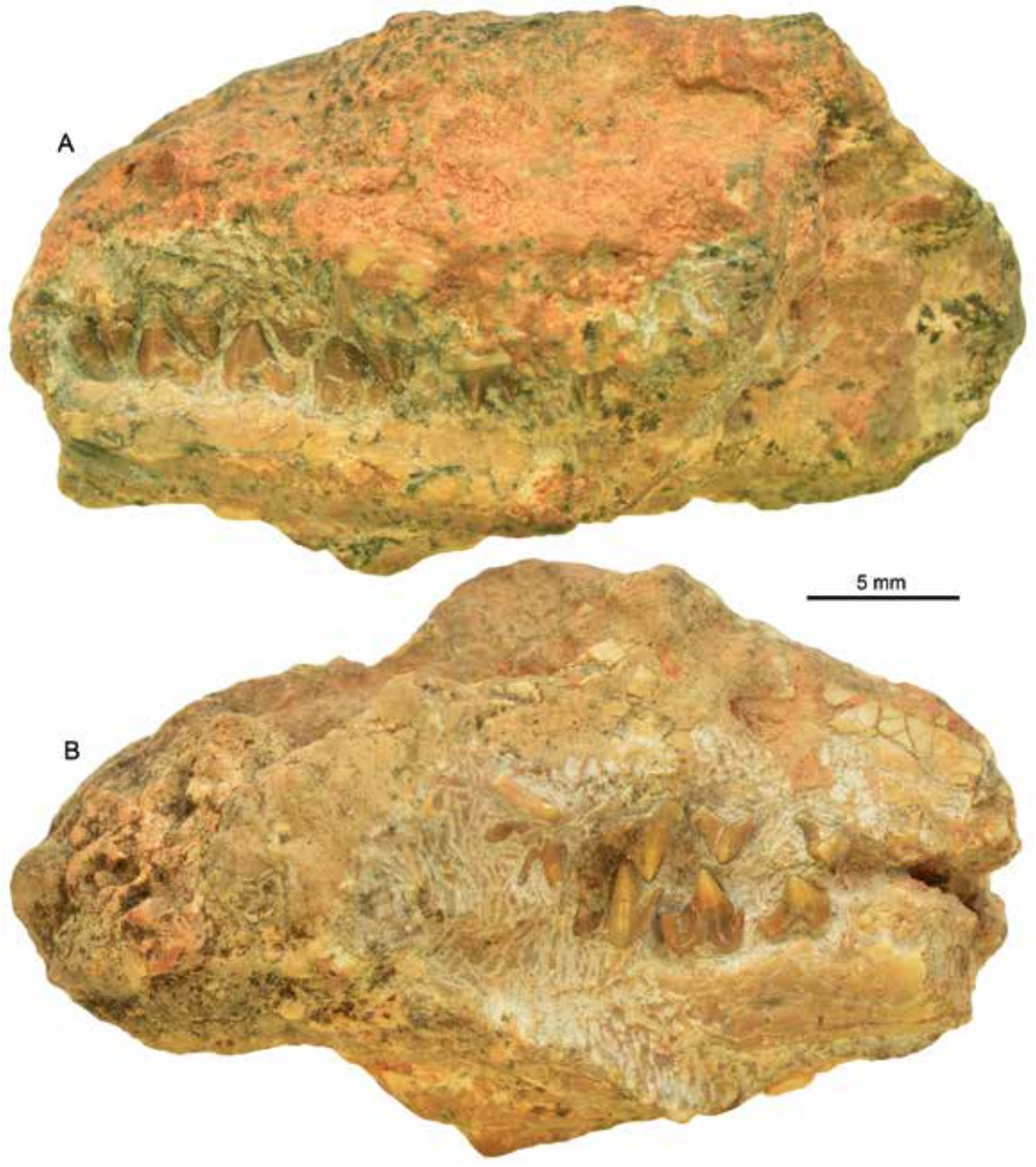

FIG. 18. Anterior part of skull of *Hsiangolestes youngi*, IVPP V5802: **A.** left lateral and **B.** right lateral views.

FIG. 19. *Hsiangolestes youngi* skull, IVPP V5797: **A.** ventral and **B.** right lateral views.

The metacrista is a well-developed sharp ridge in M1 and is reduced in M2–3. The ridge starts from the apex of the metacone and runs steeply posterolabially, but is interrupted by a notch near the base of the metacone, and then continues to meet the metastyle at the posterolabial corner of the stylar shelf. A well-developed cusp is at the middle of the metacrista ridge. The metastylar shelf is well developed in M1–2, but lacking in M3. Both the paraconule and metaconule are well developed in all three molars, but they decrease in size from M1 to M3. The conules are located in the midline of the tooth in M1–2, but slightly lingually in M3. The paraconule is usually larger and stronger than the metaconule. The preparaconule crest is a well-developed sharp, thin ridge. There is a small cusp on the ridge in M2. The preparaconule crest starts from the apex of the paraconule, runs anterolabially, and connects to the parastyle at the anterolabial corner of the stylar shelf. The ridge is separated from the paracrista by a wide, shallow depression. The posterior surface of the paraconule and the anterior surface of the metaconule are broad and smooth, without a distinct postparaconule crest and premetaconule crest respectively, but have a deep depression between the postparaconule crest and the premetaconule crest. The postmetaconule crest is a well-developed sharp, thin ridge. It starts from the apex of the metaconule, runs posterolabially, and terminates at the base of the crown near the posterior surface of the metacone. There is a small cusp on the postmetaconule crest, which is especially clear in M2. The hypocone is well developed in M1–2, but reduced to a tiny cusp in M3. The hypoconal shelf is large and projects posterolingually in M1–2, but is very reduced in M3. It runs labially from near the lingual side of the protocone to the midline of the tooth. There is a small cusp on the ridge of the hypoconal shelf, which is clearer in M2 than in M1. The precingulum is distinct in M1–2. It runs from the base of the crown near the anterior surface of the protocone to the midline of the crown. The ectocingulum runs along the labial base of the crown. There are no posterior cingula or lingual cingula. The ectoflexus is flat without a distinct curve and extends along the labial edge of the crown.

The lower molars slightly increase in size from m1 to m2, and the m3 is the longest among the lower molars (figs. 11, 15A, B, 16). The trigonid is well developed and triangular. It is much taller than the talonid and widely open lingually. The protoconid, paraconid, and metaconid are well developed. The protoconid is the tallest cusp of the tooth. It is conical with a sharp apex. The labial surface of the protoconid is narrow and convex and the posterior surface is flat. Its lingual surface is flat or slightly concave in different individuals. The paraconid is shorter than the protoconid and slightly shorter and more labially situated than the metaconid. It is notably compressed anteroposteriorly and bladelike. The anterior surface of the paraconid is flat or slightly convex in different individuals. The posterior surface of the paraconid is slightly convex. The lingual surface is narrow and slightly convex. The apex of the paraconid is continuously connected with the paracristid. The paracristid is divided into two crests by a deep carnassial notch, connecting with the paraconid lingually and with the protoconid labially. These two crests compose a widely open V-shape with the apex of V at the middle of the crest. The metaconid is slightly shorter than the protoconid, but taller than the paraconid and conical at the apex. Both the anterior and posterior surfaces of the metaconid are flat. Its lingual surface is wide and convex. The protocristid begins slightly under the apex of the metaconid and is separated by a notch at the middle of the crest, forming a relatively narrow V-shape to connect the protoconid. A ridge is situated at the middle of the posterior wall of the metaconid and separated from the cristid obliqua by a notch. The cristid obliqua is very short and starts at the labial side of the posterior wall of the metaconid. The talonid is not compressed anteroposteriorly, but the talonids of m1–2 are shorter than those of m3. The hypoflexid is relatively deep. The hypoconid, hypoconulid, and entoconid are well developed. The hypoconid is

the largest among the talonid cusps and conical with a pointed apex. The lingual surface of the hypoconid is slightly concave, but the labial surface is convex. The hypoconulid is situated at the end of the talonid close to the hypoconid. It is slightly shorter and smaller than the hypoconid in m1–2, but about same size as the hypoconid in m3. The anterior surface of the hypoconulid is slightly concave, but the posterior is convex. The entoconid is distinct, situated at the posterior part of the entocristid. It is smaller than both hypoconid and hypoconulid. The labial surface of the entoconid is slightly concave, but the lingual is convex. A tiny, distinct cusp is situated at the end of the entocristid near the lingual side of the posterior wall of the metaconid. The talonid basin is narrow, oblique, and open lingually. The precingulid is short and robust, running from the middle of the base of the anterior wall of the paraconid to the middle of the base of the anterior wall of the protoconid. There are no lingual, labial, or posterior cingulids.

Dentary

The dentary is long and slender and has a gently convex ventral border (figs. 11, 17). The depth of the dentary under p1–4 is about the same, and it is slightly deeper under m1–3. There are two distinctive, large, circular mental foramina. The anterior one is located under the posterior edge of p1, and the posterior one is under and between p3–4. An additional small mental foramen occurs in the left side of IVPP V7434. The mandibular condyle is transversely wide and elongated mediolaterally. The lateral side of the articular surface of the condyle is flat and the medial side is cylindrical and slightly convex dorsoventrally. The condyle fits the glenoid fossa well. The masseteric fossa is quite deep, and is bordered by a strong coronoid crest anteriorly and the condyle crest posteriorly. The angular process is well developed, slender, and thin. It extends posteriorly at the level of the condylar process. The coronoid process is strongly developed, very high and wide anteroposteriorly. It extends about 90° to the tooth row.

Skull

Zheng and Huang (1984) generally described the holotype of *Hsiangolestes youngi* (IVPP V7353), an anterior part of the skull with nasal, premaxilla, maxilla, frontal, parietal, palate, and partial zygomatic arch. We describe and reconstruct the cranial morphology based on several complete skulls (IVPP V5346, 5792, 5797, 7454), some partial skulls, and a serial section of a skull (IVPP V7438). The size of the skulls of *Hsiangolestes youngi* varies, ranging from 38 mm (V5346) to 57 mm (V5797) in length from the anterior edge of the premaxilla to the occipital condyle (figs. 7, 8). The skull is long with tapering snout, somewhat like *Leptictis*, but the nasofacial region is not as elongate as in the latter. In dorsal view, the narrowest part of the skull is at a point between orbital and temporal fossa. The zygomatic arch is slender and moderately expanded laterally. The braincase is slightly expanded at the point just posterior to the frontal-parietal suture and is increasingly inflated, to reach its greatest width and height above the zygomatic process of the squamosal. The braincase wall is convex in the glenoid fossa region and becomes concave from this point to the posterior end of the skull after this inflation (figs. 20, 21, 22B, 23). In lateral view, the skull is slightly convex, highest at the braincase area (figs. 19B, 22B, 23). In ventral view, the snout is narrowed between P2–3. The length from the tip of the snout to the end of the palate at the level of the M3 occupies slightly less than a half of the entire skull length. The basicranium region (from the anterior edge of the piriform fenestra to the posterior edge of the mastoid process) is short (figs. 12, 13, 19A).

Premaxilla: The premaxilla is poorly preserved in most of the specimens. A partial right premaxilla is preserved in IVPP V5792 (figs. 10, 20). The anteriormost and palatine parts of the premaxilla are missing in all specimens. The pre-

FIG. 20. *Hsiangolestes youngi* skull, IVPP V5792, dorsal view.

FIG. 21. *Hsiangolestes youngi* skull, IVPP V5346, dorsal view.

FIG. 22. *Hsiangolestes youngi* skull, IVPP V5797: **A.** dorsal and **B.** left lateral views.

maxilla is a small, roughly triangular bone. In dorsal view, the premaxilla-nasal suture is short and straight. The posterodorsal process of the premaxilla ends at a point above the level of P1 and about one-third the length of the nasals (fig. 20). In lateral view, the premaxillary-maxillary suture runs from a point above the anterior edge of the canine to the level above P1. In palatal view, the premaxilla curves posteriorly between the I3 and the canine (fig. 12). The incisive foramen is large and oval. Its anterior extremity is just behind the incisor, and the posterior edge is approximately at the level of the middle of the canine.

Nasal: Nasal bones are well preserved in V5346, 5792, 7454. Except for slight damage, V5346 preserved most of the anterior end of the nasal. In dorsal view, the nasal bone occupies about one-third the skull length and extends posteriorly to the level above the M1 (figs. 20, 21, 22A). The nasals are relatively short compared to *Leptictis* (Novacek, 1986: fig. 6) and *Zalambdalestes* (Wible et al., 2004: fig. 18), in which the nasals occupy almost half the skull length. The nasals of *Hsiangolestes* are narrow, elongate, and slender in dorsal view. It is basically similar in width, but slightly wider at its anterior end and decreasing in width after its junction with the maxillary-frontal suture. It is most likely that the anteriormost edges of the nasals do not extend beyond the anterior edge of the premaxilla. The nasals have a broad contact with the maxilla and frontal at the point above the P3 (figs. 24A, C). The nasal-maxilla suture is straight, and the nasal-frontal suture is straight near the junction of the nasal-maxilla and nasal-frontal suture and bends medioposteriorly to meet the opposite nasal-frontal suture at the level above M1. The posterior outline of the nasal is U-shaped in dorsal view, which is similar to those of *Leptictis* and different from those of *Zalambdalestes*. The nasal is widely separated from the lacrimal by the frontal and has no contact with the lacrimal. The dorsal surface of the nasal bone is flat, and the lateral surface bends ventrally and articulates with the premaxilla anteriorly and with the maxilla and frontal posteriorly.

FIG. 23. *Hsiangolestes youngi* skull, IVPP V5346, left lateral view

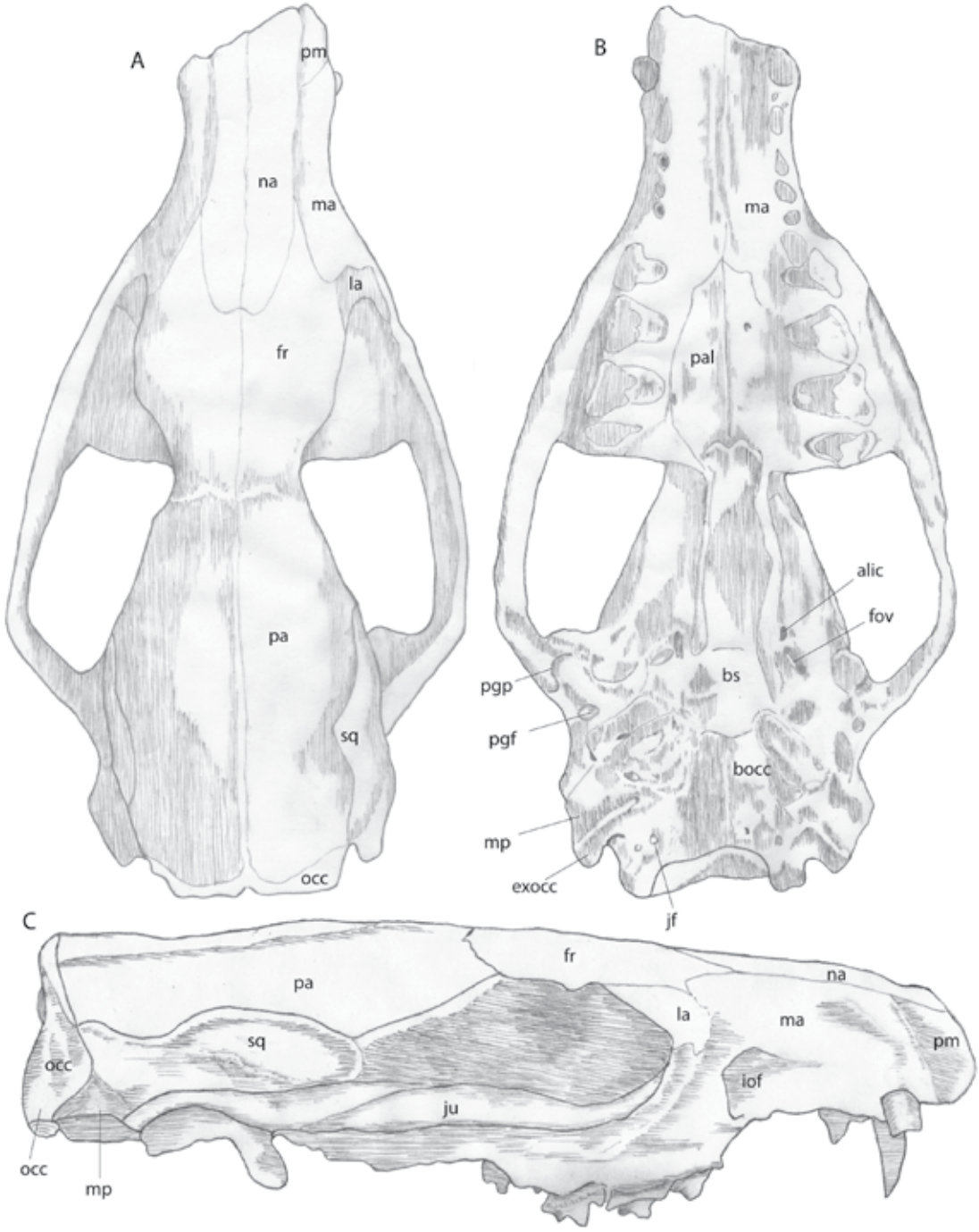

FIG. 24. Drawing of *Hsiangolestes youngi* skull: **A.** dorsal, **B.** ventral, and **C.** lateral views (based on IVPP V5792 with reference of others).

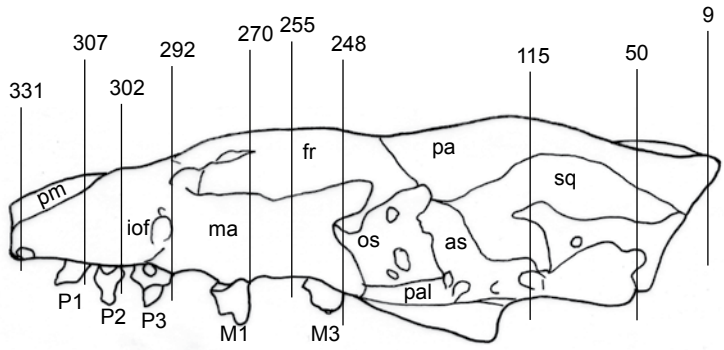

FIG. 25. *Hsiangolestes youngi*, IVPP V7438, serial section location.

Nasal Cavity: We describe the nasal cavity based on the serial sections of a complete skull IVPP V7438. The nasal cavity and its related structures are well preserved between section 233, which is cut at the level of the cribriform plate, and the section 355, where it is near the posterior edge of the incisive foramen (fig. 25).

The nasal cavity extends longitudinally, and is relatively narrow and trapezoidal, anterior to P2, but it is larger posteriorly and rectangular in cross section posterior to P4 (figs. 25, 26). The roof of the nasal cavity anterior to P3 is mainly composed of the nasal bones (figs. 11, 21, 26: sections 307–331). The premaxilla contributes a small portion to the upper part of the anterior-most lateral wall of the nasal cavity anterior to P1 (figs. 21, 26: section 331). The maxilla occupies most of the lateral wall of the nasal cavity at the level anterior to P3 (figs. 11, 20, 21, 26: sections 300–331). At the level of P2–3, the frontal bone (fig. 26: section 300) contributes a small portion to the upper part of the lateral wall of the nasal cavity. The frontal then enlarges posteriorly, and it articulates with the nasal medially and with the maxilla laterally. At the level of P4, the lacrimal (fig. 26: section 289) contributes a small portion to the upper part of the lateral wall of the nasal cavity, but this lacrimal contribution increases posteriorly until it comprises almost half of the middle part of the lateral wall above P4 and M1, where it articulates dorsally with the frontal and ventrally with the perpendicular lamina of the palatine (fig. 27: section 278). Posterior to M2, the roof of the nasal cavity is mainly composed of the frontal (fig. 27: sections 260–267). At the level of the middle of M1, the perpendicular lamina of the palatine bone contributes a small portion to the lower part of the lateral wall (fig. 27: section 278). This portion enlarges posteriorly to form the lower half of the lateral wall, where it articulates with the frontal above (fig. 27: sections 260, 267). The posterior part of the lateral wall after M2 is mainly composed of the orbital part of the frontal (figs. 25, 28: sections 238–260). At the level of M3, the orbitosphenoid contributes a small portion to the upper portion of the lateral wall underneath the frontal sinus (fig. 28: section 236). The floor of the nasal cavity anterior to P4 is composed of the palatine process of the maxilla, separating the respiratory from the digestive passageway. The dorsal surface of the palatine process of the maxilla forms part of the floor of the ventral nasal meatus, and its ventral surface forms part of the roof of the oral cavity. The palatine process of the maxilla articulates with the vomer medially (fig. 26: sections 289–323). The horizontal lamina of the palatine contributes a small portion to the middle part of the floor at the level of the middle of P4 (fig. 26: section 289), and this portion enlarges lateroposteriorly to the level of M3. The posterior part of the floor of the nasal cavity is formed by the horizontal lamina of the palatine, and the medial part of the horizontal lamina is raised to form the palatine crest (fig. 28: section 248). The anterior part of this crest articulates with the

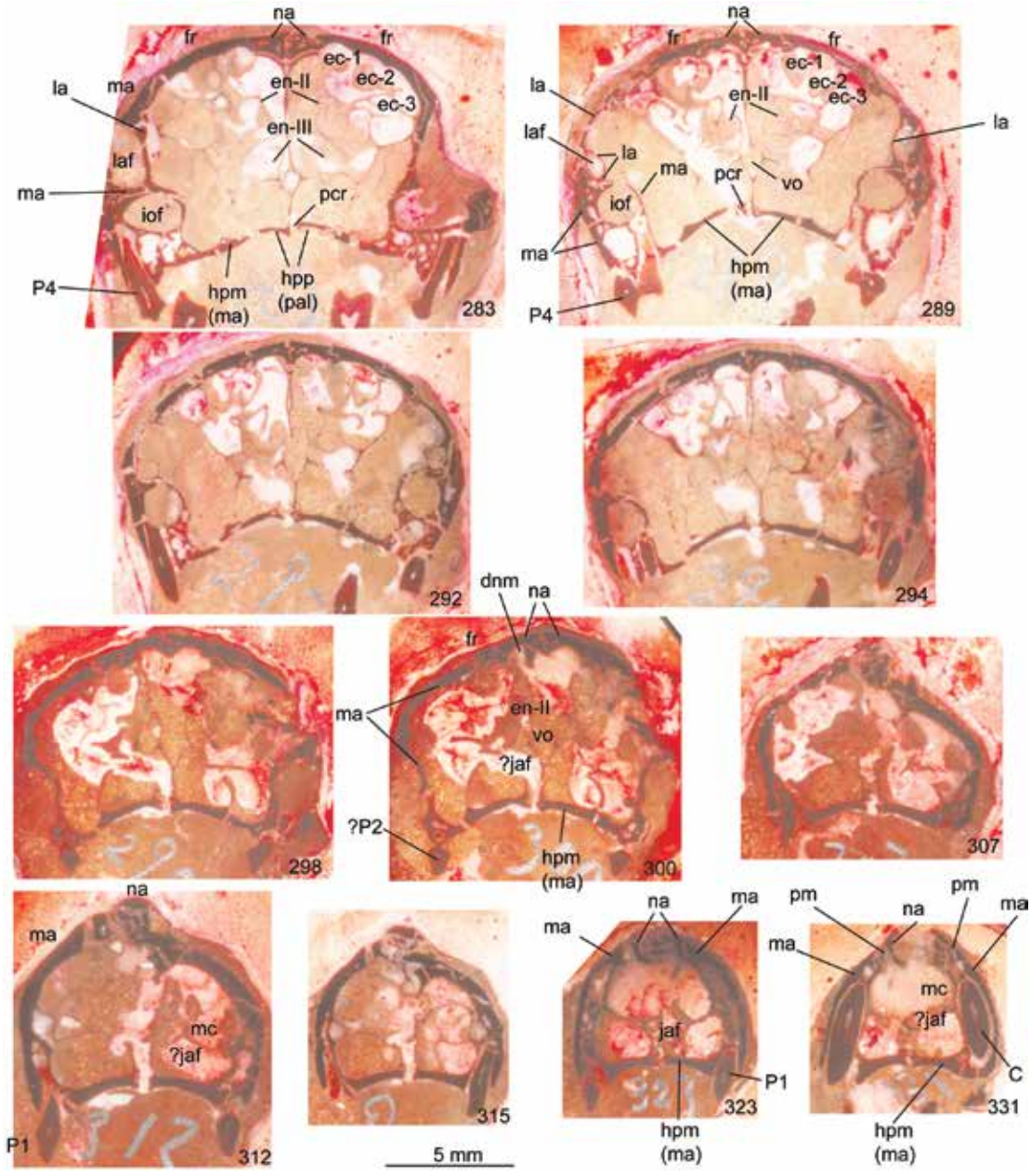

FIG. 26. *Hsiangolestes youngi*, IVPP V7438, serial sections 283–331 (from back forward).

vomer (fig. 26: sections 283, 289). The choanae are aligned with the posterior border of the horizontal lamina of the palatine, and are shown well in section 246 and specimens IVPP V5346, 5792, and 7454 (figs. 12, 13). The nasal cavity is divided into right and left halves (nasal fossa) by the nasal septum, which is composed of a bony part posteriorly and a cartilaginous portion anteriorly. Each nasal fossa is largely occupied by the maxilloturbinate anteriorly and the lateral masses

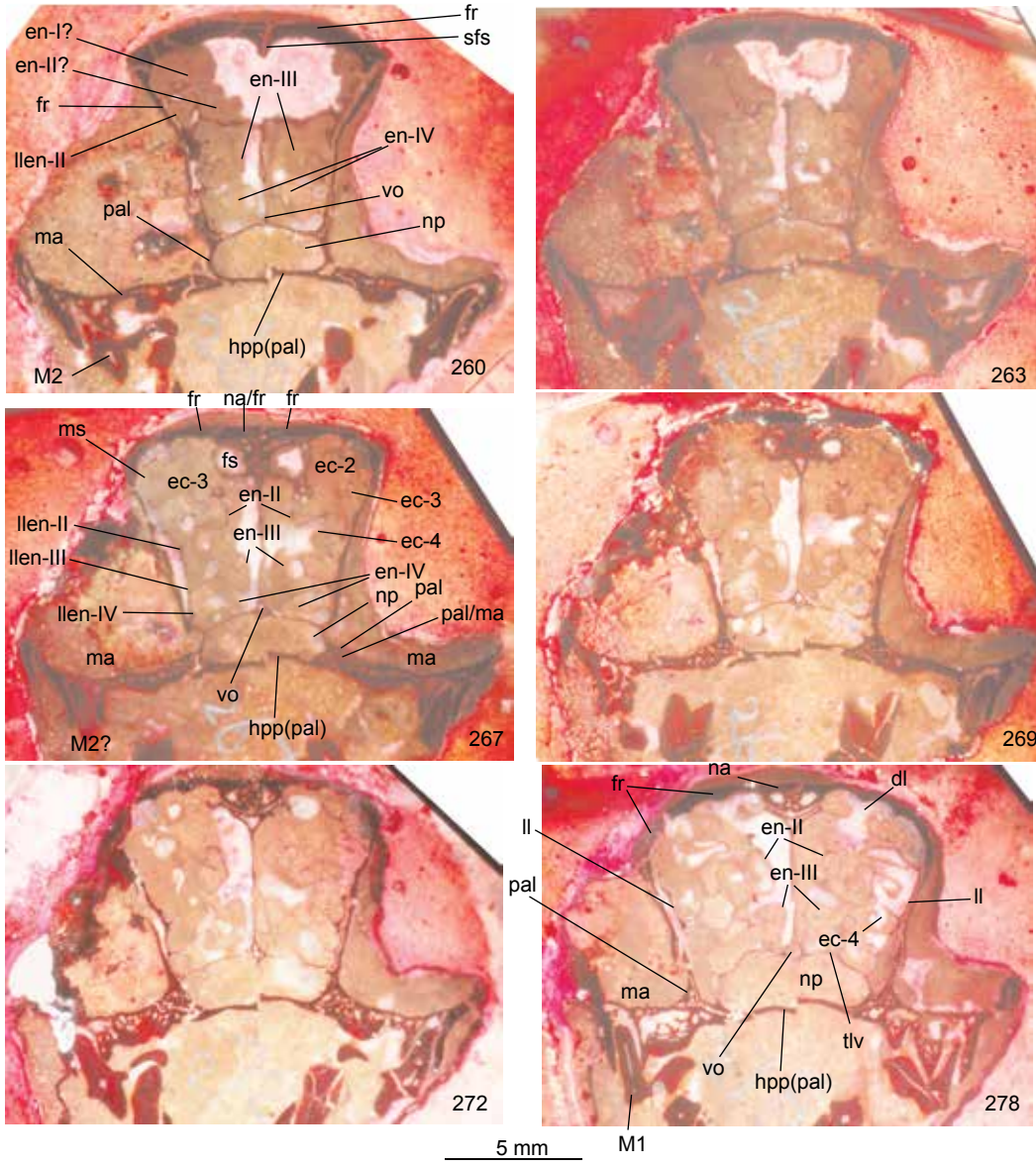

FIG. 27. *Hsiangolestes youngi*, IVPP V7438, serial sections 260–278 (from back forward).

of the ethmoid (or ethmoidal labyrinth) posteriorly. The maxilloturbinates arise from a single basal lamina (the maxilloturbinate crest) attached to the medial wall of the maxilla, and protrude into and occupy the anterior part of the nasal fossa. The maxilloturbinate is simple and preserved at the level between the first and third premolar (fig. 26: sections 300–331). It arises from the lamina on the medial surface of the maxilla and bifurcates dorsoventrally into two small laminae (fig. 26: sections 312–331). The dorsal lamina turns dorsolaterally and the ventral lamina turns ventrolaterally; however, both the dorsal and ventral laminae have not formed spirals. The maxilloturbinate of *Hsiangolestes* is similar to those of some creodontids and carniv-

oran-grade mammals, such as *Hyaenodon* and viverrids, in having a simple pattern and bifurcating into dorsal and ventral laminae (Joeckel et al., 1997: 442, figs. 5, 6). At the level of P1, we can see that the medial surface (nasal surface) of the maxilla has several crests. The maxilloturbinate crest can be seen at the level near the incisive-maxillary suture (fig. 26: sections 312–331) and extends posteriorly at the level of P2–3. The ventral and dorsal ethmoid crests are not clear. The ventral surface of the nasal bone forms the dorsal nasal meatus at its anterior part, which bears the nasoturbinates (fig. 26: sections 298, 300). The posterior part of the nasal ventral surface bounds the dorsal part of the lateral mass of the ethmoid (fig. 27: section 278). The septum of the frontal sinus separates the frontal sinus into two halves and is continuous anteriorly with the septal process of the nasal bone (figs. 27, 28: sections 243–269). The nasal surface of the lacrimal has a small ethmoid crest for articulating with the ethmoid bone.

The bony nasal septum is composed of a perpendicular plate of ethmoid bone (mesethmoid), which articulates with the septal processes (inner table) of the frontal (figs. 27, 28: sections 243–267) and nasal bones (figs. 25, 27: sections 267–289) above and the sagittal portion of the vomer below, and forms the ventral half of the nasal septum. It fuses posteriorly with the cribriform plate of the ethmoid bone, a sievelike partition between the nasal and cranial cavities, and extends as the cartilaginous part anteriorly. The cribriform plate of the ethmoid bone occurs about 2 mm posterior to the posterior edge of the horizontal lamina of the palatine (fig. 28: section 236), and it articulates with the frontal dorsally and the presphenoid ventrally (fig. 28: sections 237–246). It is protected by the orbitosphenoid (fig. 28: sections: 236–243) and the perpendicular lamina of the palatine (fig. 28: sections 243, 246) laterally. The lateral mass of the ethmoid bone (ethmoidal labyrinth) is largely composed of delicate bony scrolls (ethmoturbinates) that attach to the external lamina of the ethmoid bone by basal lamina laterally and to the cribriform plate of the ethmoid bone posteriorly. The external lamina of the ethmoid bone is divided into dorsal, lateral, and ventral (transverse) parts (roof, side, and floor plates respectively). The dorsal lamina is in contact with the frontal and nasal part of the perpendicular plate of the ethmoid bone, which can be seen in a few slides (fig. 27: sections 267–278). The lateral lamina is well developed along the lateral wall of the nasal cavity and partly covers the side of the ethmoturbinates (figs. 27, 28: sections 255–278). The ventral (transverse) lamina continues from the ventral part of the lateral lamina medially to the vomer in a transverse, dorsally convex arch (fig. 27: sections 272, 278). It is fused to the medial surfaces of the maxilla and closely connects to the horizontal part of the vomer, forming a partition separating the ethmoturbinates in the nasal fundus from the nasopharynx (fig. 27: section 278). The ethmoturbinates of *Hsiangolestes* are divided into four major long, deeply extending endoturbinates (endoturbinate I to IV) that almost reach the nasal septum medially. The lamella of endoturbinate II and III are split to form two olfactory plates respectively, so that the total number of the endoturbinates of *Hsiangolestes* is six. Usually, endoturbinate I is the longest and attaches to the medial wall of the nasal bone as the dorsal nasal concha (nasal turbinate or nasoturbinate). Endoturbinate I of *Hsiangolestes* is not as well preserved as the other ones. Based on its position, we identify a line very close to the nasal septum and to the roof of the nasal cavity at the level of P3–4 as endoturbinate I (fig. 26: sections 294–300). Tracing this line back to the position near the cribriform plate at the level of M2, we can see that the turbinates arise from the dorsal lamina near the frontal (fig. 27: section 260), which is the same as the origin of endoturbinate I in most eutherians. Endoturbinate II of *Hsiangolestes* is the best preserved, and so far the longest, in the serial section, and its anterior edge extends at least to the level between P2–3 (figs. 25, 26, 27, 28: sections 248–300). It arises from its basal lamina near the middle of the lateral lamina (fig. 27: section 267).

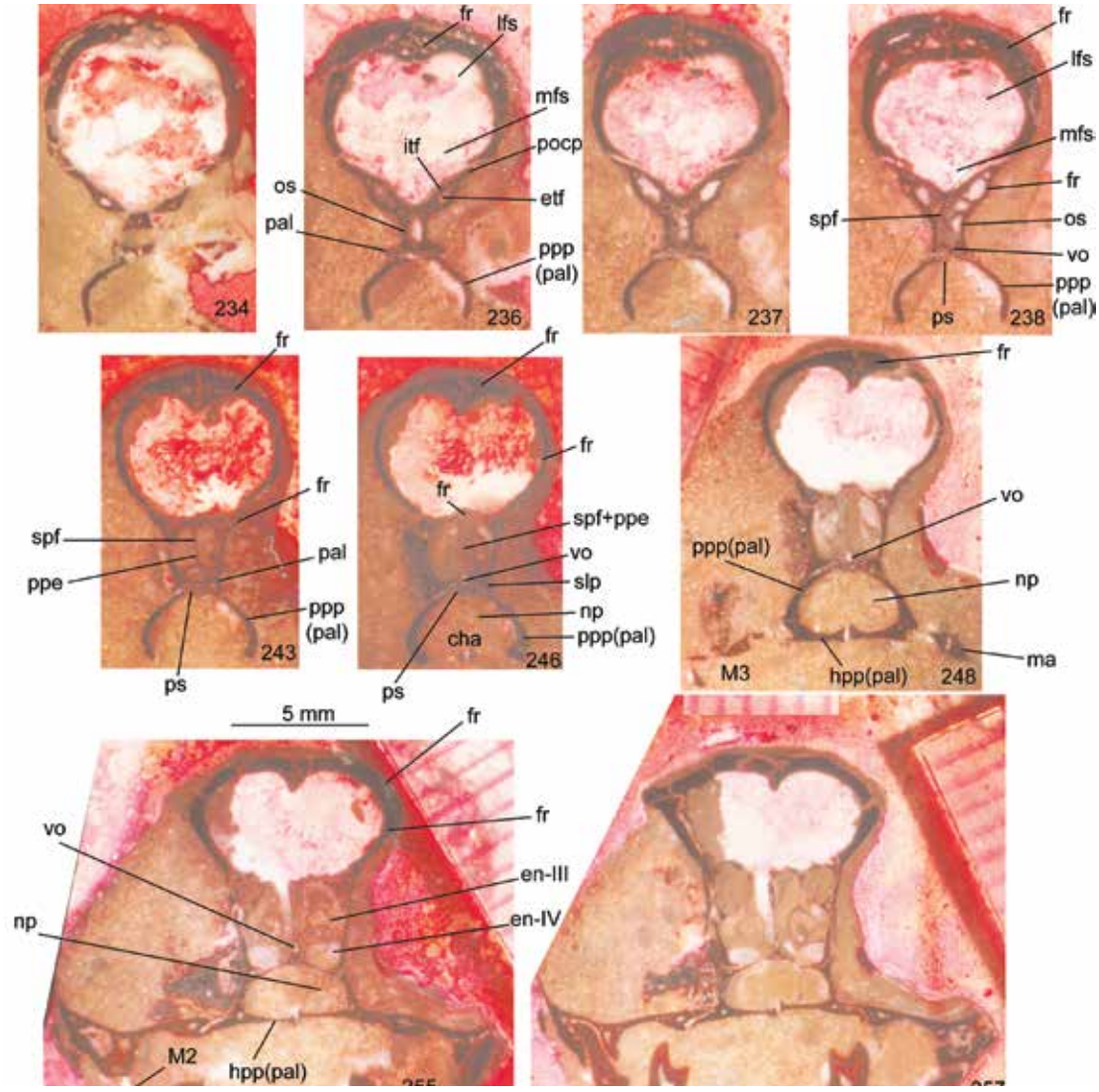

FIG. 28. *Hsiangolestes youngi*, IVPP V7438, serial sections 234–257 (from back forward).

In the region at the level between P4 and M1, it divides into two major scrolls, the medial and the lateral, which widen and extend transversely. The medial major scroll has one and a half turns. It turns ventrally after its split point, then toward the medial septum, then continues dorsally, and finally turns lateroventrally. The lateral major scroll turns dorsally after its split point and then bifurcates at the level of M1 into two mediolaterally situated small single scrolls. These two small scrolls rolled against each other (fig. 27: sections 267–272). The small medial scroll then increases in size to the size of the major medial scroll, but the lateral small one is smaller than the medial one (figs. 25, 26, 27: sections 272–292). Endoturbinate III of *Hsiangolestes* are also well preserved and slightly shorter than endoturbinate II, and they are roughly the same morphology as the second. It arises from its basal lamina of the lateral lamina beneath the endoturbinal II (fig. 27:

section 260) and its anterior edge extends at least to the level of P4 (fig. 26: section 289). In the region at the level between M1–2, it divides into two mediolaterally situated unequal-sized major scrolls, which become widened transversely. The medial major scroll makes one and a half turns before rolling ventrally, first after the split point, then toward the medial septum, after which it turns dorsally higher than the lateral major scroll, partly embracing the lateral one, before finally turning lateroventrally. The lateral major scroll splits into two small scrolls after its split point, and these then turn in opposing directions (fig. 27: sections 267–278). A very short turbinate splits from the basal lamina of endoturbinate III (fig. 27: section 272). Endoturbinate IV is much shorter and simpler than the II and III, and is well preserved in the posterior part of the nasal cavity (figs. 27, 28: sections 255–272). It arises from the basal lamina of the lateral lamina under endoturbinate III near the floor of the nasal cavity and is enlarged anteriorly. The turbinate has a single scroll with one and a half turns, which turns medially first, then dorsally when it is close to the medial septum, and finally turns laterally and curves ventrally (figs. 27, 28: sections 255–269). The anterior edge of endoturbinate IV ends at the level of the posterior part of M1 (fig. 27: sections 269, 272). In most extant mammals, the turbinates have a single scroll turn ventrally, except endoturbinate I, which turns dorsally (Miller, 1964; Moore, 1981). The lamina of the endoturbinate in different extant mammals will split to more olfactory plates; however, the scrolls usually turn ventrally. Unlike in extant mammalian groups, the scrolls of endoturbinates II, III, and IV of *Hsiangolestes* turn dorsally, which is similar to those of *Rhombomylus* (Meng et al., 2003). *Hsiangolestes* has four endoturbinates and endoturbinate II is split into two olfactory plates; however, it differs from the former in having endoturbinate III also split into two olfactory plates. Moore (1981: 248) mentioned "so far as placental memmals are concerned, it seems that the four endoturbinals with the lamella of the second divided to form two virturally independent olfactory plates represents an early, primitive condition." The splitting of endoturbinate III to increase the number of olfactory plates in *Hsiangolestes* may indicate a slight departure from the primitive condition. The number and arrangement of the ectoturbinates varies greatly in mammalian genera or species. To distinguish the ectoturbinates from the endoturbinates, we use Arabic numbers to describe the ectoturbinates. *Hsiangolestes* has four small, more superficially lying ectoturbinates (ectoturbinate 1–4). Ectoturbinate 1 (the position and morphology similar to *Rhombomylus*, Meng et al., 2003) is a single scroll situated dorsolaterally to endoturbinate I, which turns laterodorsally (figs. 26, 27: sections 272–300). Ectoturbinate 2 arises from its dorsal lamina at the frontal sinus posteriorly and bifurcates into two mediolaterally situated small scrolls. The medial one turns medially first and then dorsally, and the lateral one turns laterodorsally (figs. 26, 27: sections 267–294). Ectoturbinate 3 arises from its lateral lamina at the frontal sinus, extends dorsally dorsal to endoturbinate II, and bifurcates into two dorsoventrally situated scrolls. The dorsal one turns dorsolaterally after its split, and the ventral one turns medially first and then laterally after its split (figs. 26, 27: sections 263–294). Ectoturbinate 4 arises from the lateral lamina between endoturbinates II and III, and is a single scroll turning dorsolaterally (fig. 27: sections 263–278). *Hsiangolestes* differs from *Leptictis* that has two ectoturbinates (Novacek, 1986). Each nasal fossa is further divided by the nasal conchae (turbinates) into four major channels, the dorsal, middle, ventral, and common nasal meatuses. In *Hsiangolestes*, the dorsal nasal meatus is represented by a cleft between endoturbinate I and the nasal bone at the dorsal part of the nasal fossa (fig. 26: sections 294–300). The middle nasal meatus, the space between the nasoturbinate and the maxilloturbinate, may be seen in sections 312–315. The ventral nasal meatus, the passageway between the maxilloturbinate and the floor of the nasal cavity, and the common nasal meatus, a narrow space between the median per-

pendicular septum and the maxilloturbinate, can be seen in sections 315–331. The maxillary sinus in *Hsiangolestes* is very large (figs. 26, 27: sections 278–300). Longitudinally, it extends at least from the level of middle of M1 to the anterior edge of P3. The posterior part of the maxillary sinus is a small, narrow chamber separated by the ethmoturbinate into an upper part at the upper lateral corner and a lower part at the lower lateral corner of the nasal cavity (fig. 27: sections 260, 263). It gradually enlarges in size both dorsoventrally and transversely, and reaches its maximum at the level of the infraorbital foramen at P4, where it occupies the entire lateral area of the nasal cavity and about 40%–50% of the transverse cross section (fig. 26: sections 289–294), and then it reduces in size anteriorly. The lateral wall of the maxillary sinus is composed of the frontal posteriorly (fig. 27: sections 260, 263), and the lacrimal and maxilla anteriorly. In addition to the maxillary sinus, most mammals possess a frontal sinus. Usually, this sinus is located between the outer and inner tables of the frontal bone, and is divided into lateral and medial parts. *Hsiangolestes* has a well-developed frontal sinus (fig. 28: sections 234–246). The frontal sinus is reduced in size anteriorly and rectangular. It is divided by the septal process of the nasal bone into two small cavities at the level of M2 (fig. 27: sections 267–269) and ends at the level of M1 (fig. 27: sections 269–272).

Maxilla: The maxilla is the largest element in the facial region and an important part of the orbital region. It occupies the entire lateral surface of the facial region, contributes half the ventral surface of the palatine region, forms the ventral part of the orbital fossa, possesses a well-developed zygomatic process, and has a big infraorbital canal. In lateral view, it is shorter and deeper anteriorly and longer and narrower posteriorly (figs. 19B, 22B, 23). The sutures with neighboring bones are well preserved in IVPP V5346, 5792, and 7454 (fig. 24). In dorsal view, the maxilla is narrow and rectangular (figs. 20, 21, 22a, 24A). It contacts the premaxilla anterolaterally, the nasal medially, and the lacrimal and frontal posteriorly. The maxillary-premaxilla suture is short, and extends anterolaterally from the nasal process of the premaxilla at the level of the anterior edge of P1 to the diastema between the canine and last incisor. The maxillary-nasal suture is straight and occupies less than one-third the nasal length. The maxillary-frontal suture is a relatively short, oblique line, extending from the maxilla-nasal junction anteriorly to the maxilla-lacrimal junction posteriorly. In *Leptictis*, the maxillary-frontal suture is broad, due to the poor facial exposure of the lacrimal (Simpson, 1931; Novacek, 1986). *Hsiangolestes* is very different from *Leptictis* in having a relatively shorter maxillary-frontal suture; however, compared with didelphids and *Zalambdalestes* (Wible et al., 2004), in which the large facial extension and posterior expansion of the nasal almost excluded the contact between maxilla and frontal, the contact of maxilla and frontal in *Hsiangolestes* is broader. *Hsiangolestes* is similar to *Archaeoryctes* (Zheng, 1979), and *Hunanictis* (Li et al., 1979) in having a relatively shorter maxillary-frontal suture, but differs from *Archaeoryctes* and *Hunanictis* in having the suture oblique to the skull length, instead of transverse to the skull length as in *Archaeoryctes* and *Hunanictis*. The maxillary-lacrimal suture, well exposed on the dorsal surface, is a broad semicircular line and projects anteriorly. The lateral surface of the maxilla is basically smooth without indication of any foramina. Its alveolar border is irregular. There is indication there are three alveoli for the fourth premolar and all three molars and two for premolars 1–3. The large root of the canine extends posteriorly dorsal to the posterior edge of P1 (fig. 26: section 323). The infraorbital canal lies dorsal to the posterior edge of P3 and alveoli of P4. The infraorbital canal is short but large. Its anterior opening (infraorbital foramen) is small, situated at the level above the posterior edge of the P3, and circular in cross section. The canal gradually increases in size posteriorly, so the posterior opening is larger than the anterior and is transversely oval, with the long axis perpendicular to the length of the skull. This opening lies within the orbital wing of the maxilla at the level above P4

and lateral to the triple junction of the lacrimal, palatine, and maxilla. The wall of the infraorbital canal is mainly formed by the maxilla, but the lacrimal may contribute a little at the upper-medial aspect of the wall of the canal (fig. 26: section 289, 292). The length of the infraorbital canal is considered important evidence of relationships among the "insectivoran" mammals and with other eutherians (Butler, 1956; Novacek, 1986). Anterior to the infraorbital foramen is a small (about 2.5 mm w, 2 mm h in V7454, 2 mm w, 1.5 in V5346, 4 mm w, 2.5 mm h in V5792) shallow, oval depression, longitudinally situated at the level dorsal to P2–3. This depression in V7454 and 5792 is clearly marked by a thin ridge, but not in V5346, which makes the depression look deeper in V7454 and 5792 than in V5346. It extends from the level at the anterior edge of P2 posteriorly close to the infraorbital foramen. Unlike the well-excavated antorbital fossa in *Leptictis*, which is located anterior to the zygomatic process and bordered by the Y-shaped process of the jugal (Novacek, 1986: 30, figs. 1, 2, 10), this depression in *Hsiangolestes* is shallow, situated just anterior to the infraorbital foramen, and far from the zygomatic process of the maxilla. The zygomatic process of the maxilla is simple, thin, and slender, extending posteriorly and horizontally (fig. 24C). It is dorsobliquely articulated with the jugal bone. The palatal process of the maxilla is the largest component of the hard palate, occupying almost half the area of the hard palate (figs. 12, 13, 19A, 24B). It is rectangular. Its anterior part is narrow and flat. There is a longitudinally extended groove-like depression along the midline of the hard palate in the ventral surface. The maxillary-palatine suture runs obliquely from the posterior edge of the P3 to anterior P4, forming a V-shape with the apex of the V directed anteriorly. This suture then continues running posteriorly along the medial side of P4 to the posterior edge of M3. The posterior part of the palatal process of the maxilla, located posteromedial to M1–3, is small and narrow due to the enlargement of the palatine bone. The posterior border of the maxilla is straight, perpendicular to the midline of the skull. The dorsal surface of the palatine process of the maxilla forms part of the floor of the ventral nasal meatus (figs. 26, 27: sections 269–331). The orbital process of the maxilla is a major component of the orbital region, forming most of the floor of the orbit, which is large and flat, and in which the roots of M1–3 are exposed. The maxilla forms most of the wall of the infraorbital canal (fig. 26: sections 283–298). It is fully excluded from the medial wall and the rim of the orbit, due to well-developed frontal, palatal, and lacrimal bones in that region. The orbital process of the maxilla contributes a very small portion to the lower region of the medial wall of the orbit. The orbital process of the maxilla is bounded by the lacrimal anterodorsally. There is no contact between the orbital process of the maxilla and the frontal in the medial wall because of a large intrusion of the palatine bone in that region (figs. 19B, 22). The maxillary-lacrimal suture is short and curved. The maxillary-jugal suture is straight and runs from the triple junction of the lacrimal, zygomatic process of the maxilla, and jugal bones to the posterior end of the maxilla. The maxillary-palatine suture is straight and runs along the bottom of the medial wall of the orbit. Two small foramina are situated at the medial anterior wall of the maxilla, the sphenopalatine anteriorly, and the posterior palatine posteriorly. The zygomatic arch is moderately wide. The middle part of the arch is parallel to the longitudinal midline of the skull.

Lacrimal: The lacrimal is a prominent bone, well preserved in IVPP V5346, 5792, and 7454 (figs. 19B, 20, 21, 22, 23). The lacrimal has a distinctive, large, crescental facial process (figs. 24A, C, 32). The surfaces of the facial process of the laccrimal is flat and smooth. The facial process of the lacrimal contacts the maxilla and frontal in a short arc, projecting anteriorly at the level of the anterior edge of P4. The lacrimal is a large element in the anteromedial wall of the orbital region, and is trapezoidal. The sutures with surrounding bones are best preserved in V7454 (fig. 11). The lacrimal contacts the frontal and palatine posteriorly, the maxilla ventrally, and the palatine at the posteroventral aspect in the orbit.

The lacrimal-maxilla suture is straight and extends into the infraorbital foramen. The lacrimal-frontal suture is short, straight, and extends dorsoventrally. The lacrimal-palatine suture is 3-shaped with the apex anterior. The lacrimal foramen is single and large, situated at the anterior extremity of the lacrimal, and confined within the orbital region. The foramen is surrounded by the lacrimal. Its posterior opening is oval and lies at the level of the posterior edge of P4 (figs. 22B, 23, 26: sections 283–304). There is no "translacrimal canal" or lacrimal tubercle.

Jugal: The jugal is completely preserved on the right side of V7454 and both sides of IVPP V5792 (figs. 11, 20). The jugal is a sizable component; however, its robustness varies. The jugal in V5792 is slenderer than that in V7454. The body of the jugal is compressed lateromedially, convex laterally and concave medially. Anteriorly, the jugal contacts the lacrimal with a diagonal suture in the facial region and a short straight suture in the orbital region (fig. 24C). The jugal contacts the zygomatic process of the maxilla with a simple, straight suture, which runs from the level of M3 horizontally and then contacts the maxilla obliquely to meet at the jugal-lacrimal-maxilla triple junction, at the level of P4. The posterior process ("posterior spine" of Novacek, 1986: 38, fig. 13) is long and contacts the zygomatic process of the squamosal by a diagonal suture, running from the level of the middle of the zygomatic arch to end a little in front of the glenoid process. The jugal occupies almost the half of length of the zygomatic arch.

Frontal: The frontal is a distinctive bone composing the roof of the skull and is also a large element of the orbital region. In dorsal view, the frontal is short compared with the parietal and nasal, occupying about one-third the roof length. It is roughly butterfly shaped (figs. 20, 21, 22A, 24A). Anteriorly, there are two wing-shaped wedges extending between the nasal and maxilla and separating them at the level above P3. The frontal-nasal suture is short, extending laterally from the point where the nasal bone meets at the midline of the skull to the triple junction, where the frontal, maxillary, and nasal meet, at above the level of P3. Both sides of the frontal-nasal sutures meet at the midline of the skull to form a V shape, with the apex of the V directed posteriorly. The frontal-maxillary suture runs posteriorly from the triple junction where the nasal, frontal, and maxilla meet, and ends at the triple junction, where the frontal, maxilla, and lacrimal meet. The frontal-lacrimal suture is very short and curves at the anterior edge of the orbit. Posteriorly the frontal contacts the parietal. The frontal-parietal suture is short, straight, and runs diagonally, from the midline of the skull in a V-shape obliquely to meet the parietal-alisphenoid suture at the posterior edge of the orbit. The supratemporal crest is weak, extending from the point where the paired frontal-parietal sutures meet, to the supraorbital process of the frontal at the posterior edge of the orbit. The supraorbital process of the frontal is a distinct posterolateral projection, tapering at the tip and confining the posterior edge of the orbit. Posterior to the supraorbital process, the frontal becomes narrower and continues to the point where it meets the parietal. The narrowest part of the skull is posterior to the supraorbital process of the frontal and close to the frontal-parietal suture, which also marks the posterior rim of the orbit (figs. 20, 21, 24A). The supraorbital crest is very weak or faint in most parts of the orbit, but distinctive and well developed near the supraorbital process. The frontal has a very large orbital process, which extends ventrally almost to the ventral border of the medial wall of the orbit (figs. 10, 19B, 23, 32). The orbital process of the frontal is roughly triangular, and is wide along the posterior rim of the orbit and anterior rim of the temporal fossa. It narrows at the ventral border of the medial wall of the temporal fossa, contacting the palatine. Anteriorly, it contacts the lacrimal. The frontal-lacrimal suture is a straight line, running ventrally from the top of the orbital rim about a half the height of the medial wall of the orbit, meeting the palatine at the junction of the frontal-lacrimal and frontal-palatine sutures (figs.

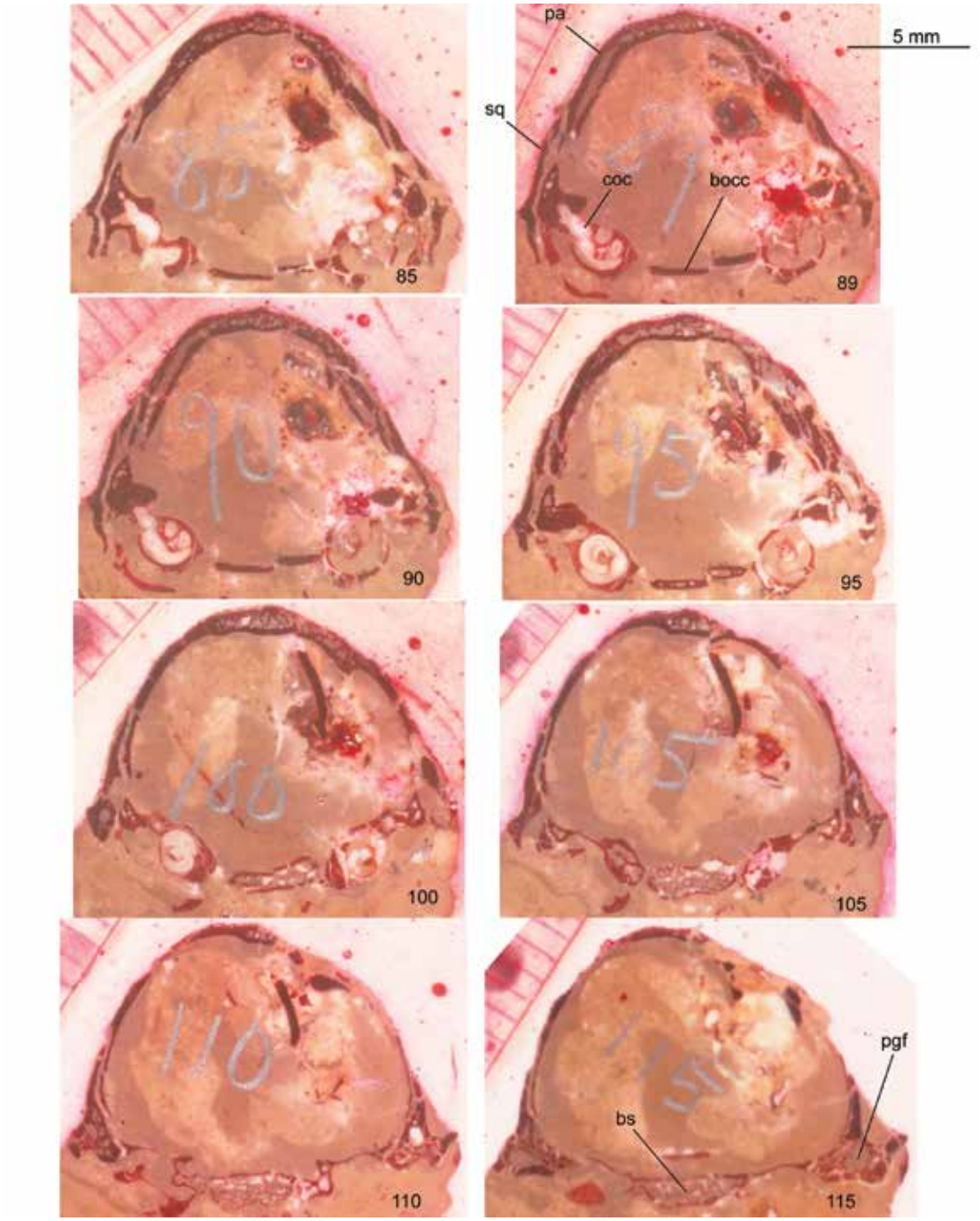

FIG. 29. *Hsiangolestes youngi*, IVPP V7438, serial sections 85–115 (from back forward).

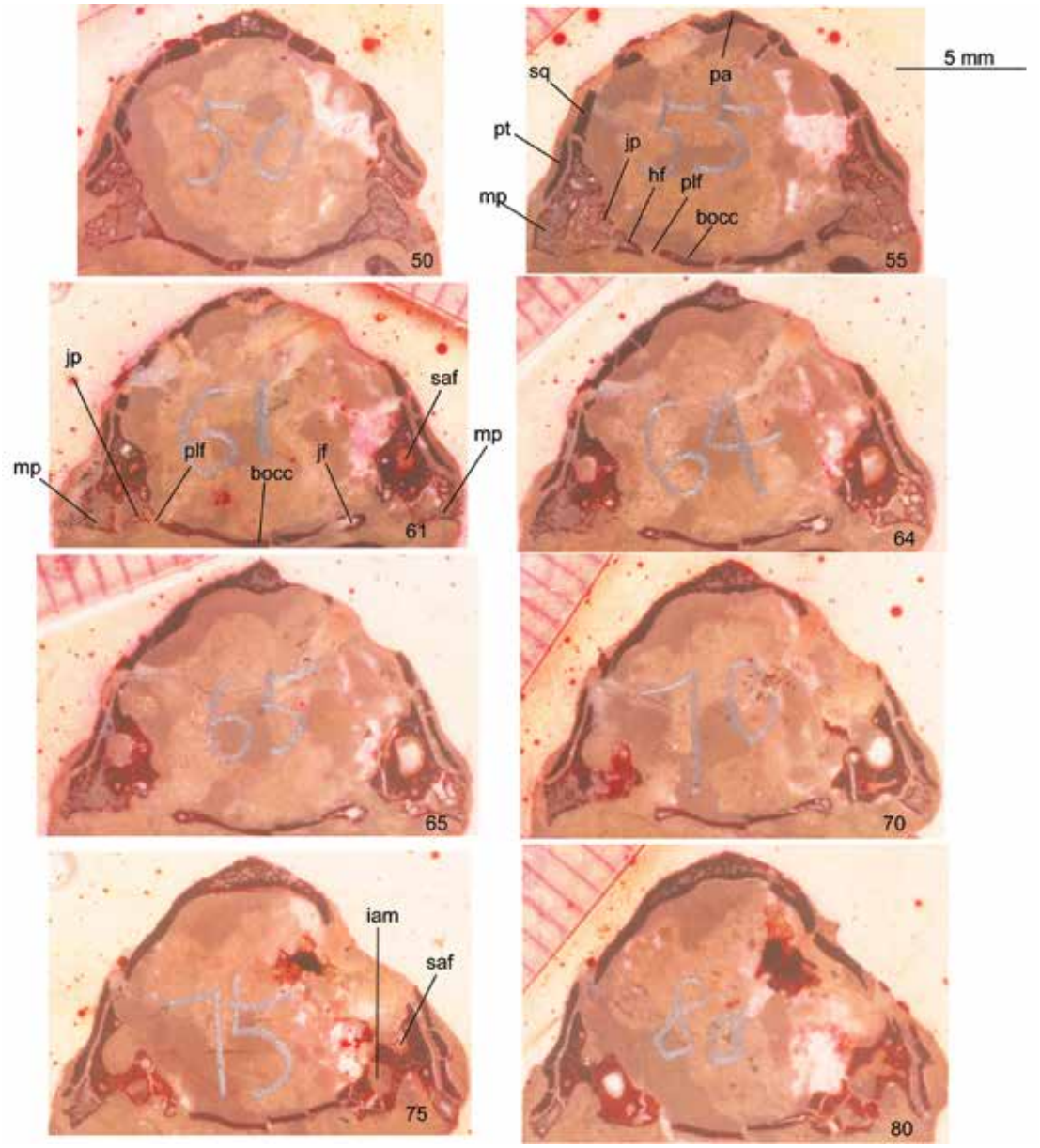

FIG. 30. *Hsiangolestes youngi*, IVPP V7438, serial sections 50–80 (from back forward).

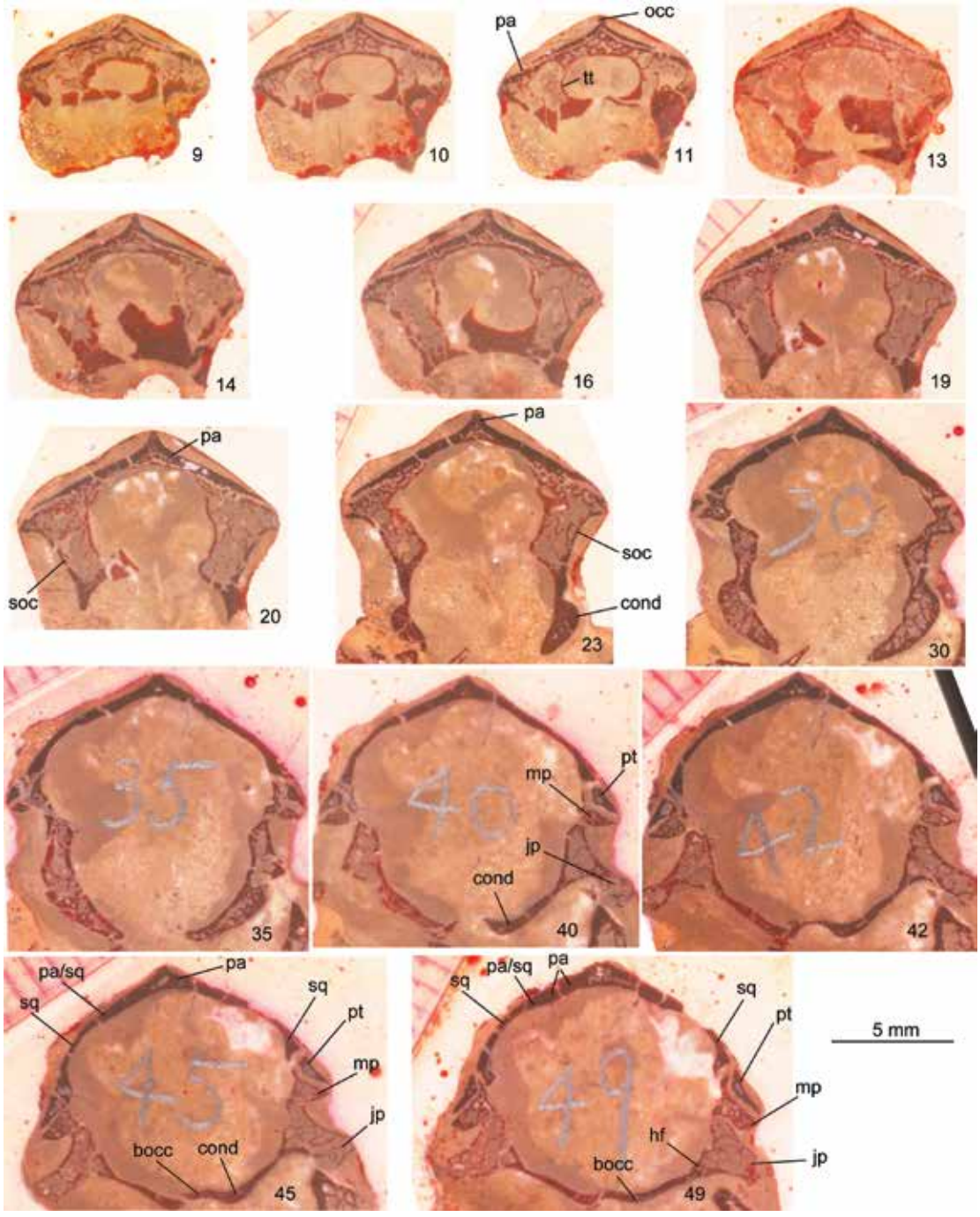

FIG. 31. *Hsiangolestes youngi*, IVPP V7438, serial sections 9–49 (from back forward).

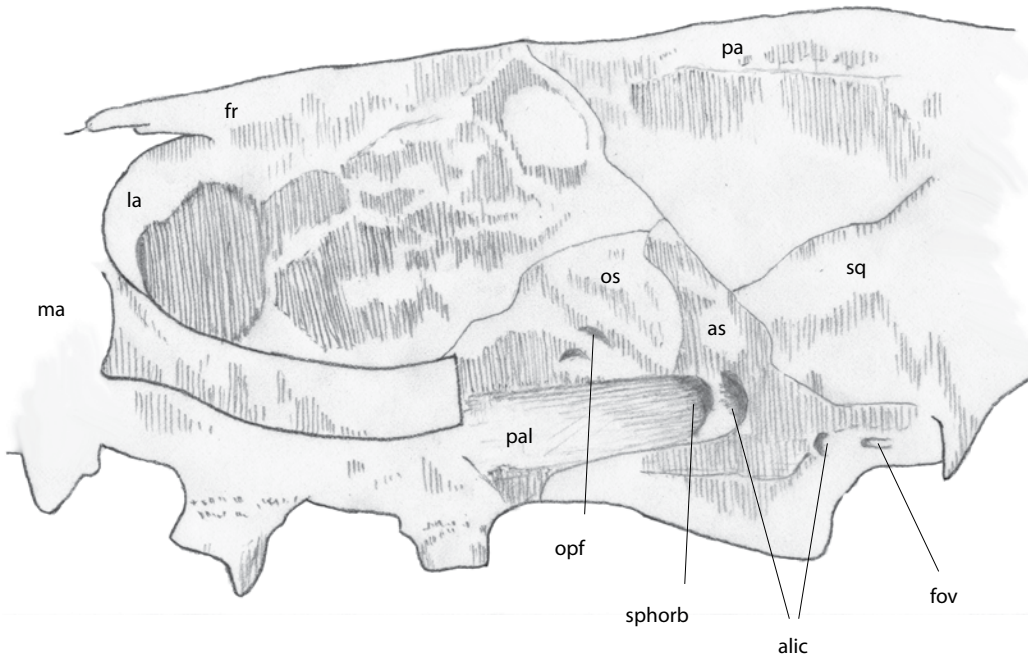

FIG. 32. Drawing of temporal region of *Hsiangolestes youngi* skull (based on IVPP V5436).

24C, 32). Posterior to the frontal-lacrimal suture, the frontal contacts the palatine in a circular suture, which then extends ventrally to reach the ventral border of the orbit and contact the palatine. Posteriorly, the frontal contacts the alisphenoid, and the frontal-alisphenoid suture is short, straight, and obliquely situated between the frontal-parietal and alisphenoid-orbitosphenoid sutures. The frontal has a broad contact with the orbitosphenoid in the posterior medial wall of the temporal region. The frontal-orbitosphenoidal suture is irregular in shape, and extends ventrally from the junction of the frontal-alisphenoid and frontal-orbitosphenoid sutures, passing the ethmoid foramen, to the ventral border of the temporal fossa, where it contacts the palatine. In the ventral border of the temporal fossa, the frontal contacts the palatine in a very short suture. The frontal is separated from the maxilla by the palatine in the orbital region (fig. 32).

Palatine: The palatine is clearly seen in IVPP V5346, 5792, and 7454. It is a large bone, occupying more than one-third the length of the palate and having a large expansion in the orbital region. It is triangular in palatal view and contacts the maxilla laterally and anteriorly (figs. 12, 13, 19A, B). The palatal-maxillary suture in ventral view runs antero-obliquely at the level of the posterior edge of M3 to meet the opposite palatal-maxillary suture at the level of the anterior edge of P4, forming a triangle with the apex pointed anteriorly. There is a clear foramen, identified as the middle palatine foramen, at the level of P4 about 2 mm medial to the palatine-maxillary suture in both sides of V7454 and the left side of V5346. This foramen opens anteriorly into a shallow, continuous groove, reaching the palatine-maxillary suture near the apex of the triangle. Three small nutrition foramina clearly seen in the left side of the palate in V5346 lie in an oblique line medial to the maxillary-palatine suture. The posterior pair is situated at the level of the posterior edge of M1 and the anterior one at the level of the middle of M1. These foramina are not clearly seen on the right side of the specimen due to

breakage in that area. There is no clear indication of the anterior and posterior palatine foramina. The posterior edge of the palatine at the level of M3 is arch shaped, curving deeply anteriorly, where the posterior palatine foramen is usually located. The posterior edge of the palatine foramen bends medially and merges laterally with the postpalatine torus. The postpalatine torus is strong, rounded, and curves in an arch anteriorly, making the middle part of the posterior edge of the palate biconcave in outline. The wings of the postpalatine torus run medially to meet at the midline of the palate, forming a rounded prominence that projects posteriorly as the postpalatine spine. The postpalatine spine is small and located at the level of the posterior edge of M3. Posterior to the postpalatine torus, the palatine narrows as the perpendicular part of the palatine and contacts the pterygoid posteriorly.

The palatine has a large expansion in the orbital region (figs. 10, 22B, 23). The orbital pricess of the palatine forms the medial part of the orbital floor, which is defined by the palatine-maxillary suture laterally (fig. 32). The palatine-maxillary suture is interdigitated and zigzag, running from the point medial to the anterior edge of the root of M3, anteriorly along the medial side of the roots of M2 and making a U turn medially and anteriorly to the root of M1, to contact the lacrimal at the posterior edge of the infraorbital foramen. The palatine-lacrimal suture is roughly V-shaped, with the apex of the V pointed ventrally, and located at the lower-anterior aspect of the medial wall of the orbit. Due to the large expansion of the palatine in the orbital region, the maxilla is entirely excluded from contact with the frontal in this region (fig. 32). In the lower-anterior medial wall of the orbit and posterior to the lacrimal, the palatine has an oval expansion, which contacts the lacrimal in a short, straight palatine-lacrimal suture anteriorly and the frontal in a curving suture dorsoposteriorly. The palatine contacts the frontal posterior to the oval palatine expansion in a horizontal straight suture along the medial side of the floor of the orbit. Next to and above the floor is the longitudinally oriented palatine recess, which is bounded by the palatine-frontal suture medially and the palatine-maxillary suture laterally. At the anterior extremity of the palatine recess, there are two foramina. A large, elliptical sphenopalatine foramen is situated dorsally, and a small, round, dorsal palatine foramen is situated ventral to it. The postpalatine foramen is oval, slightly smaller than the sphenopalatine foramen, and is located in the middle of the palatine recess. Posterior to the palatine recess, the palatine has a little contact with the ventral projection of the orbitosphenoid dorsally and with the alisphenoid ventrally. The palatine-orbitosphenoid suture is a very short curved line, and the palatine-alisphenoid suture is a simple straight line.

Parietal: The parietal and the sutures of the parietal with surrounding bones are well preserved in IVPP V5346, 5792, and 7454. The parietal is a large element in the roof of the skull and side wall of the temporal fossa, occupying almost half the length of the skull and covering the entire cranial cavity (figs. 20, 21, 22A, 24A). It is roughly rectangular, elongated anteroposteriorly, and widened and strongly expanded immediately posterior to the orbital constriction, indicating expansion of the cerebral hemispheres. The dorsal surface of the parietal is basically smooth. A distinct convex expansion area in the dorsal surface occurs from the level of the glenoid fossa to the posterior end of the zygomatic arch, and becomes slightly concave posterior to this area. The parietal contacts the frontal anteriorly and the squamosal and alisphenoid ventrolaterally, and ends at the lambdoidal crest posteriorly. The parietal-frontal suture is V-shaped in the midline of the skull roof, which is formed by a V-shaped posterior process of the frontal, fitting between the inverse V-shaped anterior process of the parietal, and the suture then runs lateroventrally to the upper part of the side wall of the temporal fossa, to end at the triple junction of the parietal, frontal, and alisphenoid (figs. 10, 20, 21, 23, 32). The parietal-alisphenoid suture immediately continues

from the triple junction of the parietal, frontal, and alisphenoid and runs ventroposteriorly a short distance to end at the triple junction of the parietal, alisphenoid, and squamosal. The parietal-alisphenoid suture is short, simple, and straight. The parietal-squamosal suture starts at the triple junction of the parietal, squamosal, and alisphenoid and runs posteriorly along the side wall of the temporal fossa to end at the lambdoidal crest. The suture is a coarsely interdigitated, roughly S-shaped line, and is longest compared to the parietal-frontal and the parietal-alisphenoid suture. A low, slender, but distinct sagittal crest immediately begins from the apex of the V-shaped parietal-frontal suture, gradually becomes strong and pronounced posteriorly, and extends along the midline of the skull roof to reach the lambdoidal crest. In IVPP V5346, there is a small rectangular bone located next to the sagittal crest on both sides of the sagittal crest, which seems likely an interparietal (?) based on its position (fig. 21). It has a distinct interdigitated curved suture with the parietal. It contacts the parietal anteriorly, and is bounded by the lambdoidal crest posteriorly. The suture of this small bone with the parietal runs from the lateroposterior aspect of the skull to a point about 2 mm anterior to the lambdoidal crest, but does not contact the squamosal. This bone can also be seen in the left side of the skull of IVPP V7454, but it does not appear on the right side of the skull of V7454 or either side of the skull of V5792. If this small bone is an interparietal, the inconsistency of its appearance in these specimens may be due to age differences. It is not fused with the parietal in a young individual, such as V5346, but partially or fully fused with the parietal in the adults, such as V7454 and 5792.

Presphenoid: The presphenoid is preserved in IVPP V5436 and 7454 (figs. 13, 23B). In ventral view, the presphenoid is a long, narrow bone in the roof of the deep recess. It is bounded laterally by the entopterygoid crests of the pterygoid. Anteriorly, it contacts the vomer in a V-shaped suture, lateral to which is a concave area. There is a weak keel along the midline of the presphenoid, which can be seen more clearly in the posterior part. The presphenoid-basisphenoid suture is a simple straight line situated approximately at the middle of the deep recess.

Orbitosphenoid: The orbitosphenoid is well preserved in IVPP V5346 and 7454, and is a large element forming most of the posterior part of the medial wall of the orbit. The orbitosphenoid is elongated dorsoventrally and roughly rectangular (figs. 11, 23). It contacts the frontal dorsally in a horizontally situated brace-shaped suture with the apex pointed ventrally (fig. 32). Anteriorly, it contacts the frontal in a curved suture that extends to the ventral border of the orbital wall, so that the orbitosphenoid has no contact with the palatine anteriorly. Posteriorly, it contacts the alisphenoid in a simple, dorsoventrally extended straight line. Ventrally, the orbitosphenoid contacts the alisphenoid and palatine. The orbitosphenoid-palatine suture is coarsely interdigitated and extends along the ventral border of the orbit (fig. 32). The orbitosphenoid-alisphenoid suture continues from the orbitosphenoid-palatine suture posteriorly to reach the sphenopalatine foramen. A large, oval optic foramen is situated just dorsal of the triple junction of the orbitosphenoid, the alisphenoid, and the palatine. It is located almost horizontally at the middle part of the orbitosphenoid. Closely anteroventral to the optic foramen is a small circular foramen (?suboptic foramen). The sphenorbital fissure is located near the orbitosphenoid-alisphenoid suture, mainly in the alisphenoid. The anterior end of the sphenorbital fissure is situated in the orbitosphenoid.

Alisphenoid: The alisphenoid is well preserved in IVPP V5346, 5792, and 7454 (figs. 11, 23). It is a large, complex, irregularly shaped element contributing to the posterior part of the temporal region of the skull. Its orbital exposure is large and it extends dorsally to the upper rim of the temporal fossa (figs. 24C, 32) It contacts the frontal anterodorsally, parietal and squamosal posterodorsally, the orbitosphenoid anteriorly, the pterygoid and palatine ventrally, and the

petrosal posteriorly and ventrally. The alisphenoid-frontal suture is very short and straight. The alisphenoid-parietal and the alisphenoid-squamosal sutures are simple and straight. The alisphenoid-pterygoid suture is short and simple, running posterobliquely from the juncture of the palatine and pterygoid to the base of the pterygoid. The alisphenoid-orbitosphenoid suture is coarsely interdigitated and runs from a point ventral to the juncture of the frontal, the orbitosphenoid, and the alisphenoid, ventrally to the ventral edge of the medial wall of the temporal fossa. The alisphenoid forms the sloping posterior wall of the temporal fossa (figs. 32, 33). At the ventral side of the slope are several foramina. The sphenorbital fissure is a large circular foramen. It is situated at the ventral end of the alisphenoid-orbitosphenoid suture and separated from the optic foramen by a thin bony septum. Posterior to the sphenorbital fissure and separated from it by a bony septum is the anterior opening of the alisphenoid canal. The alisphenoid canal is moderately long, defined laterally by a thin bony septum. The posterior opening of the alisphenoid canal is much smaller than the anterior one and situated closely anterior to the foramen ovale, that usually transmits the mandibular branch of the trigeminal nerve. The foramen ovale is large, elongate, and situated anterior to the petrosal and medial to the alisphenoid-petrosal suture (fig. 33). This foramen is facing ventrally and has no foramina next to it.

Ventrally, the alisphenoid contacts the palatine anteriorly, the pterygoid ventrally, and the petrosal ventroposteriorly (figs. 13, 33). The alisphenoid-palatine suture is coarsely interdigitated. The alisphenoid-pterygoid suture is a short, simple, V-shaped line posterior to the ectopterygoid fossa. Lateral to the ectopterygoid fossa is a prominent, triangular ectopterygoid crest of the alisphenoid, for the attachment of the external pterygoid muscles. This crest slopes dorsomedially to form the lateral wall of the ectopterygoid fossa. Posteriorly, the ectopterygoid fossa broadens in a smooth surface just anteromedial to the foramen ovale. Its posterior edge reaches the anterior rim of the tympanic cavity. The alisphenoid-petrosal suture runs just anterior to the petrosal. The alisphenoid contacts the presphenoid and basisphenoid ventrally. Both alisphenoid-presphenoid and alisphenoid-basisphenoid sutures are very short and simple.

Basisphenoid: The basisphenoid is well preserved in IVPP V5436, 5792, and 7454. It is a narrow, roughly trapezoidal bone that contacts the presphenoid anteriorly, basioccipital posteriorly, and the pterygoid and alisphenoid laterally (figs. 12, 13, 24B). The presphenoid-basisphenoid suture is situated at the level of the sphenorbital fissure, and the basisphenoid-basioccipital suture at the level of the anterior edge of the tympanic cavity. Both sutures are simple, short, and straight.

Pterygoid: The slender pterygoid extends from the posterior palatine process to a point anteromedial to the anterior opening of the alisphenoid canal (figs. 12, 13, 24B). It contacts the palatine anterodorsally and the alisphenoid dorsoposteriorly. The short pterygoid-palatine suture is coarsely interdigitated and V-shaped, with the apex of the V directed posteriorly. It runs from the posterior edge of the palatine process posteriorly to meet the pterygoid-alisphenoid suture near the lateral crest of the pterygoid. The pterygoid-alisphenoid suture is curved and coarsely interdigitated, running around the pterygoid. The pterygoid is bifurcated, with a long major medial branch and a short lateral branch.

Squamosal: The squamosal and its sutures with surrounding bones are well preserved in IVPP V5346, 5792, and 7454. The squamosal is a large element in the temporal region and comprises the posterior portion of the lateral wall of the skull (figs. 10, 19B, 20, 21, 23). In the medial wall of the temporal fossa, it contacts the parietal dorsally and the alisphenoid ventroanteriorly. The parietal-squamosal suture is a long, coarsely interdigitated line (figs. 24C, 32). The suture is somewhat horizontally situated, S-shaped, running posteriorly from the triple junction of the parietal, alisphenoid, and squamosal to the lower half of the lambdoid crest. The surface of the

squamosal is smooth without any foramina, convex at its anterior part, and slightly concave posteriorly. About 1 mm anterior to the lowest point of the lambdoid crest, there is a strong crest running horizontally, and extending anteriorly to a point where the zygomatic turns immediately laterally to form the posterior part of the zygomatic arch. This is the postzygomatic crest. The postzygomatic crest borders the root of the zygomatic arch dorsally. A deep, long fossa, the suprameatal fossa, is located under the postzygomatic crest. The zygomatic process forms the posterior half of the zygomatic arch. Both the anterior and posterior part of the dorsal border of the zygomatic process is thin and sharp, but the middle part is slightly wider and flat. The zygomatic process extends horizontally posteriorly, but its ventral border extends anterodorsally, so that the zygomatic arch tapers at its anterior end and overlaps with the jugal at the level of the anterior edge of the temporal fossa. The medial surface of the zygomatic process is slightly concave. The posterolateral surface of the zygomatic process of the squamosal has a slightly concave area (suprameatal fossa in Novacek, 1986: 47, fig. 17) that is located just above the external acoustic meatus; however, the lateral surface of the zygomatic process becomes convex anteriorly, and there is no suprameatal fissure in front of the suprameatal fossa in *Hsiangolestes*. In ventral view, the glenoid fossa is large, transversely elongated, and slightly concave. The surface of the glenoid fossa is smooth (figs. 12, 13, 24B). The postglenoid process is large and deep. It is wider at the base of the process and narrower at its tip, forming a triangular wall that covers most of the medial part of the posterior border of the glenoid fossa. A large, irregularly shaped postglenoid foramen is located at the base of the posterior wall of the postglenoid process. Posterior to the postglenoid foramen, the meatal surface of the squamosal forms a long, sharp ridge on its ventral side (fig. 33). The meatal surface is slightly curved ventrally, well below the roof of the tympanic cavity, and a distinct ridgelike posttympanic process marks its posterior boundary. In lateral view, the posttympanic process is triangular. The dorsal part of the posttympanic process connects with the mastoid process, forming the squamosal-mastoid suture. The squamosal-mastoid suture is a simple, straight line in its dorsal part, becoming zigzag and interdigitated in the lower part. In ventral view, the squamosal-mastoid suture is short and simple, with the posttympanic process anterior and the mastoid process posterior. The petrotympanic fissure (Glaserian fissure) is not well preserved in IVPP V5346 and 5792. In IVPP V7454, there is a deep fissure on the squamosal-tympanic suture at the anterior part of the tympanic cavity, which most likely is the petrotympanic fissure. At the lower posterior region of the temporal fossa, the squamosal has a short connection with the alisphenoid. The squamosal-alisphenoid suture is irregularly shaped, running ventrally from the triple junction of the parietal, squamosal, and alisphenoid, then turning posteriorly dorsal to the pterygoid process in a simple straight line, making a turn medially at the middle of the glenoid fossa and then running posteriorly to end at the anterior lateral wall of the tympanic cavity. The very short squamosal-petrosal suture lies at the level of the posterior part of the postglenoid foramen, where the squamosal forms the lateral wall of the epitympanic recess.

Petromastoid: The mastoid and petrosal usually are fused. We describe these bones and the tympanic cavity as a complex. The mastoid petrosal is well preserved in IVPP V5346, 5792, and 7454 (figs. 33, 34, 35).

The petrosal is wedged in at the base of the skull between the sphenoid and occipital. Its base is fused with the squamosal and mastoid portion. The apex is received into the angular interval between the posterior border of the sphenoid and the basilar part of the occipital.

In ventral view, the petrosal is dominated by a large, almond-shaped promontorium in the tympanic cavity, which is a prominent element in the basicranial region. The promontorium is broadest in its posterior edge and tapers toward

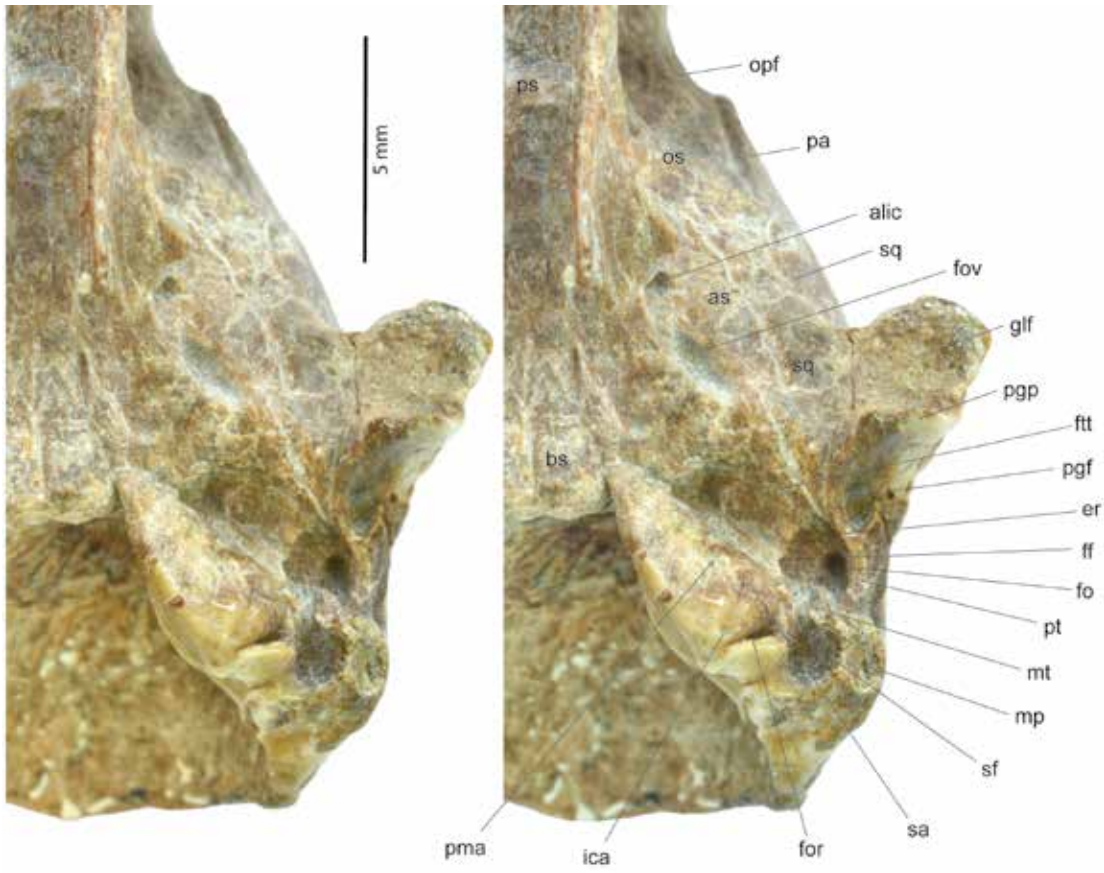

FIG. 33. *Hsiangolestes youngi*, IVPP V5436, stereophotograph of left ear region in ventral view.

the anteromedial corner of the tympanic cavity. The medial edge of the promontorium contacts the basisphenoid. Its lateral edge touches the thin bony roof, the tegmen tympani, of the tympanic cavity, where the tegmen tympani curves to contact the alisphenoid anteriorly with a short simple suture and the squamosal with a curved, interdigitated suture laterally. The promontorium is separated from the basioccipital by a large posterior lacerate foramen at its posteromedial aspect, and connects to the mastoid by a stout bony bridge posteriorly. A very short simple suture between the promontorium and mastoid can be seen in IVPP V5792 and V7454. The ventral surface of the promontorium is slightly convex and smooth. A large transversely oval foramen, the fenestra rotunda (cochleae), is situated at the posterior wall of the promontorium. The fenestra rotunda faces posteriorly. A well-developed dorsal rim of the promontorium extends more posteriorly and overhangs the antrum of the fenestra rotunda, so that the fenestra rotunda is fully covered by the dorsal rim as seen in V5346, or partially covered as in V7454. Medial to the fenestra rotunda, there is a distinct bony ridge (petrosal ridge, seen clearly in V7454), running from the posteromedial aspect of the promontorium and extending along the medial edge of the promontorium to the anteromedial aspect. Lateral to the fenestra rotunda is a large, circular fenestra ovalis (vestibuli). The fenestra ovalis is slightly smaller than the fenestra rotunda and opens laterally. Anterior to the fenestra rotunda, there is a distinct shallow

FIG. 34. *Hsiangolestes youngi*, IVPP V7454, stereophotograph of right ear region in **A.** turning lateral side to ventral and **B.** ventral views.

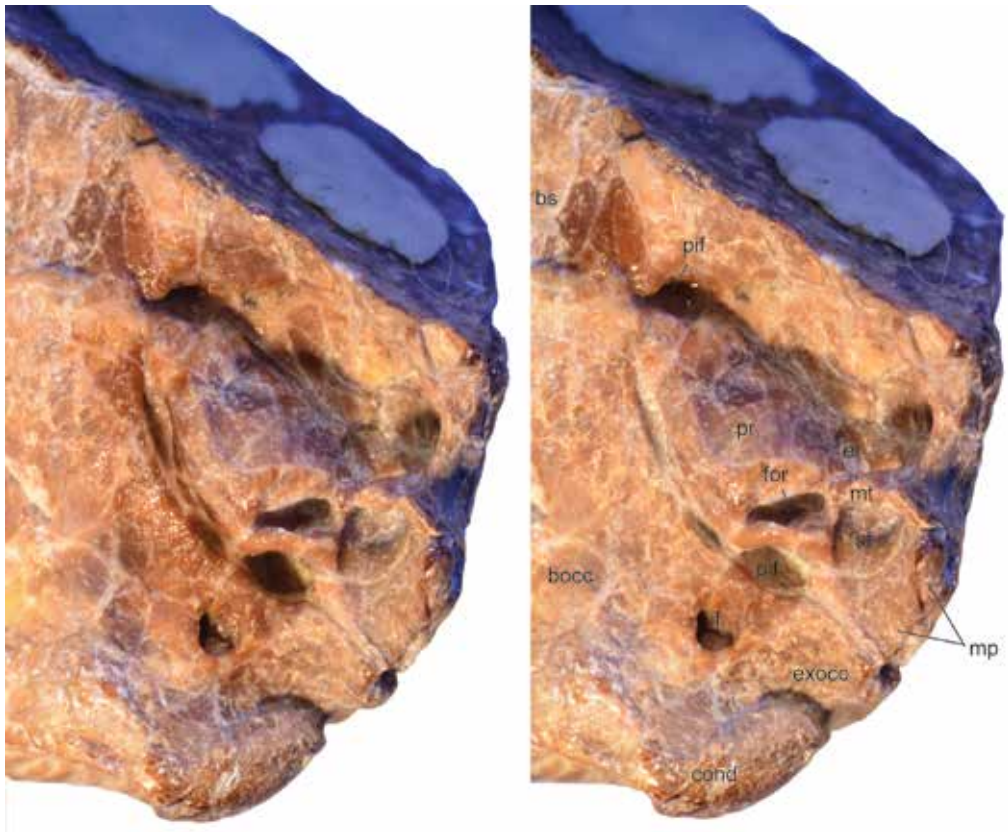

FIG. 35. *Hsiangolestes youngi*, IVPP V7454, stereophotograph of left ear region in ventral view.

groove, the sulcus for the internal carotid artery. The groove can be seen clearly at the medial side of IVPP V5346. It runs laterally from the posterior end of the petrosal ridge at the posteromedial aspect of the promontorium. It bifurcates soon into two branches in front of the fenestra rotunda: one continuing laterally toward the fenestra ovalis for the stapedial artery, and the other turning anteriorly for the promontory artery. The stapedial groove meets the medial rim of the fenestra ovalis. The sulcus for the promontory artery has left a short, clear trace after its branching from the sulcus for the internal carotid artery at the middle of the posterior edge of the promontorium. It becomes obscure for the rest of its pathway.

Lateral and anterior to the fenestra ovalis, there is a canal covered by a thin bony plate. Its posterior opening, a round foramen, is situated anterolateral to the fenestra ovalis and its anterior opening connects with the piriform fenestra. We identify it as the facial canal and its posterior opening as the stylomastoid foramen. The facial nerve comes out through the facial canal and stylomastoid foramen, and runs posteriorly to reach a large, deep fossa for the stapedial muscle that is situated posterolateral to the fenestra ovalis, lateral to the fenestra rotunda, and is partially covered by the mastoid tubercle ventrally. The fossa is bounded by the promontorium-mastoid suture posteriorly and the squamosal-mastoid suture laterally. Medial to this fossa is a bony bridge at the posterior end of the promontorium, which connects the promontorium and the mastoid bone and separates the fossa from the posterior lacerate foramen. The posterior lacerate

foramen is large, elliptical, and situated at the posteromedial aspect of the promontorium. It is surrounded by the promontorium anterolaterally and the basioccipital posteromedially, and is separated from the jugular foramen by the basioccipital. The posterior lacerate foramen transmits the cranial nerves IX, X, and XI. At the posteromedial aspect of the promontorium is a very large, circular foramen, the jugular foramen, containing the internal jugular vein. Presence of a distinct jugular foramen separate from the posterior lacerate foramen is a primitive condition for eutherians (Novacek, 1986: table 3). This foramen is situated in the suture between the petrosal and the basioccipital. Anterior to the posterior lacerate foramen is a narrow furrow that extends from the anterior tip of the foramen to the anteromedial aspect of the promontorium. It separates the promontorium from the basioccipital posteriorly and the basisphenoid along the promontorium-basisphenoid suture. In the right side of IVPP V5792, the promontorium is well fused with the basisphenoid. Anterolateral to the promontorium is a shallow fossa for the muscle tensor tympani. The fossa is shallow and elliptical, which can be seen in the right side of IVPP V5792. Anteromedial to the fossa for the muscle tensor tympani is a very large oval piriform fenestra, which is situated at the anterior wall of the tympanic cavity. The epitympanic recess is well preserved in all the specimens. It is large and round, covered by the squamosal laterally, and lies next to the facial canal medially. On the right side of IVPP V7454, there are two fragments of ear ossicles preserved in the epitympanic recess (fig. 34A).

There is no bony tympanic bulla preserved in any of the specimens. An almost complete ectotympanic (tympanic ring) is preserved on the right side of IVPP V7454, which is slightly moved from its original position (figs. 34A, B). The tympanic ring is inclined. Its dorsal part is broken, so that both anterior and posterior crura are separated from the body. It is annular in shape. The dorsal plate of the tympanic ring is separated and much narrower than the ventral part, and each dorsal plate has a round projection laterally. The ventral part of the tympanic ring is wider and flat. The lateral side of the tympanic ring is smooth and circular; however, the medial side of the ring has a widely open U-shaped concave area at its anterior edge.

In the intracranial view of the left side of the medial surface of the petrosal in IVPP V5346 and the cross sections of IVPP V7438, the most prominent features are two circular fossae, a large subarcuate fossa in the dorsal side and another shallow depression, which is the entrance of the internal acoustic meatus and the opening for facial nerve into facial canal in the ventral (fig. 30: sections 61–75). The subarcuate fossa is deep, oval, and transversely situated. The ventral depression for the internal acoustic meatus and facial foramen is oval and slightly smaller than the subarcuate fossa. Two small foramina are situated in the shallow depression, the internal acoustic meatus slightly anteroventrally and the facial foramen, slightly posterodorsally. There is a long, narrow groove along the dorsomedial edge of the promontorium, running from the posteromedial aspect of the promontorium to its anteromedial aspect. This groove may be interpreted as the sulcus of the inferior petrosal sinus. A small foramen is situated on this groove, just dorsal to the fenestra rotunda.

The mastoid is a prominent element and is best preserved in IVPP V5792 and V7454. It is located between the ventral end of the dorsal nuchal line laterally and the jugular process ventromedially (figs. 33, 34A, B, 35). In ventral view, the mastoid is roughly rectangular. Medially, it contacts the jugular process of the occipital in a short, straight suture. Laterally, it contacts the posttympanic process of the squamosal in a simple curved line. Anteriorly, the mastoid connects the promontorium of the petrosal by a stout bony bridge with a very short simple suture medially and the tympanic bone with a short simple suture laterally, which is fused in some individuals. The mastoid has a well-developed distinctive spherical tubercle, which is located medial to the mastoid-posttympanic suture and

extends almost to the lateral side of the promontorium (figs. 33, 34A, B, 35). Dorsal to the mastoid tubercle, there is a deep, round fossa, and a bony plate connecting with the mastoid tubercle and extending dorsally to reach the tegmen tympani in the tympanic cavity. The posterior edge of the mastoid is widely open and U-shaped. The surface of the mastoid is smooth, broad, and slightly concave, without a deep groove.

In lateral view, the mastoid forms the posteriormost part of the skull. It is roughly T-shaped and narrow, with a smooth surface. It contacts the squamosal anteriorly with a simple curved mastoid-squamosal suture, and the lambdoid crest of the occipital dorsally with a very short, straight suture. The mastoid continues from the lambdoid crest of the occipital, contacting the lower part of the lambdoid crest.

In occipital view, the mastoid has a very narrow exposure at the lower lateral aspect of the occipital region. It is rectangular and bends medially, forming a deep furrow with the exoccipital on the other side. Ventral to the mastoid-occipital suture in the furrow, there is a small foramen that may be a mastoid foramen. Medially, the mastoid contacts the exoccipital in a narrow, deep furrow, and dorsally contacts the supraoccipital with a short simple suture.

Occipital: The occipital is well preserved in IVPP V5792 and V7454. The sutures of the occipital with neighboring bones can be seen best in V7454. In posterior view, the occipital is trapezoidal, narrower dorsally, and wider ventrally. The occipital projects posteriorly beyond the lambdoid crest. The supraoccipital occupies the whole middorsal part in occipital view of the skull and is trapezoidal. The surface of the supraoccipital is slightly concave at its middle part, and has no median crest. The supraoccipital contacts the lambdoid crest dorsally and the exoccipital laterally. The ventral part of the supraoccipital forms the dorsal rim of the foramen magnum. The supraoccipital-exoccipital suture is a simple straight line, running from the lateral side of the lambdoid crest to the dorsal rim of the foramen magnum at a knob. Lateral to the supraoccipital-exoccipital suture is a prominent vertical ridge that separates the supraoccipital from the exoccipital. The exoccipital is roughly rectangular and extends in a slope anterolaterally from this ridge. A distinctive wide and deep furrow separates the exoccipital from the mastoid. The mastoid has a broad exposure in occipital view and extends anteriorly into the furrow. The dorsal atlantal facet at the edge of the foramen magnum is widely open, oval, with two knobs at the supraoccipital-exoccipital suture. The paroccipital process is well developed, and is large and elongate dorsoventrally. It contacts the exoccipital dorsally and the mastoid process laterally. The paroccipital-exoccipital suture is simple, short, transversely situated in the occipital region, and the mastoid-paroccipital suture is simple and straight. The paroccipital is separated from the condyle by a wide notch, which is formed by the ventral border of the exoccipital. The paroccipital is well separated from the mastoid process by a distinctive straight suture in ventral view, and it contacts the basioccipital anteriorly in a short, simple suture that reaches the middle of the medial rim of the posterior lacerate foramen. The foramen magnum is oval, oriented transversely, and faces posteriorly. The dorsal rim of the foramen has two knobs, which divide the rim into three parts. The dorsal lobe of the occipital condyle is transverse, slender, and separated from the opposite side by a wide gap. The lobe has a strong convex curvature. The anterior border of the occipital condyle has a sharp crest that separates it from the exoccipital. The ventral lobe of the occipital condyle can be seen only in IVPP V7454. It is slightly convex and extends transversely. A single small circular foramen, the hypoglossal foramen, is situated anterior to the anterior edge of the occipital condyle (fig. 34A, B). Anterolateral to the hypoglossal foramen is the jugular foramen, which is very large and situated just at the basioccipital-petrosal suture (figs. 34A, B, 35).

The basioccipital, a large element in the posteroventral part of the skull, is a narrow trapezoid, extending anteroposteriorly (figs. 34A, B,

35). It consists of the ventral lobe of the occipital condyle, the shallow area between the condyle and the low paroccipital process, and the posterior lacerate foramen. The basioccipital contacts the basisphenoid anteriorly, the petrosal laterally, and the rest of the occipital posteriorly. The basioccipital-basisphenoid suture is a short straight line and situated at the level at the anterior edge of the petrosal. The basioccipital-petrosal suture is a coarsely interdigitated, straight line along the medial border of the petrosal. Posterior to the basioccipital is the ventral lobe of the occipital condyle.

Postcranium

Vertebrae and Rib: Four cervical vertebrae are preserved with the skull in IVPP V7454 (figs. 36, 37). Some postcranial elements are preserved with the skull V5797, including a partial rib, pelvic girdle, femur, tibia, and almost complete left and right pedes. We consider that these postcranial elements most likely belong to the same individual as the skull IVPP V5797 based on the position and preservation (figs. 38A, 38B).

The atlas, axis, and third and fourth cervical vertebrae are articulated with the skull in IVPP V7454 (figs. 36, 37). The axis and the third and fourth cervical vertebrae are twisted during fossilization, so that the spinous process of the axis is posteriorly located at the right side of the posterior edge of the dorsal arch of the atlas near the intervertebral foramen of the atlas.

The atlas is well preserved except the ventral part. The dorsal (neural) arch of the atlas is completely preserved. The surface of the arch is smooth and flat, and has no clearly developed dorsal tubercle. However, there is a well-preserved, V-shaped curve at the position where the bifurcated dorsal tubercle should be located, which may indicate that a weak bifurcated dorsal tubercle may have been present. Both right and left intervertebral foramina are well preserved. They are large and round. The left side of the transverse process is almost completely preserved, but the right side of the transverse process is slightly damaged. The transverse process is large, thin, and wing shaped. The transverse process is situated at the posterior part of the body. The alar notch is deep and curved posteriorly. Ventral to the transverse process is a large, round transverse foramen for the vertebral artery. The left cranial articular fovea for the left condyle is better preserved than the right one; however, neither ventral parts of the articular fovea is preserved. The cranial articular fovea is roughly oval and extends dorsoventrally. The articular surface is slightly concave. Both right and left caudal articular fovea for the axis is completely preserved. The articular fovea is roughly round. The surface of the caudal articular fovea is flat and directed posteriorly.

The axis is best preserved, with only the right transverse process slightly damaged. The body of the axis is short and has a prominent keel at the middle of the ventral side. The surface of the ventral side of the body is smooth, concave along the keel. The dens (odontoid process) is well developed, cranioventrally oriented, and anterior to the body. Posterior and lateral to the dens is a slightly convex cranial articular surface (facies articularis dorsalis of Wible, 2009: 50, fig. 21). The dorsal spinous process is long, thin, and overhangs the cranial and caudal articular surfaces of the vertebral body. The anterior tip of the spinous process is located at the level of the anterior edge of the cranial articular surface. The posterior tip of the spinous process touches the third cervical vertebrae in the specimen, possibly due to deformation of the third cervical vertebrae. The transverse process is a small projection, extending posterolaterally from the posterior edge of the posterior opening of the transverse foramen. The transverse foramen is well preserved on both sides of the axis at the dorsal part of the vertebrate body. A thin bone in lateral view separates the anterior and posterior opening of the transverse foramen. The caudal articular surface is well preserved and is roughly round and slightly concave.

The third cervical vertebra and the anterior part of the fourth cervical vertebra are articu-

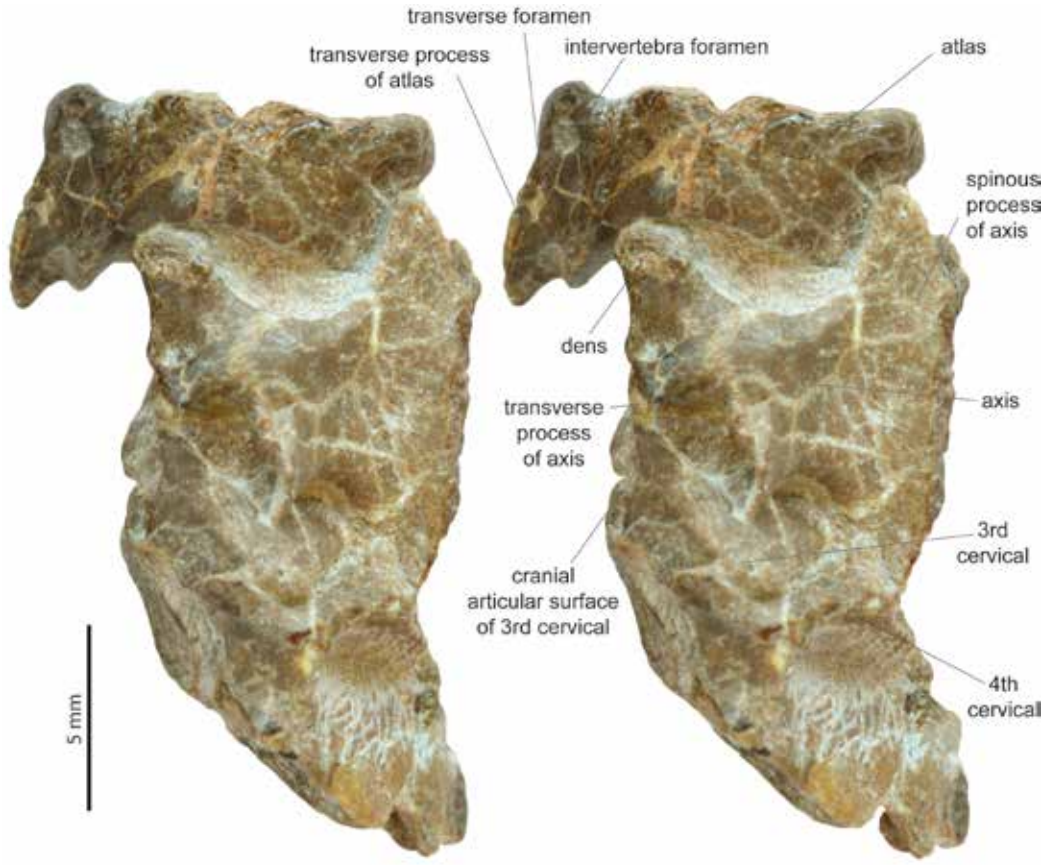

FIG. 36. *Hsiangolestes youngi*, IVPP V7454, stereophotograph of cervical vertebrae in lateral view.

lated with the axis. The third is slightly shorter and narrower than the fourth. The bodies of the third and fourth cervical vertebrae are short and have a well-developed keel at the middle of the ventral side. The ventral surface of the body, along both sides of the keel, is strongly concave. There is no indication of the spinous process on the third cervical vertebra, or it is not well preserved, and the spinous process is not preserved on the fourth cervical vertebra. The cranial articular surfaces of the third and fourth cervical vertebrae are well preserved. They are roughly round and flat. The caudal articular surface is preserved only in the third cervical vertebra, which is articulated with the cranial articular surface of the fourth cervical vertebra. The transverse foramen is well preserved in both the third and fourth cervical vertebrae. It is large and round. The transverse process is preserved only at the right side of the third cervical vertebra. It is long and extends posterolaterally from the lateral side of the transverse foramen.

Several postcranial bones preserved with the skull IVPP V5797 (fig. 38). The preserved part of rib (fig. 39C) is very thin and short. The proximal end is widely curved and distal end is straight. The cross section of the rib is roughly round.

Pelvic Girdle: An incomplete right pelvic girdle is preserved (fig. 39B). The ilium and ischium are slender and narrow. The ilium has an elongate wing, and its preserved part is about 14 mm. The lateral surface of the ilium wing is not well preserved and most of the surface has been damaged. The partial superior gluteal fossa is

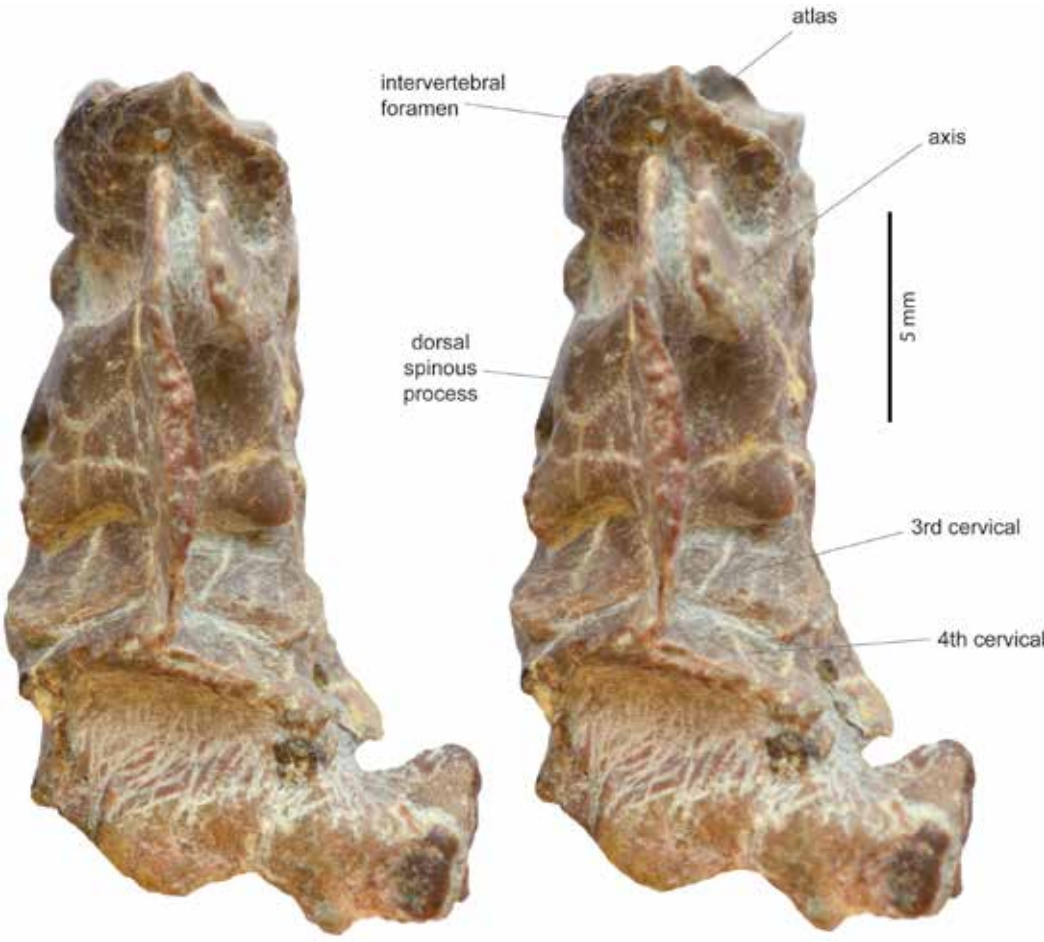

FIG. 37. *Hsiangolestes youngi*, IVPP V7454, stereophotograph of cervical vertebrae in dorsal view.

preserved at the lower posterior region. The surface of the fossa is slightly concave. The ventral surface of the ilium wing is damaged. The medial surface of the ilium wing is narrow and slightly concave along the middle part of the ilium body. The acetabulum is a nearly round open socket with the diameter about 6 × 6 mm. Most of the edge of the acetabular fossa is not well preserved, so that the lunate surface is not clearly seen. The well-preserved anterior body of the ischium is about 8 mm in length; it extends posteriorly along the same axis as the ilium and is thicker than the latter. The lateral surface of the ischium is strongly convex with two longitudinally elongated facets along the midline of the body. The dorsal margin of the anterior body of the ischium is smooth with a well-preserved greater sciatic notch. The anterior body of the ischium bears a low ischiatic spine. The medial surface of the ischium is smooth, strongly concave at its anterior part. The pubis is not preserved.

Femur: A distal portion of the left femur is preserved (fig. 39A). The preserved part is about 23 mm. The femoral body is narrow and straight, its dorsal surface strongly convex and plantar surface flat. The cross section of the femoral body is oval, about 4.5 × 3.5 mm in diameter. The patellar trochlea is long, narrow, and well defined by the trochlear ridges. The lateral trochlear ridge is slightly higher than the medial one.

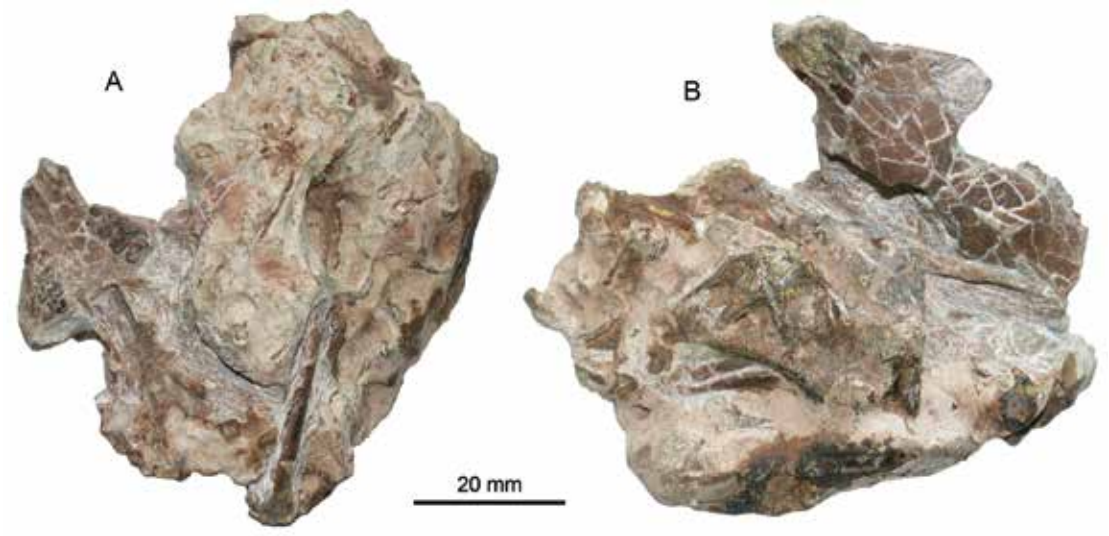

FIG. 38. *Hsiangolestes youngi*, IVPP V5797, skull and postcranial bones: **A.** ventral and **B.** dorsal views of skull, showing preservation before preparation.

Both of the femoral condyles are well preserved, but the lateral surface of the lateral condyle is slightly damaged. The lateral condyle is slightly larger than the medial one and extends further, both distally and posteriorly. The lateral surface of the condyle is slightly convex and the medial surface is flat. The intercondylar fossa is long, deep, and rectangular. The fossa is separated and well defined by the sharp ridges on both dorsal and plantar sides. There is a roughly triangular shallow depression on the upper aspect of the lateral surface of the lateral condyle.

Tibia: A nearly complete right tibia is preserved (fig. 39D). It is about 31 mm in length. The body of the tibia is slender and gently curved. The upper part of the dorsal surface of the tibia is strongly convex and has a sharp and narrow ridge, the tibial crest. The lower part of the dorsal surface of the body is convex. The tibial crest extends mediolaterally about half the length of the tibia. The lateral surface of the tibia is flat, but has a deep lateral tibial fossa near the upper part of the tibial crest. The medial surface of the body of the tibia is slightly convex and has no clear medial tibial fossa. Both lateral and medial condyles of the tibia are not preserved. The upper part of the plantar surface of the tibia is concave, but its lower part is flat. A possible left tibia shows that the articular surface for the astragalus is strongly concave, and transversely situated (fig. 40). The medial malleolus of the tibia is round, strongly projecting medially, and separated from the tibia by a narrow notch.

Fibula: A fragmentary distal end of the left fibula may be preserved, but its morphology is not clear (fig. 40).

Calcaneus: A partial left calcaneus is preserved and articulated with the astragalus; however, the articular surface is not well preserved (fig. 40). The peroneal process can be seen clearly. It projects ventrally and is triangular in lateral view.

Astragalus: A partial left astragalus is preserved, but was dislocated, with damage to the mediodorsal surface, so that the trochlea and astragalotibia facet cannot be seen (fig. 40). The astragalus is articulated with the distal end of the calcaneus, but not articulated with the tarsals below, due to a lateral shift during burial. The body of the astragalus is long and rectangular in anterior view. The head of the astragalus is separated from the body by a relatively long and nar-

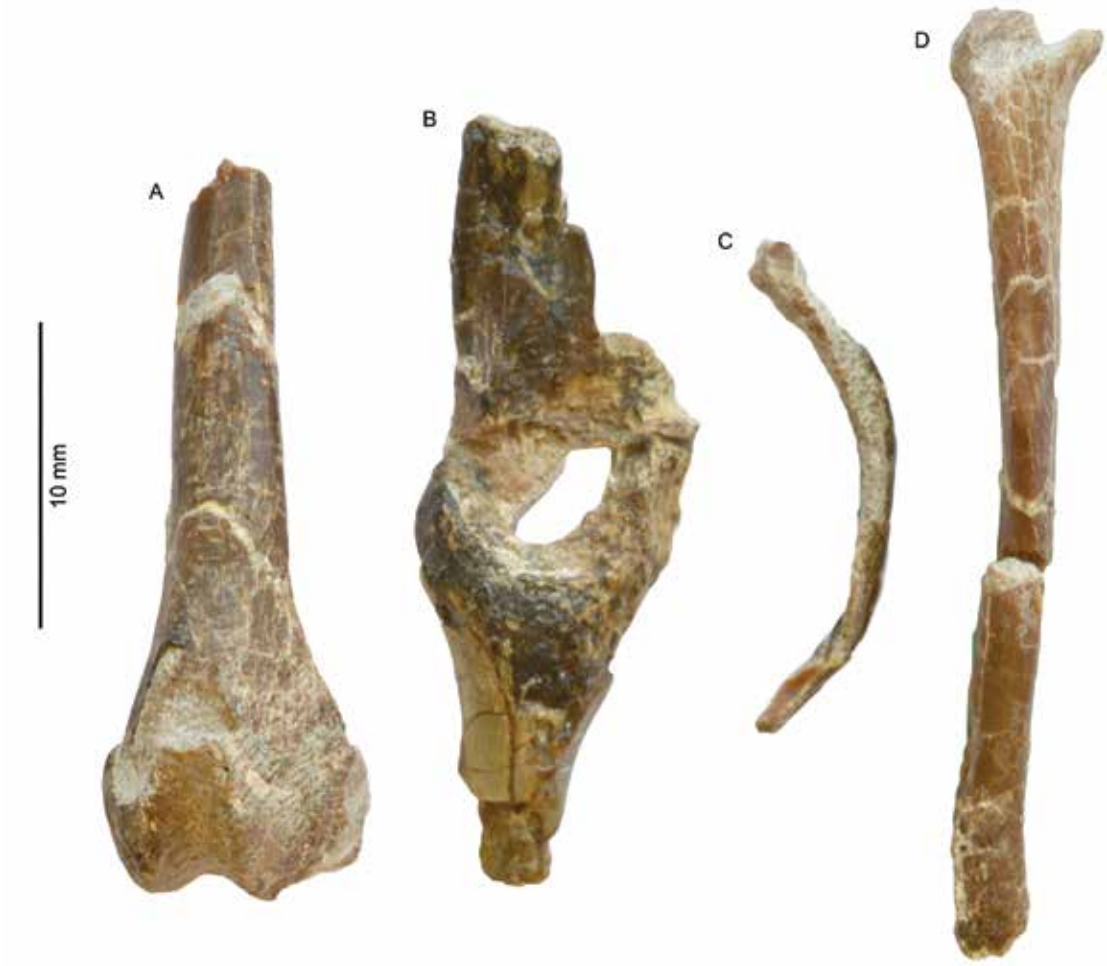

FIG. 39. *Hsiangolestes youngi*, IVPP V5797: **A.** left femur; **B.** right pelvic girdle; **C.** rib; **D.** right tibia.

row neck. In anterior view, the head of the astragalus is oval and extends transversely. Its dorsal surface is gently convex, and the ventral surface (astragalo-navicular facet) is strongly convex and almost round. The astragalus has no contact with the cuboid.

Navicular: The navicular is large and composed of two parts, the body (4 mm medial-lateral, 1 mm proximal-distal) and the plantar process (2 mm medial-lateral, 4 mm proximal-distal) (figs. 40, 42). The body is proximodistally compressed. The proximal and distal surfaces of the body of the navicular are semilunar. The proximal surface is concave, transversely extending, and articulated with the head of the astragalus only. The distal surface contacts the entocuneiform medially, the mesocuneiform at its middle part, and the ectocuneiform laterally. It may contact the cuboid at its lateral aspect. The dorsal surface of the navicular is rectangular, rough, and slightly convex. The plantar process of the navicular is very large, massive, thick, and rectangular. It extends distally directly from the navicular body at a right angle and is situated at the opposite of the navicular body. The plantar surface of the plantar process is convex and rough. The proximal end of the plantar surface of the plantar process has a short, shallow depres-

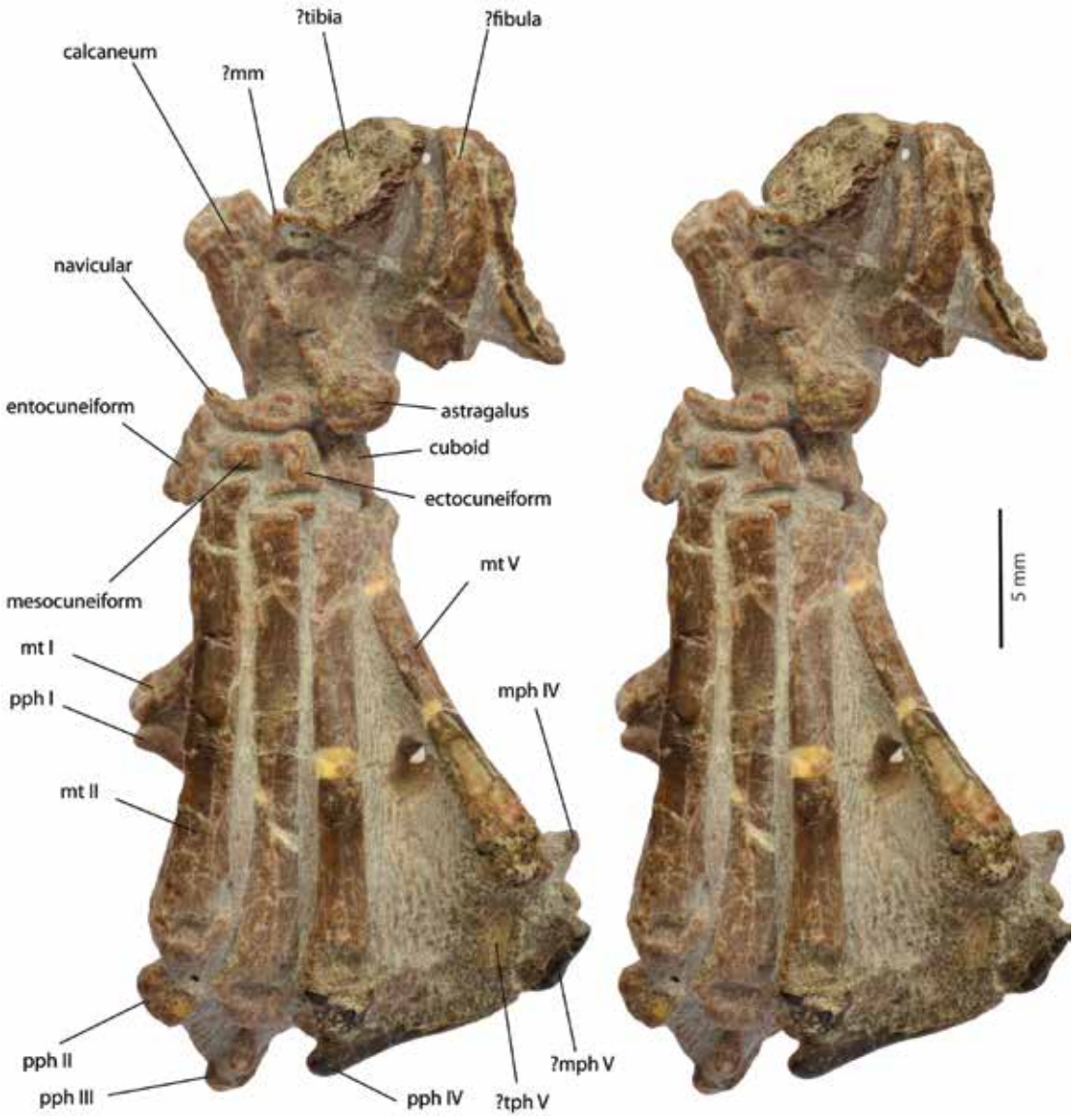

FIG. 40. *Hsiangolestes youngi*, IVPP V5797, stereophotograph of left pes in plantar view.

sion. A small, nearly round, concave surface in the proximal surface of the plantar process may be the calcano-navicular facet. The navicular entirely covers the proximal end of the entocuneiform.

Cuboid: The cuboid is well preserved in the left foot (figs. 40, 42). However, the cuboid in the right foot was distorted and dislocated, so that its distal surface was squeezed over the proximal surface of the metatarsal IV (figs. 42, 43). The cuboid is larger than the ectocuneiform and almost square (3 mm medial-lateral, 3 mm proximal-distal, 1 mm dorsal-plantar). The dorsal surface of the cuboid is flat, partially faces dorsally, turns laterally, and is gently convex. The cuboid has a big process at its proximal-medial

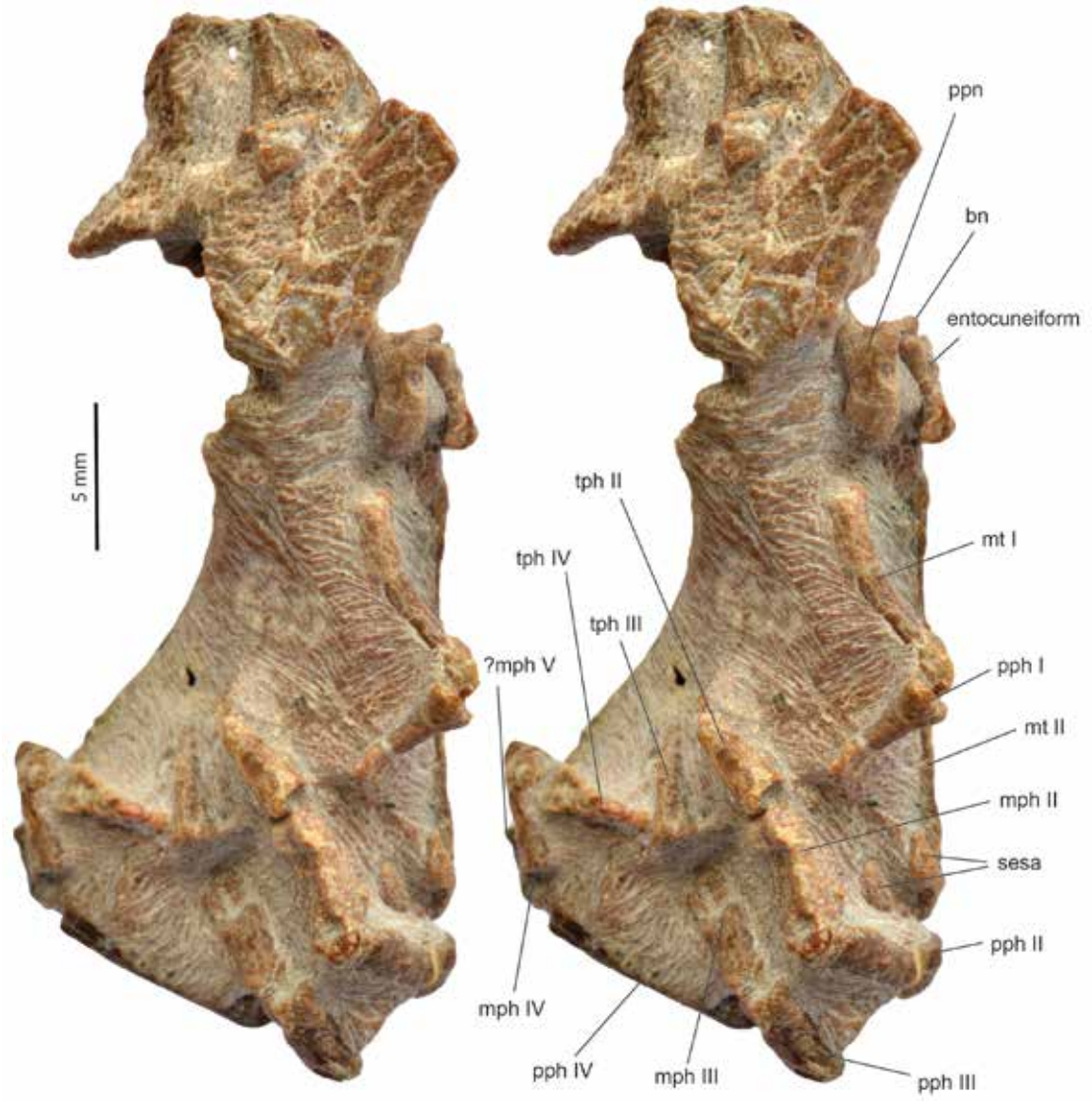

FIG. 41. *Hsiangolestes youngi*, IVPP V5797, stereophotograph of left pes in palmar view.

aspect that probably contacted the navicular. The medial edge of the cuboid is strongly curved. The cuboid has a distinct process at its upper lateral aspect, projecting laterally. The cuboid contacts the metatarsal IV medially with a slightly concave surface. It contacts the metatarsal V at its distolateral aspect.

Ectocuneiform: The ectocuneiform is much larger than the mesocuneiform and almost square (2.4 mm medial-lateral, 2.3 mm proximal-distal) (figs. 40, 42). Its medial edge is strongly curved laterally, and its dorsal surface is gently convex. The ectocuneiform contacts the navicular at the lateral aspect of the navicular, the mesocuneiform at the upper medial aspect of the ectocuneiform, and the cuboid laterally. The articular surface of the ectocuneiform-navicular is slightly convex. The ectocuneiform mainly

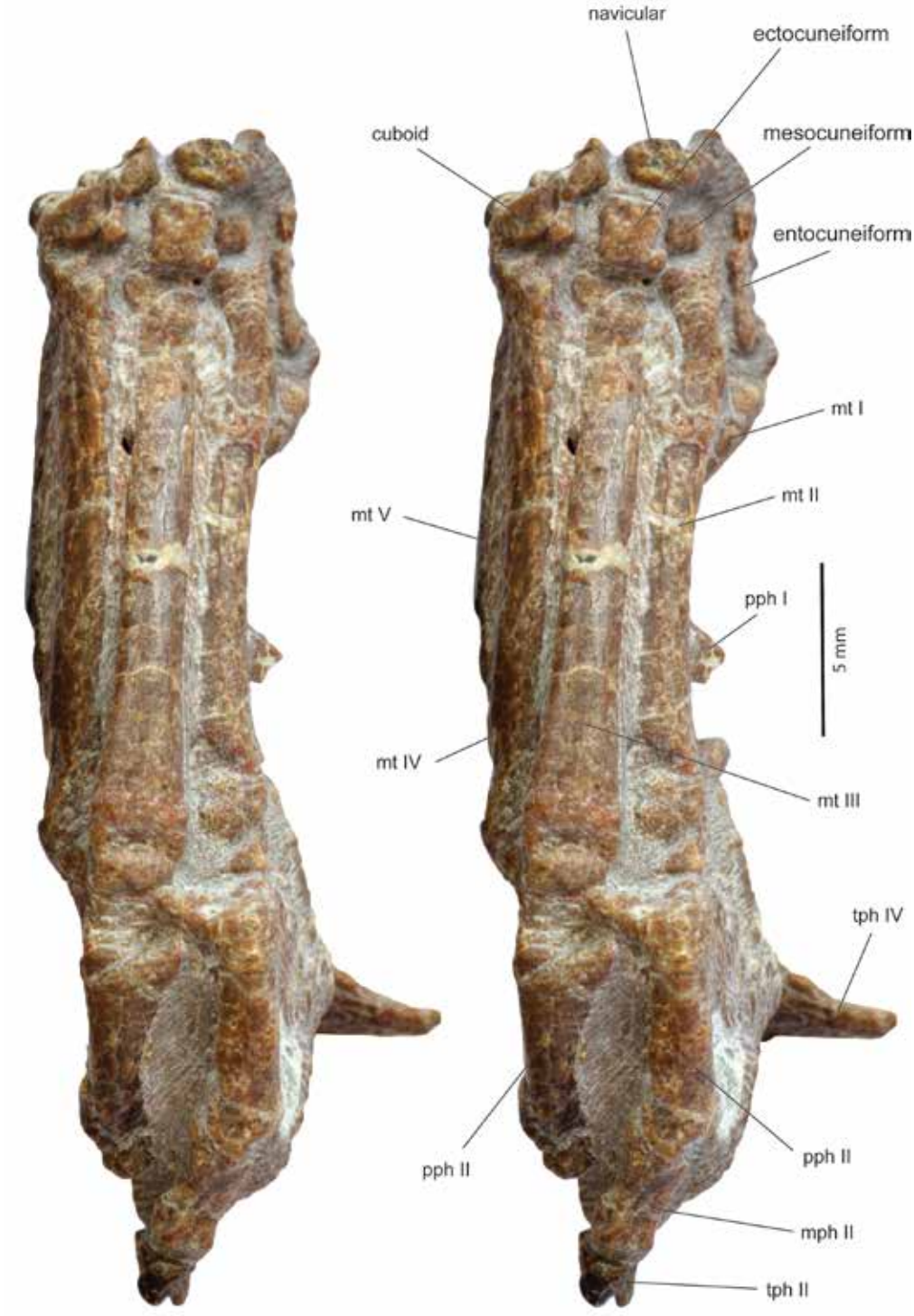

FIG. 42. *Hsiangolestes youngi*, IVPP V5797, stereophotograph of right pes in plantar view.

contacts the metatarsal III at its distal end, and may contact the metatarsal II at its medial distal aspect and the metatarsal IV at its lateral distal aspect. The articular surfaces of both the ectocuneiform-mesocuneiform and the ectocuneiform-metatarsal III are gently concave.

Mesocuneiform: The mesocuneiform is the smallest among the tarsals (figs. 40, 42). The mesocuneiform is proximodistally compressed and flat. In dorsal view, it is rectangular, transversely extended (1.9 mm medial-lateral, 1 mm proximal-distal). It contacts the navicular proximally at the middistal part of the body of the navicular, the entocuneiform medially at the middle part of the lateral side of the entocuneiform, the ectocuneiform laterally at the mediopoximal aspect of the ectocuneiform, and the metatarsal II distally. The mesocuneiform-navicular and the mesocuneiform-ectocuneiform facets are flat. The mesocunieform-entocuneiform facet is gently convex, and the mesocuneiform-metatarsal II facet is slightly concave.

Entocuneiform: The entocuneiform is large, rectangular (2.3 mm medial-lateral, 5 mm proximal-distal, 1.3 mm dorsal-plantar) (figs. 40, 42). The dorsal surface of the entocuneiform is slightly damaged, but basically flat. The entocuneiform is completely covered by the navicular at its proximal end, so that it has no contact with either the calcaneus or the astragalus. The entocuneiform contacts the navicular at the medial aspect of the navicular body and the medial aspect of the plantar process of the navicular in a gentle curved line. It contacts the mesocuneiform at the middle part of the medial surface of the mesocuneiform. The entocuneiform contacts the metatarsal II in its lateral-distal aspect just beneath the entocuneiform-mesocuneiform contact. The entocuneiform contacts the metatarsal I distally in a concave surface.

Metatarsals: All of the metatarsals are nearly completely preserved in both left and right feet (figs. 40, 41, 42, 43). They are basically articulated at their original position, except the left metatarsal I, which was shifted from its original position to the plantar side, and the right metatarsals I and V, which were curved plantarly because the right metatarsals are gently pressed together. Metatarsal II–V closely contact each other at their proximal end and separate slightly from one another distally. Metatarsal I is the shortest among the metatarsals (about a half the length of metatarsal III) and is much slenderer than the others. Metatarsal III is the longest and the most robust. Metatarsal II is slightly shorter than metatarsal IV, and metatarsal IV is slightly shorter than metatarsal III, but both of them are as robust as metatarsal III. Metatarsal V is much more slender than metatarsals II–IV, and is shorter than metatarsal II–IV, but much longer than metatarsal I. Metatarsals II–V are relatively flat dorsoplantarly. The plantar surfaces of the metatarsals are slightly arched and have a short keel at the distal ends. The dorsal surface of metatarsal I is flat and less expanded at the distal end. A small plantar tuberosity is situated at the proximal end of the metatarsals, and the plantar tuberosity in metatarsal III is larger than the others. The proximal surface of the metatarsals is dorsoplantarly elongated and narrower at the plantar side. The distal ends of the metatarsals are smooth and rounded[, without a ridge. A pair of sesamoid bones are associated with distal ends of the left metatarsal II and right metatarsal V (figs. 41, 43).

Phalanges: The proximal phalanges of the hallux are well preserved in both the right and left foot (figs. 40, 41, 42, 43). They (4.5 mm proximal-distal) are much shorter and more slender than their counterparts in phalanges II–V. The proximal end of the proximal phalange of the hallux (2 mm medial-lateral) is twice as wide as its distal end (1 mm) and both proximal and distal ends project dorsally, so that the dorsal surface is concave at its middle part, and its plantar surface is slightly convex. The proximal surface is concave and has a deep sulcus (groove) at its middle part, extending dorsoplantarly. The plantar surface of the distal end of the proximal phalanges of the hallux is strongly convex. The proximal phalanges II, III, and IV are about the same in length (8 mm) and longer than the pha-

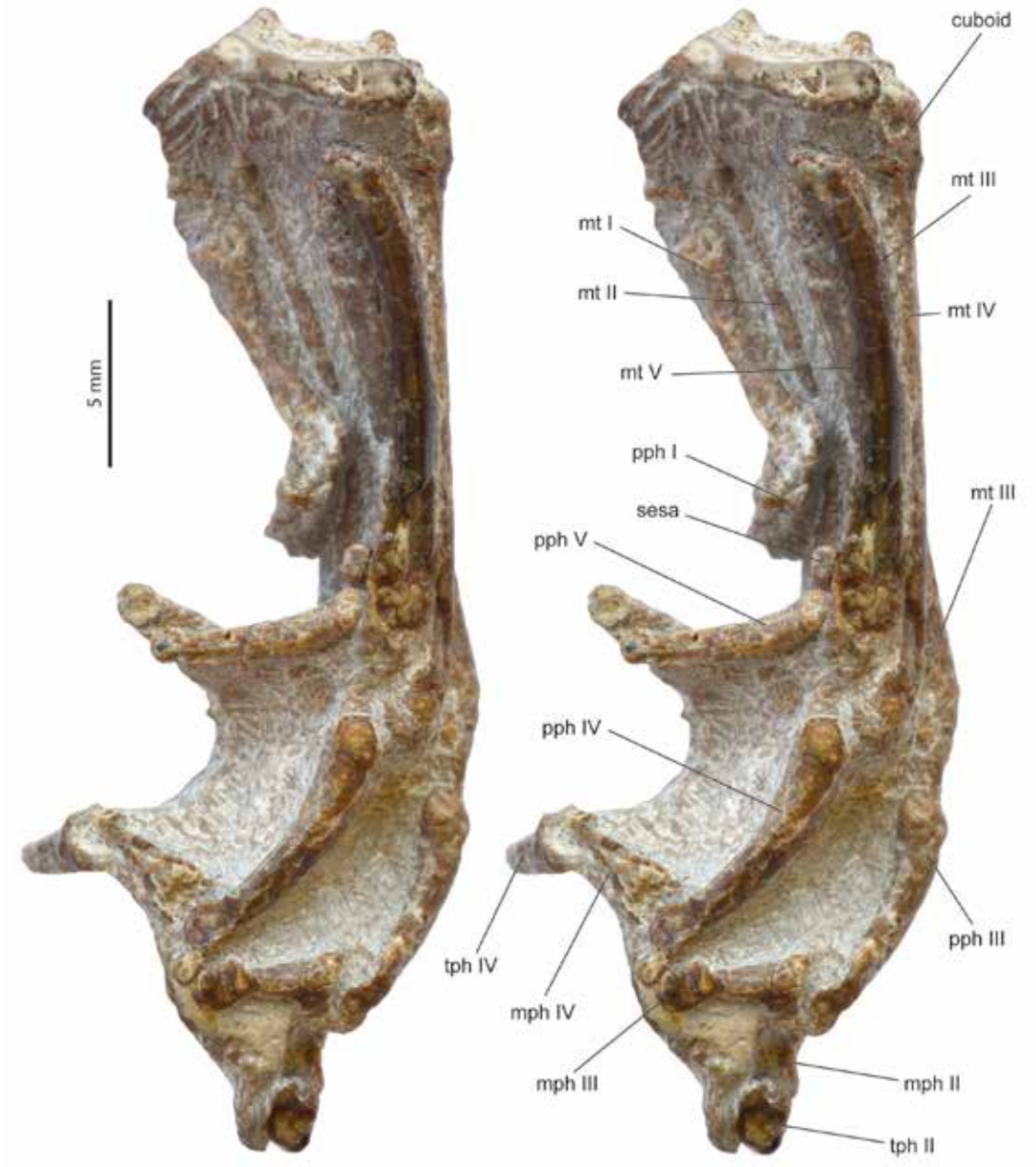

FIG. 43. *Hsiangolestes youngi*, IVPP V5797, stereophotograph of right pes in palmar view.

langes V (6 mm). Their dorsal surfaces are gently convex and slightly curve plantarly. Their proximal articular facet is somewhat rectangular, gently concave. It has a deep sulcus at the midline, extending dorsoplantarly. The dorsal surface of their distal ends is somewhat flattened, and the plantar surface is spherical. The middle phalanges of the right and left phalanges II, III, and IV are well preserved, but some of them were bent at the plantar side of the foot during burial (figs. 41, 43). They are much shorter (4.5 mm proximal-distal) than the proximal phalanges. Both

the proximal and distal ends of the middle phalanges are expanded transversely and dorsoplantarly, so that the phalanges are narrower at the middle. The dorsal surface is relatively flat and the plantar surface is gently concave at the middle. The proximal articular facet is about square and forms a shallow depression at the middle part, which is bordered by the lateral and medial ridges. The distal articular facet is about spherical, with a relatively deep groove at its plantar side, and the facets extend to the dorsal and plantar sides. The terminal phalanges are well preserved in the right phalange IV and left phalanges II, III, and IV. The terminal phalanges are about the same length as the middle phalanges (4.5 mm proximal-distal), slender, transversely compressed, and clawlike. They taper from the proximal end toward the distal end. The dorsal surface is strongly convex and ridgelike at its middle part. The plantar surface has a large round tubercle at its proximal end and becomes narrow, ridgelike, and relatively flat toward the tip. The proximal articular facet is roughly oval and elongated dorsoplantarly. It is strongly concave and forms a depression surrounded by ridges. The distal end is narrow and pointed.

Family Cimolestidae Marsh, 1889

Naranius Russell and Dashzeveg, 1986

Type Species: *Naranius infrequens*, Russell and Dashzeveg, 1986

Included Species: *Naranius hengdongensis* (*N.* cf. *infrequens* of Ting, 1995, 1998), new species.

Distribution and Age: Early Eocene (Bumbanian Asian Land Mammal Age), Bumban Member of Naran-Bulak Formation, Tsagan-Khushu, Nemegt Basin, Mongolia; Early Eocene (Bumbanian Asian Land Mammal Age), Lingcha Formation, Hengyang Basin, Hunan Province, China.

Revised Diagnosis: This is a very small animal with considerably reduced P2–3 and p2–3 smaller than both preceding and subsequent premolars, P3 with two roots (char. 31), P4 anterior and posterior edge symmetrical (char. 48), p2 with posterior accessory cuspule (char. 54), presence of diastema posterior to p2 (char. 56), molar protocone without labial shift (char. 97), postcingulum situated lingual to metaconule position (char. 100), presence of rudimentary hypocone (char. 101), M3 without hypocone (char. 108), and M3 without metacone (char. 109).

Naranius hengdongensis, new species

Figures 44–52; tables 1–3

Naranius cf. *infrequens* Ting, 1995, 1998.

Type Specimen: IVPP V7439, a complete skull with associated mandibles, with a small piece of enamel of right I, partial left and right I2, left and right I3, left and right C–M3, fragmentary left i1, partial i2, left i3, left c–m2, right c, right p1–2, and right p4–m3 (field number, 82002).

Referred Specimens: IVPP V5352, nearly complete skull with associated mandibles, with partial left C, left P1–M3, left c, and left and right p4–m3; IVPP V5353, most of skull with associated mandibles, with very fragmentary left M1–3, right P4, right M2–3, fragmentary left p4–m2, and right p4–m3 (field number: 76003); IVPP V7440 (? Insectivora gen et sp. nov. of Ting, 1995), anterior half of skull with associated mandibles, with left I3, right I1–3, left and right C, left and right P2–M3, and left and right i1–m3 (field number: 82001).

Distribution and Age: Early Eocene (Bumbanian Asian Land Mammal Age), Lingcha Formation, Hengyang Basin, Hunan Province, China.

Etymology: Species named for the Hengdong County, Hengyang Basin, Hunan Province, China, where the fossils were collected.

Diagnosis: *Naranius hengdongensis* differs from the type species, *N. infrequens*, in having longer diastema posterior to p1 (char. 52), p4 without cingulid (char. 69), metacrista prominent instead of salient (extending from side of metacone to metastyle) (char. 87), preprotocrista

extending labially past base of paracone (char. 89), only one mental foramen (char. 131), coronoid process vertically situated (char. 135), and with large infraorbital canal (char. 160).

Dentition

Dental Formula: 3.1.4.3/3.1.4.3. The dental formula of *Naranius*, 3-1-4-3, was proposed by Russell and Dashzeveg (1986) based on the holotype, a left mandibular fragment with p3–m1 and alveoli of p1–2 (PSS 20-73). Lopatin (2006) reported upper dentition with left maxillary fragment with P2–M2 (PIN 3104/1001) and left maxillary fragment with M1–3 (PIN 3104/1003); however, those specimens are not associated. The specimens IVPP V5353, V7439 and V7440 provide the best-preserved dentition, indicating that the dental formula of *Naranius* is 3.1.4.3/3.1.4.3.

In IVPP V7440, there are three left and right upper premolars preserved. We suggest that it is most likely this is a juvenile individual and its P1 has not erupted (fig. 44A, B). Study of the sequence of dental eruption (Slaughter et al., 1974: 116, table 1) indicates that the eruption sequence of the upper dentition of some eutherians is as follows:

Tenrecidae
- *Tenrec ecaudatus* M1-M2-M3-P4-P2-P3
- *Setifer setosus* M1-M2-M3-P2-P3-P4
- *Microgale dobsoni* M1-M2-M3-P4/P2-P3

Leptictidae
- *Ictops bicuspis* DP1-M1-M2-M3-P2/P4-P3

Erinaceidae
- *Echinosorex gymnurus* DP1-M1-M2-M3-P4/P2-3
- *Hylomys suillus* DP1-M1-M2-M3-P4-P3-P2
- *Erinaceus* sp. M1-M2-M3P4/P3-2
- *Atelerix pruneri* M1-M2-M3-P4-P3/P2

Macroscelididae
- *Nasilio brachyrhynchus* DP1-M1-M2-P4-P3/M3-P2
- *Elephantulus* (mixture of species) DP1-M1-M2-P4-P3-P2

Tupaiidae
- *Tupaia glis* M1-M2-M3-P2-P4-P3

The sequence of tooth eruption of some leptictids and erinaceids shows that the molars erupted before the permanent premolars (Slaughter et al., 1974). The DP1 is the first to be erupted in *Leptictis* (*Ictops) bicuspis*, *Echinosorex gymnurus*, and *Hylomys suillus*, and this may suggest that the permanent P1 may be the last one to be erupted, although documented DP1 replacements in mammals are rare enough to be cautious of such occurrences (Uhen, 2000; Asher et al., 2017; McKay et al., 2022). This situation occurs in IVPP V7349, in which the right P1–4 and left P2–4 are fully erupted; however, the left P1 is much smaller than the right, which is just erupting (fig. 45). The specimen IVPP V7440 possesses only left and right P2–4; however, the four lower premolars are all erupted. Based on the sequence of the tooth eruption and last erupting of P1 in IVPP V7349, we consider that the DP1 of IVPP V7440 was just lost, and P1 has not erupted.

Incisors: The right I1–3 and left I3 are well preserved in IVPP V7440 (fig. 44A, B), and the right I2–3 and left I3 are preserved in IVPP V7349 (fig. 45). The I1 is preserved only on the right side of the premaxilla of IVPP V7440, which is also the only known I1 among all of the specimens of this genus. I1 is small with a pointed tip and a long root, and situated in the anterior tip of the premaxilla. Its anterior surface is slightly convex, and its lateral surface is flat. The I2 and I3 are situated behind the I1 and closely spaced with each other at the lateral side of the premaxilla. The posterior edge of I3 is close to the premaxilla-maxillary suture. The I2 is about the same size and morphology as I3. The crown of I2 is blunt, peglike, oval in cross section, and thicker mediolaterally. A small oval wear facet occurred on the medial side of the anterior edge of the crown. The anterior edge of the crown of I2 is somewhat perpendicular to the toothrow, and the posterior edge slightly leans anteriorly. The I3 is laterally compressed and peglike. The anterior edge of I3 is slightly curved, so that the tip of the crown is slightly pointing posteriorly. There is a short anteroposterior gap

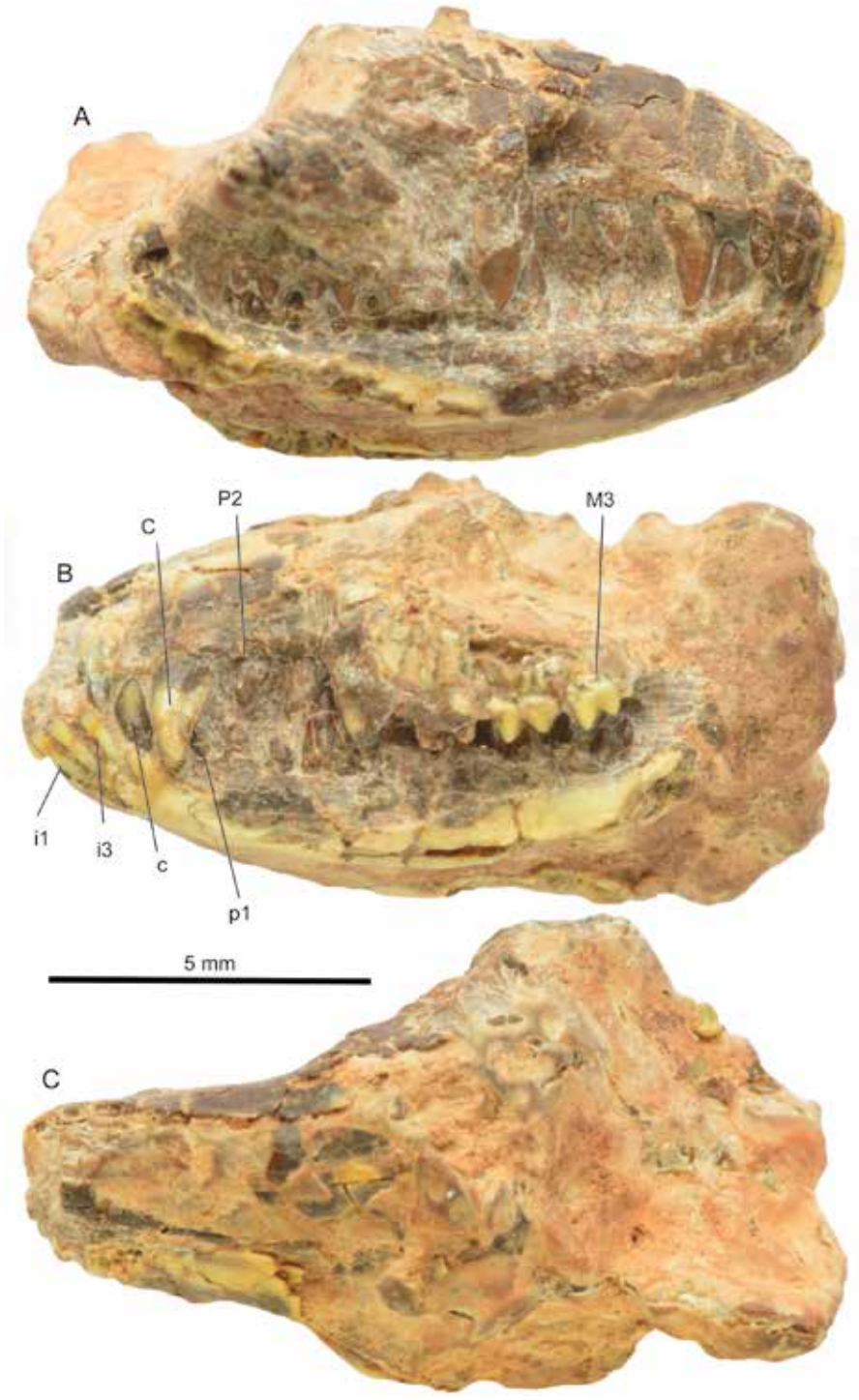

FIG. 44. Anterior part of skull of *Naranius hengdongensis*, sp. n., IVPP V7440: **A.** right lateral, **B.** left lateral, and **C.** dorsal views.

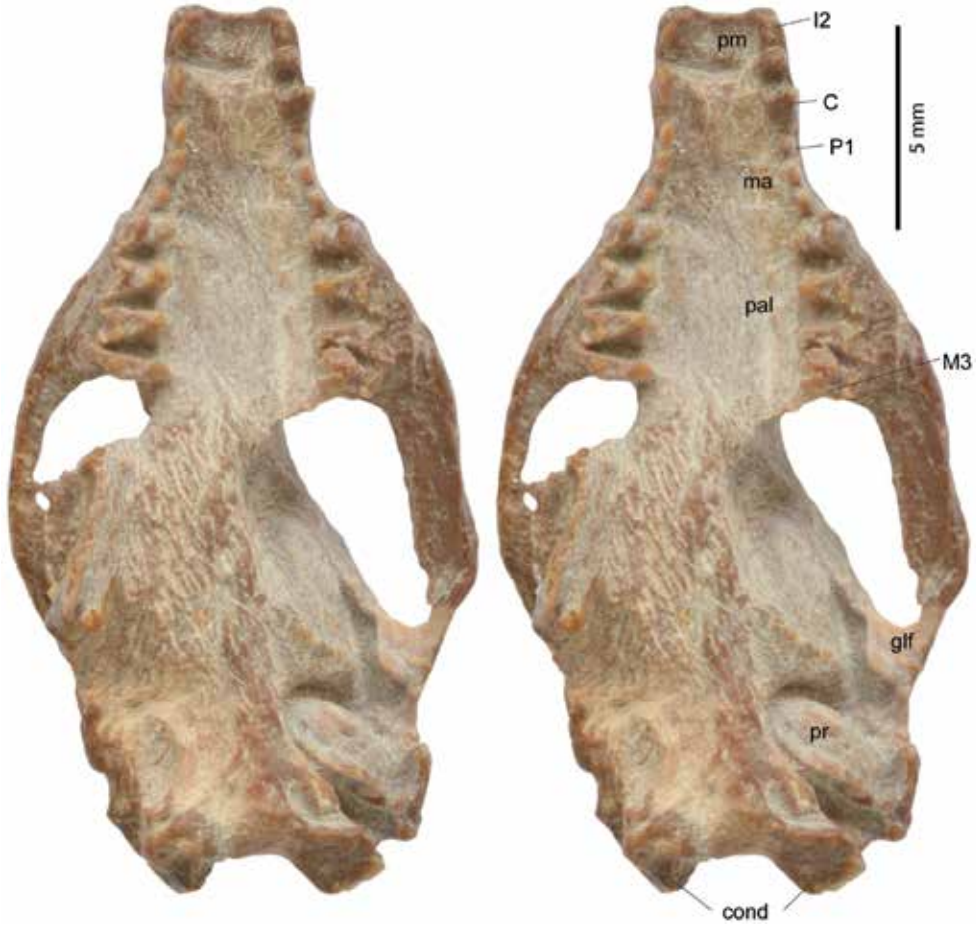

FIG. 45. Skull of *Naranius hengdongensis*, sp. n., IVPP V7439, stereophotograph in ventral view.

(about 0.7 mm in length) between I3 and the canine and this space held the lower canine in occlusion. This situation is proved in IVPP V5352 and V7440, in which the lower canines occupied the spaces. In the original description, Russell and Dashzeveg (1986) proposed the dental formula as 3.1.4.3 based on the lower dentition; however, the authors did not provide any information on the lower incisors. Lopatin (2006: 325) described "the incisors are small, similar in size, with i2 somewhat larger than the others," based on the alveoli." The lower incisors are well preserved in both the right and left side of the mandible of IVPP V7440 and i2–3 are also preserved in IVPP V7349. Three lower incisors are closely crowded in the anterior edge of the mandible. The i1 is small, square in anterior view, single rooted, and situated at the anterior extremity of the mandible. Its anterior surface is flat, smooth, and faces anteriorly. The i2 is laterally situated to the i1. The i3 is closely behind i2, but it is at the lateral side of the mandible. The i2 is slightly larger than the i1 and much larger than i3. Both i2 and i3 are mediolaterally flattened, and single rooted.

Canines: Both upper and lower canines are well preserved in IVPP V7439 and V7440. The upper canine is about 1 mm behind I3 and just posterior to the premaxilla-maxillary suture (figs. 44A, B, 45). The upper canine is much

larger than the upper incisors and the first three upper premolars. It is single rooted, with a single transversely compressed sharp cusp, and in lateral view resembles a right-angled triangle. The anterior edge of the upper canine is somewhat perpendicular to the tooth row. The posterior edge leans anteriorly with a gentle ridge extending from the tip to the base of the crown. The crown is slightly convex labially and flat lingually. The lower canine is closely behind the i3 and much smaller than the upper canine (figs. 44A, B, 46). It is a single rooted, unicuspid tooth, transversely compressed, triangular in lateral view, and somewhat premolariform. The anterior edge is curved anteriorly in the middle and then leans posteriorly, and the posterior edge is somewhat perpendicular to the tooth row. The crown is flat lingually and convex labially. The tip of the cusp is not sharp, as is the upper canine. In occlusion, the lower canine is in front of the upper.

Premolars: The premolars are characteristic of *Naranius* in having upper P2–3 and lower p2–3 smaller than P1/p1 and considerably smaller than P4/p4 (figs. 44A, B, 45, 46A–F). The P1–4 are well preserved in both the right and left maxilla of IVPP V7439, V7440, and in the left maxilla of V5352 (fig. 47B), and the P2–4 are well preserved in the right maxilla of V5353 (fig. 48A). The size and morphology of premolars varies slightly in different individuals. The P1 and P2 are closely placed and P3 and P4 are closely placed, but there is gap between P2 and P3.

The P1 is a small, simple tooth, situated about 1 mm posterior to the canine in V7439, but closer to the canine in V5352 (fig. 47A, B). It possesses a laterally compressed single cusp without posterior accessory cusp. The main cusp is piercing with a sharp edge extending posterobliquely from the tip of the cusp to the base of the crown. The anterior edge of the tooth is smooth and straight dorsoventrally. The tip of the main cusp tilts slightly posteriorly. There is a deep groove in the middle of the root that can be seen clearly on the labial side of the tooth in V7439, indicating the tooth is either two rooted or bifurcated. The groove is not seen in V5352. Both crown and root of P1 in V5352 are simpler than in V7439.

The P2 is similar to P1 in size and closely behind P1 (figs. 44A, B, 45). It is a small, single-cusped, two-rooted tooth. The main cusp is piercing and laterally compressed, with a sharp posterior ridge extending from the tip of the main cusp to the base of the tooth. The labial side of the main cusp is slightly convex. There is a faint projection at the end of the posterior ridge near the base of the tooth in V7439, but it is a distinct cusp in V5353 (fig. 48A). The anterior edge of the main cusp is smooth and almost straight dorsoventrally.

The P3 is the smallest tooth among the premolars, smaller than P1 and P2 and considerably smaller than P4 (figs. 44A, B, 45). It is a low-crowned, single-cusped tooth, laterally compressed, and situated about 0.5 mm behind the P2 in V7439. It is double rooted. The labial side of the tooth is flat and the lingual side is slightly convex. Its anterior edge is smooth and slightly curves anteriorly with the tip of the main cusp directed posteriorly. The posterior edge has a sharp ridge, extending labially from the tip of the tooth to its base. The tooth bears a projection (heel) at the base of the tooth in V7439, which is a distinct cusp in V5353 (fig. 48A).

The P4 is the largest tooth among the upper premolars and is semimolariform, with three roots (figs. 44A, B, 45). It is about the same size as M1, triangular in occlusal view, and it possesses protocone and paracone, but no indication of a metacone or conules. The paracone is large, piercing, and towers above all other cusps. The apex of the paracone is at about the midpoint of the tooth length, with a long, sharp metacrista extending from the tip to the base of the crown. Its anterior surface is broad and smooth, and the paracrista is a gentle ridge on the lingual side. The labial surface of the paracone is slightly convex. The parastyle is near the base of the paracone, separated from the paracone by a narrow, shallow depression. The metastyle is well devel-

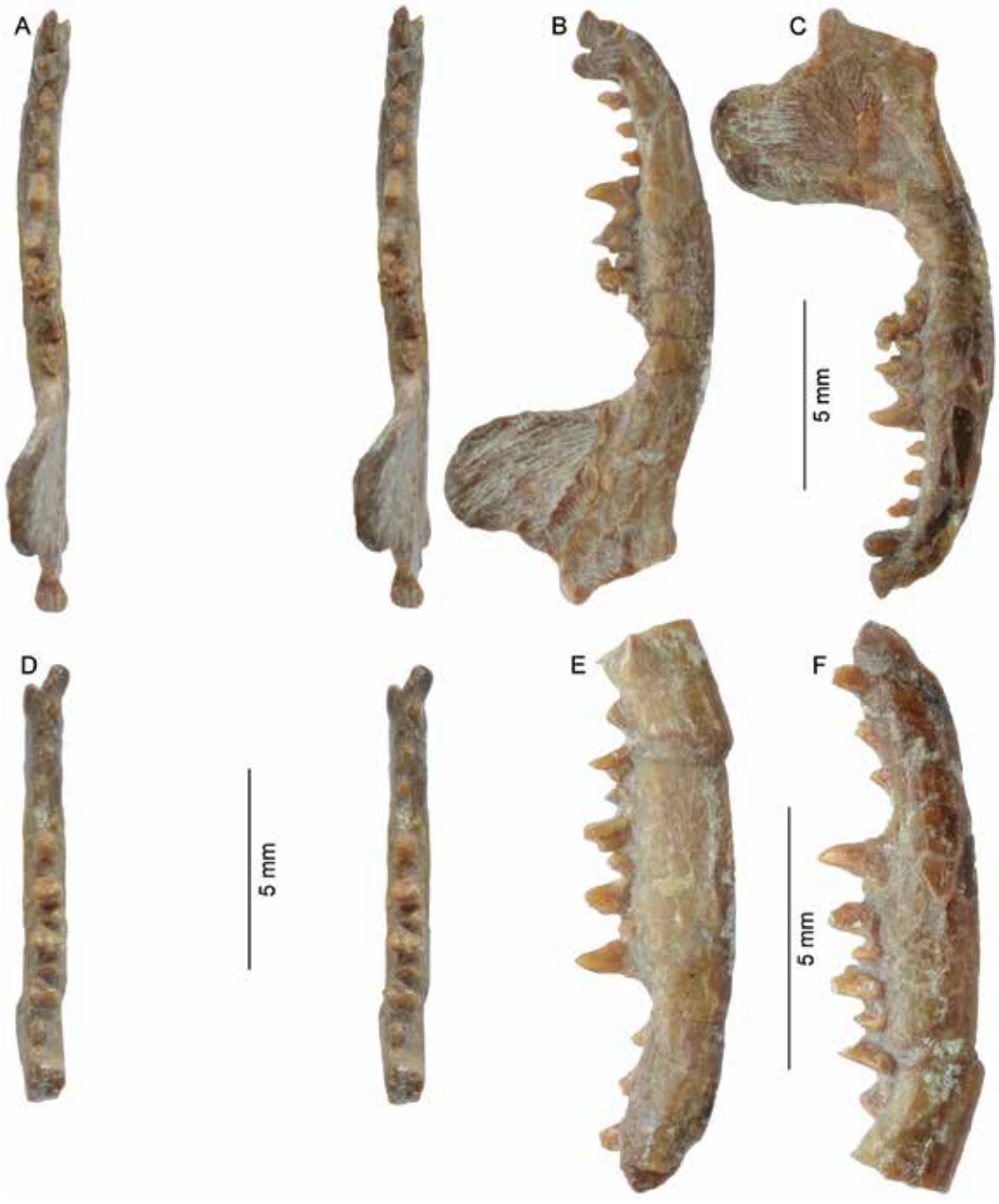

FIG. 46. Lower jaws of *Naranius hengdongensis*, sp. n., IVPP V7439: **A.** stereophotograph of left lower jaw in occlusal view; **B.** lingual view of left lower jaw; **C.** labial view of left lower jaw; **D.** stereophotograph of right lower jaw in occlusal view; **E.** lingual view of right lower jaw; **F.** labial view of right lower jaw.

oped and separated from the metacrista by a notch. The protocone is a sharp, conical cusp, but much shorter than the paracone, and situated just opposite the paracone. The preprotocrista and postprotocrista run steeply from the protocone to connect the ridges from the parastyle and metastyle respectively. There is no sign of anterior, posterior, and lingual cingula, but a weak ectocingulum occurred near the parastyle and metastyle.

The p1 is a small, single-rooted tooth, but it is much larger than p2 and p3 (fig. 46A–F). The root is large. The crown is laterally compressed with both labial and lingual sides slightly convex. The main cusp is large, piercing, with a sharp anterior ridge running down anteriorly and then bending posteriorly near the base of the crown. There is a small poorly developed posterior accessory cusp at the posterior end of the crown. The cusp is not separated from the posterior ridge. The posterior ridge is sharp and runs down lingually. It is separated from the posterior projection by a notch. There is a triangular surface on the posterior surface of the crown limited by the posterior ridge lingually.

The p2 is a very small, two-rooted tooth, about half the size of p1 (fig. 46A–F). It is about 1 mm posterior to p1 in IVPP V7439. The two roots are about equal in size. The crown is laterally compressed with both labial and lingual sides slightly convex at the middle. The tooth bears a main large cusp and a small posterior accessory cusp that is not separated from the posterior ridge. The main cusp is conical, and the apex of the cusp is situated at the midpoint of the tooth length. Its anterior edge is round and smooth and projects anteriorly at its middle part. The posterior edge has a very gentle ridge extending from the tip of the tooth and turning lingually to the base. The posterior accessory cusp is not as well developed as in p1 and is placed slightly labially at the end of the posterior ridge. There is no sign of any cingulids.

The p3 is about the same size as p2, and both of them are considerably smaller than p4 (fig. 46A–F). The p3 is about 1mm posterior to the p2 in IVPP V7439. It has two equal-sized roots, and possesses a main cusp and a distinct posterior accessory cusp. The crown is laterally compressed with both labial and lingual surface slightly convex. The main cusp is conical. The anterior surface of the crown is round, smooth, and projects anteriorly. The posterior surface has a gentle ridge extending from the tip of the main cusp to contact the posterior accessory cusp at the slightly labial side of the base of the crown. There is no sign of any cingulid.

The p4 is the largest tooth among the lower premolars and about the same length and width as m1 (fig. 46A–F). The crown is laterally compressed, with labial side slightly convex, and the lingual side flat. It has two roots. The posterior root is larger and stronger than the anterior one. The main cusp is tall, piercing, and towers above the others. The anterior surface of the crown is round and smooth and runs steeply to contact a faint cusp near the base of the crown. The cusp projects anteriorly. There is no indication of a metaconid. The posterior surface is a triangular, smooth surface limited by a sharp ridge lingually and a gentle ridge labially. The lingual ridge extends from the tip of the protoconid and ends near the base of the cusp. The talonid is well developed, but not basined. A short, sharp ridge divides the talonid into two unequal parts, wider labially and narrower lingually. There is no indication of cingulids.

Molars: Both right and left upper molars are well preserved in IVPP V5352, 5353, 7349, and 7440 (figs. 44A, B, 45, 47A, B, 48A, C, D). All three upper molars are transverse and compressed anteroposteriorly. They are three rooted, the lingual root the largest and most robust, and the labial roots are parallel to one another and about equal in size. M2 is the largest among the upper molars and M3 the smallest. All upper molars have high, piercing cusps. The protocone is about the same height as the paracone, but slightly more robust. Both anterior and posterior faces of the protocone are steep. The preprotocrista and postprotocrista are well-developed thin, sharp ridges. The paracone and metacone

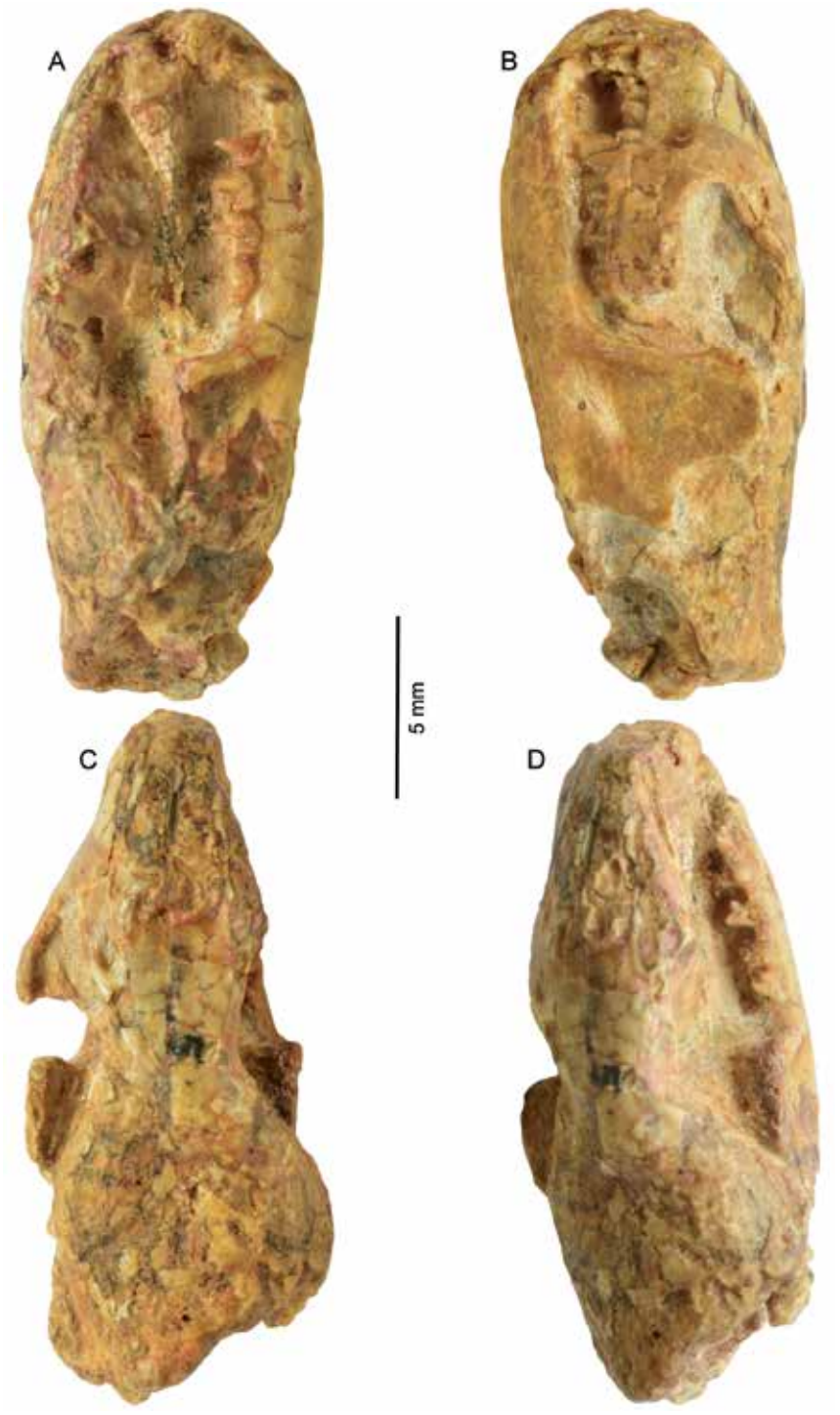

FIG. 47. Skull and lower jaw of *Naranius hengdongensis*, sp. n., IVPP V5352: **A.** right lateral, **B.** left lateral, **C.** dorsal, and **D.** right dorsal-lateral views.

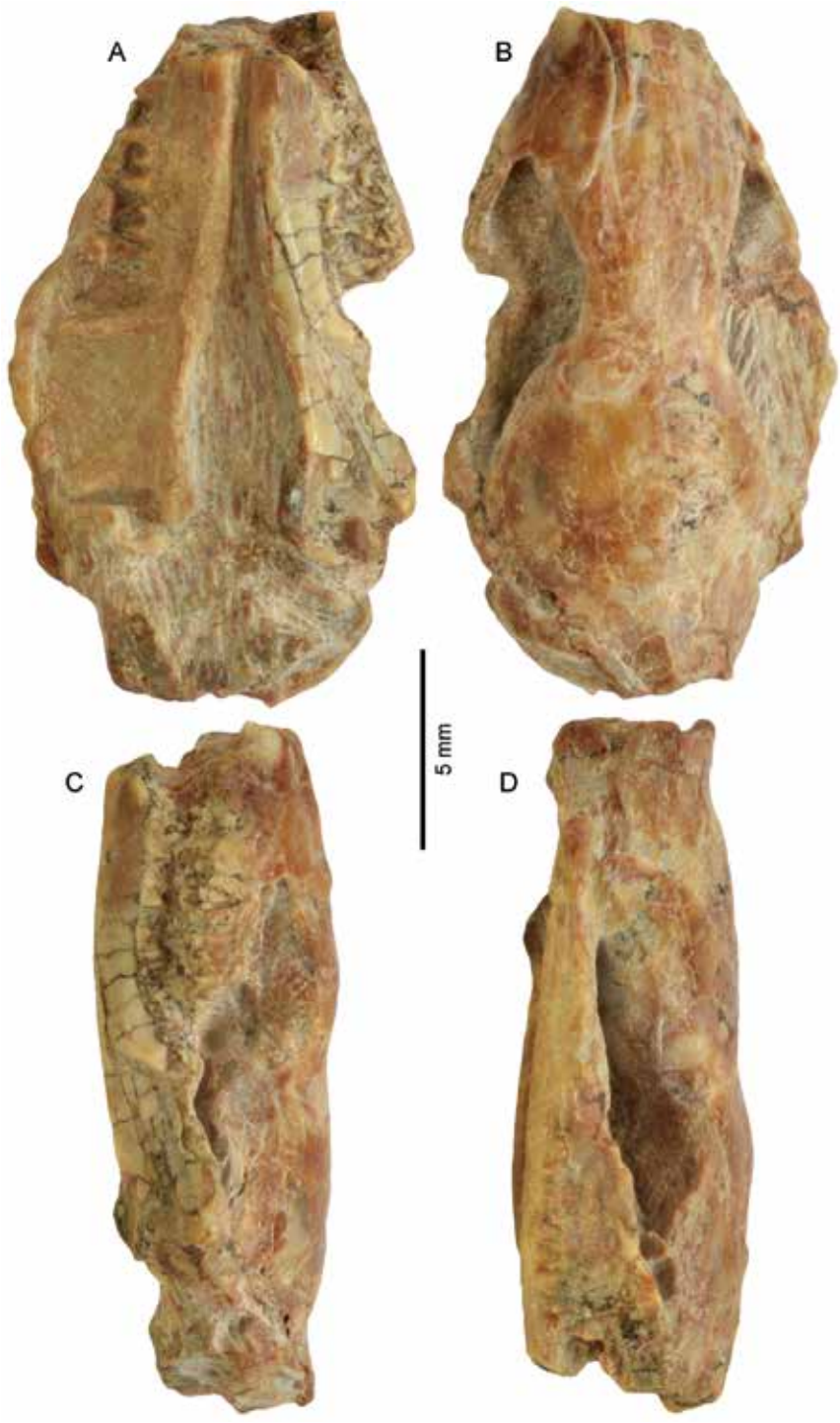

FIG. 48. Skull and lower jaw of *Naranius hengdongensis*, sp. n., IVPP V5353: **A.** ventral, **B.** dorsal, **C.** left lateral, and **D.** right lateral views.

are well separated and approximately parallel at the labial edge of the crown. The paracone is taller than the metacone; however, the metacone is reduced in size and smaller than the paracone in M3. Both lingual and labial surfaces of the paracone and metacone of M1–3 are slightly convex. The paracrista is a weak ridge in M2, terminating at the base of the paracone, and is absent in M1 and M3. The parastylar shelf is well developed in the three molars, forming a pronounced stylar shelf lobe. The parastyle cusp is distinct. The metacrista is distinct in M 1–2 and separated from the metastyle by a notch. The metastylar shelf is well developed in M1–2, but is not developed in M3. The paraconule and metaconule are distinct. The conules are located in the midline of the tooth in M1–2. The preparaconule crest is a thin ridge, connecting with the preprotocrista. The posterior surface of the paraconule and the anterior surface of the metaconule are broad and smooth, without a distinct postparaconule crest and premetaconule crest, respectively. The postmetaconule crest is a distinct thin, sharp ridge, which terminates at the base of the crown near the posterior surface of the metacone. The hypocone is weak and can be seen in M2 in V7439, but not in M1 and M3. A weak hypoconal shelf is seen in M1–2 in V7440, projecting posterolingually, but is absent in M3 of IVPP V5353 and 7439. The ectocingulum runs along the labial base of the crown. The ectoflexus is deeply curved. The development of pre- and postcingulae varies among the individuals.

The lower molars slightly increase in size from m1 to m3 (fig. 46A–F). The trigonid basin is not well developed and is considerably compressed anteroposteriorly. It is at least twice as tall and slightly wider than the talonid. The protoconid and metaconid are well developed and about equal in size. The protoconid is conical with a piercing apex. The labial side of the protoconid is narrow and convex, and the anterior and the posterior sides are flat. The paraconid is reduced and much shorter and smaller than both protoconid and metaconid. It is located more labially than the metaconid. The paracristid connects the paraconid and protoconid without interruption. There is no carnassial notch on the paracristid. The metaconid is conical at the apex. Both anterior and posterior surfaces of the metaconid are flat. The posterior surface of the protoconid and metaconid form a dorsoventrally oriented wall perpendicular to the toothrow. The protocristid begins at the apex of the metaconid and is separated by a wide notch at the middle of the crest, forming a relatively wider V-shape to connect the protoconid. The cristid obliqua is very short and starts at the middle of the posterior wall of the trigonid. The hypoflexid is deep. The talonid in m1–2 is short and compressed anteroposteriorly, but is elongated and enlarged in m3. The hypoconid and hypoconulid are well developed and situated at the posterior end of the talonid. The hypoconid in m1–2 is slightly larger than the hypoconulid, but the hypoconulid of m3 is larger than the hypoconid, and situated at the very end of the talonid. The entoconid is smaller than the hypoconid and hypoconulid. The talonid basin is open lingually. The precingulid is narrow and short. There are no labial and posterior cingulids.

Dentary

The dentary is completely preserved in IVPP V7439, and incompletely preserved in V5352, V5353, and V7440 (figs. 44A, B, 46A–D, 47A, B, 48A, C, D).

The dentary is long, slender, and gently convex at the middle part of the ventral border. The dentary under m1 is slightly deeper than the rest of the body. There are no clear mental foramina in any of the specimens, except one small foramen under m1 on the right side of the dentary of V5352. The mandibular condyle is small and elongated anteroposteriorly. The dorsal side of the articular surface of the condyle is flat and slightly curved at its posterior end, indicating the basic movement is anteroposteriorly. The condyle is situated slightly higher than the tooth row. The masseteric fossa is quite deep, bordered by a strong coronoid crest anteriorly and the

condyle crest posteriorly. The angular process is small, slender, thin, and has no posterior projection. The coronoid process is strongly developed, very high, and wide anteroposteriorly.

Skull

The outline of the skull is long with a narrow snout. In dorsal view, the narrowest part of the skull is at the midpoint where the orbital and temporal fossae are separated (figs. 47C, 48B, 49). The zygomatic arch is very thin, slender, and moderately expanded laterally. The skull is slightly expanded at the point posterior to the orbital-temporal fossa connection and increasingly inflated to reach its greatest width and height above the zygomatic process of the squamosal. The surface of the skull is convex from the glenoid fossa region to the end of the skull. In lateral view, the contour of the skull is slightly convex and higher at the braincase area (fig. 50). In ventral view, the snout is narrowed between P2–3 (fig. 45). The area from the tip of the snout to the end of the palate with M3 is slightly less than a half the length of the skull. The basicranium region (from the anterior edge of the piriform fenestra to posterior edge of the mastoid process) is short, about one-fifth the length of the skull.

Premaxilla: The premaxilla is almost completely preserved on the right side of V7440, and partially preserved in V7439 (figs. 44A, B, 49, 50A). Wible et al. (2004: 39) refer to the portion of the premaxilla anterior to the I1 as the "rostral process," noting that in *Zalambdalestes* it projects considerably farther forward than the nasals. The rostral process of the premaxilla in the Glires is enlarged (Meng et al., 2003: 132); however, most eutherians have a small rostral process of the premaxilla, such as in *Leptictis*. Judging from the space between the vestige of the right I1 to the fragment of the left I2 of IVPP V7439, it seems that the anteriormost region of the premaxilla of *Naranius hengdongensis* is wide; however, it is difficult to judge whether the wide rostrum region of the premaxilla supported the enlarged I1s or this portion of the premaxilla is projecting beyond the I1s. The premaxilla of *Naranius hengdongensis* is relatively large, contributing about two-fifths the length of the preorbital region, and is a half-ellipse in lateral view (figs. 44B, 47C, 49. 50A). In dorsal view, the premaxilla ends at the point above the posterior edge of the canine (figs. 49, 50A). The premaxillary-nasal suture is straight, occupying more than one-third the length of the nasal in dorsal view. The premaxillary-maxillary suture is oblique in lateral view, running from the point above the anterior edge of the canine, then turning dorsoventrally and ending at the point closely above the posterior edge of I3. It is situated between I3 and the canine in the occlusal view.

Nasal: The nasals are well preserved in IVPP V7439 and 7440, and partially preserved in V5352 and 5353. In dorsal view, the nasals are narrow, slender, and occupy more than one-third the skull length and their posterior edge extends to the level of the middle of the upper rim of the orbit and above the anterior edge of M3 (figs. 44C, 47C, 48B, 49, 50). The posterior border of the nasal is W-shaped. The preserved part of the anterior extremity of the nasal is flat, situated posterior to the point of the contact with the anterior edge of the premaxilla. The anteriormost end of the nasal does not extend beyond the anterior edge of the premaxilla. The nasals are basically equal in width along their entire length. The nasals have broad contact with the maxilla and relatively narrow contact with the frontal in dorsal view. The nasal-premaxillary suture and the nasal-maxillary suture are a continuous straight line. The nasal-frontal suture is a short, W-shaped line with the apices of the "W" directed posteriorly. The nasal is separated from the lacrimal by the maxilla and has no contact with the lacrimal.

Maxilla: The maxilla is a large element in the facial region. It occupies most of the lateral surface of the facial region, possesses a well-developed zygomatic process, and has a moderately long infraorbital canal. In lateral view, it is rectangular, shorter and deeper anteriorly, and longer and narrower posteriorly (figs. 44B, 47C,

FIG. 49. Skull of *Naranius hengdongensis*, sp. n., IVPP V7439, dorsal view.

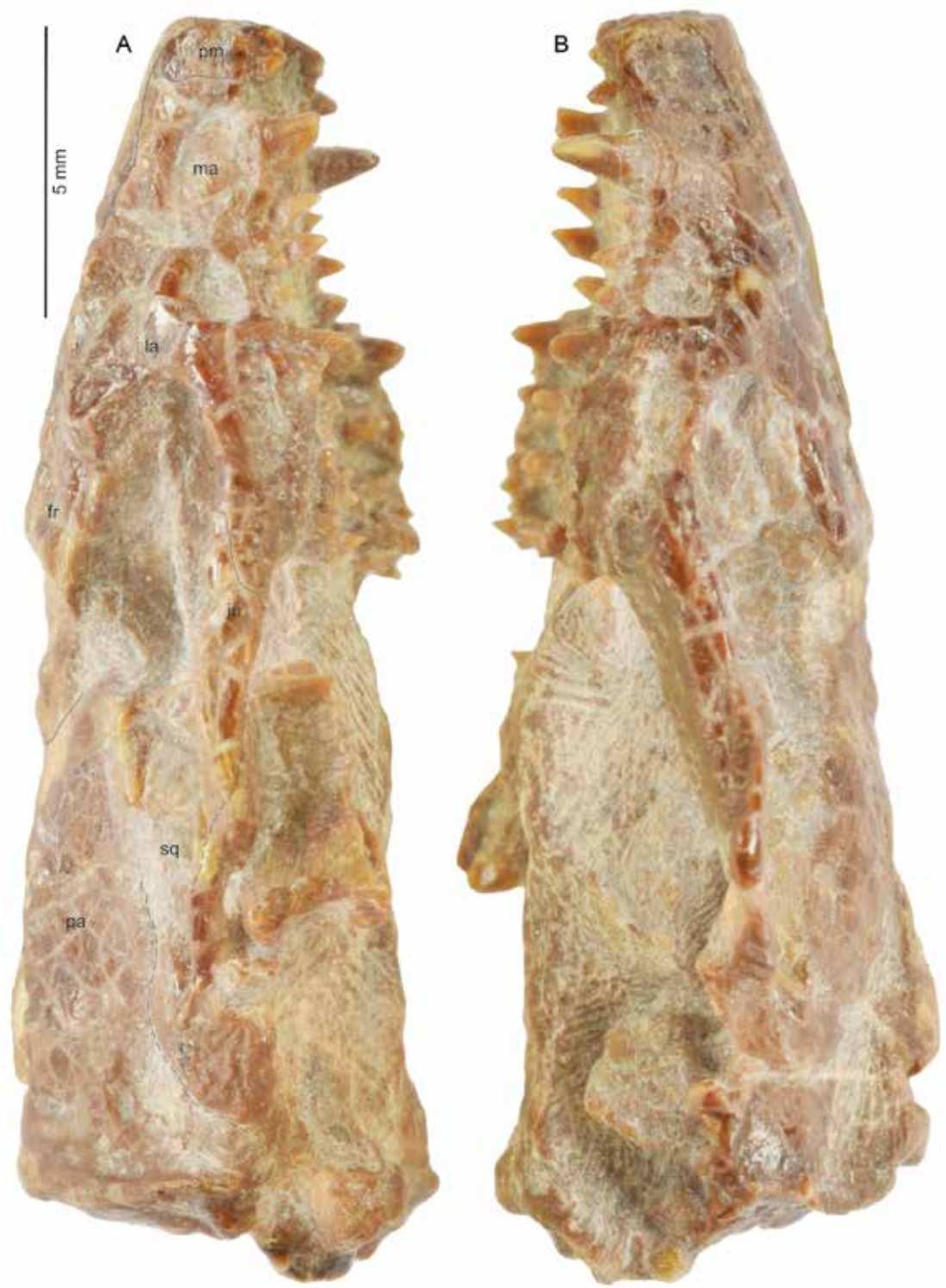

FIG. 50. Skull of *Naranius hengdongensis*, sp. n., IVPP V7439: **A.** right lateral and **B.** left lateral views.

48B, C, 49, 50, 51). The sutures with neighboring bones are preserved in IVPP V7439. In dorsal view, the maxilla is narrow and rectangular, seen on the left side of IVPP V7439 (fig. 49). It contacts the premaxilla anteriorly, the nasal medially, and the lacrimal and frontal posteriorly. The maxillary-premaxillary suture, clearly seen in IVPP V7439, is short, straight, and bends anterolaterally from the nasal process of the premaxilla at the level of the anterior edge of P1 to the level of the anterior edge of the canine. The maxillary-nasal suture is straight and occupies about two-thirds the length of the nasal. The maxillary-frontal suture is better preserved in the left side of V7439, while the right side has some distortion. The suture is short, W-shaped, with the apices of the "W" directed posteriorly in dorsal view. The maxillary-lacrimal suture is defined at the anterior rim of the orbit, because the lacrimal has no facial process. The lateral surface of the maxilla is basically smooth without indication of any foramen (figs. 44B, 47C, 49, 50, 51). Its alveolar border is relatively straight. There are three alveoli for the fourth premolar and for each of three molars; two for the first and second premolars; and one for the third premolar. The infraorbital canal is short, about 1mm in length, but large and circular in cross section. The anterior opening of the infraorbital canal is about 0.9 mm in diameter. It is situated above the level between the P3 and the P4, and the posterior opening is above the posterior edge of the P4. The posterior opening lies within the orbital wing of the maxilla at the level above P4. There is no antorbital fossa anterior to the infraorbital foramen. A suture between the zygomatic process and the jugal defines the zygomatic process of the maxilla posteriorly, which can be seen in the right side of the skull in IVPP V7439; however, this suture on the left side of the skull is obscure. The zygomatic process of the maxilla is wider dorsoventrally at its anterior part, tapering posteriorly near the suture between the zygomatic process and jugal. The suture between the zygomatic process and jugal is coarsely interdigitated and straight, extending obliquely from anterior to posterior. The sutures between the maxilla, the lacrimal, and the frontal in the orbit are preserved in IVPP V5353. The maxilla contacts the frontal at the upper part of the orbital region in a W-shaped line, with the apices of the W directed anteriorly (figs. 50A, 51). It contacts the lacrimal in a short, curved line. The maxilla has no contact with the frontal in the medial wall of the orbit, because of the large expansion of the palatine in the orbital region, separating the maxilla and the frontal.

Lacrimal: The lacrimal is preserved in IVPP V7439 and V5353. It is roughly rectangular (figs. 48B, 49, 50A, 51). The surface of the lacrimal is smooth. The lacrimal foramen is of moderate size, a feature that can be seen in the left side of V5353. The lacrimal has no facial process and its anterior edge is defined within the orbit. The lacrimal contacts the maxilla dorsoventrally and the frontal and palatine posteriorly. The sutures of the lacrimal with these bones in the orbital region are short, simple lines. There is no lacrimal tubercle.

Jugal: The jugal is completely preserved in both sides of IVPP V7439, and partially preserved in V5353. The jugal is long, slender, and widely expands laterally (figs. 48B, 49, 50A). The body of the jugal is compressed lateromedially, slightly convex laterally, and flat medially. Anteriorly, the jugal contacts the maxilla with a short, straight suture in the orbital region, and the suture extends laterally at the level of the posterior edge of P4. The jugal and the maxilla form the inferior rim of the orbit. The posterior process (posterior spine of Novacek, 1986: 38) is long and contacts with the zygomatic process of the squamosal by a diagonal suture, running from the anterior part of the zygomatic arch to contact the zygomatic process of the squamosal, far from the glenoid process. The jugal occupies more than half the length of the anterior part of the zygomatic arch.

Frontal: The dorsal part of the frontal on the roof of the skull is best preserved in IVPP V5353 (fig. 48B). The posterior part of the frontal is damaged in V7439 (fig. 49). In dorsal view, the

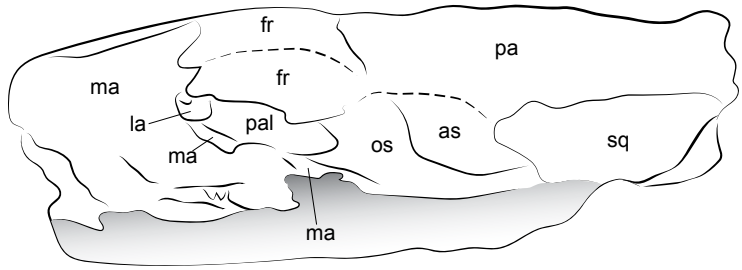

FIG. 51. Drawing of temporal region of skull of *Naranius hengdongensis*, sp. n. (based on IVPP V 5353).

frontal is shorter compared with the parietal and nasal, and is about one-third the length of the skull (figs. 48B, 49). It is rectangular and extends longitudinally along the midline of the skull. It is slightly convex at the posterior part of the roof in V5353. In V5353, there is a sliver of bone extending anteriorly between the nasal and maxilla that is not clearly shown in other specimens due to damage in that area. It contacts the nasal anteriorly in a coarsely interdigitated W-shaped suture in dorsal view. Laterally, the frontal-maxillary suture extends from the frontal-nasal suture posteriorly to contact the parietal (figs. 48C, 50A). The frontal-parietal suture can be seen only in IVPP V5353. It is a short, straight line, extending anterolaterally from the point where both sides of the frontal-parietal suture meet at the midline of the skull to the top rim of the anterior edge of the temporal fossa. There is no supratemporal crest, and no clear supraorbital crest and supraorbital process. The frontal has a very large orbital process, which extends ventrally almost to the ventral border of the medial wall of the orbit. The orbital process of the frontal is well preserved in IVPP V7439 and V5353; however, the sutures of the frontal and neighboring bones are best preserved on the left side of V5353. The orbital process of the frontal is roughly triangular, wider at the dorsal edge of the orbital fossa and narrows ventrally about halfway down on the medial wall of the orbital fossa to contact the palatine. Anteriorly, it contacts the lacrimal. The frontal-lacrimal suture is a short, straight line, running dorsoventrally from the top of the orbital rim at the triple junction of the frontal, maxilla, and lacrimal, down almost halfway on the medial wall of the orbit to meet the palatine at the junction of the frontal-lacrimal and frontal-palatine sutures. Posterior to the frontal-lacrimal suture, the frontal has a broad contact with the palatine. The frontal-palatine suture is a slightly curved line that occupies half the length of the temporal region, running horizontally and posteriorly from the triple junction of the frontal, lacrimal, and palatine to meet the orbitosphenoid at the middle of the temporal fossa. Posteriorly, the frontal contacts the parietal at the upper posterior aspect of the orbital fossa with a very short frontal-parietal suture. The frontal has a broad contact with the orbitosphenoid in the posteromedial wall of the temporal region. The frontal-orbitosphenoidal suture is slightly curved, and extends from the frontal-palatine suture dorsally to meet the parietal at the triple junction of the frontal, parietal, and orbitosphenoid. The frontal has no contact with the alisphenoid bone, and is separated from the alisphenoid by the orbitosphenoid at the upper posterior region of the temporal fossa. The frontal is separated from the maxilla by both the palatine and orbitosphenoid.

Palatine: The palatine is preserved in IVPP V7439 and V5353. The surfaces of the palatine bone in palatal view in both specimens appear to have been damaged during fossilization, so that the size, shape, and related structures of the palatine, such as the palatine foramina and the postpalatine torus, postpalatine spine, etc., cannot be seen clearly (fig. 45). Most likely, the palatine does not join to form the orbital floor. The pala-

tine has a large expansion in the anterior part of the medial wall of the orbital region, which can be seen in both IVPP V5353 and V7439. The orbital expansion of the palatine is horizontally located and occupied almost half the depth of the anterior part of the medial wall of the orbit (figs. 50, 51). The orbital expansion cannot be seen clearly in the palatal view, and it is irregularly shaped in orbital view, widest at the middle and narrowed on both ends. Its anterior end contacts the lacrimal. The palatal-lacrimal suture is a short straight line, and runs dorsoventrally from the triple junction of the frontal, lacrimal, and palatine to meet the triple junction of the lacrimal, palatine, and maxilla. The palatine has a long contact with the frontal. The palatine-frontal suture is a simple straight line located about 1 mm below the top rim of the orbital fossa, running horizontally from the triple junction of the frontal, lacrimal, and palatine, to end at the triple junction of the frontal, orbitosphenoid, and palatine posteriorly. At the bottom of the orbital fossa, the palatine contacts the maxilla in a simple, straight suture. Posteriorly, the palatine contacts the orbitosphenoid in a short zigzag suture, running dorsoventrally from the triple junction of the frontal, palatine, and orbitosphenoid, to end at the triple junction of the orbitosphenoid, palatine, and maxilla at the bottom of the orbital fossa. Both the sphenopalatine foramen and postpalatine foramen are not well preserved in our specimens. The palatine is separated from the alisphenoid by the orbitosphenoid, and has no contact with the alisphenoid.

Parietal: The parietal and the sutures of the parietal with surrounding bones are well preserved in IVPP V5353 and V7439, and partially preserved in V5352. The parietal is a large element in the skull roof and upper part of the side wall of the temporal fossa, occupying about one-third the length of the skull roof (figs. 47C, 48B, 49, 50A, 51). It is elongate anteroposteriorly, roughly rectangular, and very narrow in the posterior orbital region and widened and strongly expanded immediately posterior to the orbital constriction, with the widest part at the middle and posterior temporal region. The parietal is convex dorsally and laterally and extends along the lateral flank of the posterior part of the skull. The posterior part of the parietal is flat. The dorsal surface of the parietal is smooth. The parietal contacts the frontal anteriorly, the squamosal and alisphenoid ventrolaterally, and the lambdoid crest posteriorly (figs. 49, 50A). The parietal-frontal suture can be seen clearly only in IVPP V5353, and this suture is damaged in V5352 and V7439. The parietal-frontal suture is a simple, wide-open V-shaped line. It starts at the midline of the skull roof, extending laterally to the posterior edge of the orbit and ventrally in a short distance to end at the triple junction of the parietal, frontal, and orbitosphenoid in the medial wall of the temporal region (on the right side of V5353, the orbitosphenoid is not as well preserved as in V7439 and the left side of V5353). The parietal-orbitosphenoid suture is very short, simple, and straight (fig. 51). It immediately continues from the triple junction of the parietal, frontal, and orbitosphenoid and runs posteriorly. The parietal-orbitosphenoid suture ends at the triple junction of the parietal, orbitosphenoid, and alisphenoid, where the parietal-alisphenoid suture immediately continues. The parietal-alisphenoid suture runs a short distance posteriorly to end at the triple junction of the parietal, alisphenoid, and squamosal. The parietal-alisphenoid suture is short, simple, and straight. The parietal-squamosal suture starts at the triple junction of the parietal, squamosal, and alisphenoid, and runs for a very short distance posteriorly along the side wall of the temporal fossa, turning to the dorsal surface of the skull and ending at the lambdoidal crest. This suture is coarsely interdigitated. It is longer than the parietal-frontal, the parietal-orbitosphenoid, and the parietal-alisphenoid sutures. The sagittal crest cannot be seen in IVPP V5352 and V7439 due to the damage in that area; however, in V5353, there is a very short and weak sagittal crest in the midline of the skull in front of the lambdoidal crest.

Presphenoid: The presphenoid is not well preserved in any specimens.

Orbitosphenoid: The orbitosphenoid is best preserved in IVPP V5353 and partially preserved in V7439. The orbitosphenoid is a large element in the posteromedial wall of the temporal fossa (figs. 48D, 51). It is irregular and extends anteroposteriorly with a long ventral border. Dorsally, it contacts mainly the frontal with a simple straight suture (fig. 51). Continuing from the orbitosphenoid-frontal suture, the orbitosphenoid has a small semicircular intrusion into the parietal at its dorsal posterior aspect. Anteriorly, the orbitosphenoid contacts the palatine in a U-shaped suture with its apex pointed posteriorly. Posteriorly, it contacts the alisphenoid with a curved line. The orbitosphenoid-alisphenoid suture continues from the orbitosphenoid-parietal suture and runs posteriorly, then turns anteriorly at the dorsal rim of the sphenorbital fissure. Ventrally, it contacts the maxilla at the bottom of the temporal fossa. The orbitosphenoid-maxillary suture continues from the palatine-maxillary suture and extends posteriorly along the bottom of the medial wall of the temporal fossa and ends at the dorsal rim of the sphenorbital fissure. The optic foramen is large and oval. It is situated at the posterior recess of the orbitosphenoid, separated from the sphenorbital fissure by a thick bony septum. The sphenorbital fissure is located near the orbitosphenoid-alisphenoid suture, but mainly in the alisphenoid.

Alisphenoid: The alisphenoid is best preserved in IVPP V5353. It is a large, irregularly shaped element in the posterior part of the medial wall of the temporal fossa (figs. 48D, 51). It contacts the orbitosphenoid anteriorly, the parietal dorsally, and the squamosal posteriorly (fig. 51). The orbitosphenoid-alisphenoid suture is a simple straight line, running anterodorsal-posteroventrally from the triple junction of the parietal, orbitosphenoid, and alisphenoid to the bottom of the temporal fossa. A short, curved orbitosphenoid-parietal suture, at the upper dorsal aspect of the alisphenoid, separates the alisphenoid from the frontal. There is no alisphenoid-frontal contact. The dorsal part of the alisphenoid-parietal suture is simple and straight, extending posteriorly almost horizontally from the triple junction of the orbitosphenoid, parietal, and alisphenoid, and turning ventrally to end at the triple junction of the alisphenoid, parietal, and squamosal. The alisphenoid-squamosal suture is a simple, curved line, which continues from the alisphenoid-parietal suture and runs ventrally. The alisphenoid-pterygoid contact and the epipterygoid process of the alisphenoid are not well preserved. The alisphenoid forms the sloping posterior wall of the temporal fossa; however, the ventral side of the slope is not well preserved, so that the sphenorbital fissure and the alisphenoid canal cannot be seen clearly.

Basisphenoid: The basisphenoid is not clearly preserved in any specimens.

Squamosal: The squamosal and its sutures with surrounding bones are well preserved in IVPP V7439 and partially preserved in V5353. The squamosal is a moderate-sized element in the temporal region that comprises the lower posterior portion of the lateral wall of the skull (figs. 48B, D, 49, 50A, 51). In the medial wall of the temporal fossa, it contacts the parietal dorsally and the alisphenoid anteroventraly (figs. 48D, 49, 50A, 51). The parietal-squamosal suture is better seen in IVPP V5353. It is a long, course, irregularly curved line. The suture is horizontally situated, running posteriorly from the triple junction of the parietal, alisphenoid, and squamosal to end laterally near the lambdoid crest. The surface of the squamosal is smooth without any foramina, convex at its anterior part and slightly concave posteriorly. The postzygomatic crest is very weak or not well preserved in any of the specimens. There is no indication of a distinct suprameatal fossa (suprameatal triangle or mastoid fossa). The zygomatic process is well preserved in IVPP V7439 (figs. 49, 50). It forms the posterior half of the zygomatic arch. Both the ventral and dorsal border of the zygomatic process is very narrow, thin, and sharp. The zygomatic process extends horizontoposteriorly, but the ventral border extends anterodorsally, so that the zygomatic arch tapers at its anterior end and

overlaps with the jugal at the level of the anterior edge of the temporal fossa. The zygomatic process is slender and elongate and meets the jugal at a diagonal suture. The medial surface of the zygomatic process is basically flat. The posterolateral surface of the zygomatic process of the squamosal is slightly convex.

In ventral view, the glenoid fossa is large, square, slightly concave, and elongated anteroposteriorly (figs. 45, 52). The surface of the glenoid fossa is smooth. The postglenoid process is not well preserved in any specimen. Based on the left side of IVPP V7439, where the process is partially preserved, the postglenoid process is large, compressed anteroposteriorly, and transversely located (figs. 45, 52). The medial part of the postglenoid process is triangular, situated at the medial aspect. The lateral part is small, located at the lateral aspect. There is a wide concave area in the medial side of the posterior wall of the postglenoid process. The postglenoid foramen is not well preserved in the specimens. Based on the left side of IVPP V7439, where the posterior wall of the postglenoid process is better preserved, there is no indication of the postglenoid foramen, so the postglenoid foramen may be either small or absent. Posterior to the postglenoid process, the meatal surface of the squamosal is short and narrow. Its ventral side is a sharp ridge. The meatal surface curves ventrally, well below the roof of the tympanic cavity, and its posterior boundary is marked by a distinct ridgelike posttympanic process.

In lateral view, the posttympanic process is prominent, compressed mediolaterally, and triangular (fig. 52). The ventral part of the posttympanic process connects with the mastoid process, forming the squamosal-mastoid suture. The squamosal-mastoid suture is short, simple, and straight, with the posttympanic process anteriorly and the mastoid process posteriorly located. The petrotympanic fissure (Glaserian fissure) is not well preserved. At the lower posterior region of the temporal fossa, the squamosal has a short connection with the alisphenoid. The squamosal-alisphenoid suture is irregularly shaped, running ventrally from the triple junction of the parietal, squamosal, and alisphenoid, then turning posteriorly, horizontally, and also ventrally and ending at the anteromedial aspect of the postglenoid fossa (fig. 52). The squamosal has a long connection with the petrosal at its medial side. The squamosal-petrosal suture is a simple curve.

Petromastoid: The mastoid-petrosal portion of the skull is well preserved on the right side of IVPP V5352 and the left side of V7349 (fig. 52).

In ventral view, the petrosal is a very prominent element in the basicranial region, occupying almost half the region (fig. 52). It is dominated by a large promontorium in the tympanic cavity. The promontorium of V5352 is fusiform, but almond shaped in V7349. The promontorium is broadest at its posterior edge and tapers toward the anteromedial aspect of the tympanic cavity. The surface of the promontorium is strongly convex ventrolaterally. The medial connection of the petrosal with neighboring bones is not clear, due to the poor preservation. The lateral edge of the promontorium touches the thin bony roof, the tegmen tympani, of the tympanic cavity, which can be seen in V7439 (fig. 52). The tegmen tympani contacts the squamosal with a curved, interdigitated suture laterally, which continues to run posteriorly to contact the posttympanic process of the squamosal with a short, simple squamosal-mastoid suture at the posterolateral aspect of the skull. The promontorium connects the mastoid by a stout bony bridge posteriorly. The promontorium-mastoid suture can be seen in V7439. It is very short and straight, running from the triple junction of the posttympanic process of the squamosal, mastoid, and promontorium laterally. The fenestra rotunda and the fenestra ovalis can be clearly seen in V5352. There are three foramina situated at the mediposterior aspect of the promontorium. The fenestra rotunda (cochleae) is small, oval, and elongated obliquely, situated at the mediposterior aspect of the promontorium, which differs from that in most mammals in position. The

FIG. 52. *Naranius hengdongensis* sp. n., IVPP V7439, stereophotograph of left ear region in ventral view.

fenestra rotunda faces posteromedially. There is no dorsal rim to cover the fenestra rotunda. Dorsoposterior to the fenestra rotunda is a large, circular foramen. Dorsomedial (almost in the intracranial surface) to the fenestra rotunda is a small foramen that is most likely the opening of the aqueductus cochleae (cochlear aqueduct). It carries the perilymphatic duct to the subarachnoid space. There is a robust bony ridge at the posterior end of the petrosal, which can be seen clearly in V7439. The fenestra ovalis (vestibuli) is situated at the lateroposterior aspect of the promontorium, anterior to the bony bridge connecting the mastoid process. The fenestra ovalis is small, oval, elongated, and opens laterally. Anterior to the fenestra rotunda, there is a shallow groove, the sulcus for the internal carotid artery. The groove can be seen clearly at the medial side of IVPP V5352, and runs laterally from the posterior end of the petrosal ridge at the posteromedial aspect of the promontorium toward the fenestra ovalis, which is for the stapedial artery. In V5352, there is a bony ring preserved at the middle of the ventral side of the promontorium. There is a long, narrow groove that can clearly be seen in V7439, but not in V5352, along the dorsomedial edge of the promontorium, running from the posteromedial aspect of the promontorium to its anteromedial aspect. This groove may be interpreted as the sulcus for the inferior petrosal sinus (Novacek, 1986: 54, fig. 20).

The tympanic cavity is better preserved in IVPP V7439. Lateral to the fenestra ovalis in the tympanic cavity, there is a large, deep, round fossa, the epitympanic recess (fig. 52). Lateral to the epitympanic recess, the tympanic contacts the squamosal laterally. The tensor tympani fossa is not well preserved in the specimen. Posterior to the epitympanic fossa is a round fossa for attachment of the stapedial muscle. The medial edge of the promontorium, the basisphenoid, and basioccipital are not well preserved and separated by a wide gap, so that the posterior lacerate foramen, jugular foramen, and their relationship with surrounding bones cannot be determined. The piriform fenestra is situated at the anterior wall of the tympanic cavity.

In the intracranial view of the promontorium of V5352, where the basisphenoid and basioccipital are not preserved, we can see that a large, deep, and round subarcuate fossa is transversely situated on the dorsal side. The ventral part of the subarcuate fossa is broken, so that the internal acoustic meatus cannot be observed.

The mastoid is a distinctive element, which is best preserved in IVPP V7439 (fig. 52). In ventral view, the mastoid is roughly rectangular. Medially, it contacts the jugular process of the occipital in a short, straight suture. Laterally, it contacts the posttympanic process of the squamosal in a simple straight line. Anteriorly, the mastoid connects with the promontorium of the petrosal by a stout bony bridge with a very short simple suture medially and the tympanic bone laterally. The posterior edge of the mastoid forms the ventral border of the occipital region of the skull lateroposteriorly. The surface of the mastoid is smooth, broad, and slightly damaged. The mastoid is not exposed in the lateral side of the skull.

In occipital view, the mastoid is very distinct and has a broad exposure at the lower lateral aspect of the occipital region. It is roughly rectangular. It contacts the supraoccipital in a short, simple suture dorsally and the exoccipital laterally in a longer curved line. At the lower medial edge it contacts the jugular process of the occipital.

Occipital: The occipital is incompletely preserved in IVPP V-5352, V5353, and V7439. In occipital view, the occipital is roughly semicircular. The occipital does not project posteriorly beyond the lambdoid crest. The supraoccipital occupies the whole middorsal part of the posterior wall of the skull and is semicircular. The surface of the supraoccipital is slightly convex. The supraoccipital contacts the lambdoid crest dorsally and the exoccipital ventrally. The ventral part of the supraoccipital is not well preserved, but it forms the dorsal rim of the foramen magnum, judging from the shape of the preserved part. The supraoccipital-exoccipital suture can be seen in the left side of V7439. It is a simple straight line, running obliquely laterally from the middle of the dorsal rim of the foramen magnum to the triple junction of the mastoid process, supraoccipital, and exoccipital. The exoccipital is smaller than the supraoccipital and roughly triangular. It contacts the mastoid process at the triple junction of the mastoid, supraoccipital, and exoccipital. The mastoid is exposed in occipital view and extends laterally to the supraoccipital. There is no clear mastoid foramen. The paroccipital process is large and transversely elongated. It contacts the exoccipital dorsally and the mastoid process laterally in the posterior wall of the skull. The paroccipital-exoccipital suture is not well preserved. The paroccipital is well separated from the mastoid process by a wide gap. The foramen magnum is not well preserved, but appears to have been circular. The occipital condyle and basioccipital region are not well preserved.

Comments on *Naranius americanus*

The genus *Naranius* has been known as an Asian endemic taxon. It is represented by the type species, *N. infrequens*, which was discovered from the early Eocene Bumban Member of the Nemegt Formation, Mongolia, and the new species, *N. hengdongensis*, which was from the early Eocene Lingcha Formation of the Hengyang Basin, Hunan Province, China. *Naranius americanus* is the only reported species of *Naranius* outside Asia. The holotype of *N. Americanus*, a left m3 (CM 81283), and a referred specimen with right m2 (CM 81282), were collected from the upper part of the Tuscahoma Formation, Lauderdale County, Mississippi (early Wasatchian of the Gulf Coastal Plain; Beard and Dawson, 2009). The authors refer the specimen to the genus *Naranius* basically because of its small size and some similarities of lower molars to that of *N. infrequens*, such as "relatively tall trigonids and long talonids of the lower molars, the open lingual margins of the lower molars, and the relatively small size of the lower molar paraconids which are nonetheless located fairly high on the trigonid, near the base of the corresponding metaconid" (Beard and Dawson, 2009: 204). The

similarities that the authors mentioned above are mainly primitive characters that occurred in many early insectivorans. *N. americanus* differs from *N. infrequens* in having the m2 talonid longer, cristid obliqua of m2 and m3 labially located, indistinct hypoconulid of m2, and less open lingual side of the talonid. The most characteristic feature for *Naranius* is the considerably reduced and small P2–3 and p2–3, for which we are not aware in *N. americanus*. Also, we do not have any information on the upper dentition of *N. americanus*. The classification of *N. americanus* is very uncertain based on available evidence.

? DIDYMOCONIDAE

Figures 53–54; tables 1, 2

Specimen IVPP V7441 (? Insectivora gen. et sp. uncertain, of Ting, 1995) is an anterior part of a skull. It has four right and two left fragmentary teeth and two alveoli on the right side and one alveolus on the left side after the fourth tooth (field number: 76003) (fig. 53).

A round root represents the canine. It is single rooted and strong. There are four fragmentary teeth preserved on the right side behind the canine (figs. 53A, 54B). The lingual part of the first two teeth is preserved. They are close together, two rooted with simple major cusps and a small heel, and are strongly compressed transversely. The crown of the third tooth is better preserved and separated from the second one by a short diastema. It is larger and wider than the first two teeth, compressed transversely, and has two roots, a large major cusp, and a basin-shaped posterior edge. Its lingual cingulum is distinct, situated at the posterior half of the tooth, and the labial cingulum is much shorter than the lingual one and situated at the posterior end of the tooth. The most lingual part of the fourth tooth is preserved on both left and right side. The fourth tooth is closely positioned behind the third and is triangular. It has a conical, low protocone and a large inflated parastyle. Two crests extend from the protocone toward the labial edge of the tooth. The protoconule and the metaconule are distinct and situated on the crests. Based on the broken middle and labial part of the tooth, it should have a large cusp at the middle of the tooth. Well-preserved right and left alveoli behind the fourth tooth indicate that there is definitely another tooth behind the fourth tooth. There is a partial lingual ridge behind the fifth tooth on the right side, which indicates that the sixth tooth may occur in V7441. The portion of the maxilla posterior to the last alveolus is very thin.

In dorsal view, the nasal is narrow, extending posteriorly at the level above the alveolus of the fifth tooth (figs. 53B, 54A). The nasal-maxillary suture is simple and straight. Posteriorly, it contacts the frontal in a V-shaped suture with the apex of the V pointing posteriorly. The maxilla is large and broad (figs, 53B, C, 54A–C). It contacts the frontal in a short, curved suture. The orbital foramen is large and round, situated above the posterior edge of the third tooth. In ventral view, the maxilla occupies about two-thirds the length of the palatal area. It is narrow and straight, and extends from the canine to the posterior edge of the second tooth and laterally to the fourth tooth. The maxilla contacts the palatine in a V-shaped suture, with the apex of the V at about the level between the third and fourth teeth. The surface of the maxilla is flat and smooth. The palatine is long, narrow, and irregular in shape, and has a flat and smooth surface. On the left side of the palatine, there are three palatine foramina: one situated at the level of the anterior edge of the third tooth, one at the level of the posterior edge of the fourth tooth that is paired with its left counterpart, and one at the level of the fifth tooth. The postpalatine torus is well developed and has a ridgelike anterior edge. In lateral view, the maxilla occupies a large area of the orbital region, and extends ventrally, almost reaching the ventral border of the medial wall of the orbital fossa (figs. 53C, 54C). It contacts the lacrimal at its anterior aspect. The maxilla-lacrimal suture is not well preserved. The maxilla contacts the palatine in a zigzag suture ventrally

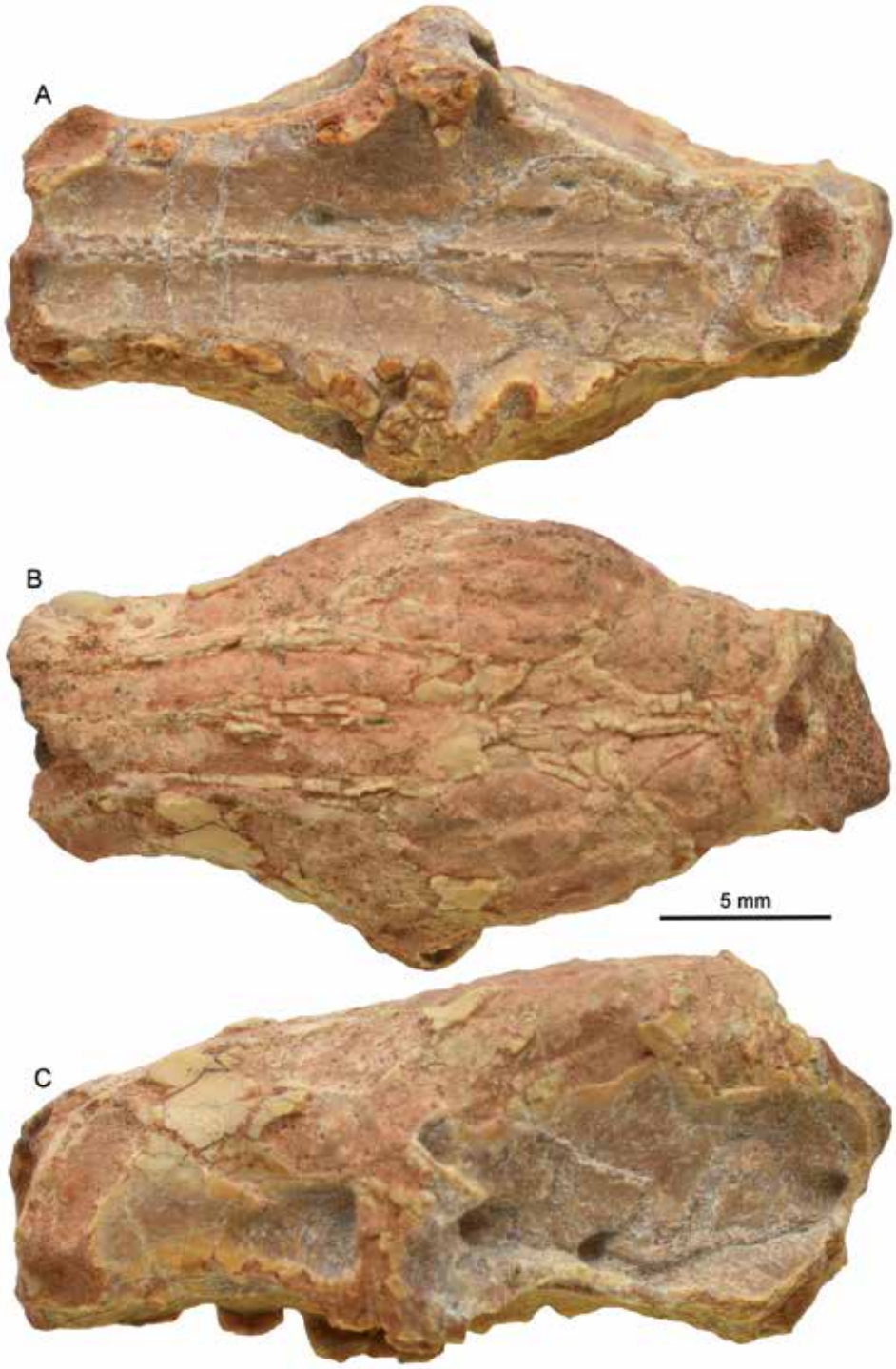

FIG. 53. Anterior part of skull of ?Didymoconidae, IVPP V7441: **A.** ventral, **B.** dorsal, and **C.** left lateral views.

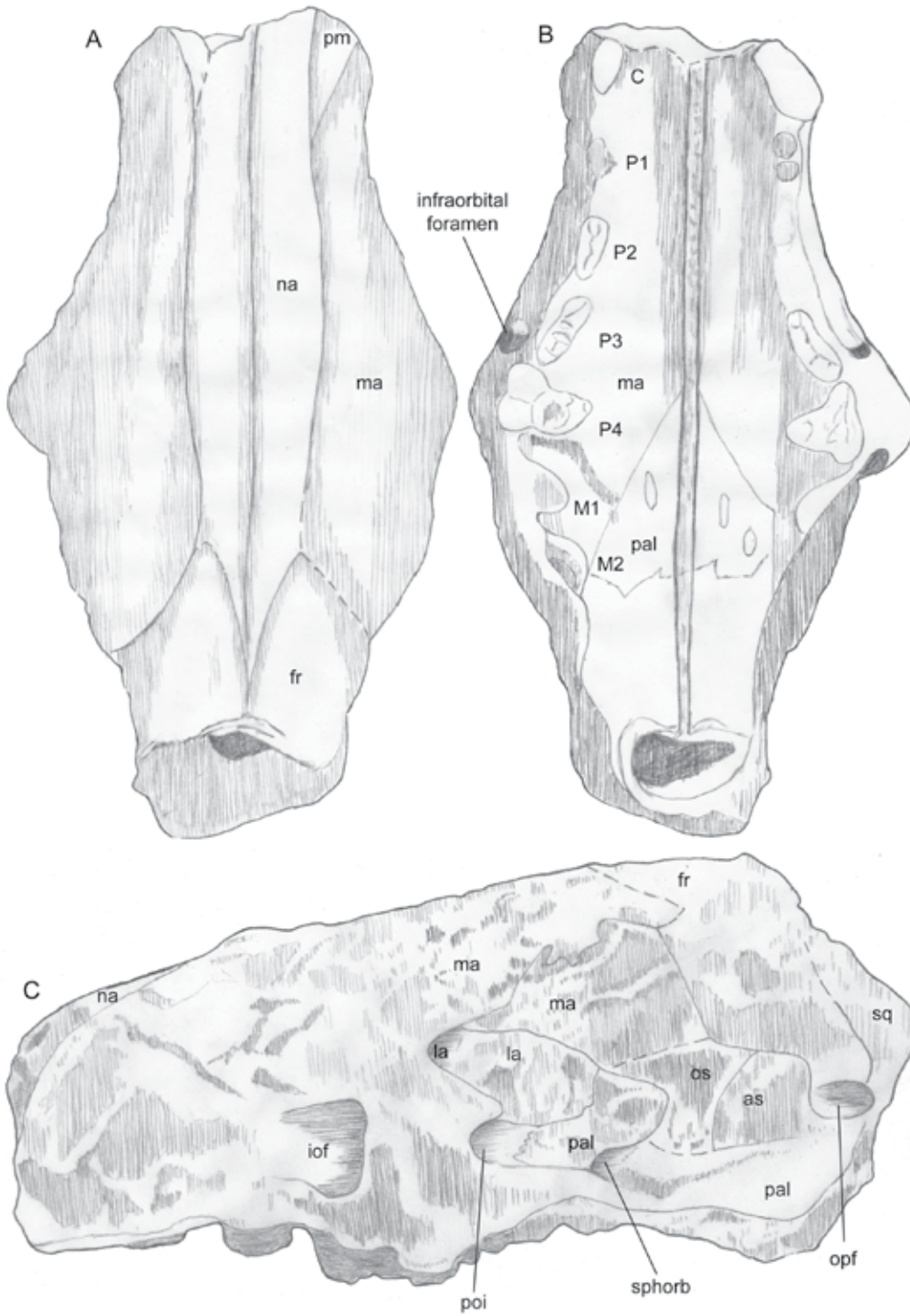

FIG. 54. Drawing of anterior part of skull of ?Didymoconidae: **A.** dorsal, **B.** ventral, and **C.** left lateral views (based on IVPP V7441).

and the frontal in a wide-open V-shaped suture posteriorly. Its ventral posterior end contacts the orbitosphenoid in a simple and straight line. Posterior to the maxilla-orbital suture is the orbitosphenoid. It contacts the frontal dorsally, the alisphenoid posteriorly, and the palatine ventrally. The frontal extends about one third ventrally in the medial wall of the temporal fossa, and is triangular. The alisphenoid is large and rectangular. It contacts the squamosal posteriorly with an oblique suture. A small ethmoid foramen is situated at the dorsal anterior aspect of the orbitosphenoid. The optic foramen is large, situated at the dorsal edge of the frontal, and covered by a well-developed ridge dorsally. A partial squamosal is preserved behind the alisphenoid-squamosal suture. The lacrimal is large and irregular in shape, and its surface is smooth and curved. The lacrimal foramen is small and separated from the posterior opening of the orbital foramen by a strong ridge, so that the lacrimal foramen seems situated in a small fossa above the orbital foramen. The palatine occupies most of the ventral border of the orbit and temporal fossa (figs. 53A, 54B). The anterior part of the palatine extends dorsally, occupying about half the medial wall of the orbital fossa and contacting the maxilla. The sphenopalatine foramen is large and round, situated at the level above the sixth tooth. Posterior to the sphenopalatine foramen is the dorsal palatine foramen. It is smaller than the sphenopalatine foramen, narrow, oval, and extending anteroposteriorly.

IVPP V7441 is much smaller than *Archaeoryctes notialis* (Zheng, 1979), and about the size of *Hunanictis inexpectatus* (Li et al., 1979) or slightly larger. The first three teeth behind the canine of IVPP V7441 are two-rooted premolars. The morphology of the third tooth is somewhat similar to that of the P3 of *Archaeoryctes notialis*, but differs from the later in being more compressed and having no lingual projection of the tooth. It differs from *Hunanictis inexpectatus* in having a less-developed protocone. The morphology of the fourth tooth is similar to the P4 of *Archaeoryctes notialis* in its triangular shape and its strongly developed paracone situated in the middle part of the crown, protocone situated slightly anteriorly, and well-developed parastyle and metastyle. It differs from the later in that it is less molarized. It differs from *Hunanictis inexpectatus* in having a less-developed protocone. If the fourth tooth is P4, it means that IVPP V7441 had four premolars with a two-rooted P1. The very thin portion of the maxilla after the last alveolus indicates that V7441 may have had only two teeth after the fourth tooth. Based on the two alveoli after the fourth tooth and morphology, it is likely that V7441 had four premolars and two molars, which means it probably represents a new didymoconid with unmolarized P1–3 and submolarized P4. The classification of IVPP V7441 remains uncertain until better material is found.

? INSECTIVORAN-GRADE MAMMAL

Figure 55; tables 1, 2

The specimen IVPP V7442 (? Insectivora gen. et sp. uncertain, of Ting, 1995) is a fragmentary anterior part of skull. It has the root of the right canine, fragmentary crown of right four teeth (? P1–4 or P2–M1), and two alveoli after the fourth tooth (?M1–2 or M2–3) (field number: 76004) (fig. 55).

IVPP V7442 is about one third smaller than IVPP V7441 and *Hunanictis inexpectatus*. The canine is large and has a single round root. The first tooth is small and single rooted, and separated from both the canine and P2 by a short diastema. The second tooth is double rooted. The third tooth is slightly larger than the second, with two roots, and closely situated behind the second. The fourth tooth is triangular and follows close behind the third. The fifth tooth is situated behind the fourth tooth with a large diastema. The sixth tooth is situated behind the fifth tooth with a large diastema, and it is smaller than the fifth tooth.

The skull is somewhat compressed, so that the sutures of most bones are not clear. The anterior

part of the skull is narrow. In dorsal view, the nasals are long, extending posteriorly to the level above the last tooth, to contact the frontal. The nasal-maxilla suture is simple and straight. The nasal-frontal suture is not well preserved, and is U-shaped and simple based on the preserved part of the nasal-frontal contact. The maxilla has a very narrow exposure in dorsal view, and extends ventrally near the nasal-maxilla suture. The maxillary-frontal suture is short and curved, extending anteriorly from the triple junction of the nasal, maxilla, and frontal. The frontal is short, but wide in dorsal view. The frontal-parietal suture is a simple, wide-open U-shaped line, curving anteriorly. The parietal has a large exposure in dorsal view. Its surface is slightly convex at the middle. The squamosal has a narrow exposure in dorsal view and contacts the parietal in a simple, straight suture. In ventral view, the maxillary occupies more than half the palatal area. It contacts the palatine in a V-shaped suture with the apex of the V pointing anteriorly. The maxillary-palatine suture runs anteromedially from a short distance posterior to the last tooth, to the level of the fourth tooth. The palatine is triangular, and has a well-developed, round postpalatine torus. The pterygoid process is long and thin. In lateral view, the lacrimal is not well preserved. The maxilla is large and deep anterior to the infraorbital foramen. The anterior opening of the infraorbital foramen is situated above the level of the fourth tooth. The maxilla has a large exposure in the orbital region. It is irregular in shape and extends ventrally to reach the ventral border of the orbital fossa. It contacts the frontal in a short, oblique suture, and contacts the palatine at its posterior end. The sphenopalatine foramen is large, round, and situated at a level above the maxilla-palatine suture. The frontal has a triangular exposure in the medial wall of the temporal region. It contacts the parietal posteriorly in a short simple suture. The parietal has a very small exposure in the dorsal part of the medial wall of the temporal region and separates the frontal and squamosal. The squamosal has a large exposure at the posterior part of the temporal fossa. The orbitosphenoid and alisphenoid occupy the most posterior part of the medial wall of the temporal fossa, but the orbito-alisphenoid suture is not clear. The palatine has a large exposure at the medial wall of the temporal fossa, which reaches the middle of the medial wall of the temporal fossa.

The dentition of IVPP V7442 is poorly preserved. It may represent an "insectivoran" mammal based on the triangular fourth tooth. Its classification will remain uncertain until more material is recovered.

PHYLOGENETIC ANALYSIS

We selected 36 species, representing 34 genera, for the phylogenetic analysis. Each genus is represented by one species, except *Naranius*, represented by two species, *N. infrequens* and *N. hengdongensis*, and *Nuryctes*, represented by two species, *N. qinlingensis* with lower dentition and *N. alayensis* with upper dentition. The selected taxa include some basal "insectivorans" as major comparative components: *Aaptoryctes ivyi, Centetodon chadronensis*, *Cimolestes magnus*, *Eoryctes melanus*, *Leptictis dakotensis*, *Micropternodus borealis*, *Palaeoryctes puercensis*, *Palaeosinopa veterrima*, and *Pantolestes natans*. To test the relationship of *Hsiangolestes youngi* and *Naranius hengdongensis* with other Asian early Paleogene insectivorans, we choose some recently reported Asian fossil "insectivorans" with relatively better preserved specimens for comparison, including *Asionyctia guoi*, *Bumbanius rarus*, *Carnilestes palaeoasiaticus*, *Changlelestes dissetiformis*, *Eochenus sinensis*, *Eogalericius butleri*, *Eosoricodon terrigena*, *Gobigeolabis verigranum*, *Jarveia minuscula*, *Luchenus erinaceanus*, *Naranius infrequens*, *Nuryctes alayensis, Nuryctes* (*Neoryctes*) *qinlingensis*, *Praolestes nanus*, *Prosarcodon lonanensis*, *Sarcodon pygmaeus*, *Scileptictis simplus*, *Sinosinopa sinensis*, *Tsaganius ambiguus*, *Voltaia minuta*, and *Zhigdenia nemegetica*. We choose two Cretaceous eutherians, *Asioryctes nemegetensis* and *Maelestes gobiensis*, as outgroups. The extant lipotyphlan taxa are *Blarina brevicauda*

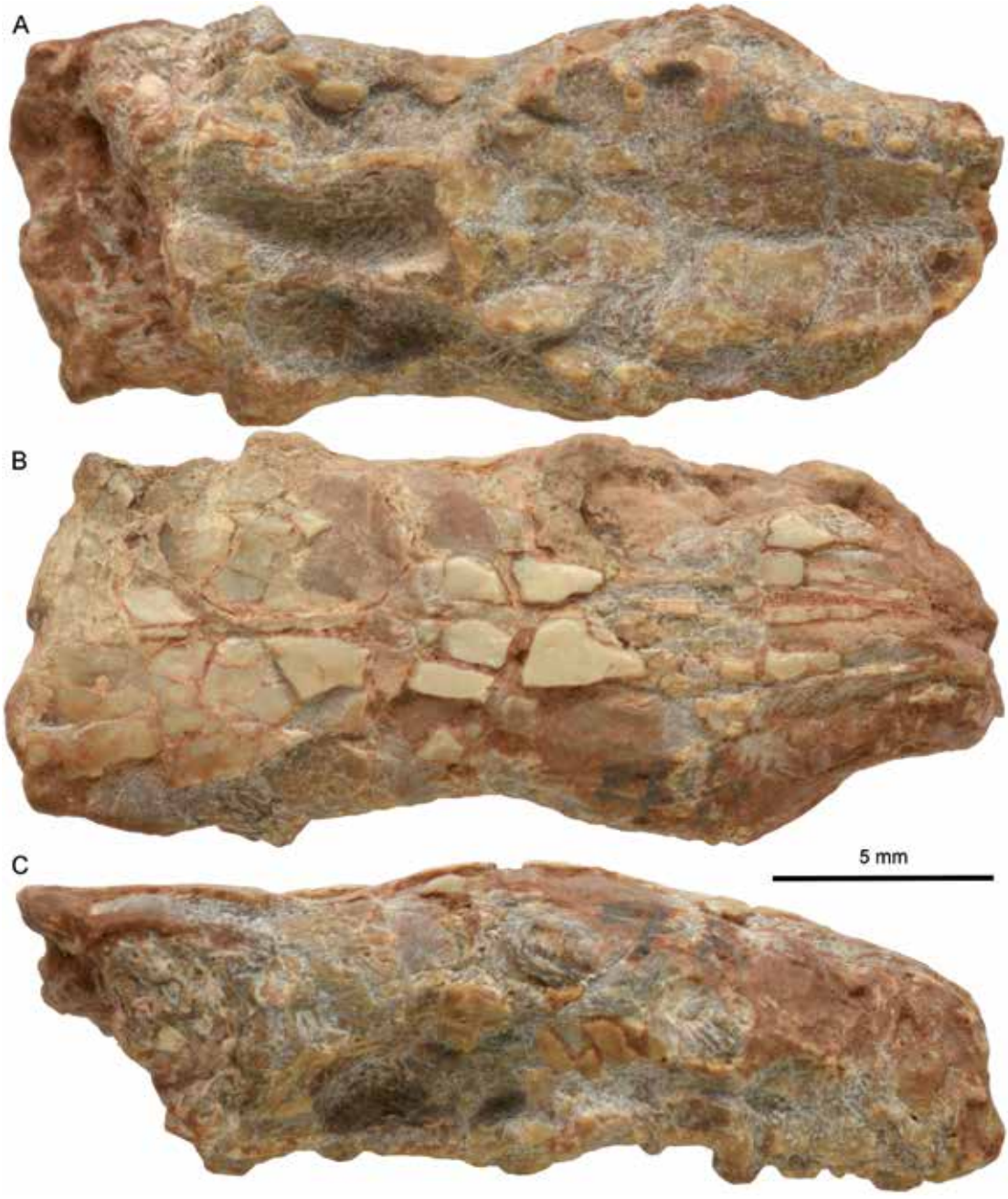

FIG. 55. Anterior part of skull of ?Insectivora, uncertain, IVPP V7442: **A.** ventral, **B.** dorsal, and **C.** right lateral views.

and *Erinaceus europaeus*. The sources of selected taxa are listed in appendix 1.

The characters are selected mainly from those of Wible et al. (2009). We made some changes in the description and character states from Wible et al. (2009), based on our observations. These are marked in the character list with an asterisk. We also chose some characters from Butler (1947), Novacek (1986), Asher et al. (2002), and Lopatin (2006), for which we present the source of data for each character. The characters and character states are presented in appendix 2. We compiled 290 characters and 667 states over 36 terminal taxa by using McClade 4 with observations on the specimens as well as casts and from literature. These are shown in Taxon-Character Matrix. Numbers (0–5) refer to states of those characters. "/" means "either/or" "&" means "and" the taxa have both characters. Both "/" and "&" are treated as "/" in the phylogenetic analysis. The number of scored character states (nonmissing data) and the completeness of each taxon (the number of nonmissing data divided by the total number of characters, 290 for skull and dental and 130 for dental in this case) are listed at the end of the sequence for each taxon in Taxon-Character Matrix. S&D refers to scored numbers of skull and dental characters; D refers to scored numbers of dental characters.

Initial coding of data matrix is done in MacClade (Maddison and Maddison, 2005) and is later manipulated in Mesquite (Maddison and Maddison, 2018). Missing character is designated "?" and inapplicable characters "-." Missing or inapplicable characters have several causes. First, character states may be unknown due to a lack of preservation, i.e., missing characters. This is especially common in the Asian early Paleogene insectivorans. Other than *Hsiangolestes youngi* and *Naranius hengdongensis*, most Asian taxa did not have skulls and only a few of them have the dentaries preserved. Therefore, character states of Asian taxa are mainly based on the dentition; however, some of the taxa did not even have complete dentition. For example, *Tsaganius ambiguus* and *Voltaia minuta* are represented only by the lower dentition and their dental character completeness is 31%. Second, certain character states are not applicable to a given taxon, i.e., inapplicable characters. For example, the morphology and size of P/p1 and M/m3 cannot be coded for the taxa that lack these teeth, such as lack of P/p1 in *Aaptoryctes ivyi*, *Asionyctia guoi*, *Blarina brevicauda*, *Eoryctes melanus*, *Erinaceus europaeus*, *Micropternodus borealis*, *Nuryctes* (*Neoryctes*) *qinlingensis*, *Palaeoryctes puercensis*, and *Zhigdenia nemegetica*; and lack of M/m3 in *Carnilestes palaeoasiaticus* and *Prosarcodon lonanensis*. Third, in some cases, the morphology of a taxon may be unobservable, for example, because of damage of the labial side of P4–M1 in *Zhigdenia nemegetica* or information lacking in the references, and these cases are treated as missing characters here. Characters are equally weighted. Parsimony analysis is initially explored by PAUP (Phylogenetic Analysis Using Parsimony, PAUP* 4.0, Macintosh Beta Version 10) (Swofford, 2014) and later in TNT (Goloboff and Catalando, 2016). We used New Technology search option in TNT (options: Sectorial Search, Ratchet, Drift, Tree Fusing, and finding minimum length 1000 times). TNT found 35 equally parsimonious trees with a length of 983 steps. Figure 56 is the majority rule consensus tree based on the 35 shortest trees with numbers in red indicating percent of support and black numbers in circles being node numbers assigned by TNT.

Sarcodontidae

Our cladistic analysis on the 36 terminal taxa with over 290 cranial and dental characters (fig. 56: node 62) supports the monophyletic clade of Sarcodontidae, including *Hsiangolestes*, *Sinosinopa*, *Prosarcodon*, and *Sarcodon*. Monophyly of the family is well supported by several cranial (chars. 134, 224, 242) and dental (1, 9, 56, 73, 74, 112, 114) synapomorphies, and supported by 100% of shortest tree discovered by TNT. In the majority rule tree, *Hsiangolestes* is in an Asian

clade, with three other Asian genera, *Sinosinopa*, *Prosarcodon*, and *Sarcodon* (fig. 56: node 62). Three cranial synapomorphies, coronoid process width (char. 134), foramen ovale composition (char. 224), and basisphenoid tympanic process (char. 242), are unknown (coded as missing) in *Sinosinopa*, *Prosarcodon*, and *Sarcodon*. Number of postcanine tooth (char. 1), number of lower incisor (char. 9), and M1 width (char. 73) in *Sarcodon,* M1 width (char. 73) and M2 parastyle and metastyle lobe labial extension (char. 74) in *Prosarcodon*, and number of lower incisor (char. 9) and diastema posterior to p2 (char. 56) in *Sinosinopa* are unknown. *Hsiangolestes* has several autamorphies: I1 subequal to I2 in size (char. 6), presence of a diastema posterior to P2 (char. 30), P3 paracone greatly enlarged (char. 32), P4 less asymmetrical (char. 48), p3 subequal to p2 in size (char. 57), p3 protoconid subequal to that of p4 (char. 58), paracrista weak (char. 85), protocristid transversely situated (char. 116), talonid multicuspid basined (char. 118), internal carotid artery course transpromontorial (char. 245), and fenestra cochlear posteromedially situated to fenestra vestibule (char. 264).

Hsiangolestes was first identified as a didymoconid (Zheng and Huang, 1984), and was later assigned to Cimolesta (McKenna and Bell, 1997) and Lipotyphla (Lopatin and Kondrashov, 2004; Lopatin, 2006) respectively. Our study indicates that *Hsiangolestes* is neither related to our redefined Cimolestidae (*Cimolestes* + *Naranius*; see Phylogenetic Analysis below) nor to Lipotyphla as McKenna and Bell (1997) and Lopatin (2006) suggested. We assigned *Hsiangolestes* to the new family Sarcodontidae, order incertae sedis. In the majority rule tree (fig. 56: node 70), *Hsiangolestes* is sister to *Sinosinopa-Prosarcodon-Sarcodon*. This clade is supported by seven dental synapomorphies (chars. 23, 42, 47, 66, 99, 113, 125). Absence of P3 protocone (char. 33), not well-developed protocone on P4 (char. 39), and P4 less asymmetrical (char. 48) in *Hsiangolestes* shows less-molariform premolar, which indicates that *Hsiangolestes* is more primitive. Morphologically, the dentition of *Hsiangolestes* is the most similar to that of *Sinosinopa* among the Sarcodontidae.

The next node in the majority rule tree, where *Prosarcodon* and *Sarcodon* are clustered (fig. 56: node 69), is strongly supported by six dental synapomorphies (chars. 69, 87, 96, 100, 106, 115). *Prosarcodon* and *Sarcodon* are sister group in 100% of shortest trees. *Prosarcodon*, represented by type species *P. lonanensis*, was originally assigned to Micropternodontidae under Palaeoryctoidea, Soricomorpha, Lipotyphla (McKenna et al., 1984; McKenna and Bell, 1997). *Sarcodon*, represented by *S. pygmaeus*, Matthew and Granger, 1925, was first referred to order uncertain (? Carnivorous Marsupial). Szalay and McKenna (1971) assigned it to the family Deltatheridiidae, Palaeoryctoidea, Insectivora. It was placed within Micropternodontidae under Palaeoryctoidea, Soricomorpha, Lipotyphla by McKenna and Bell (1997). Postcingulum extending lingual to metaconule (char. 100) shared by *Prosarcodon* and *Sarcodon* show more similarities in their dental morphology compared with *Hsiangolestes*. The distinctive character in *Prosarcodon* is presence of two molars (char. 70), which indicate that this clade may represent a subfamily of the family Sarcodontidae differing from *Hsiangolestes* and *Sinosinopa* as Lopatin (2006) suggested.

In reporting some new Asian early Paleocene to middle Eocene insectivoran-grade mammals, Lopatin and Kondrashov (2004) proposed two lineages of the family Micropternodontidae. They suggested that *Prosarcodon lonanensis*, *Prosarcodon matures* (Lopatin and Kondrashov, 2004), *Sarcodon pygmaeus*, *Sarcodon minor* (Meng et al., 1998), *Sarcodon zhai* (Huang, 2003), *Hyracolestes ermineus* (Matthew and Granger, 1925), *Metasarcodon udovichenkoi* (Averianov, 1994), *Metasarcodon reshetovi* (Lopatin and Kondrashov, 2004), and *Carnilestes palaeoasiaticus* represented a separate Asian micropternodontid lineage and established a new subfamily, Sarcodontinae, under Micropternodontidae. Another proposed lineage, including Asian *Hsiangolestes youngi*, *Sinosinopa sinensis*, *Bogdia*

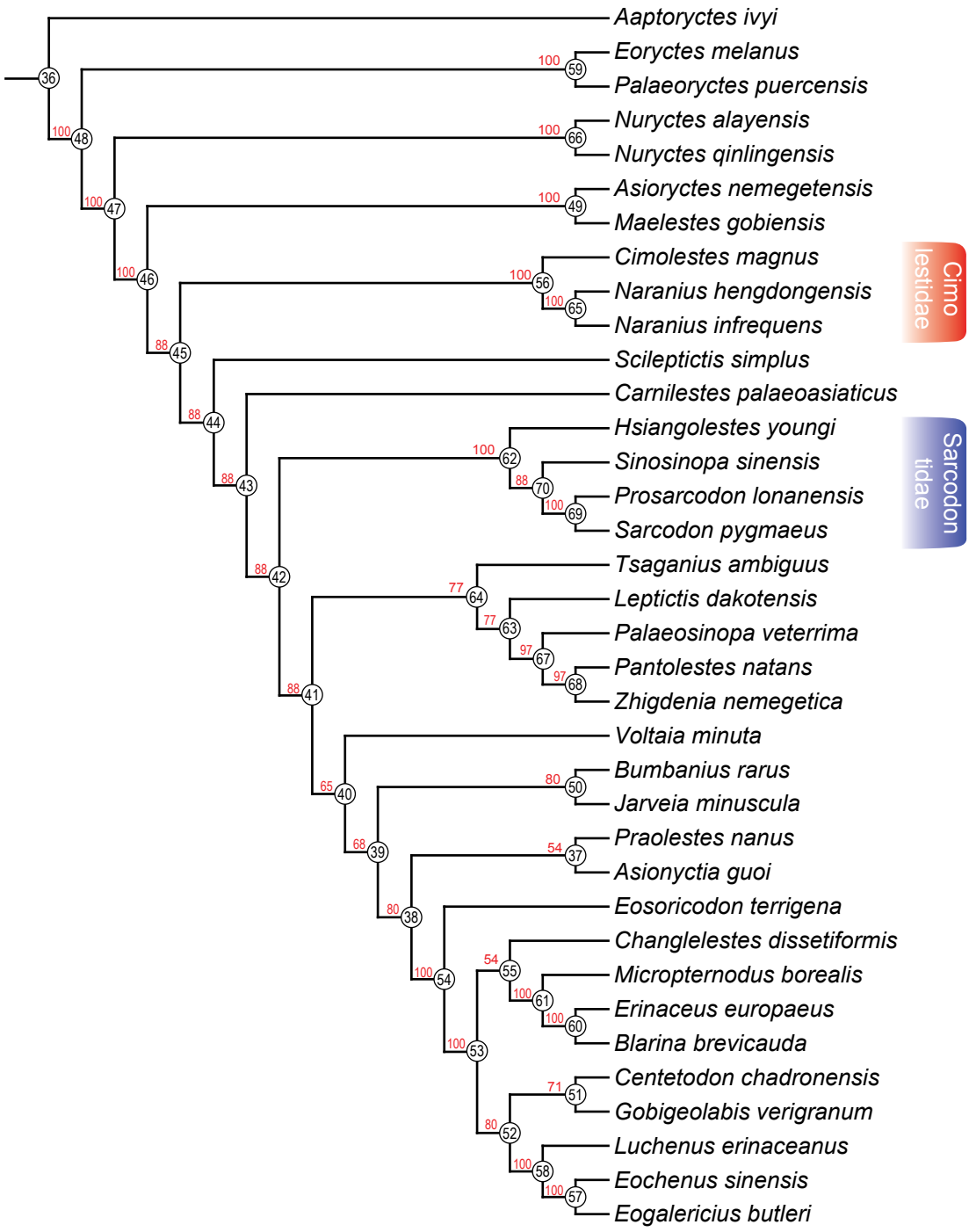

FIG. 56. Majority rule consensus tree (cut-off = 50, tree length = 983, consistency index = 0.389, retention index = 0.461 from 35 equally parsimonious trees discovered by TNT (New Technology search using Sectorial Search, Ratchet, and Tree fusing, setting Find minimum length at 1000 times) (Goloboff and Catalando, 2016).

orientalis (Dashzeveg and Russell, 1985), and North American *Micropternodus* and *Clinopternodus*, was under the subfamily Micropternodontinae. They also mentioned that their Sarcodontinae "clearly differs from Micropternodontinae in lacking the M3/3 and in the absence of the hypoconal shelf on the P4 and M2" (Lopatin and Kondrashov, 2004: 183). Lopatin (2006) later listed Sarcodontinae and Micropternodontinae under family Micropternodontidae (Soricomorpha, Lipotyphla). We propose raising Sarcodontinae to the family level Sarcodontidae. Differing from Sarcodontinae proposed by Lopatin and Kondrashov (2004), the family Sarcodontidae includes *Hsiangolestes*, *Sinosinopa*, *Prosarcodon*, and *Sarcodon*, whereas *Carnilestes* is excluded. Although, we did not choose *Metasarcodon* for phylogenetic analysis, its dental morphology is similar to that of *Sarcodon* and *Prosarcodon*. We include it in the family Sarcodontidae. In describing *Prosarcodon*, McKenna et al. (1984) suggested that *Prosarcodon*, *Sarcodon*, and *Sinosinopa* were soricomorph lipotyphlans, mainly based on the presence of a piriform fenestra in *Prosarcodon*. Although, a piriform fenestra occurred in some extant soricids, it was considered a primitive character "very like *Palaeoryctes*" (Butler, 1988: 135) and with "moot significance" (MacPhee and Novacek, 1993: 27), which by itself is insufficient to indicate a Soricomorpha relationship. Therefore, this character was not listed as a valid synapomorphy for the lipotyphlans (Butler, 1988; MacPhee and Novacek, 1993). The rest of the cranial characters of *Prosarcodon* described by McKenna et al. (1984) are basically primitive characters for eutherians (Butler, 1988; MacPhee and Novacek, 1993).

Another clade in the majority rule tree (fig. 56: node 54), clustering 10 lipotyphlan (or eulipotyphlan) genera (*Eosoricodon*, *Gobigeolabis*, *Changlelestes*, *Centedoton*, *Micropternodus*, *Blarina*, *Erinaceus*, *Luchenus*, *Eogalericius*, and *Eochenus*), is strongly supported by six dental synapomorphies (chars. 58, 85, 110, 118, 121, 127). *Eosoricodon terrigetta* and *Gobigeolabis verigranum* have been identified as a nyctitheriidid and a geolabidid soricomorph lipotyphlan respectively (Lopatin, 2006). *Changlelestes dissetiformis* was identified as a soricomorph (Tong and Wang, 1993, 2006), and was later considered as an erinaceidid lipotyphlan (Lopatin, 2006). *Micropternodus* is in a clade with extant lipotyphlan genera, *Blarina* and *Erinaceus* (fig. 56: node 61). The clade is strongly supported by one cranial (char. 156) and six dental synapomorphies (chars. 21, 32, 40, 47, 78, 130). Asian erinaceidid lipotyphlan taxa, *Luchenus ernaceanus* (Tong and Wang, 2006), is in a clade with other two Asian erinaceidid lipotyphlan, *Eogalericius butleri* (Lopatin, 2004) and *Eochenus sinensis* (Wang and Li, 1990) (fig. 56: node 58). This clade is supported by one cranial (char. 143) and eight dental synapomorphies (chars. 40, 49, 58, 66, 84, 85, 91, 113). The family Sarcodontidae and the lipotyphlan clade are paraphyletic (fig. 56).

It is beyond the scope of our work to consider the higher-level relationships of lipotyphlan mammals in detail, but we will make some brief comments on the issue related to the phylogenetic relationship of *Hsiangolestes*. The order Lipotyphla today include families Erinaceidae, Soricidae, Talpidae, and Solenodontidae (Asher, 2018b). Butler (1988) proposed six derived characters supporting the monophyly of the Lipotyphla (Erinaceidae and Soricomorpha), including absence of the cecum, reduction of the pubic symphysis, large maxillary contribution to the orbital wall, mobile snout or proboscis, reduction of the jugal, and the hemochorial placenta. MacPhee and Novacek (1993) later reviewed the six characters and suggested that absence of the cecum, reduction of the pubic symphysis, and large maxillary contribution to the orbit (less certainly) can be considered as the basis for defining Lipotyphla as a monophyletic group, while the other three characters are inappropriate. Unfortunately, the pelvic girdle of *Hsiangolestes* described in this paper did not preserve the relevant part of the pubic symphysis. Almost all extant lipotyphlans show a large maxillary contribution to the orbital wall, and the

maxilla interposes between the lacrimal and the frontal dorsally and the palatine ventrally, separating the palatine from the lacrimal and the frontal (MacPhee and Novacek, 1993). In *Hsiangolestes*, the frontal extends deeply ventrally and occupies the most anterior part of the orbital wall, so that the maxilla is almost fully excluded from the orbital wall and contributes only a very small portion to the lower aspect of the orbital wall. The maxilla mainly comprises the anterior part of the orbital floor. There is no contact between the maxilla and the frontal in the medial wall of the orbit, because of a large intrusion of the palatine bone in that region. In *Hsiangolestes*, the maxilla does not separate the palatine from the lacrimal and the frontal as in the lipotyphlans; instead, it is more similar to the leptictids in this aspect. For reference, we also compare *Hsiangolestes* to the lipotyphlans in some other characters proposed by Butler (1988). *Hsiangolestes* differs from the lipotyphlans in having a longer infraorbital canal, large jugal, normal postglenoid process, and obliquely positioned tympanic membranes.

The taxa included in the Sarcodontidae have been referred to the family Micropternodontidae (McKenna et al., 1984; Ting and Li, 1987; Ting, 1998; Lopatin and Kondrashov, 2004; Lopatin, 2006). The family Micropternodontidae Stirton and Rensberger, 1964 (= Micropternodidae Stirton and Rensberger, 1964) was originally established only for the North American taxon, *Micropternodus*, including *M*. (*Kentrogomphios*) *borealis* and *M*. *morgani*. The phylogenetic position of *Micropternodus* has been controversial since it was first reported (Matthew, 1903). Matthew (1903: 205) considered that the genus "must be placed among the Zalambdodonta, with no very near relatives among living species, although it is not so strikingly different from modern types." It has been also placed within Solenodontidae (Schlaikjer, 1933; Scott and Jepson, 1936), Nyctitheriidae (White, 1954; McDowell, 1958), Apternodontidae (Hough, 1956), "insectivorans" in a broad sense (Russell, 1960), and Erinaceoidea (Stirton and Rensberger, 1964). In his overall review of insectivorans, Van Valen (1966) first included the Asian taxon, *Sarcodon pygmaeus*, in micropternodontid and later established a new order Deltatheridia, in which he listed *Sarcodon* with *Micropternodus*, as other Palaeoryctidae under his new order, and a year later, he grouped *Sarcodon* and *Micropternodus* in the family Micropternodontidae in the order Deltatheridia (Van Valen, 1967). Van Valen (1966: 61) mentioned considerable similarities between *Sarcodon* and *Micropternodus*, but the prominent characters are the "development of the metacrista and the general configuration of the hypocone region." Szalay and McKenna (1971: 287, 288) realized that the lower dentition of *Sarcodon* differs from that of *Micropternodus,* and suggested that "the similarity of the upper molars of *Sarcodon,* but not the lower molars, to those of *Micropternodus* is the result of convergence" and that "*Micropternodus* is probably a nyctitheriid insectivore, but we hold that *Sarcodon* is similar to *Micropternodus* partly because nyctitheres originated from Cretaceous palaeoryctoid stock via *Batodon*." McKenna et al. (1984), however, reconsidered that *Micropternodus* is similar to Asian *Sinosinopa*, *Sarcodon*, and *Prosarcodon*, among palaeoryctoids and palaeoryctoid-like derivatives, because it has *Sarcodon*-like hypocones on P4–M2. Although McKenna et al. (1984: 13) realized that the highly specialized snout of *Micropternodus* separates it from Asian genera by a considerable morphological distance, the authors mentioned "they do not alter cladistics relationships based upon postulated shared-derived cheek-tooth patterns" and included *Prosarcodon*, *Sarcodon*, and *Sinosinopa* in Micropternodontidae under superfamily Palaeoryctoidea of order Soricomorpha (McKenna et al., 1984). The major character to connect *Sarcodon* to *Micropternodus* provided by both Van Valen (1966) and McKenna et al. (1984) is an enlarged jutting hypocone and expanded hypoconal shelf. Actually, the dental morphology of *Sarcodon* is very different from that of *Micropternodus*. The hypocone in *Sarcodon* is smaller and situated much further lingually than the proto-

cone, and the hypocone shelf is smaller and expanded linguoposteriorly. The upper molar of *Sarcodon* is basically triangular. On the other hand, the hypocone in *Micropternodus* is larger and aligned with the protocone, and the hypocone shelf is largely expanded posteriorly, so that the upper molar of *Micropternodus* is square. Butler (1988: 135) suggested that *Micropternodus* "is much too specialized to be considered as a primitive soricomorph; more probably it is a palaeoryctoid that has paralleled the Soricomorpha in some respects." Our study supports the monophyletic clade Sarcodontidae for Asian taxa *Hsiangolestes*, *Prosarcodon*, *Sarcodon*, and *Sinosinopa*. *Micropternodus* is excluded from this clade, indicating that *Micropternodus* is not related to Asian forms previously assigned to "micropternodontids" (now sarcodontids). We agree with Asher (2002: 109) that the "affinity of *Micropternodus* must await an analysis that has a better sample of erinaceomorphs, soricomorphs, palaeoryctids, and Asian micropternodontids." We suggest that the family Micropternodontidae may best be restricted to *Micropternodus borealis* and its North American allies, as Stirton and Rensberger (1964) had proposed.

Naranius

Our cladistics supports the monophyletic clade of Cimolestidae, including *Naranius* and *Cimolestes* (fig. 56: node 56). Monophyly of the family Cimolestidae is well supported by five dental synapomorphies (chars. 43, 54, 99, 113, 125). In the majority rule tree, *Cimolestes* is sister to *Naranius*. The next node (fig. 56: node 65) that united two species of *Naranius*, *N. infrequens* and *N. hengdongensis*, is strongly supported by five dental synapomorphies (chars. 56, 97, 100, 101, 108). Presence of a rudimentary hypocone on the upper molars (char. 101) indicates the derived feature of *Naranius* compared to *Cimolestes*. *N. infrequens* has several autapomorphies: p4 talonid with one cusp (char. 68), centrocrista straight (char. 86), absence of notch on metacrista (char. 88). *N. hengdongensis* has three autapomorphies: m3 larger than m2 (char. 130), one mental foramen (char. 131), and broad coronoid process (char. 134). *Naranius* was previously considered an Asian endemic taxon, found in Mongolia and China. The only species assigned to *Naranius* outside Asia is *N. americanus* from the early Wasatchian, Red Hot local fauna, uppermost Tuscahoma Formation, Lauderdale County, Mississippi (Beard and Dawson, 2009). This species is represented by two isolated teeth, left m3 and right m2. Based on Beard and Dawson (2009: 204–205), the similarities between *N. infrequens* and North American specimens are "relatively tall trigonids and long talonids of lower molars, the open lingual margins of the lower molars, and the relatively small size of the lower molar paraconids (which are nonetheless located fairly high on the trigonid, near the base of the corresponding metaconid." These characters are plesiomorphic characters, common to the early eutherians and insectivorans. *N. infrequens* differs from *N. americanus* in having its paraconid relatively medially located, paraconid very low, crest connecting protoconid and paraconid less developed, cristid obliqua joining the postvallid in the middle instead of buccally in *N. americanus*, talonid not basined, and no crest connecting hypoconulid and entoconid instead of a crest between hypoconulid and entoconid in *N. americanus*. Affinities of *N. americanus* await analysis with better-preserved materials.

CONCLUSIONS

The phylogenetic analysis of Asian early Paleogene insectivoran-grade eutherians has been difficult due to the lack of well-preserved material. In this monograph, we describe some best-preserved skulls, mandibles, and postcranial skeletons of *Hsiangolestes* and *Naranius*. Based on cladistic analysis of 36 taxa and 290 cranial and dental characters, we propose a new family Sarcodontidae, including *Hsiangolestes*, *Sinosinopa*, *Sarcodon*, *Prosarcodon*, and *Metasarcodon*. These taxa were previously assigned to the family Micropternodontidae, which was established

for the North American genus *Micropternodus*. Our study indicates that *Micropternodus* is not related to any genus included in the new family Sarcodontidae. We suggest that the family Micropternodontidae may best be restricted to *Micropternodus* and its North American allies. Our cladistic analysis indicates that family Sarcodontidae is not closely related to Lipotyphla. *Naranius* is an Asian endemic taxon related to the family Cimolestidae. The systematic position of *Naranius americanus*, the only reported species outside of Asia, is uncertain.

ACKNOWLEDGMENTS

The specimens described in this monograph were collected by many colleagues in 1976, 1982–1987, and 2000 field seasons in the Hengyang Basin, Hunan Province, China. We express our sincere thanks to Jinling Li, Chuankuei Li, Zhanxiang Qiu, the late Defa Yan, Yuanqing Wang, Yuan Wang, and Shuhua Xie of the Institute of Vertebrate Paleontology and Paleoanthropology, Chinese Academy of Sciences, Beijing; to Paul L. Koch of the University of California, Santa Cruz; to William C. Clyde of the University of New Hampshire, Durham; and to the late Malcolm C. McKenna of the American Museum of Natural History, New York, and Priscilla McKenna, for their hard work during collecting.

We greatly benefited from the long-term support of the late Judith A. Schiebout of the LSU Museum of Natural Science, Louisiana State University, and the late Minchen Chow (Mingzheng Zhou) of Institute of Vertebrate Paleontology and Paleoanthropology for their discussions and suggestions on the issues related to this project and revision of the manuscript. Special thanks go to John R. Wible of the Carnegie Museum of Natural History for his important suggestions and discussions on character analysis; to Robert J. Asher of the Museum of Zoology, University of Cambridge, for discussions on taxon selection; to K. Christopher Beard of the Carnegie Museum of Natural History (now at the University of Kansas) for his assistance and discussion on *Naranius americanus*; to Yongsheng Tong of the Institute of Paleontology and Paleoanthropology for assisting with comparison with the specimens from the Wutu Fauna and discussing the classification; and to Chuankuei Li and Bin Bai of the Institute of Paleontology and Paleoanthropology for providing the primary information on the field locations. We especially thank Zhexi Luo of the University of Chicago who advised and helped in processing the serial section of the specimen V7438 when he worked at the Museum of Comparative Zoology at Harvard University in 1990. For kindly providing reprints and comparative casts, we thank Alexey V. Lopatin of the Paleontological Institute, Russian Academy of Sciences, Moscow, Russia, Alexander O. Averianov of the Zoological Institute, Russian Academy of Sciences, Saint Petersburg, Russia, Kenneth D. Rose of Johns Hopkins University, Rachel H. Dunn of Des Moines University, Philip D. Gingerich of the University of Michigan, Ann Arbor, and Thierry Smith of the Royal Belgian Institute of Natural Sciences, Brussels, Belgium. We cordially thank Robert Asher and Zhexi Luo for their insightful reviews and substantial suggestions of this manuscript, and in particular, we are grateful to Asher for his willingness to review our paper a second time. We thank Robert Voss of the AMNH for his guidance and handling of editorial issues of this paper. We thank Mary Knight of the AMNH for copyediting, formatting, and guidance in the publication process.

Michael G. Harvey of the Department of Biological Sciences, Louisiana State University (now at the University of Michigan Museum of Zoology, Ann Arbor) helped in use of the PAUP program for phylogenetic analysis and construction of the cladogram. Lorene E. Smith of the LSU Museum of Natural Science, Louisiana State University, helped with image-editing software. Jinghua Ge of Louisiana State University (now at the University of Illinois at Chicago, Illinois) helped in digital reconstruction of the ear region of the specimen V7438. Mary Lee Eggart and Gabe Harrell of Louisiana State University helped to digitize the serial section slides. The preparation lab of the Institute of Vertebrate Paleontology and Paleoanthropology, Chinese

Academy of Sciences, Beijing, provided the tools for preparing specimens via Shuhua Xie and Wei Zhou. Samuel McLeod and Vanessa Rhue of the Natural History Museum of Los Angeles County assisted Ting's research in their collection. Yanping Song of Los Angeles assisted in the photographic manipulations. Aiichiro Nakano of the University of Southern California and Lijun Zhang of the California Institute of Technology helped arrange the research trips to the Natural History Museum of Los Angeles County. We express our cordial thanks to all of them.

This work would have not been completed without the generous financial and material support from several institutions and grants. The field work was supported by National Geographic Grant 6528-99 (U.S.) to Suyin Ting (PI), Paul L. Koch, and William C. Clyde, and the Major Basic Research Project of Ministry of Science and Technology, China (2006CB806400) to Yuanqing Wang. The Institute of Vertebrate Paleontology and Paleoanthropology, Beijing, and the Hengdong County Government Office helped to arrange the field trips. The project has been supported by the Hubert Charitable Foundation. Ting especially expresses her sincere thanks to the late Ruth Hubert and Cathy Fox (daughter of Ruth) for their long-term support for her research at the LSU Museum of Natural Science, Louisiana State University. Lastly, we thank our families for their long-turm support in our professional careers. S. Ting thanks the late Zhengzhi Huang, Lei Huang, Yan Huang, Zheng Jing, Fanny Pan, Abrielle Huang, and Madeleine Huang; X. Wang thanks Yanping Song and Alex Wang; J. Meng thanks Yu Liu, Amy Meng, and Matthew Meng.

REFERENCES

417 Geological Team, Hunan Geological Bureau. 1979. Preliminary report on Cretaceous–early Tertiary lithofacies and paleogeography of Hengyang Basin. *In* Y. Chang (editor), Cretaceous–early Tertiary lithofacies and paleogeography of south-central region: 140–150. Beijing: Geology Publishing House.

Álvarez-Carretero, S., et al. 2022. A species-level timeline of mammal evolution integrating phylogenomic data. Nature 602: 263–267.

Asher, R.J. 2018a. Diversity and relationships within crown mammals. *In* F.E. Zachos and R.J. Asher (editors), Handbook of zoology: Mammalia: 39–57. Berlin: Walter de Gruyter.

Asher, R.J. 2018b. Taxonomy, trees, and truth in historical mammalogy. *In* F.E. Zachos and R.J. Asher (editors), Handbook of zoology: Mammalia: 301–351. Berlin: Walter de Gruyter.

Asher, R.J., M.C. McKenna, R.J. Emry, A.R. Tabrum, and D.G. Kron. 2002. Morphology and relationships of *Apternodus* and other extinct, zalambdodont, placental mammals. Bulletin of the American Museum of Natural History 273: 1–117.

Asher, R. J., et al. 2017. Dental eruption and growth in Hyracoidea (Mammalia, Afrotheria). Journal of Vertebrate Paleontology 37 (3): e1317638.

Averianov, A.O. 1994. A new species of *Sarcodon* (Mammalia, Palaeoryctoidea) from the lower Eocene of Kirgizia. Geobios 27: 255–258.

Averianov, A.O. 1995. Nyctitheriid insectivores from the upper Paleocene of southern Kazakhstan (Mammalia, Lipotyphla). Senckenbergiana Lethaea 75: 215–219.

Bai, B., Y.Q. Wang, and J. Meng. 2018. The divergence and dispersal of early perissodactyls as evidenced by early Eocene equids from Asia. Communications Biology 2018 (1) 115: 1–10.

Beard, C.K., and M.R. Dawson. 2009. Early Wasatchian mammals of the Red Hot local fauna, Uppermost Tuscahoma Formation, Lauderdale County, Mississippi. Annals of Carnegie Museum 78: 193–243.

Bowen, G.J., et al. 2002. Mammalian dispersal at the Paleocene/Eocene boundary. Science 295: 2062–2065.

Bowen, G.J., P.L. Koch, J. Meng, J. Ye, and S. Ting. 2005. Age and correlation of fossiliferous late Paleocene–early Eocene strata of the Erlian Basin, Inner Mongolia, China. American Museum Novitates 3473: 1–26.

Butler, P.M. 1939. Studies of the mammalian dentition. Differentiation of the postcanine dentition. Proceedings of the Zoological Society of London B109 (1): 1–36.

Butler, P.M. 1947. The evolution of carnassial dentition in the Mammalia. Proceedings of the Zoological Society of London 116: 198–220.

Butler, P.M. 1948. On the evolution of the skull and teeth in the Erinaceidae, with special reference to

fossil material in the British Museum. Proceedings of the Zoological Society of London 118: 446–500.

Butler, P.M. 1956. The skull of *Ictops* and the classification of the Insectivora. Proceedings of the Zoological Society of London 126: 453–481.

Butler, P.M. 1972. The problem of insectivore classification. *In* K.A. Joysey and T.S. Kemp (editors), Studies in vertebrate evolution: 253–265. Edinburgh: Oliver & Boyd.

Butler, P.M. 1988. Phylogeny of the insectivores. *In* M.J. Benton (editor), The phylogeny and classification of the tetrapods, vol. 2: Mammals. Systematics Association special volume 35B: 117–141. Oxford: Clarendon Press.

Cande, S.C., and D.V. Kent. 1995. Revised calibration of the geomagnetic polarity timescale for the late Cretaceous and Cenozoic. Journal of Geophysical Research 100: 6093–6095.

Chu, C. 1986. Late Late Cretaceous red beds of Hunan. Journal of Stratigraphy 10: 54–59.

Clemens, W.A., and L.S. Russell. 1965. Mammalian fossils from the upper Edmonton Formation. *In* Vertebrate paleontology in Alberta. University of Alberta Bulletin of Geology 2: 32–40.

Croft, W.N. 1950. A parallel grinding instrument for the investigation of fossils by serial sections. Journal of Paleontology 24: 693–698.

Dashzeveg, D. 1988. Holarctic correlation of nonmarine Paleocene-Eocene boundary strata using mammals. Journal of the Geological Society (London) 145: 473–478.

Dashzeveg, D., and D.E. Russell. 1985. A new middle Eocene insectivore from the Mongolian People's Republic. Geobios 18: 871–875.

Douady, C.J., and E.J.P. Douzery. 2003. Molecular estimation of eulipotyphlan divergence times and the evolution of "Insectivora." Molecular Phylogenetics and Evolution 28: 285–296.

Douady, C.J., M. Scally, M.S. Springer, and M.J. Stanhope. 2004. "Lipotyphlan" phylogeny based on the growth hormone receptor gene: a reanalysis. Molecular Phylogenetics and Evolution 30: 778–788.

Dunn, R.H., and K.D. Rose. 2015. Evolution of early Eocene *Palaeosinopa* (Mammalia, Pantolestidae) in the Willwood Formation of the Bighorn Basin, Wyoming. Journal of Paleontology 89: 665–694.

Foley, N.M., et al. 2023. A genomic timescale for placental mammal evolution. Science 380 (6643): eabl8189.

Gaughran, G.R.L. 1954. A comparative study of the osteology and mycology of the cranial and cervical regions of the shrew, *Blarina brevicauda*, and the mole, *Scalopus aquaticus*. Miscellaneous Publications, Museum of Zoology, University of Michigan 80: 1–76.

Gingerich, P.D. 1982. *Aaptoryctes* (Palaeoryctidae) and *Thelysia* (Palaeoryctidae?): new insectivorous mammals from the late Paleocene and early Eocene of western North America. Contribution from the Museum Paleontology, the University of Michigan 26: 37–41.

Goloboff, P.A., and S.A. Catalano. 2016. TNT version 1.5, including a full implementation of phylogenetic morphometrics. Cladistics 32: 221–238.

Gould, G.C. 1995. Hedgehog phylogeny (Mammalia, Erinaceidae) — the reciprocal illumination of the quick and the dead. American Museum Novitates 3131: 1–45.

Gould, G.C. 2001. The phylogenetic resolving power of discrete dental morphology among extant hedgehogs and the implications for their fossil record. American Museum Novitates 3340: 1–52.

Guan, S.Z. 1979. Cretaceous and early Tertiary ostracode assemblage from the south-central region and related stratigraphic subdivision and correlation. *In* Institute of Vertebrate Paleontology and Paleoanthropology and Nanjing Institute of Geology and Paleontology (editors), The Mesozoic and Cenozoic Red Beds of South China: 121–131. Beijing: Science Press.

Guan, S.Z. 1989. The age of the Dongtang Formation in the Hengyang Basin of Hunan, and the Cretaceous and Tertiary boundary. Acta Geologica Sinica 63: 59–72.

Hough, J. 1956. A new insectivore from the Oligocene of the Wind River Basin, Wyoming, with notes. Journal of Paleontology 30: 531–541

Hsu, V., T.M. Ge, A.K. Baksi, L.M. Fan, and J. Liu. 1990. Late Cretaceous magnetostratigraphy from a red basin in central China and a preliminary radiometric date for the K-N (Cretaceous Normal) superchron. American Geophysical Union, 1990 fall meeting, Abstract 71: 1298.

Hu, J.M., and D.M. Zheng. 1980. On the age of Chejiang Formation of Hengyang Basin. Petroleum and Natural Gas Geology 1:159–165.

Huang, X.S. 2003. Mammalian remains from the late Paleocene of Jiashan, Anhui. Vertebrata PalAsiatica 41: 42–54.

Huxley, T.H. 1880. On the application of the laws of evolution to the arrangement of the Vertebrata, and more particularly of the Mammalia. Proceedings of the Zoological Society of London 43: 649–662.

Joeckel, R.M., H.W. Bond, and G.W. Kabalka, 1997. Internal anatomy of the snout and paranasal sinuses of *Hyaenodon* (Mammalia, Creodonta). Journal of Vertebrate Paleontology 17: 440–446.

Kennett, J.P., and L.D. Scott. 1991. Abrupt deep-sea warming, palaeoceanographic changes, and benthic extinctions at the end of Paleocene. Nature 353: 225–229.

Kielan-Jaworowska, Z. 1975a. Preliminary description of two new eutherian genera from the late Cretaceous of Mongolia. *In* Results of the Polish-Mongolian Paleontological expeditions—Part VI. Palaeontologia Polonica 33: 5–16.

Kielan-Jaworowska, Z. 1975b. Evolution of the therian mammals in the late Cretaceous of Asia. Part I. Deltatheridiidae. Results of the Polish-Mongolian palaeontological expeditions—Part VI. Palaeontologia Polica 33:103–132.

Kielan-Jaworowska, Z. 1981. Evolution of the therian mammals in the late Cretaceous of Asia. Part VI. Skull structure in *Kennalestes* and *Asioryctes*. Results of the Polish-Mongolian Palaeontological Expeditions, Part IX. Palaeontologia Polonica 42: 25–71.

Kielan-Jaworowska, Z., T.M. Bown, and J.A. Lillegraven. 1979. Eutheria. *In* J.A. Lillegraven, Z. Kielan-Jaworowska, and W.A. Clemens (editors). 1979. Mesozoic Mammals, the first two-thirds of mammalian history: 221–259. Berkeley: University of California Press.

Koch, P.L., J.C. Zachos, and P.D. Gingerich. 1992. Correlation between isotope records in marine and continental carbon reservoirs near the Paleocene/Eocene boundary. Nature 358: 319–322.

Koch, P.L., J.C. Zachos, and P.D. Gingerich. 1995. Stable isotope stratigraphy and paleoclimatology of the Paleogene Bighorn Basin (Wyoming, USA). Palaeogeography, Palaeoclimatology, Palaeoecology 115: 61–89.

Kondrashov, P.E., A.V. Lopatin, and S.G. Lucas. 2004. Late Paleocene (Gashatan) Nyctitheriidae (Mammalia, Lipotyphla) from Mongolia. Bulletin of New Mexico Museum of Natural History and Science 26: 185–193.

Li, C.K., and S. Ting. 1983. The Paleogene mammals of China. Bulletin of Carnegie Museum of Natural History 21:1–93.

Li, C.K., and S. Ting. 1985. Possible phylogenetic relationship of Asiatic eurymylids and rodents, with comments on mimotonids. *In* W.P. Luckett, and J.-L. Hartenberger (editors), Evolutionary relationships among rodents: a multidisciplinary analysis: 35–58. New York: Plenum Press.

Li, C.K., C.S. Chiu, D.F. Yan, and S.H. Hsieh, 1979. Notes on some early Eocene mammalian fossils of Hengtung, Hunan. Vertebrata PalAsiatica 17: 71–80.

Li, H.M. 1965. The early Tertiary fossil plants from Chashanao, Hengyang basin, Hunan. Acta Palaeontologica Sinica 13: 540–547.

Liang, M.S., and W. Zhang. 1984. The Tertiary ostracods of China. *In* Li Y.T. (editor), The Tertiary system of China: 297–305. Beijing: Geological Publishing.

Lillegraven, J.A. 1969. Latest Cretaceous mammals of upper part of Edmonton Formation of Alberta, Canada, and review of Marsupial-placental dichotomy in mammalian evolution. University of Kansas Paleontological Contributions 50 (Vertebrata 12): 7–85. Lawrence: University of Kansas Publications.

Lillegraven, J.A., C.M. McKenna, and L. Krishtalka. 1981. Evolutlionary relationships of middle Eocene and younger species of *Centetodon* (Mammalia, Insectivora, Geolabididae) with a description of the dentition of *Ankylodon* (Adapisoricidae). University of Wyoming Publications 45: 1–112.

Linnaeus, C. 1758. Systema naturae per regna tria naturae, secundum classes, ordines, genera, species, cum characteribus, differentiis, synonymis, locis. Vol. 1: Regnum animale. 10th ed. Stockholm: Societatis Zoologicae Germanicae.

Liu, X., and D.Y. Fu. 1986. Sedimentary facies and the tectonic development of the Hengyang Basin, Hunan Province. Bulletin of the Chinese Academy of Geological Sciences 13: 13–36.

Lopatin, A.V. 2004a. A new genus of the Galericinae (Erinaceidae, Insectivora, Mammalia) from the middle Eocene of Mongolia. Paleontological Journal 38: 319–326.

Lopatin, A.V. 2004b. The first finding of Geolabididae (Soricomorpha, Mammalia) in Asia (Upper Paleocene of Mongolia). Paleontological Journal 38: 672–679.

Lopatin, A.V. 2005. A new soricomorph insectivore (Soricomorpha, Mammalia) from the Eocene of Mongolia and the origin of shrews (Soricidae). Doklady Biological Sciences 401: 144–146.

Lopatin, A.V., 2006. Early Paleogene insectivore mammals of Asia and establishment of the major groups of Insectivora. Paleontological Journal 40 (suppl. 3): S205–405.

Lopatin, A.V., and A.O. Averianov. 2004. New Palaeoryctidae (Mammalia) from the Eocene of Kyrgyzstan and Mongolia. Paleotological Journal 38: 556–562.

Lopatin, A.V., and P.E. Kondrashov. 2004. Sarcodontinae, a new subfamily of micropternodontid insectivores from the early Paleocene–middle Eocene of Asia. Bulletin of New Mexico Museum of Natural History and Science 26: 177–184.

Luo, Z.X., and E.R. Eastman. 1995. Petrosal and inner ear of a squalodontoid whale: implications for evolution of hearing in *Odontosetes*. Journal of Vertebrate Paleontology 15: 431–442.

MacPhee, R.E.E., and M.D. Novacek. 1993. Definition and relationships of Lipotyphla. *In* F.S. Szalay, M.D. Novacek, and M.C. McKenna (editors), Mammal phylogeny: placentals: 13–31. New York: Springer-Verlag.

Maddison, D.R., and W.P. Maddison. 2005. MacClade 4: analysis of phylogeny and character evolution. Version 4.08a. Sunderland, MA: Sinauer Associates.

Maddison, W.P., and D.R. Maddison. 2018. Mesquite: a modular system for evolutionary analysis. Version 3.51. [http://www.mesquiteproject.org]

Marsh, O.C. 1889. Discovery of Cretaceous Mammalia. American Journal of Science S3-38: 81–92.

Matthew, W.D. 1901. Additional observations on the Creodonta. Bulletin of the American Museum of Natural History 14 (1): 1–38.

Matthew, W.D. 1903. The fauna of the *Titanotherium* beds at Pipestone Springs, Montana. Bulletin of the American Museum of Natural History 19 (6): 197–226.

Matthew, W.D. 1909. The Carnivora and Insectivora of the Bridger Basin, Middle Eocene. Memoirs of the American Museum of Natural History 9 (6): 291–576.

Matthew, W.D. 1913. A zalambdodont insectivore from the basal Eocene. Bulletin of the American Museum of Natural History 32 (17): 307–314.

Matthew, W.D., and W. Granger. 1925. Fauna and correlation of the Gashato Formation of Mongolia. American Museum Novitates 189: 1–12.

Matthew, W.D., W. Granger, and G.G. Simpson. 1929. Additions to the fauna of the Gashato Formation of Mongolia. American Museum Novitates 376:1–12.

McDowell, S.B. 1958. The Greater Antillean insectivores. Bulletin of the American Museum of Natural History 115 (3): 117–214.

McKay, C. J., et al. 2022. Dental development and first premolar homology in placental mammals. Vertebrate Zoology 72: 201–208.

McKenna, M.C. 1963. New evidence against the tupaioid affinities of the mammalian family Anagalidae. American Museum Novitates 2158: 1–16.

McKenna, M.C. 1968. *Leptacodon*, an American Paleocene nyctithere (Mammalia, Insectivora). American Museum Novitates 2317: 1–12.

McKenna, M.C., and S.K. Bell, 1997. Classification of Mammals, above the species level, with contributions from G.G. Simpson, R.H. Nichols, R.H. Tedford, K.E. Koopman, G.G Musser, N.A. Neff, J. Shoshani, D.M. McKenna. New York: Columbia University Press, 547 pp.

McKenna, M.C., X.X. Xue, and M.Z. Zhou. 1984. *Prosarcodon lonanensis*, a new Paleocene micropternodontid Palaeoryctoid insectivore from Asia. American Museum Novitates 2780: 1–17.

Meng, J., R.-j. Zhai, and A.R. Wyss. 1998. The late Paleocene Bayan Ulan fauna of Inner Mongolia, China. In K.C. Beard, and M.R. Dawson (editors), Dawn of the age of mammals in Asia. Bulletin of Carnegie Museum of Natural History 34: 148–185.

Meng, J., Y.M. Hu, and C.K. Li. 2003. The osteology of *Rhombomylus* (Mammalia, Glires): implications for phylogeny and evolution of Glires. Bulletin of the American Museum of Natural History 275: 1–245.

Meredith, R.W., et al. 2011. Impacts of the Cretaceous terrestrial revolution and KPg extinction on mammal diversification. Science 334: 521–524.

Miller, M.E. 1964. Anatomy of the dog. Philadelphia: W.B. Saunders Company, 544 pp.

Missiaen, P., and T. Smith. 2005. A new Paleocene nyctitheriid insectivore from Inner Mongolia (China) and the origin of Asian nyctitheriids. Acta Plaeontologica Polonica 50: 513–522.

Moore, W.J. 1981. The mammalian skull. New York: Cambridge University Press, 369 pp.

Nessov, L.A. 1987. Results of search and investigation of Cretaceous and early Paleogene mammals on the territory of the USSR. Ezhegodnik Vsesoyuznogo Paleontologicheskogo Obshchestva 30: 199–218.

Ni, X.J., Y.Q. Wang, Y.M. Hu, and C.K. Li. 2004. A euprimate skull from the early Eocene of China. Nature 427: 65–68.

Novacek, M.J. 1986. The skull of leptictid insectivorans and the higher-level classification of eutherian mammals. Bulletin of the American Museum of Natural History 183: 1–111.

O'Leary, M.A., et al. 2013. The placental mammal ancestor and the post–K-Pg radiation of placentals. Science 339: 662–667.

Qi, T., 1987. The middle Eocene Arshanto fauna (Mammalia) of Inner Mongolia. Annals of Carnegie Museum 56: 1–73.

Ren, J.N., K. Tamaki, S.T. Li, and J.X. Zhang. 2002. Late Mesozoic and Cenozoic rifting and its dynamic setting in eastern China and adjacent areas. Tectonophysics 344: 175–205.

Russell, D.A. 1960. A review of the Oligocene insectivore *Micropternodus borealis*. Journal of Paleontology 34: 940–949.

Russell, D.E., and D. Dashzeveg. 1986. Early Eocene insectivores (Mammalia) from the People's Republic of Mongolia. Palaeontology 29: 269–291.

Schlaikjer, E.M. 1933. Contributions to the stratigraphy and paleontology of the Goshen Hole Area, Wyoming. I. A detailed study of the structure and relationships of a new zalambdodont insectivore from the middle Oligocene. Bulletin of the Museum of Comparative Zoology 76: 1–27.

Scott, W.B., and G.L. Jepson. 1936. The mammalian fauna of the White River Oligocene, Part I Insectivora and Carnivora. Transactions of the American Philosophical Society 28: 1–153.

Simpson, G.G. 1931. A new insectivore from the Oligocene, Ulan Gochu horizon, of Mongolia. American Museum Novitates 505: 1–22.

Slaughter, B.H., R.H. Pine, and N.E. Pine. 1974. Eruption of cheek teeth in Insectivora and Carnivora. Journal of Mammalogy 55: 115–125.

Springer, M.S., M.J. Stanhope, O. Madsen, and W.W. de Jong. 2004. Molecules consolidate the placental mammal tree. Trends in Ecology & Evolution 19: 430–438.

Stirton, R.A., and J.M. Rensberger. 1964. Occurrence of the insectivore genus *Micropternodus* in the John Day Formation of central Oregon. Bulletin of the Southern Californian Academy of Sciences 63: 57–80.

Swofford, D. 2014. PAUP* 4.0, Phylogenetic analysis using parsimony (PAUP), Macintosh beta version 10, distributed by Sinauer Associates, Inc., Sunderland, MA.

Szalay, F.S., and M.C. McKenna. 1971. Beginning of the age of mammals in Asia: the late Paleocene Gashato fauna, Mongolia. Bulletin of the American Museum of Natural History 144: 271–314.

Tarver, J. E., et al. 2016. The interrelationships of placental mammals and the limits of phylogenetic inference. Genome Biology and Evolution 8 (2): 330–344.

Thewissen, J.G.M., and P.D. Gingerich. 1989. Skull and endocranial cast of *Eoryctes melanus*, a new palaeoryctid (Mammalia: Insectivora) from the early Eocene of Western North America. Journal of Vertebrate Paleontology 9: 459–470.

Thomas, E., and N.J. Shackleton. 1996. The Paleocene-Eocene benthic foraminiferal extinction and stable isotope anomalies. Geological Society London Special Publications 101: 401–441.

Tien, C.C., 1936. Orogenic movements in Hunan. Bulletin of Geological Society of China 15: 453–365.

Tien, C.C., H.C. Wang, and T.Y. Hsu. 1933. The geology of Changsha, Hsiangtan, Hengshan, Hsianghsiang, Hengyang, and Shaoyang districts, central Hunan. Bulletin of Geological Survey of Hunan (Geology 2) 15: 29–31.

Ting, S. 1993. A preliminary report on an early Eocene mammalian fauna from Hengdong, Hunan Province, China. *In* F. Schrenk and K. Ernst (editors), Kaupia, Darmstädter Beiträge zur Naturgeschichte 3: 201–207.

Ting, S. 1995. An early Eocene mammalian fauna from Hengdong, Hunan Province, China. Ph.D. dissertation, Department of Geology and Geophysics, Louisiana State University, Baton Rouge, 200 pp.

Ting, S.1998. Paleocene and early Eocene Land Mammal Ages of Asia. Bulletin of Carnegie Museum of Natural History 34: 124–147.

Ting, S., and C.K. Li. 1984. The structure of the ear region of *Rhombomylus* (Anagalida, Mammalia). Vertebrata PalAsiatica 22: 92–102.

Ting, S., and C.K. Li. 1987. The skull of *Hapalodectes* (?Acreodi, Mammalia), with notes on some Chinese Paleocene mesonychids. Vertebrata PalAsiatica 25: 161–186.

Ting, S., J. Meng., and M.C. McKenna. 2002. The osteology of *Matutinia* (Simplicidentata, Mammalia) and its relationship to *Rhombomylus*. American Museum Novitates 3371: 1–33.

Ting, S., et al. 2003. Biostratigraphic, chemostratigraphic, and magnetostratigraphic study across the Paleocene/Eocene boundary in the Hengyang Basin, Hunan, China. GSA Special Paper 369: 521–536.

Ting, S., et al. 2004. New early Eocene mammalian fossils from the Hengyang Basin. Bulletin of Carnegie Museum of Natural History 36: 291–302.

Ting, S., et al. 2011. Asian early Paleogene chronology and mammalian faunal turnover events. Vertebrata PalAsiatica 49:1–28.

Tong, Y.S. 1997. Middle Eocene small mammals from Liguanqiao basin of Henan Province and Yuanqu basin of Shanxi Province, central China. Palaeontologia Sinica whole number 186, new series C 26: 1–256.

Tong, Y.S. 2003. *Nuryctes*, a new generic name to replace *Neoryctes* Tong, 1997 (Mammalia, ?Insectivora, Palaeoryctidae). Vertebrata PalAsiatica 41: 88.

Tong, Y.S., and J.W. Wang. 1993. A new soricomorph (Mammalia, Insectivora) from the early Eocene of Wutu Basin, Shandong, China. Vertebrata PalAsiatica 31: 19–32.

Tong, Y.S., and J.W. Wang. 1998. A preliminary report on the early Eocene mammals of the Wutu fauna, Shandong Province, China. Bulletin of Carnegie Museum of Natural History 34: 186–193.

Tong, Y.S. and J.W. Wang. 2006. Fossil mammals from the early Eocene Wutu formation of Shandong Province. Palaeontologia Sinica 192, new series C 28: 1–192.

Tong, Y.S., Y.Q.Wang, and Q. Li. 2006. Subdivision of the Paleogene in Lingcha Area of Hunan Province and Early Eocene mammalian faunas of China. Geological Review 52: 153–162.

Uhen, M.D. 2000. Replacement of deciduous first premolars and dental eruption in archaeocete whales. Journal of Mammalogy 81 (1): 123–133.

Van Valen, L. 1966. Deltatheridia, a new order of mammals. Bulletin of the American Museum of Natural History 132: 5–124.

Van Valen, L. 1967. New Paleocene insectivores and insectivore classification. Bulletin of the American Museum of Natural History 135: 219–278.

Wang, B.Y., and C.T. Li. 1990. First Paleogene mammalian fauna from northeast China. Vertebrate PalAsiatica 28: 165–205.

Wang, X., and R.J. Zhai. 1995. *Carnilestes*, a new primitive lipotyphlan (Insectivora: Mammalia) from the early and middle Paleocene, Nanxiong Basin, China. Journal of Vertebrate Paleontology 15: 131–145.

White, T.E. 1954. Preliminary analysis of the fossil vertebrates of the Canyon Ferry Reservoir Area. Proceedings of the United States National Museum 103: 395–437.

Wible, J.R., M.J. Novacek, and G.W. Rougier. 2004. New data on the skull and dentition in the Mongolian Late Cretaceous eutherian mammal *Zalambdalestes*. Bulletin of the American Museum of Natural History 281: 1–144.

Wible, J.R., G.W. Rougier, M.J. Novacek, and R.J. Asher. 2007. Cretaceous eutherians and Laurasian origin for placental mammals near the K/T boundary. Nature 447: 1003–1006; and 1–139 (supplementary information available on line at http:www.nature.com/nature/journal/v447/n7147/suppinfo/nature05854.html).

Wible, J.R., G.W. Rougier, M.J. Novacek, and R.J. Asher. 2009. The eutherian mammal *Maelestes gobiensis* from the later Cretaceous of Mongolia and the phylogeny of Cretaceous Eutheria. Bulletin of the American Museum of Natural History 327: 1–123.

Wyss, A.R. 1987. Notes on Prototheria, Insectivora, and Thomas Huxley's contribution to mammalian systematics. Journal of Mammalogy 68: 135–138.

Young, C.C. 1944. Note on the first Eocene mammal from south China. American Museum Novitates 1268: 1–3.

Young, C.C., M.N. Bien, and Y.Y. Lee. 1938. "Red Beds" of Hunan. Bulletin of Geological Society of China 18: 259–300.

Zachos, J.C., et al. 2003. A transient rise in tropical sea surface temperature during the Paleocene-Eocene thermal maximum. Science 302: 1551–1554.

Zhang, J.J. 1982. The age of the Chejiang Formation in Hengyang Basin. Journal of Stratigraphy 6: 140–143.

Zheng, J.J. 1979. A new genus of Didymoconidae from Paleocene, Jiangxi Province, China. *In* Institute of Vertebrate Paleontology and Paleoanthropology, and Nanjing Institute of Geology and Paleontology (editors), The Mesozoic and Cenozoic Red Beds of South China: 360–365. Beijing: Science Press.

Zheng, J.J., and X.S. Huang. 1984. A new didymoconid (Mammalia) from the Early Eocene of Hunan. Vertebrata PalAsiatica 22: 198–207.

Zhang, Z.L. 1979. The Cretaceous pollen assemblage of middle-south region of China. *In* Institute of Vertebrate Paleontology and Paleoanthropology, and Nanjing Institute of Geology and Paleontology (editors), The Mesozoic and Cenozoic Red Beds of South China: 132–140. Beijing: Science Press.

Zhu, M., et al. 2010. High-resolution carbon isotope record for the Paleocene-Eocene thermal maximum from the Nanyang Basin, Central China. Chinese Science Bulletin 55: 3606–3611.

APPENDIX 1

Taxa Selected and Sources of Data

The following list of taxa was used in the phylogenetic analysis. We include taxa plus their author and year citation, followed by citations of major sources of information about each taxon, separated from the taxa by a long dash (—).

Outgroups

Asioryctes nemegetensis Kielan-Jaworowska, 1975 — Kielan-Jaworowska, 1975a, 1975b, 1981; Kielan-Jaworowska et al., 1979

Maelestes gobiensis Wible et al., 2007 — Wible et al., 2007, 2009

Ingroups

Aaptoryctes ivyi Gingerich, 1982 — Gingerich, 1982

Asionyctia guoi Missiaen and Smith, 2005 — Missiaen and Smith, 2005

Blarina brevicauda (Say, 1823) — Gaughran, 1954

Bumbanius rarus Russell and Dashzeveg, 1986 — Russell and Dashzeveg, 1986; Lopatin, 2006

Carnilestes palaeoasiaticus Wang and Zhai, 1995 — Wang and Zhai, 1995

Centetodon chadronensis Lillegraven, McKenna, and Krishtalka, 1981 — Lillegraven et al., 1981

Changlelestes dissetiformis Tong and Wang, 1993 — Tong and Wang, 1993, 2006

Cimolestes magnus Clemens and Russell, 1965 — Clemens and Russell, 1965; Lillegraven, 1969

Eochenus sinensis Wang and Li, 1990 — Wang and Li, 1990

Eogalericius butleri Lopatin, 2004 — Lopatin, 2004a, 2006

Eoryctes melanus Thewissen and Gingerich, 1989 — Thewissen and Gingerich, 1989

Eosoricodon terrigena Lopatin, 2005 — Lopatin, 2005, 2006

Erinaceus europaeus Linnaeus, 1758 — Gould. 1995, 2001; Wible et al., 2009

Gobigeolabis verigranum Lopatin, 2004 — Lopatin, 2004b, 2006

Hsiangolestes youngi Zheng and Huang, 1984 — Zheng and Huang, 1984

Jarveia minuscula Nessov, 1987b — Nessov, 1987; Averianov, 1995; Kondrashov et al., 2004; Lopatin, 2006

Leptictis dakotensis Leidy, 1869 — Lillegraven, 1969; Novacek, 1986; Wible et al., 2009

Luchenus erinaceanus Tong and Wang, 1998 — Tong and Wang, 1998, 2006

Micropternodus borealis Matthew, 1903 — Matthew, 1903; White, 1954; Hough, 1956; Russell, 1960

Naranius infrequens Russell and Dashzeveg, 1985 — Russell and Dashzeveg, 1985; Lopatin, 2006

Naranius hengdongensis (*N.* cf. *infrequens*, Ting, 1995, 1998), new species — this paper

Nuryctes (*Neoryctes*) *qinlingensis* Tong — Tong, 1997, 2003

Nuryctes alayensis Lopatin and Averianov, 2004 — Lopatin and Averianov, 2004; Lopatin, 2006

Palaeoryctes puercensis Matthew, 1913 — Matthew, 1913; McDowell, 1958; Van Valen, 1966

Palaeosinopa veterrima Matthew, 1901 — Matthew, 1901; Dunn and Rose, 2015

Pantolestes natans Matthew, 1909 — Matthew, 1909

Praolestes nanus Matthew, Granger, and Simpson, 1929 — Matthew et al., 1929; Szalay and McKenna, 1971; Kondrashov et al., 2004; Lopatin, 2006

Prosarcodon lonanensis McKenna, Xue, and Zhou, 1984 — McKenna et al., 1984; Lopatin and Kondrashov, 2004; Lopatin, 2006

Sarcodon pygmaeus Matthew and Granger, 1925 — Matthew and Granger, 1925; Matthew et al., 1929; Szalay and McKenna, 1971; Lopatin and Kondrashov, 2004; Lopatin, 2006

Scileptictis simplus Tong and Wang, 2006 — Tong and Wang, 1998, 2006

Sinosinopa sinensis Qi, 1987 — Qi, 1987

Tsaganius ambiguus Russell and Dashzeveg, 1985 — Russell and Dashzeveg, 1985; Lopatin, 2006

Voltaia minuta Nessov, 1987 — Nessov, 1987; Lopatin, 2006

Zhigdenia nemegetica Lopatin, 2006 — Lopatin, 2006

APPENDIX 2

Character and Character States

The following list of character descriptions and their states are used in our phylogenetic analysis. Character numbers correspond to those in our data matrix (See online supplement: https://doi.org/10.5531/sd.sp.59). Character numbers followed by an asterisk (*) denotes some modification to the cited source for the character.

Dentition

Character 1. Number of postcanine tooth (Wible et al., 2009: 3): eight or more (0); seven (1); six (2); or five or fewer (3).

Character 2. Upper diastema (Wible et al., 2009: 4): small, between incisors and canine (0); small, between canine and premolars (1); enlarged (2); or absent (3).

Character 3. Lower diastema behind incisors (Wible et al., 2009: 5): absent or small (0); enlarged (1).

Character 4. Number of upper incisors (Wible et al., 2009: 7*): five (0); four (1); three (2); two (3).

Character 5. Anteriormost upper incisor alveoli (Wible et al., 2009: 9): approximately on the midline (0); separated by a narrow gap (1); separated by a broad gap (2).

Character 6. Anteriormost upper incisor size (Wible et al., 2009: 10*): subequal to or slightly larger than subsequent (0); greatly enlarged (1); smaller than subsequent (2).

Character 7. Anteriormost upper incisor shape (Wible et al., 2009: 11*): conical (0); mediolaterally compressed (1); anteroposteriorly compressed (2); crown with one major and two small cuspate (3); crown with one major and two small cuspates (4); spatulate (5).

Character 8. Position of ultimate upper incisors (Wible et al., 2009: 14): in premaxilla (0); between maxilla and premaxilla (1); in maxilla (2).

Character 9. Number of lower incisors: more than three (0); three (1); two (2); and one (3).

Character 10. Anteriormost lower incisor size (Asher et al., 2002: 75; Wible et al., 2009: 15): subequal to or slightly larger than subsequent incisors (0); greatly enlarged (1); tiny or smaller than subsequent incisors (2).

Character 11. Anteriormost lower incisor shape (Wible et al., 2009, 16*): conical (0); mediolaterally compressed (1); anteroposteriorly compressed (2); crown with one major and a small cuspate (3); spatulate (4); deeply bifurcated (5).

Character 12. Procumbent anteriormost lower incisor (Wible et al., 2009: 17*): absent (0); present (1); horizontally projecting (2).

Character 13. Procumbent posterior lower incisors (Wible et al., 2009: 21): absent (0); present (1).

Character 14. Posterior lower incisor cusps or size (Asher et al., 2002: 73*): single (0); dual (1); triple or more (2); i2 substantially larger than other incisors (3).

Character 15. Upper canine (Wible et al., 2009: 23): present, large (0); present, small (1); absent (2).

Character 16. Number of upper canine roots (Wible et al., 2009: 24): two (0); one (1); three (2).

Character 17. Upper canine crown (Asher et al., 2002: 54*): premolariform (0); bulbous (1); incisiform (2).

Character 18. Lower canine (Wible et al., 2009: 25): present, large (0); present, small (1); absent (2).

Character 19. Number of lower canine roots (Wible et al., 2009: 26): two (0); one (1).

Character 20. Procumbent lower canine (Wible et al., 2009: 27): absent (0); present (1).

Character 21. Lower canine crown: premoliariform (0); caniniform (1); incisiform (2); bulbous (3).

Character 22. Number of premolars (Wible et al., 2009: 29*): five or more (0); four (1); three (2); two (3); one (4).

Character 23. Procumbent first upper premolar (P1) (Wible et al., 2009: 32): absent (0); present (1). (Score is inapplicable for taxa with three premolars).

Character 24. First upper premolar roots (Wible et al., 2009: 33): two (0); one (1); three (2).

Character 25. First upper premolar crown: unicuspid (0); mediolaterally compressed (1); crown with one major cuspate and a small cuspate posterior to the major one (2).

Character 26. First upper premolar size: small, subequal to subsequent premolar (0); smaller than subsequent premolar (1); larger than subsequent premolar (2).

Character 27. Diastema posterior to first upper premolar (Wible et al., 2009: 34): absent (0); present (1).

Character 28. Second upper premolar crown: unicuspid (0); with anterior accessory cusp (1); with posterior accessory cusp or heel (2).

Character 29. Second upper premolar roots: two (0); one (1); three (2).

Character 30. Diastema posterior to second upper premolar: absent (0); present (1).

Character 31. Penultimate upper premolar roots (Wible et al., 2009: 39*): two (0); three (1); one (2).

Character 32. Penultimate upper premolar paracone (Novacek, 1986: dental feature 10): greatly enlarged (0); slightly larger (1); not enlarged (2).

Character 33. Penultimate upper premolar protocone (Wible et al., 2009: 36): absent (0); small or lingual bulge (1); with an enlarged basin (2).

Character 34. Penultimate upper premolar metacone (Wible et al., 2009: 37*): absent (0); present (1).

Character 35. Penultimate upper premolar parastylar lobe (Wible et al., 2009: 38): absent or small (0); well developed (1).

Character 36. Penultimate upper premolar metastylar lobe: absent or small (0); well developed (1).

Character 37. Penultimate upper premolar size related to preceding upper premolar: larger (0); slightly larger (1); reduced, smaller (2).

Character 38. Penultimate upper premolar strongly oblique: absent (0); present (1).

Character 39. Ultimate upper premolar protocone (Wible et al. 2009: 40*): shorter than paracone (0); approaches paracone in height (1).

Character 40. Ultimate upper premolar metacone (Wible et al., 2009: 41): absent (0); swelling (1); large (2).

Character 41. Ultimate upper premolar hypocone: absent or reduced (0); present (1); large (2).

Character 42. Ultimate upper premolar paracone related to preceding premolar: shorter than or subequal to (0); taller (1).

Character 43. Ultimate upper premolar conules (Wible et al., 2009: 45*): absent (0); present, lower than protocone (1); present, level with protocone (2).

Character 44. Ultimate upper premolar para- and metastylar lobes (Wible et al. 2009: 42): absent or insignificant (0); subequal (1); parastylar lobe larger (2); metastylar lobe larger (3).

Character 45. Ultimate upper premolar precingulum: (Wible et al., 2009: 43): absent (0); present (1).

Character 46. Ultimate upper premolar postcingulum (Wible et al., 2009: 44*): absent (0); present (1).

Character 47. Ultimate upper premolar size (occlusal surface) related to first upper molar (Wible et al., 2009: 46): smaller or subequal (0); larger (1).

Character 48. Maximum degree of asymmetry of ultimate upper premolar (ratio of posterior/anterior edges) (Butler, 1947: 209): 1:1.2 (0); 1.3:1.4 (1); 1:5 or higher (2).

Character 49. First lower premolar roots (Wible et al., 2009: 48): two (0); one (1). (Score is inapplicable for taxa with three premolars).

Character 50. Procumbent first lower premolar: absent (0); present (1).

Character 51. First lower premolar cusps: unicuspid (0); with heels or basal cusps (1).

Character 52. Diastema posterior to first lower premolar (Wible et al., 2009: 49): absent or less than one tooth root for whichever is smaller of adjacent tooth (0); present, subequal to one tooth-root diameter or more (1).

Character 53. Second lower premolar roots: two (0); one (1).

Character 54. Second lower premolars cusps: unicuspid (0); with anterior accessory cuspule (1); with posterior accessory cuspule or heel (2); with both anterior and posterior accessory (heel) cuspule (3).

Character 55. Size of second lower premolars related to preceding lower premolar: larger or subequal (0); smaller (1).

Character 56. Diastema posterior to second lower premolar: absent or less than one tooth-root diameter (0); subequal to one tooth-root diameter or more (1).

Character 57. Penultimate lower premolar size: larger than preceding premolar (0); smaller or subequal to preceding premolar (1).

Character 58. Penultimate lower premolar protoconid: taller than subsequent premolar protoconid (0); shorter than subsequent premolar protoconid (1); subequal to subsequent premolar protoconid (2).

Character 59. Penultimate lower premolar paraconid (Wible et al., 2009: 52): absent, indistinct, or small (0); present and distinct (1).

Character 60. Penultimate lower premolar metaconid (Wible et al., 2009: 53*): absent (0); swelling (1).

Character 61. Penultimate lower premolar talonid cusps (Wible et al., 2009: 54): absent or one (0); two (1); three (2).

Character 62. Penultimate lower premolar cingulid (Asher et al., 2002: 81*): absent (0); present (1).

Character 63. Diastema posterior to third lower premolar: absent or less than one tooth-root diameter (0); present, subequal to one or a half of a tooth-root diameter or more (1). (Score is inapplicable for taxa with three lower premolars)

Character 64. Ultimate lower premolar paraconid (Wible et al., 2009: 55): absent or indistinct (0); distinct but low (1); distinct and high (2).

Character 65. Ultimate lower premolar metaconid (Wible et al., 2009: 56): absent (0); swelling or rudimentary (1); large (2).

Character 66. Ultimate lower premolar talonid (Wible et al., 2009: 57*): narrower than trigonid (0); as wide as trigonid (1).

Character 67. Ultimate lower premolar talonid shape: heel (0); median longitudinal ridge (1); basined (2); transverse ridge (3).

Character 68. Ultimate lower premolar talonid cusps (Wible et al., 2009: 58*): one (0); two (1); three (2); ridge without cusps (3).

Character 69. Ultimate lower premolar cingulid (Wible et al., 2009: 60*): absent (0); present, anteriorly or anterolingually (1); present, posteriorly or posterolabially (2).

For characters 70–130, unless noted in the character description, molar features are scored for the first and second molar when available.

Character 70. Number of molars (Wible et al., 2009: 61*): three (0); two (1).

Character 71. Upper molar type (Butler, 1939; Lopatin, 2006): zalambdodont (0); protodilambdodont (Lopatin, 2006L 214, fig. 4a; upper molar paracone and metacone clearly detached, but not froming characteristic W-shaped centrocrista) (1); entodilambdodont (a) (Lopatin, 2006: 214,

fig. 4b; upper molar W-shaped centrocrista with apices located on parastyle, paracone, matacone, and metastyle, lower molar with distinct hypoconulid) (2); entodilambdodont (b) (Lopatin, 2006: 214, fig. 4c, d; differing from above entodilambdodont in having larger hypocone shelf) (3); ectodilambdodont (Lopatin, 2006: 214, fig. 4e; upper molar W-shaped centrocrista with apices located on parastyle, paracone, mesostyle, metacone, and metasyle and with large hypocone shelf, lower molar with high hypoconid and hypoconulid lingually located or disappeard) (4). (See Lopatin, 2006: 213–215 for detail).

Character 72. First upper molar length: subequal to subsequent molar (0); shorter (1); longer (2). (Score is inapplicable for taxa lacking three molars.)

Character 73. First upper molar width: subequal to subsequent molar (0); narrower (1); wider (2). (Score is inapplicable for taxa lacking three molars.)

Character 74. Labial extent of M2 parastylar and metastylar lobes (Wible et al., 2009: 66*): parastylar lobe more labial (0); lobes subequal (1); metastylar lobe more labial (2); lobes absent (3). (Score is inapplicable for taxa lacking three molars)

Character 75. Labial extent of M1 parastylar and metastylar lobes: parastylar lobe more labial (0); lobes subequal (1); metastylar lobe more labial (2); lobes absent (3).

Character 76. M1–2 parastylar lobe relative to paracone (Wible et al., 2009: 67*): parastylar lobe anterolabial to paracone (0); parastylar lobe anterior to paracone (1).

Character 77. Parastyle (Wible et al., 2009: 70*): subequal to or larger than stylocone (0); distinct, but smaller than stylocone (1); vestigial to absent (2).

Character 78. Mesostyle (Wible et al., 2009: 72*): absent (0); present (1).

Character 79. Metastyle (Wible et al., 2009: 74*): large (0); small to indistinct (1).

Character 80. Ectocingulum (buccal cingulum) (Butler, 1947): present (0); rudimentary or absent (1).

Character 81. Deep ectoflexus (Wible et al., 2009: 76): only on penultimate molar (0); on penultimate and preceding molars (1); strongly reduced (2); or absent (3).

Character 82. Metacone size relative to paracone (Wible et al., 2009: 77): noticeably smaller (0); slightly smaller (1); subequal or larger (2); absent or merged with paracone (3).

Character 83. Metacone position relative to paracone (Wible et al., 2009: 78): labial (0); approximately at same level (1); lingual (2).

Character 84. Metacone and paracone bases (Wible et al., 2009: 79): adjoined (0); separated (1).

Character 85. Paracrista (Wible et al., 2009: 80*): distinct, from side of paracone to parastyle (0); weak, from base of paracone (1); absent (2).

Character 86. Centrocrista (Wible et al., 2009: 82): straight (0); V-shaped (1); weak or absent (2).

Character 87. Metacrista (Wible et al., 2009: 83*): prominent, from side of metacone to metastyle (0); salient (1); weak, from base of metacone (2); absent (3).

Character 88. Notch metacrista: absent (0); deep notch (1); carnassial notch (2).

Character 89. Preprotocrista (Wible et al., 2009: 85): does not extend (0); extends labially slightly past or at base of paracone (1); extends labially past base of paracone or absent (2).

Character 90. Postprotocrista (Wible et al., 2009: 86): extends to midlingual surface of metacone (0); extends distal to metacone (1); postprotocrista absent (2).

Character 91. Development of postvallum shear (Wible et al., 2009: 87*): present, only by metacrista (0); present, with postprotocrista not reaching labially below the base of the metacone (1); metacrista extending to metastylar lobe (2); weak or absent (3).

Character 92. Paraconule (Wible et al., 2009: 88*): weak or absent (0); prominent, closer to protocone (1); prominent, closer to paracone (2); midway to paracone (3).

Character 93. Metaconule (Wible et al., 2009: 89*): weak or absent (0); prominent, closer to protocone (1); prominent, closer to metacone (2); midway to metacone (3).

Character 94. Internal conular cristae (Wible et al., 2009: 90): indistinct (0); distinct and winglike (1). (Score is inapplicable for taxa without prominent conule.)

Character 95. Protocone anteroposterior expansion (Wible et al., 2009: 93): none, subequal to paracone (0); expanded, larger than paracone (1).

Character 96. Protocone procumbency (Wible et al., 2009: 94): absent (0); present (1).

Character 97. Degree of labial shift of protocone (distance from protocone apex to lingual border vs. total tooth width, in %) (Wible et al., 2009: 95): no labial shift (10%– 20%) (0); moderate labial shift (21%–30%) (1); substantial labial shift (≥31%) (2).

Character 98. Protocone height (Wible et al., 2009: 96): low (0); tall, approaching paracone and metacone (1); subequal to paracone and metacone (2).

Character 99. Precingulum (Wible et al., 2009: 97): absent or weak (0); present, but not reaching labially past the paraconule or paraconule position (1); present, reaching labially past the paraconule or paraconule position (2).

Character 100. Postcingulum (Wible et al., 2009: 98): absent or weak (0); present, lingual to metaconule or metaconule position (1); present, reaching labially past metaconule or metaconule position (2); present, extending to labial margin (3).

Character 101. Hypocone on postcingulum (Wible et al., 2009: 99*): absent (0); rudimentary (1); small (2); large (3).

Character 102. Hypoconal shelf: absent (0); narrow (1); moderate (2); wide (3); greatly enlarged (4).

Character 103. Pre- and postcingulum (Wible et al., 100*): separated (0); continuous lingually (1). (Score is inapplicable for taxa without pre- and postcingulum).

Character 104. Number of roots of M1–2 (Wible et al., 2009: 101*): three (0); four (1).

Character 105. Number of roots on ultimate upper molar (Wible et al., 2009: 102*): three (0); two (1); four (2).

Character 106. Ultimate upper molar width relative to penultimate molar (Wible et al., 2009:104): subequal (0); smaller (1).

Character 107. Ultimate upper molar conules: absent (0); present (1).

Character 108. Ultimate upper molar hypocone: absent (0); present (1).

Character 109. Ultimate upper molar metacone: present, distinct (0); weak or absent (1).

Character 110. Paraconid height relative to metaconid (Wible et al., 2009: 107): shorter (0); subequal (1); taller (2).

Character. 111. Paraconid on lingual margin (Wible et al., 2009: 108): absent (0); present (1).

Character. 112. Paraconid shape (Novacek, 1986: dental feature 28*): conical (0); crestiform or bladelike (1).

Character 113. Paracristid (Wible et al., 2009: 110*): notched (0); deep or carnassial (1); continuous curve without notch (2).

Character 114. Trigonid configuration (Wible et al., 2009: 111*): open, with paraconid anteromedial, paracristid-protocristed angle more than 50° (0); more acute, with paraconid more posteriorly placed, paracristid-protocristid angle between 36°–49° (1); anteroposteriorly compressed, paracristid-protocristid angle 35° or less (2). (Score is inapplicable for taxa lacking a paraconid.)

Character 115. Protoconid height (Wible et al., 2009: 112): tallest cusp on trigonid (0); subequal to para- and/ or metaconid (1); smaller than para and/or metaconid (2).

Character 116. Protocristid orientation (Wible et al., 2009: 113): oblique (0); transverse (1).

Character 117. Anterior and labial cingular cuspute (Wible et al., 2009: 114): present, without a distinct cingular shelf posteroventrally directed from it (0); present with a distinct cingular shelf posteroventrally directed from it (1); present with distinct cinular shelf continuing along buccal border (2); absent (3).

Character 118. Talonid (Wible et al., 209: 115): small heel or minute (0); multicusped basin (1).

Character 119. Cristid obliqua (Wible et al., 2009: 116*): complete, attaching to base of metaconid (0); complete, attaching to notch in protocristid (1); complete, attaching below posterior middle of protoconid or labially placed (2).

Character 120. Trigonid height relative to talonid height (Wible et al., 2009: 117): twice or more (0); less than twice (1); subequal (2).

Character 121. Anteroposterior shortening at base of trigonid relative to talonid (Wible et al., 2009: 118): trigonid long (more than 75% of tooth length) (0); some shortening (50%–75% of tooth length) (1); anteroposterior compression of trigonid (less than 50% of tooth length) (2).

Character 122. Talonid width relative to trigonid (Wible et al., 2009: 119*): talonid very narrow, subequal to base of metaconid (0); talonid narrower than trigonid (1); talonid subequal to trigonid (2); talonid wider than trigonid (3).

Character 123. Hypoconulid (Wible et al., 2009: 120): absent (0); in posteromedial position near the midpoint of transverse talonid width (1); lingually placed with slight proximity to entoconid (2); in close proximity to entoconid (3).

Character 124. Hypoconulid of ultimate lower molar (Wible et al., 2009: 121): short and erect (0); tall and sharply recurved (1); large, posteriorly procumbent (2); absent (3).

Character 125. Entoconid (Wible et al., 2009: 122): absent (0); smaller than hypoconid and/or hypoconulid (1); or subequal to or larger than hypoconid and/or hypoconulid (2).

Character 126. Entocristid: present (0); weak or absent (1).

Character 127. Labial postcingulid (Wible et al., 2009: 126): absent (0); present (1).

Character 128. Hypoflexid (Meng et al., 2003: 70): shallow (0); deep (1).

Character 129. First lower molar size relative to subsequent lower molar: subequal or larger (0); smaller (1).

Character 130. Ultimate lower molar size relative to penultimate lower molar (Wible et al., 2009: 127): subequal or larger (0); smaller (1).

Dentary

Character 131. Number of mental foramina (Wible et al., 2009: 128): two or more (0); one (1).

Character 132. Anteriormost mental foramen (Wible et al., 2009: 129*): below incisors (or anteriormost dentary) (0); below anteriormost premolar (1); more posterior (2). (Taxa with only one mental foramen are scored here.)

Character 133. Posteriormost mental foramen (Wible et al., 2009: 130*): below penultimate premolar (under anterior end of functional postcanine row) (0); below ultimate premolar (1); at ultimate premolar and first molar junction or more posterior (2). (Score is inapplicable for taxa with only one mental foramen.)

Character 134. Coronoid process width (Wible et al., 2009: 134): broad, roughly two molar lengths (0); narrow, subequal to or less than one molar length (1).

Character 135. Tilting of coronoid process (measured as angle between anterior border of coronoid process and horizontal alveolar line of all molars) (Wible et al., 2009: 135*): reclined (≥120°) (0); less than vertical (~110°) (1); near vertical (2).

Character 136. Ventral border of masseteric fossa (Wible et al., 2009: 137*): absent (0); present as a well-defined and thin crest (less than half the height of the mandibular ramus) (1); present as a low and broad crest (more than half the height of mandibular ramus) (2).

Character 137. Condyloid crest (Wible et al., 2009: 140): absent (0); present (1).

Character 138. Angular process orientation (Wible et al., 2009: 143): posteriorly directed (0); medially inflected (1); posteroventrally directed (2); posterodorsally directed (3).

Character 139. Angular process length (Wible et al., 2009: 144): less than dentary ramus length (0); equal or greater than dentary ramus length (1).

Character 140. Angular process shape (Wible et al., 2009: 145): tapering, base wider than tip (0); rounded, base as wide as tip (1).

Character 141. Angular process vertical position (Wible et al., 2009: 146): at posteroventral border of dentary (0); posterodorsal, at or near alveolar border (1).

Character 142. Root of angular process relative to condylar process (Wible et al., 2009: 147): level with or posterior to condylar process (0); anterior to condylar process (1).

Character 143. Condylar process (Wible et al., 2009: 148): with posteriorly directed peduncle (0); without peduncle (1).

Character 144. Condyle shape (Wible et al., 2009: 149): ovoid (0); cylindrical (1); anteroposteriorly elongate (2).

Character 145. Condyle position relative to tooth row (Wible et al., 2009: 150): at about same level (0); slightly above (1); above by more than molar length (2).

Character 146. Symphysis shape (Wible et al., 2009: 151): tapered (0); deep (1).

Character 147. Symphysis posterior extent (Wible et al., 2009: 152): p1 or more anterior (0); p2 (1); p3 or more posterior (2).

Character 148. Symphysis (Wible et al., 2009: 153): mobile (0); fused (1).

Character 149. Vertical position of mandibular foramen (Wible et al., 2009: 157): anteriorly placed, near back of dentition (0); near ventral margin, at root of angle (1); recessed dorsally from ventral margin but below alveolar plane (2); recessed dorsally from ventral margin, at or above alveolar plane (3).

Character 150. Mandibular foramen dorsal to prominent longitudinal ridge (Wible et al., 2009: 158): present (0); absent (1).

Character 151. Depth of dentary body (Wible et al., 2009: 131): slender and long (0); or deep and short (1).

Character 152. Masseteric fossa: shallow, is not or is bordered by coronoid crest anteriorly (0); deep, bordered by strong coronoid crest (1).

Skull

Character 153. Premaxilla, facial process dorsal extent (Wible et al., 2009: 160): does not reach nasal (0); reaches nasal (1).

Character 154. Premaxilla, facial process posterior extent (Wible et al., 2009: 161): does not extend beyond canine (0); extends beyond canine but does not contact frontal (1); extends beyond canine and contacts frontal (2).

Character 155. Premaxilla, facial process with distinct fingerlike posterodorsal process (Wible et al., 2009: 162): present (0); absent (1).

Character 156. Exits of infraorbital canal (Wible et al., 2009: 164): multiple (0); single (1); canal absent (2).

Character 157. Infraorbital foramen position (Wible et al., 2009: 165): dorsal to ultimate premolar (0); dorsal to penultimate premolar or more anterior (1); dorsal to first molar or more posterior (2). (Score is inapplicable for taxa without an infraorbital canal.)

Character 158. Infraorbital canal length (Wible et al., 2009: I66): long (more than one

molar length) (0); short (less than one molar length) (1). (Score is inapplicable for taxa without an infraorbital canal.)

Character 159. Flaring of cheeks behind infraorbital foramen as seen in ventral view (Wible et al., 2009: 167): present (0); absent (1).

Character 160. Infraorbital canal of large caliber (Novacek, 1986: cranial and jaw feature 11): present (0); absent (1).

Character 161. Nasal (Wible et al., 2009: 168): widest posteriorly (0); sides subparallel (1); widest anteriorly (2).

Character 162. Nasal overhangs external nasal aperture (Wible et al., 2009: 169; Novacek 1986: cranial and jaw feature 1): present (0); absent (1).

Character 163. Nasofrontal suture with medial process of frontal wedged between nasals (Wible et al., 2009: 170): present (0); absent (1).

Character 164. Nasofrontal suture position (Wible et al., 2009: 171): posterior to or even with anterior orbital rim (0); anterior to anterior orbital rim (1).

Character 165. Frontal-maxillary contact on rostrum (Wible et al., 2009: 173): absent (0); present (1).

Character 166. Maxillary process of frontal (anterior projection of frontal) (Wible et al., 2009: 174): weak or absent (0); elongate and thin (1).

Character 167. Preorbital length relative to postorbital (Wible et al., 2009: 175): less than one-third total length (0); more than one-third (1).

Character 168. Lacrimal (Wible et al., 2009: 176): present (0); absent (1).

Character 169. Facial process of lacrimal (Wible et al., 2009: 177*): large, triangular and pointed anteriorly (0); small, rectangular, or crescentic (1); absent (2). (Score is inapplicable for taxa without lacrimal).

Character 170. Lacrimal tubercle (crest) (Wible et al., 2009: 178; Novacek, 1986): present (0); absent (1). (Score is inapplicable for taxa without lacrimal).

Character 171. Lacrimal foramen exposed on face (Wible et al., 2009: 179): present (0); absent (1).

Character 172. Lacrimal foramen number (Wible et al., 2009: 180): two (0); one (1).

Character 173. Lacrimal foramen composition (Wible et al., 2009: 181): enclosed within lacrimal (0); with maxillary contribution (1); with jugal contribution (2).

Character 174. Lacrimal foramen size (Asher et al., 2002: 35): small or similar to sphenopalatine foramen (0); larger (1).

Character 175. Premaxilla, palatal process (Wible et al., 2009: 183): does not reach canine alveolus (0); reaches nearly to or to canine alveolus (1).

Character 176. Premaxillary-maxillary suture on palate (Wible et al., 2009: 184): transverse (0); wedge shaped, pointing anteriorly (1); wedge shaped, pointing posteriorly (2).

Character 177. Incisive foramina (Wible et al., 2009: 185): small, length of 1 or 2 incisors (0); intermediate length of 3 incisors (1); elongate, more than half the palate length (2).

Character 178. Incisive foramina composition (Wible et al., 2009: 186): between premaxilla and maxilla (0); within premaxilla (1).

Character 179. Palatal vacuities (Wible et al., 2009: 187): absent (0); present (1).

Character 180. Major palatine foramen (Wible et al., 2009: 188): within palatine (0); between palatine and maxilla (1); within maxilla (2); multiple small foramina (3); absent (4).

Character 181. Middle palatine foramen (Novacek, 1986: cranial feature 15): present (0); foramina joined as an elongate pair of openings or absent (1).

Character 182. Anterior extent of palatine on palate (Wible et al., 2009: 189): to level of first molar (0); more posterior (1); more anterior (2).

Character 183. Palatal expansion with regard to ultimate molar (Wible et al., 2009: 190):

even with ultimate molar (0); posterior to ultimate molar (1); anterior to ultimate molar (2).

Character 184. Postpalatine torus (Wible et al., 2009: 191): absent or weak (0); present, distinct (1).

Character 185. Maxilla with large shelflike expansion posterior to ultimate molar (Wible et al., 2009: 195): absent (0); present (1).

Character 186. Posterior edge of anterior zygomatic root (Wible et al., 2009: 196): aligned with last molar (0); with anterior molars (1); with premolars (2).

Character 187. Zygomatic process of maxilla (Wible et al., 2009: 197): present (0); vestigial (1).

Character 188. Jugal (Wible et al., 2009: 198): present (0); absent (1).

Character 189. Jugal (Wible et al., 2009: 199): contributing to anteroventral orbit and zygoma (0); contributing to zygoma (1). (Score is inapplicable for taxa without jugal.)

Character 190. Maxillary-jugal contact bifurcated (Wible et al., 2009: 200): absent (0); present (1). (Score is inapplicable for taxa without jugal and /or lacrimal.)

Character 191. Jugal-lacrimal contact (Wible et al., 2009: 201): present (0); absent (1). (Score is inapplicable for taxa without jugal and/or lacrimal.)

Character 192. Zygomatic arch (Wible et al., 2009: 202): stout (0); delicate (1); incomplete (2).

Character 193. Origin of maxillary zygoma (Asher et al., 2002: 43): at level of M1 (0); M2 (1); M3 (2).

Character 194. Roots of molars exposed in orbit floor (Wible et al., 2009: 203): absent (0); present (1).

Character 195. Palatine reaching infraorbital canal (Wible et al., 2009: 204): present (0); absent (1).

Character 196. Sphenopalatine foramen (Wible et al., 2009: 207): within palatine (0); between palatine and maxilla (1); between palatine, maxilla, and frontal (2); within maxilla (3).

Character 197. Sphenopalatine foramen proximal to maxillary foramen (Wible et al., 2009: 208): absent (0); present (1).

Character 198. Maxilla excluded from medial orbital wall (Wible et al., 2009: 209): present (0); absent (1).

Character 199. Frontal and maxilla contact in medial orbital wall (Wible et al., 2009: 210): absent (0); present (1).

Character 200. Orbital process of palatine (Wible et al., 2009: 211): present (0); absent or with thin sliver in ventromedial wall of orbit (1).

Character 201. Ethmoid exposure in medial orbital wall (Wible et al., 2009: 212): absent (0); present (1).

Character 202. Ethmoidal foramen (Wible et al., 2009: 213): between frontal and orbitosphenoid (0); within frontal (1).

Character 203. Frontal foramen on skull roof (Wible et al., 2009: 215): absent (0); present (1).

Character 204. Postorbital process (Wible et al., 2009: 216): present, prominent (0); present, weak (1); absent (2).

Character 205. Size of orbit (orbit length/skull length): small (less than 10%) (0); larger (near 20%) (1).

Character 206. Postorbital bar (Wible et al., 2009: 218): absent (0); present (1).

Character 207. Orbital process of frontal (modified from Novacek, 1986: cranial feature 28): large, confined to orbitosphenoid and palatine (0); restricted (1); ventral expansion of frontal very pronounced (2).

Character 208. Dorsal process of jugal (Wible et al., 2009: 219): weak or absent (0); strong (1).

Character 209. Optic foramen (Wible et al., 2009: 220): absent (0); present (1).

Character 210. Optic foramen position (Wible et al., 2009: 221): narrowly separated from

sphenorbital fissure (0); broadly separated from sphenorbital fissure (1); not visible in lateral view (2). (Score is inapplicable for taxa without optic foramen.)

Character 211. Orbitosphenoid (Wible et al., 2009: 222): expanded anteriorly from optic foramen (or with anterior process for forms without optic foramen) (0); expanded dorsally from optic foramen (or with dorsal process for forms without optic foramen) (1); not expanded anteriorly or dorsally (2).

Character 212. Suboptic foramen (Wible et al., 2009: 223): absent (0); present (1).

Character 213. Frontal/alisphenoid contact (Wible et al., 2009: 225): present, dorsal plate of the alisphenoid contacting frontal at anterior end (0); present, with more extensive contact with frontal (~50% of its dorsal border) (1); absent (2).

Character 214. Frontal length on midline (Wible et al., 2009: 226): subequal to slightly smaller than parietal (0); less than half that of parietal (1); more than 50% longer than parietal (2).

Character 215. Frontoparietal suture (Wible et al., 2009: 227): transverse (0); with anterior process of parietal off the midline (1); with anterior process of parietal on the midline (2).

Character 216. Sagittal crest (Asher et al., 2002: 26): single, reduced or weak (0); single, large or strong (1); double (2).

Character 217. Interparietal (Wible et al., 2009: 229): absent (0); present (1).

Character 218. Nuchal crest (Wible et al., 2009: 230): level with or anterior to foramen magnum (0); posterior to foramen magnum (1).

Character 219. Squama of squamosal (Wible et al., 2009: 232): absent (0); present (1).

Character 220. Choanae (Wible et al., 2009: 234): as wide as posterior palate (0); narrower than posterior palate (1).

Character 221. Midline rod-shaped eminence on basisphenoid (Wible et al., 2009: 240): absent (0); present (1).

Character 222. Ectopterygoid process of alisphenoid (Wible et al., 2009: 241): absent (0); ending at anterior basisphenoid (1); approaching ear region (2).

Character 223. Ectopterygoid process of alisphenoid extent (Wible et al., 2009: 242): long crest (0); narrow process (1). (Score is inapplicable for taxa without ectopterygoid process.)

Character 224. Foramen ovale composition (Wible et al., 2009: 246): in petrosal (anterior lamina) (0); between petrosal and alisphenoid (1); in alisphenoid (2); between alisphenoid and squamosal (3).

Character 225. Foramen ovale position (Wible et a., 2009: 247): on lateral wall of braincase (0); on ventral surface of skull (1).

Character 226. Alisphenoid canal (Wible et al., 2009: 248): absent (0); present (1).

Character 227. Posterior opening of alisphenoid canal (Wible et al., 2009: 249): separated from foramen ovale (0); in common depression with foramen ovale (1). (Score is inapplicable for taxa without alisphenoid canal.)

Character 228. Position of jaw articulation relative to fenestra vestibuli (Wible et al., 2009: 250): at same level as fenestra vestibuli (0); in front of fenestra vestibuli (1).

Character 229. Glenoid fossa position (Wible et al., 2009: 251): on zygoma (0); partly on braincase (1).

Character 230. Glenoid fossa shape (Wible et al., 2009: 252): concave, open anteriorly (0); troughlike (1); anteroposteriorly elongate (2); anteroposteriorly short (3); convex, open anteriorly (4).

Character 231. Glenoid fossa dorsoventral position relative to sphenoid on midline skull base (Wible et al., 2009: 253): even with sphenoid (0); higher than sphenoid (1).

Character 232. Glenoid process of jugal (Wible et al., 2009: 254): present, with articular facet (0); present without facet (1); absent (2). (Score is inapplicable for taxa without jugal.)

Character 233. Glenoid process of alisphenoid (Wible et al., 2009: 255): absent (0); present (1).

Character 234. Postglenoid process (Wible et al., 2009: 256): absent or weak (0); present (1).

Character 235. Postglenoid foramen (Wible et al., 2009: 257): absent (0); present (1).

Character 236. Postglenoid foramen position (Wible et al., 2009: 258): behind postglenoid process (0); medial or anterior to postglenoid process (1); on lateral aspect of braincase (2). (Score is inapplicable for taxa without postglenoid foramen.)

Character 237. Postglenoid foramen composition (Wible et al., 2009: 259): within squamosal (0); behind squamosal (1). (Score is inapplicable for taxa without postglenoid foramen.)

Character 238. Suprameatal foramen (Wible et al., 2009: 260): absent (0); present (1).

Character 239. Entoglenoid process of squamosal (Wible et al., 2009: 261): absent (0); present, separate from postglenoid process (1); present, continuous with postglenoid process (2).

Character 240. Carotid foramen (Wible et al., 2009: 263): within basisphenoid (0); between basisphenoid and petrosal (1); absent (2).

Character 241. Alisphenoid tympanic process (Wible et al., 2009: 265): absent (0), present (1).

Character 242. Basisphenoid tympanic process (Wible et al., 2009: 266*): absent or weak (0); present (1).

Character 243. Medial flange of petrosal (epitympanic wing medial to promontorium (Wible et al., 2009: 268): absent (0); flat (1); thickened (2).

Character 244. Rostral tympanic process of petrosal (Asher et al., 2002: 6; Wible et al., 2009: 269): absent or flat (0); moderate medial ridge (1); tall ridge or medial wall, contributing to ventral bulla (2).

Character 245. Course of internal carotid artery (Wible et al., 2009: 270): lateral (transpromontorial) (0); medial (perbullar or extrabullar) (1); course indication absent (2).

Character 246. Intratympanic vascular canal (for transpromontorial internal carotid) (Wible et al., 2009: 271): absent (0); present (1).

Character 247. Deep groove for internal carotid artery excavated on anterior pole of promontorium (Wible et al., 2009: 272): absent (0); present (1).

Character 248. Stapedial artery on promontorium (Wible et al., 2009: 274): sulcus (0); canal (1); absent (2).

Character 249. Stapedial ratio (length/width of fenestra vestibuli) (Wible et al., 2009: 275): rounded, less than 1.8 (0); elliptical, more than 1.8 (1).

Character 250. Promontorium shape (Wible et al., 2009: 278): flat (0); globose (1).

Character 251. Promontorium depth relative to basioccipital (Wible et al., 2009: 279): even with or ventral to basioccipital (0); dorsal to basioccipital (1).

Character 252. Intratympanic course of facial nerve (Wible et al., 2009: 280): opening in sulcus (0); opening anteriorly, canal posteriorly (1); opening in canal (2).

Character 253. Length of bony shelf lateral to promontorium (lateral trough or tegmen tympani) (Wible et al., 2009: 285): extended anteriorly as far as promontorium (0); confined posterolaterally (1); prolonged anterior to promontorium (2).

Character 254. Width of bony shelf lateral to promontorium (lateral trough or tegmen tympani) (Wible et al., 2009: 286): uniform (0); expanded anteriorly (1).

Character 255. Inflation of bony shelf lateral to promontorium (lateral trough or tegmen tympani) (Wible et al., 2009: 287): absent (0); present (1).

Character 256. Stapedial canal on bony shelf lateral to promontorium (lateral trough or tegmen tympani) (Wible et al., 2009: 288): absent (0); present (1).

Character 257. Tensor tympani fossa on petrosal (Wible et al., 2009: 289): shallow (0); deep circular pit (1).

Character 258. Medial process of squamosal in tympanic cavity (Wible et al., 2009: 290): absent (0); present (1).

Character 259. Epitympanic recess/fossa incudis size (Wible et al., 2009: 292): subequal (0); epitympanic recess larger (1); or no visible depression for epitympanic recess (2).

Character 260. Epitympanic recess lateral wall (Wible et al., 2009: 293): with small contribution to posterolateral wall by squamosal (0); with extensive contribution to lateral wall by squamosal (1); with no squamosal contribution (2).

Character 261. Fossa incudis (Wible et al., 2009: 294): continuous with epitympanic recess (0); separated from epitympanic recess (1).

Character 262. Fossa incudis position relative to fenestra vestibuli (Wible et al., 2009: 296): lateral (0); anterior (1).

Character 263. Stapedius fossa (Wible et al., 2009: 300): twice the size of fenestra vestibuli (0); small and shallow (1).

Character 264. Fenestra cochlear position to fenestra vestibuli (Wible et al., 2009: 303): posteromedial (0); posterior (1).

Character 265. Posterior septum shields fenestra cochleae (Wible et al., 2009: 304): absent (0); present (1).

Character 266. Paroccipital process (Wible et al., 2009: 305): vertical (0); slanted, projecting anteroventrally as flange toward back of promontorium (1); indistinct to absent (2).

Character 267. Rear margin of auditory region (Wible et al., 2009: 310): marked by deep wall (0); extended onto a flat surface (1).

Character 268. Jugular foramen size relative to fenestra cochleae (Wible et al., 2009: 312): subequal (0); larger (1).

Character 269. Jugular foramen (Wible et al., 2009: 313): confluent with (0); separated from opening for inferior petrosal sinus (1).

Character 270. Hypoglossal foramen (Wible et al., 2009: 314): two or more (0); one (1).

Character 271. Hypoglossal foramen housed in opening larger than jugular foramen (Wible et al., 2009: 315): absent (0); present (1).

Character 272. Paroccipital process of exoccipital (Wible et al., 2009: 316): weak or absent (0); prominent vertical (1); prominent posteriorly directed (2).

Character 273. Ectotympanic (Wible et al., 2009: 317): phaneric or visible in ventral view (0); or aphaneric or hidden by auditory bulla (1).

Character 274. Ectotympanic shape (Wible et al., 2009: 318): ringlike (0); fusiform (1); expanded (2).

Character 275. Anterior crus of ectotympanic broadly contacts facet on squamosal (Wible et al., 2009: 319): absent (0); present (1).

Character 276. Elongate ossified external acoustic canal (Wible et al., 320): absent (0); present (1).

Character 277. Roof of external acoustic meatus (Wible et al., 2009: 321): petrosal (0); squamosal (1).

Character 278. Entotympanic (Wible et al., 2009: 322): absent (0); present (1).

Character 279. Subarcuate fossa aperture (Wible et al., 2009: 330): not constricted (0); constricted (1); fossa absent (2).

Character 280. Internal acoustic meatus (Wible et al., 2009: 332): deep with thick prefacial commissure (0); shallow with thin prefacial commissure (1).

Character 281. Glaserian fissure (Novacek, 1986: cranial feature 42): indistinct or absent (0); distinct (1).

Character 282. Mastoid foramen (Wible et al., 2009: 336): absent (0); two in mastoid (1); one in mastoid (2); one between mastoid and supraoccipital (3).

Character 283. Lack of occipital exposure of mastoid (Wible et al., 2009: 337): absent (0); present (1).

Character 284. Dorsal margin of foramen magnum (Wible et al., 2009: 338): formed by exoccipitals (0); by exoccipitals and supraoccipital (1).

Character 285. Mastoid process (Novacek, 1986: cranial feature 57): with deep groove (0); groove faint or absent (1).

Character 286. Mastoid tubercle (Novacek, 1986: cranial feature 58): weak or absent (0); large (1).

Character 287. Small exposure of parietal on occipital surface (Novacek, 1986: cranial feature 61): absent (0); present (1).

Character 288. Exposure of supraoccipital on dorsal roof of skull (Novacek, 1986: cranial feature 63): broad (0); narrow restricted (1).

Character 289. Lambdoidal crest (Novacek, 1986: cranial feature 64): well-developed (0); weak (1).

Character 290. Posterior lacerate foramen (Novacek, 1986: cranial feature 67): small (0); large (1).

Scientific Publications of the American Museum of Natural History

American Museum Novitates
Bulletin of the American Museum of Natural History
Anthropological Papers of the American Museum of Natural History

Submission procedures can be found at http://research.amnh.org/scipubs

All issues of *Novitates* and *Bulletin* are available on the web (https://digitallibrary.amnh.org/handle/2246/5). Order printed copies on the web from:
https://shop.amnh.org/books/scientific-publications.html

or via standard mail from:
American Museum of Natural History—Scientific Publications
Central Park West at 79th Street
New York, NY 10024

♾ This paper meets the requirements of ANSI/NISO Z39.48-1992 (permanence of paper).

On the cover: Skull of *Hsiangolestes youngi*, IVPP V5792, left lateral (upper) and ventral (lower) views.